Experimental Study of Hydro-Mechanical Behaviour of Granular Materials

By

Gilbert Joseph KASANGAKI

Submitted for the degree of Doctor of Philosophy

(Civil Engineering)

Heriot-Watt University

School of the Built Environment

November 2012

Abstract

Inadequate knowledge of the behaviour of wet granular materials such as unsaturated soils or wet and sticky industrial bulk solids formed the basis of the current research project in which selected granular materials were experimentally characterised. The main objective was to investigate the hydro-mechanical behaviour. Specifically, the following were studied: effect of particle size, particle shape, drying-wetting cycles and void ratio on the water retention behaviour of granular materials, and effect of suction on the shear behaviour and flowability of granular materials. A total of 85 pressure plate tests, 13 triaxial compression tests with the axis translation technique used to control suction in unsaturated tests and 52 silo model tests were successfully conducted to respectively measure water retention characteristics, stress-strain and shear strength, and flowability of glass beads of high sphericity (~95% roundness) and Leighton Buzzard sand (~82% roundness). With these deliberately simple materials each considered factor was isolated and investigated at a time something hugely challenging to achieve with many unsaturated soils.

Many pertinent features of hydro-mechanical behaviour observed for most soils were well captured with spherical glass beads meaning that particle-water interaction alone can produce the typical unsaturated behaviour and the particle size and shape significantly affected the behaviour. Further drying-wetting cycles did not alter the WRCs of both glass beads and sand except in the saturated capillary regime suggesting that factors other than the inert water-particle interaction through the liquid bridges are responsible for the discrepancy between the first drying-wetting cycle WRC and the subsequent drying-wetting cycles WRCs often observed in clayey soils. It's discovered that the additional inter-particle bonding force introduced through the liquid bridges maintained by the matric suction serves to increase the stiffness, volumetric stability and shear strength of the material. The rate of increase of strength diminished with increase in matric suction. The study noted that the Beverloo law is valid for estimation of the dry mass discharge rate and that moisture alone is sufficient to maintain stable arching action depending on the hopper outlet. The study generated new knowledge in form of the effect of the material particle properties on the bulk hydro-mechanical behaviour of granular materials. An approach has also been proposed for estimating the flowability and minimum hopper outlet diameter for the wet noncohesive bulk solids.

To my true treasures in life, my wife and children

Declaration Statement

ACADEMIC REGISTRY
Research Thesis Submission

Name*:*	Gilbert Joseph Kasangaki		
School/PGI:	School of the Build Environment		
Version: *(i.e. First, Resubmission, Final)*	Final	Degree Sought (Award **and** Subject area)	PhD (Civil Engineering)

Declaration

In accordance with the appropriate regulations I hereby submit my thesis and I declare that:

1) the thesis embodies the results of my own work and has been composed by myself
2) where appropriate, I have made acknowledgement of the work of others and have made reference to work carried out in collaboration with other persons
3) the thesis is the correct version of the thesis for submission and is the same version as any electronic versions submitted*.
4) my thesis for the award referred to, deposited in the Heriot-Watt University Library, should be made available for loan or photocopying and be available via the Institutional Repository, subject to such conditions as the Librarian may require
5) I understand that as a student of the University I am required to abide by the Regulations of the University and to conform to its discipline.

* *Please note that it is the responsibility of the candidate to ensure that the correct version of the thesis is submitted.*

Signature of Candidate*:*		Date:	

Submission

Submitted By *(name in capitals):*	GILBERT JOSEPH KASANGAKI
Signature of Individual Submitting:	
Date Submitted:	

For Completion in the Student Service Centre (SSC)

Received in the SSC by *(name in capitals):*			
Method of Submission *(Handed in to SSC; posted through internal/external mail):*			
E-thesis Submitted *(mandatory for final theses)*			
Signature:		Date:	

Acknowledgement

First, I would like to thank my supervisors, Dr. Gabriela M. Medero and Prof. Jin Y. Ooi for accepting me as their student and for their guidance, contribution, encouragement but mostly for their patience when it came to experimental and or equipment setup challenges and failures. To me they are not just supervisors but generous friends. It was one of my greatest assets to know that my supervisors were there for me and could, in most cases, be contacted if any consulting or support was needed.

This research project was done in collaboration with Edinburgh University to which I am highly indebted. A lot of library resources that I could not get at Heriot-Watt University were accessed through the University of Edinburgh Robertson Engineering and Science Library. The project was funded by the Civil and Environmental Engineering Joint Research Institute, Edinburgh to which I am also highly indebted for the enormous facilitation for and during my study and stay in the United Kingdom. It really would have been rather difficult without such support. However, the work presented herein is solely the responsibility of the author and by no means represents the ideas of the funders.

Dr. David Toll of Durham University is also very much appreciated for his assistance with the software that was used in this research project. Mr. Joao Mendes's prior experience with the double-wall unsaturated triaxial apparatus and the Triax software was also of much use in the early stages of this study. Mr. Bernie McEleavey, the Laboratory Technician at Durham University was also so instrumental in the electrical connections that his input cannot go unacknowledged.

To the Laboratory Technician, Mr. Alastair McFarlane, I say thank you for your help and support. You often went above and beyond the call of duty in encouraging participation, supporting the goals of the research project and providing the necessary expertise especially during the setting up of, and making operational, the unsaturated triaxial apparatus. The workshop superintendent, Mr. Bill Hodder and his co-workers in the workshop helped with the fabrication of several accessories and are very much appreciated for their input. Many of the operations in the laboratory would have been a nightmare without a hand from my friends Nawras, Ali, Ogechi and other colleagues in

the laboratory and office, to whom I am indebted. Mr. Zhong Zhilug, the Laboratory Technician at the Institute for Infrastructure and Environment, University of Edinburgh is also appreciated for his cooperation during the study period of this project. Mr. Subhash Chandra Thakur your help with the mastersizing of the test samples is also very much appreciated.

Special thanks go to my parents, brothers and sisters for their love, support and guidance throughout my life and for inculcating in me the passion for knowledge. Out of the ordinary, I thank my lifelong best friend, companion and wife Annette Ateenyi, my dearly loved daughters, Prudence Amooti and Marjorie Ateenyi for their love and patience so exceedingly appreciated during my study period.

Finally, I thank the Almighty God, for obvious reasons, but especially for the countless blessings He has poured upon me in the completion of this thesis with strength, determination and discipline.

Gilbert Joseph KASANGAKI.

Table Contents

List of Tables

List of Figures

List of Acronyms and Symbols plus their Units

Notation	Description	Unit
Acronyms		
A	Area	m^2
b	Mankoc et al. (2007) fitting parameter	-
c	Apparent cohesion	kPa
c'	Effective cohesion	kPa
C	Beverloo et al. (1961) fitting parameter related to friction	kPa
C_U	Coefficient of uniformity	-
C_Z	Coefficient grading	-
C_τ	Zhang & Rudolph (1991) parameter related to shear resistance	-
C'	Mankoc et al. (2007) proportionality coefficient	-
d_p	Particle size	mm
D_{10}	Particle size for which 10% is finer (effective size)	mm
D_{30}	Particle size for which 30% is finer	mm
D_{50}	Mean particle size (Particle size for which 50% is finer)	mm
D_{50eq}	Equivalent mean spherical particle diameter	mm
D_{60}	Particle size for which 60% is finer	mm
D_o	Hopper outlet diameter	cm
D_B	Silo barrel diameter	cm
$D_{\min}$	Minimum hopper outlet diameter	cm
D_{crit_lb}	Critical outlet diameter with respect to liquid bridge induced arch	cm
e	Void ratio	-
e_0	Void ratio at peak deviator stress	-
e_{ic}	Void ratio after isotropic compression	-
e_{peak}	Void ratio after isotropic compression	-
E_m	Young's modulus of elasticity for the membrane	kPa
F_s	Bonding force between particles	kPa
g	Acceleration due to gravity	ms^{-2}

h	Height of the capillary rise	m
h_s	Hydrostatic pressure head	m
k	Alonso et al. (1990) parameter describing cohesion increase with ψ	-
k_a, k_b	Toll & Ong (2003) fitting parameters relating to $(p-u_a)$ and ψ_m	-
k_B	Beverloo et al. (1961) fitting parameter related to empty annulus	-
k_{sat}	Saturated coefficient of permeability	cms^{-1}
K	Lateral pressure coefficient	-
K_0	Lateral pressure coefficient at rest	-
K_a	Active lateral pressure coefficient	-
L	Separation distance between any two spheres	m
M	Critical state stress ratio (also known as slope of critical state line)	-
M_a	Critical state stress ratio with respect to ($p-u_a$)	-
M_b	Critical state stress ratio with respect to (u_a-u_w)	-
M_s	Saturated critical state stress ratio	-
m_b	Mass of a single particle	g
n	Porosity	-
p	Mean total stress equal to $(\sigma_1+2\sigma_3)/3$ for triaxial tests	kPa
p_0	Yield stress	kPa
p^c	Mean stress at which one may reach the saturated virgin state through suction unloading involving only elastic swelling	kPa
p_o^*	Pre-consolidation mean stress for saturated conditions	kPa
P	Partial water pressure	kPa
P_0	Saturation pressure of water vapour over flat surface of pure water	kPa
q	Deviator stress $(\sigma_1-\sigma_3)$	kPa
R	Universal gas constant	$Jmol^{-1}K^{-1}$
R_B	Radius of silo barrel (shell)	m
R_h	Relative humidity $(100P/P_0)$	%
$R*$	Ratio of hopper outlet diameter to mean particle diameter	-
r	Alonso et al. (1990) parameter defining the maximum soil stiffness	-
r_o	Radial distance of the bulk solids arch from hopper virtual apex	m

r_s	Radius of capillary tube	m
R_s & R_1, R_2	Radius of the meniscus and liquid bridge respectively	m
S_r	Degree of saturation	%
S_{r0}	Initial degree of saturation	%
S_{r1}, S_{r2}	Toll & Ong (2003) reference degrees of saturation	%
S_{ric}	Degree of saturation after isotropic compression	%
S_{rpeak}	Degree of saturation at peak deviator stress	%
SSA	Specific surface area	cm^{-1}
t	Relative temperature measured on the Celsius scale	^oC
T	Absolute temperature	^oK
t_m	Membrane thickness	mm
T_s	Surface tension	Nm
u_a	Pore air pressure	kPa
u_w	Pore water pressure	kPa
$(u_a - u_w)_b$	Bubbling pressure (also known as air-entry value)	kPa
Δu	Pressure difference across the air-water interface	kPa
V	Volume	m^3
V_m	Membrane penetration	cm^3
w	Gravimetric water content	%
w_{opt}	Optimum moisture content	%
w_r	Residual gravimetric water content	%
w_s	Saturated gravimetric water content	%
w_w	Gravimetric water content corresponding to ψ_w	%
W	Discharge rate	g/s
W_b	Number of particles collected per unit time	particles/s
W_{calc}	Calculated discharge rate	g/s
W_{obs}	Observed (measured) discharge rate	g/s
z	Depth of solids in the silo barrel	m

Notation	Description	Unit
Greek Symbols		
α	Contact angle	^{o}
α_d	Desorption (drying) contact angle	^{o}
α_w	Wetting contact angle	^{o}
α_{vG}	van Genuchten (1980) fitting parameter related to air-entry value	kPa^{-1}
β	Hopper half angle	^{o}
ε_a	Axial strain	%
ε_v	Total volumetric strain	%
ϑ	Parameter that controls rate of increase of soil stiffness with ψ_m within virgin state	-
$\lambda(0)$	Compressibility coefficient for saturated state along virgin loading	-
$\lambda(\psi)$	Compressibility coefficient for increments of net normal stress for virgin states	-
λ_ψ	Compressibility coefficient for increments of suction for virgin states	-
κ	Elastic stiffness parameter for changes in net normal stress	-
κ_ψ	Elastic stiffness parameter for changes in suction	-
κ_Θ	Shear strength envelope fitting parameter with respect to Θ	-
μ	Coefficient of friction	-
ϕ'	Effective angle of friction	^{o}
ϕ^a	Toll (1990) friction angle with respect to $(\sigma - u_a)$	^{o}
ϕ^b	Angle of friction with respect to matric suction	^{o}
ϕ_w	Angle of wall friction	^{o}
φ	Filling angle with respect to liquid bridge between particles	^{o}
ρ	Density	Mgm^{-3}
ρ_b	Bulk density	Mgm^{-3}
ρ_d	Dry density	Mgm^{-3}
ρ_s	Particle density	Mgm^{-3}
$\rho_{d\,\max}$	Maximum dry density	Mgm^{-3}
$\rho_{\max}$	Maximum density	Mgm^{-3}
$\rho_{\min}$	Minimum density	Mgm^{-3}

ρ_w	Density of water	Mgm^{-3}
ρ^c	Critical density	Mgm^{-3}
σ	Total normal stress	kPa
σ_{con}	Consolidation stress	kPa
σ_c	Unconfined yield strength	kPa
σ_{ccrit}	Critical unconfined yield strength	kPa
σ_{hw}	Principal stress needed to support weight of a stable bulk solids arch	kPa
σ_n	Wall normal stress	kPa
σ_z	Vertical stress	kPa
σ_1	Total major principal stress	kPa
σ_3	Total cell pressure (total minor principal stress)	kPa
$\sigma_3 - u_a$	Net normal stress	kPa
σ'	Effective stress $(\sigma - u)$	kPa
θ	Volumetric water content	-
Θ	Normalised volumetric water content	-
θ_r	Residual volumetric water content	-
θ_s	Saturated volumetric water content	-
υ	Angle of dilation	o
ν	Specific volume	-
ν_{w0}	Specific volume of water $(1/\rho_w)$	Mgm^3
ω_v	Molecular mass of water vapour	$kgmol^{-1}$
ψ	Total suction	kPa
ψ_m	Matric suction	kPa
ψ_a	Air-entry value	kPa
ψ_r	Residual value	kPa
ψ_w	Water-entry value	kPa
ψ^*	Matric suction in excess of ψ_a, $[(u_a - u_w) - \psi_a]$	kPa
ψ_0	Hardening parameter of the suction increase yield curve	kPa
χ	Soil parameter related to the degree of saturation	-
ξ	Gallipoli et al. (2003) bonding parameter	-

List of Publications by the Candidate

Kasangaki G.J., Medero G.M., Ooi J.Y., 2012, *Factors influencing water retention characteristics of granular materials*, Proceedings of the Workshop on Advances in Multiphysical Testing of Soils and Shales, AMTSS, EPLF, Laussame, Switzerland, 3-5 September, in Laluoi L., Ferrari A. (Eds.): Multiphysical Testing of Soils and Shales, SSGG, 111-116

Kasangaki G.J., Medero G.M., Ooi J.Y., 2012, *Water retention characteristics of non-plastic granular materials*, Proceedings of the Second European Conference on Unsaturated Soils, E-UNSAT 2012, Napoli Italy, 20-22 June, in Mancuso C., Jommi C., & D'Onza F. (Eds.): Unsaturated Soils: Research and Applications 2012, Part 2, 197-203. DOI: 10.1007/978-3-642-31116-1_27

CHAPTER ONE

1 INTRODUCTION

1.1 Background

Wet granular materials such as unsaturated soils or wet and sticky industrial bulk solids present many engineering challenges. Their behaviour often tend to be complex due to the influence of matric suction arising from the interaction between the gas and liquid phases in the voids and cannot be easily predicted using classical theories. A sound understanding of the behaviour of unsaturated materials is relevant to the analysis and safe and economic design of most geotechnical structures including embankments, earth dams, road subgrades and subbases. These are placed and remain most of their life in unsaturated state. Many of the geohazards such as rainfall induced landslides also fall within the framework of unsaturated soils. Knowledge of the unsaturated behaviour of granular materials is also important in the analysis and design of silos for flow of the industrial bulk solids. Other areas where unsaturated behaviour is of interest are oil extraction, agronomy, flow of contaminants, etc.

Over the past few decades some advances have been made with respect to the behaviour of unsaturated soils relevant to geotechnical analyses and designs. From shear strength point of view, early researchers focussed on extending the Terzaghi's effective stress concept to unsaturated soils (e.g. Bishop, 1959). Afterwards it was recognised by many that such a concept was unable to describe the unsaturated behaviour of soils given that total stresses and suction influence the stability of soil particles differently (e.g. Jennings & Burland, 1962). Consequently, the two stress state variables (net normal stress and matric suction) concept was adopted as a necessary framework to describe unsaturated soil behaviour (e.g. Fredlund et al., 1978; Alonso et al., 1987 & 1990). Many of the subsequent formulations are variants of, and attempts to improve, the two stress state variables concept to directly incorporate the effect of degree of saturation (e.g. Vanapalli et al., 1996; Fredlund et al., 1996; Oberg and Salfors, 1997; Toll & Ong, 2003) and that of porosity (e.g. Wheeler et al., 2003).

Several mathematical equations have also been formulated to describe the water retention behaviour of particulate media in form of the relationship between water content and suction (e.g. Gardner, 1958; Brooks & Corey, 1964; van Genuchten, 1980;

Fredlund & Xing, 1994). Using these formulations and saturated soil parameters it has been possible to estimate the unsaturated shear strength (e.g. Vanapalli et al., 1996; Fredlund et al., 1996; Rassam & Cook, 2002) among other unsaturated soil properties. From practical application point of view this approach to determining shear strength seems more feasible than theories that require experimental measurement of shear strength even if such theories give predictions that are consistent with the measured experimental behaviour. This is because experimental measurements of shear strength are generally more costly, time consuming and complex to carry out. In fact use of costly highly complex measurement methods would have to be justified in terms of their economic benefits (Wheeler & Karube, 1996).

Whereas the inability of total stresses (and effective stress) based formulations to describe the behaviour of unsaturated soils is a wide recognition among the soil mechanics research community, the design of silos and other storage facilities continue to be based on analyses employing total stresses (e.g. Euro Code: BS EN 1993, 2007). As a consequence operational failures due to arching are still one of the main problems facing the industry.

It is noted that in characterising the behaviour of unsaturated soils the effect of many of the properties of the constituent particles has been ignored. The unsaturated soil behaviour has often been compared and grouped according to plasticity characteristics (e.g. Houston et al., 2006) and particle size and grading (e.g. Yang et al., 2004) while ignoring particle shape, roughness and other surface properties and the physico-chemical processes. Any constitutive parameters obtained without systematically recognising all the influential factors are likely to fall short in predicting the unsaturated material behaviour. Indeed most models can only give satisfactory results for the tested material, as evident in many studies (e.g. Leverett, 1940; Aya & Paris, 1981) and as observed by many researchers (e.g. Zhang & Li, 2011). Recognising the effect of constituent particle properties will improve an understanding of how they individually and collectively influence the unsaturated behaviour.

This research project therefore experimentally investigated the hydro-mechanical and flow behaviour of granular materials under unsaturated conditions. Distilled water and spherical glass beads were chosen to provide simple and well defined granular assemblies where the observed response can be attributed to purely glass-glass and

glass-water interaction without the presence of other complex inter-particle interactions often present in unsaturated soils. Particle size was then varied in an attempt to study its effect on the unsaturated behaviour. Finally naturally occurring Leighton Buzzard sand was tested and results compared to determine the effect of particle shape.

1.2 Objectives and Significance of the Study

The main objective of this study was to determine the hydro-mechanical behaviour of unsaturated granular materials. Specifically, the study focused on the determination of the effect of particle size, roughness and shape on the water retention characteristics for two different granular materials, namely glass beads and Leighton Buzzard sand, and their dependence on the stress history in terms of drying-wetting cycles. For these materials, the effect of matric suction and particle size on shear strength and volumetric and flow behaviour were also investigated. Using the experimental data some of the popular constitutive models in the literature were tested for their robustness. Microscopic observations have been used to add credence to the fact that soil is highly polydisperse material.

The outcome of this research project will enhance an understanding of the hydro-mechanical behaviour of granular materials among the communities that deal with particulate materials including researchers and consultants. Such communities include geotechnical community, soil scientists, agronomists and those involved in the handling and storage of the industrial bulk materials as well as researchers in the related studies. The study has contributed to knowledge by establishing a spring board for understanding how the unsaturated behaviour is influenced by the constituent particle properties. It is envisaged that extension of the study to include other factors present in many the encountered particulate materials will be helpful in improving the existing constitutive models for unsaturated soils for a wider application.

1.3 Organisation of the Thesis

This thesis is organised into Chapters, One to Eight. The relevant physical aspects of the soil-water interaction and the mechanical behaviour and modelling of unsaturated granular materials and the application to industrial material handling are reviewed and presented in Chapter 2. The experimental equipment, techniques and procedures of the laboratory testing of unsaturated materials are also reviewed and presented in this chapter.

The test materials, methods and experimental techniques and the test equipment used in the current research project are presented and described in Chapters 3 and 4 respectively.

The experimental results of this study are then presented and discussed in Chapter 5 through to Chapter 7. In Chapter 5, the water retention curves and characteristics and the micro-structural study results are presented. In Chapter 6, the stress-strain and shear strength characteristics are presented, analysed and discussed. The silo model tests results are then presented in Chapter 7.

Conclusions and recommendations are presented in Chapter 8. The thesis then ends with the appendices and references.

CHAPTER TWO

2 LITERATURE REVIEW

2.1 Introduction

Aimed at establishing state of the knowledge and identifying gaps in the current knowledge, this chapter focuses on the review of literature on the physical aspects of granular material-water interaction, mechanical behaviour and modelling of unsaturated soils as well as application to industrial material handling. It provides a platform for a better understanding of the hydro-mechanical and flow behaviour of unsaturated granular materials and a conceptual framework upon which the subsequent parts of this thesis are based.

Firstly, the physical aspects of unsaturated granular materials are presented. The material-water retention behaviour is then discussed including the determination methods for, applications and the factors influencing the water retention curve. The review proceeds with the hydro-mechanical behaviour and the constitutive modelling of unsaturated materials. In particular, the stress state variables and the associated state functions (failure criteria), the elasto-plastic models and the volumetric behaviour of unsaturated materials are discussed. The laboratory techniques for measurement and control of suction are then presented followed by application of the knowledge in industrial material handling. Concluding remarks in form of the identified gaps and hence the envisaged contribution of the current research project close this chapter.

2.2 The Concept of Suction in Granular Materials

Granular materials such as soils, glass beads, iron ores and other industrial bulk materials used in the manufacture of various products are frequently encountered in engineering projects. These materials are mostly in an unsaturated state. During transportation and storage, for instance, industrial bulk materials may attract moisture from the environment so that their voids are filled with both air and water.

In many parts of the world, mostly in arid and semi-arid regions, most of the civil engineering works are carried out within the soil that lies above the water table. In these regions, the water table is deep and annual upward flux through evaporation and evapotranspiration exceeds annual downward flux through precipitation. The soil above

water table is thus unsaturated and constitutes three phases: The solid phase related to the mineral particles, liquid phase related to the soil water and the gaseous phase related to the air within the voids. The proportions of these phases in a saturated-unsaturated soil profile are illustrated in Fig. 2.1. The gaseous phase diminishes as depth is increased finally disappearing or remaining in dissolved state below the water table. The process of excavating, remoulding, and recompacting soil also results in an unsaturated soil (Fredlund & Rahardjo, 1993; Ridley et al., 2003; Lu & Likos, 2004; Ng & Menzies, 2007). These processes are very common in engineering works.

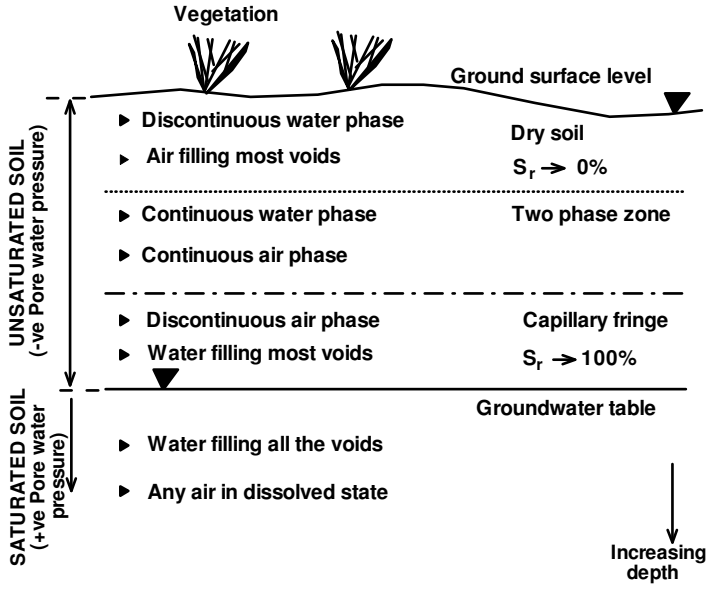

Figure 2.1: Classification of regions within a saturated-unsaturated soil profile (modified after Fredlund, 2000)

Fredlund & Morgenstern (1977) proposed a fourth phase for unsaturated soil called the contractile skin which is related to the air-water interface. This interface otherwise known as the meniscus possesses a property called surface tension, which is explained later in section 2.2.1. They argue that the air-water interface qualify to be an independent phase because its properties differ from those of the air and water phases in the soil. The contractile skin is believed to significantly influence the mechanical behaviour of unsaturated soils especially when the air phase and water phase are both continuous.

With the contractile skin recognised as the fourth phase of a system of unsaturated particulate materials such as soil or other granular materials, then in terms of behaviour the phases of an element of these materials can be visualised as a mixture of two phases

(i.e. solid particles and the contractile skin) which come to equilibrium under the action of applied stress gradients, and two other phases (i.e. air and water) that flow under the applied stress gradients. However, in the consideration of mass-volume relationships of unsaturated soils as well as other granular materials, the physical recognition of the contractile skin is unnecessary. This is because the thickness of the contractile skin is of the order of only a few molecular layers, and can therefore be considered as part of the water phase without any significant errors (Fredlund & Rahardjo, 1993).

Any soil or particulate material system with more than two phases experiences interplay of phenomena leading to suction within the material. Depending on type and state of the material, suction is due to the capillary phenomenon, water adsorption and/or dissolved salts. Consequently, suction is known as matric suction if it is only due to capillary and adsorption forces. On the other hand, if it is due to the presence of dissolved salts in the soil then it is called osmotic suction (Fredlund & Rahardjo, 1993; Lu & Likos, 2004; Ng & Menzies, 2007). These are further explained below.

2.2.1 Matric Suction

The term matric suction may be described as a measure of the energy required to remove a unit volume of pure water from the matrix of particulate material (e.g. soil) without water changing state. Being the material potential for water attraction, it is one of the most influential factors for the mechanical behaviour of unsaturated particulate materials (Fredlund & Rahardjo, 1993). In practice, matric suction, ψ_m is obtained as the difference between the pore air pressure, u_a and the pore water pressure, u_w. Thus,

$$\psi_m = u_a - u_w \qquad \text{Eq. 2-1}$$

If a particular soil-water-air system is such that the air phase is continuous throughout the system and in equilibrium with the atmosphere, then the gauge pore air pressure component of Eq. 2-1 is zero so that matric suction is simply the gauge value of the negative pore water pressure as measured through a porous tip that is in intimate contact with the soil water (Burland & Ridley, 1996). On the other hand, if the system is subjected to an air pressure greater than the atmospheric pressure but the continuous water phase is in equilibrium with the atmosphere then matric suction will simply be given by the value of the applied air pressure.

The physical mechanisms of matric suction are summarised in Fig. 2.2. The capillary action that is attributed to surface tension property of the water and water adsorption property are the source of matric suction in the soil. Water adsorption of the soil is mainly pronounced in materials such as clay minerals, which undergo high level electro-chemical activity at their negatively charged surfaces. In coarse granular materials such as glass beads, sands and gravels, water adsorption is less significant so that the capillary action may be considered as being mainly due to the surface tension of the water (Fredlund & Rahardjo, 1993; Lu & Likos, 2004). In fact in some of the studies on cohesionless materials matric suction has been termed capillary pressure (e.g. Lappalainen et al., 2009).

As shown in Fig. 2.2, surface tension develops along the water surface to equilibrate the inward forces due to an imbalance of intermolecular forces at the air-water interface. Whereas a water molecule inside the liquid experiences equal molecular attraction in all directions the one at the surface has a net attraction towards the water (Fig. 2.2a). The surface therefore curves to form an upward concave shape called the meniscus (Fig. 2.2b). The water meniscus is inversely proportional to the tube diameter. The presence of surface tension enables the water to rise and stay above the atmospheric pressure level in a small-diameter tube (Fig. 2.3a).

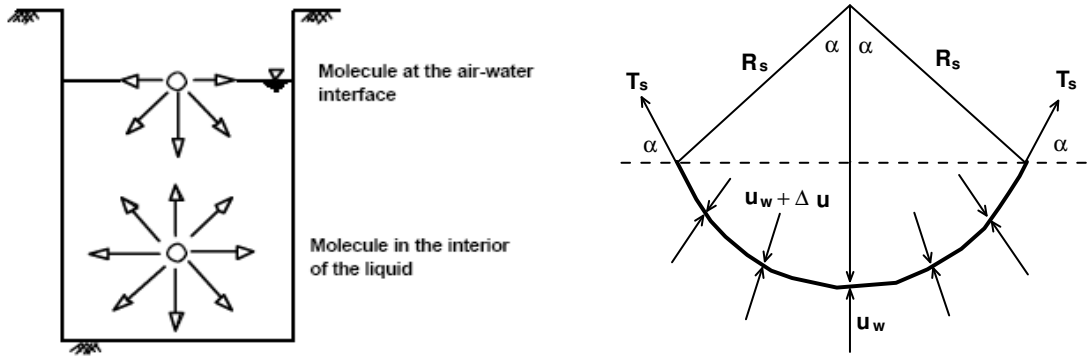

(a) *(b)*

Figure 2.2: Surface tension phenomenon: (a) Intermolecular forces, and (b) pressures and surface tension acting on the curved two-dimensional surface (after Fredlund & Rahardjo, 1993)

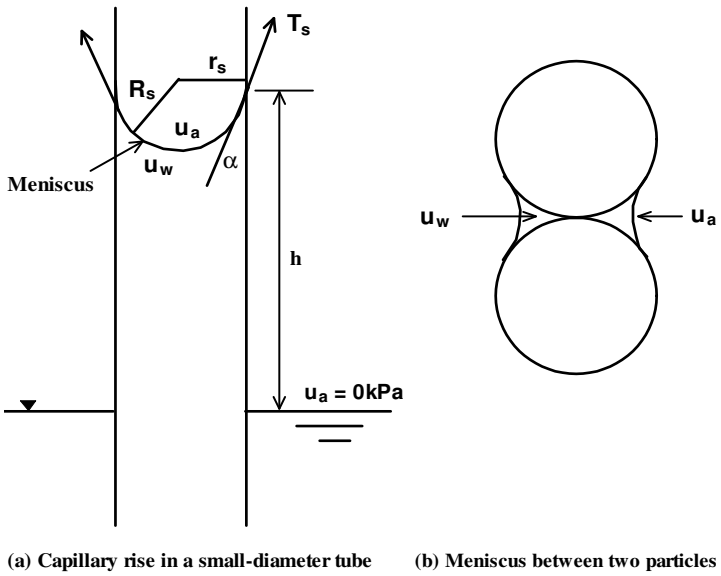

Figure 2.3: Capillary model

The capillary model in Fig. 2.3 is used to describe the behaviour of water in a porous medium such as soil (Fredlund & Rahardjo, 1993; Ridley et al., 2003; Lu & Likos, 2004). Water rises and fills the soil voids above the water table leading to a near saturation zone called the capillary fringe (see Fig. 2.1). The height of the capillary fringe, h, above the water table is a function of the pore sizes which is in turn a function of particle size and distribution within the soil system. Smaller tubes and hence finer soil particles are associated with higher capillary rise and bigger water menisci due to higher surface tension and vice versa. When the surface tension forces are balanced by the weight of the water column, the pressure difference across the air-water interface is given by Eq. 2-2. The corresponding water column height is given by Eq. 2-3a in which $R_s = \frac{r_s}{\cos\alpha}$, α being the contact angle measured into the liquid. If pure water and a clean tube are assumed then the contact angle, α is zero so that the corresponding water column height is given by Eq. 2-3b. This assumption is often assumed for soils such as sands under drying conditions (Lu & Likos, 2004).

$$\Delta u = (u_a - u_w) = \frac{2T_s}{R_s} \qquad \text{Eq. 2-2}$$

$$h = \frac{2T_s}{\rho_w g R_s} \qquad \text{Eq. 2-3a}$$

$$h = \frac{2T_s}{\rho_w g r_s} \qquad \text{Eq. 2-3b}$$

where the difference $(u_a - u_w)$ that causes the air-water interface to curve is referred to as matric suction, u_a is the air pressure, u_w is the water pressure, T_s and R_s are the surface tension and meniscus radius respectively. ρ_w is the mass density of water, g is the acceleration due to gravity and r_s is the radius of the capillary tube. For unsaturated materials exposed to the atmosphere, the air pressure is atmospheric and so the pore water pressure in Eq. 2-2 is a direct result of surface tension and the radius of the meniscus.

2.2.2 Osmotic Suction

Osmotic suction is the component of suction related to the amount and concentration of dissolved salts in the soil water. When the concentration of the dissolved salts is high, the relative humidity is low, and hence the osmotic suction is high. The physical significance of the presence of dissolved salts in the soil water is therefore to increase the amount of energy required to remove a unit volume of water from the water phase of a material up from the matric suction value. Dissolved salts do not affect the capillary phenomena and so the matric suction remains unchanged (e.g. Leong et al., 2007). Hence matric and osmotic suctions are considered independent variables.

2.2.3 Total Suction

Fredlund & Rahardjo (1993) defined total suction, ψ as the free energy of soil water. It is a measure of the energy required to remove a unit volume of water from the soil matrix to a reference system of pure liquid water at atmospheric conditions. Total suction is related to relative humidity at a given temperature by the Kelvin's thermodynamic Eq. 2-4 in which the vapour pressure above a flat surface of pure water is the reference for quantifying suction.

$$\psi = -\frac{RT}{\nu_{wo}\omega_v}\ln\left(\frac{P}{P_o}\right) = -\frac{RT}{\nu_{wo}\omega_v}\ln R_h \qquad \text{Eq. 2-4}$$

where P is the partial pore water vapour pressure, P_o is the saturation pressure of the water vapour over a flat surface of pure water at the same temperature, R is the universal (molar) gas constant and is equal to $8.31432 Jmol^{-1}K^{-1}$, ν_{wo} and ω_v are the specific volume of water given by the inverse of the density of water and the molecular mass of water vapour ($18.016 kgmol^{-1}$) respectively. $T(K)$ is the absolute temperature

and is given by $273.16+t$ with t as temperature in degrees Celsius. The ratio $\frac{P}{P_o}$ expressed as a percentage is called the relative humidity, R_h. When relative humidity is 100% suction is equal to 0kPa. A nonzero suction exists in a material with relative humidity of less than 100%.

Total suction is the sum of matric suction and the osmotic suction. When the concentration of salts, which is responsible for osmotic suction, increases, relative humidity decreases and the total suction increases and vice versa. Fredlund & Rahardjo (1993) noted that osmotic suction is more closely related to the diffuse double layer around the clay particles whereas matric suction is mainly associated with the contractile skin. It therefore means that for *clean* granular materials such as cohesionless soils and glass beads osmotic suction is negligible and so, total suction may be taken to equal to matric suction and vice versa.

Any change in total suction, which may be due to change in either one or both components of the soil suction, affects the overall equilibrium and hence the behaviour of a soil mass. However, most engineering problems involving unsaturated soils are commonly the result of environmental changes, which primarily affect the matric suction component thereby rendering osmotic suction changes generally less significant (Fredlund & Rahardjo, 1993; Rampino et al., 1999). There is some evidence in support of this reasoning. Krahn and Fredlund (1972 (in Fredlund & Rahardjo, 1993)) for instance, shown that a change in total suction is essentially equivalent to a change in matric suction (Fig. 2.4). In practice, therefore, most geotechnical engineering problems involving unsaturated soils, matric suction changes can be substituted for total suction changes and vice versa. As such a laboratory study of the hydro-mechanical behaviour of unsaturated granular materials based on only the changes in matric suction is justified.

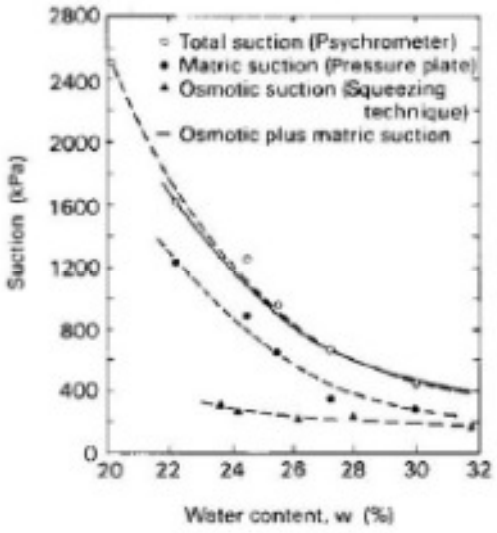

Figure 2.4: Comparison of changes in total, matric and osmotic suctions (Biglari et al., 2008; after Krahn & Fredlund, 1972)

2.3 Water Retention Behaviour of Particulate Materials

2.3.1 Definitions and properties of the water retention curve

The water retention curve (WRC) for a soil is the relationship between water content and suction (e.g. Gardner, 1958; Fredlund & Rahardjo, 1993; Barbour, 1998; Lu & Likos, 2004; Yang et al., 2004; Ng & Menzies, 2007). It shows how soil behaves during desorption and adsorption. Water content may be the proportion of volume occupied by water in the entire soil element, called the volumetric water content or the ratio of mass of water to the mass of the solid particles in the soil element, known as the gravimetric water content. Alternatively, water content could be in terms of the proportion of voids occupied by water, called the degree of saturation (e.g. Fredlund & Xing, 1994; Fredlund et al., 1996; Pham & Fredlund, 2008). In the study of bulk solids and porous media, the WRC is referred to the capillary pressure liquid saturation curve (e.g. Lappalainen et al., 2009). The capillary pressure and liquid saturation are synonymous to suction and degree of saturation respectively.

There exist a number of empirical models to describe the WRC of a soil and the capillary pressure liquid saturation curve for other particulate materials. Leong & Rahardjo (1997) gave a comprehensive review of some of the water retention curve equations. As reviewed by Leong & Rahardjo (1997) and reproduced in Table 2.1, the equations include Gardner (1958), Brooks & Corey (1964), Farrel & Larson (1972), Williams et al. (1983), McKee & Bumb (1984 and 1987), van Genuchten (1980) and

Fredlund & Xing (1994) among others. Although all the equations are of the same generic form, Leong & Rahardjo (1997) demonstrated that among these equations, the van Genuchten (1980) is second to the one by Fredlund & Xing (1994) in describing the WRC for a variety of soils. Subsequent researchers (e.g. Yang et al., 2004; Fredlund and Houston, 2009) also made the same conclusion about the Fredlund & Xing (1994). Therefore, from this point on, attention is paid to the Fredlund & Xing (1994) and van Genuchten (1980) models. The capillary pressure liquid saturation curve models, on the other hand, include Leverett (1940), Grosser et al. (1988), Attou and Ferschneider (2000), Lappalainen et al. (2009).

Table 2-1: Summary of some of the equations for SWRC in the literature

Authors	**Proposed equation**	**Unknowns**
Gardner (1958)	$\theta = \theta_r + \frac{\theta_s - \theta_r}{1 + a\psi^b}$	a b and θ_r
Brooks & Corey (1964)	$\theta = (\theta_s - \theta_r) + \left(\frac{a}{\psi}\right)^b$	a b and θ_r
van Genuchten (1980)	$\theta = \theta_r + \frac{\theta_s - \theta_r}{\left(1 + (a\psi)^b\right)^c}$	a b , c and θ_r
Williams et al. (1983)	$\ln\psi = a + b\ln\theta$	a and b
McKee & Bumb (1984)	$\theta = \theta_r + (\theta_s - \theta_r)\exp\left(\frac{a - \psi}{b}\right)$	a b and θ_r
McKee & Bumb (1987)	$\theta = \theta_r + \frac{\theta_s - \theta_r}{1 + \exp\left(\frac{\psi - a}{b}\right)}$	a b and θ_r
Fredlund & Xing (1994)	$\theta = \left[1 - \frac{\ln\left(1 + \frac{\psi}{\psi_r}\right)}{\ln\left(1 + \frac{1{,}000{,}000}{\psi_r}\right)}\right] \frac{\theta_s}{\left\{\ln\left[e + \left(\frac{\psi}{a}\right)^b\right]\right\}^c}$	a b , c and ψ_r
	$\theta = \theta_r + \frac{\theta_s - \theta_r}{\left\{\ln\left[e + \left(\frac{\psi}{a}\right)^b\right]\right\}^c}$	a b , c and θ_r

Source: *Leong & Rahardjo (1997); representation modified for convenience*

If the entire suction range from saturation to zero relative humidity conditions in the soil is considered, then the following general equation by Fredlund & Xing (1994) can be used to describe the soil-water retention curve.

$$\theta = \theta_s \left[1 - \frac{\ln\left(1 + \frac{\psi}{\psi_r}\right)}{\ln\left(1 + \frac{1{,}000{,}000}{\psi_r}\right)} \right] \left\{ \frac{1}{\ln\left[e + \left(\frac{\psi}{a}\right)^n \right]} \right\}^m \qquad \text{Eq. 2-5}$$

where ψ is the total suction (kPa), ψ_r is the residual total suction corresponding to residual water content (kPa), e is the natural number, a is a soil parameter related to the air entry value of the soil (kPa), n is the soil parameter that controls the slope at the inflection point in the soil water retention curve, and m is a soil parameter that is related to the residual water content of the soil. The parameters a, n and m are obtained from a nonlinear regression procedure outlined by Fredlund & Xing (1994). The figure 1,000,000 is the suction corresponding to zero water content and is believed to be independent of the soil type. If the analysis is made in terms of matric suction then the total suction term in Eq. 2-5 is replaced by the matric suction value.

Water content has often been used in a dimensionless form where the water content is referenced to a residual or zero water content and is defined as follows:

$$\Theta = \frac{\theta - \theta_r}{\theta_s - \theta_r} \qquad \text{Eq. 2-6}$$

where θ is the volumetric water content at any suction, θ_r is the residual volumetric water content, and θ_s is the saturation volumetric water content. For granular materials that have been sufficiently dried the residual water content may be taken to equal to zero in which case Eq. 2-6 reduces to Eq. 2-7. Additionally, if the soils total volume change is negligible, then the normalised volumetric water content becomes equal to the degree of saturation (i.e. $\Theta = S_r$).

$$\Theta = \frac{\theta}{\theta_s} \qquad \text{Eq. 2-7}$$

Fig. 2.5 shows a typical soil-water retention curve. Clearly soil can exhibit different values of suction depending on whether it is subjected to drying (decrease in water

content) or wetting (increase in water content). The difference between the wetting and drying paths of the retention curve is called the hysteresis. The water retention curve hysteresis is attributed to among other factors the "ink bottle" effect, air entrapment and the contact angle effect. These are explained in subsection 2.3.4. The hysteresis phenomenon seems not well documented in the study of particulate materials other than soils. As can be seen in Fig. 2.5, the WRC consists of three identifiable zones, namely, the capillary saturation zone, the desaturation (also known as transition) zone and the residual zone (e.g. Fredlund et al., 1996; Fredlund & Houston, 2009). These zones are respectively termed the capillary bridges zone, funicular bridges zone and pendular bridges zone in the study of industrial bulk solids and porous media (e.g. Urso et al., 1999; Lappalainen et al., 2009) and will be used interchangeably in this research project.

(a)

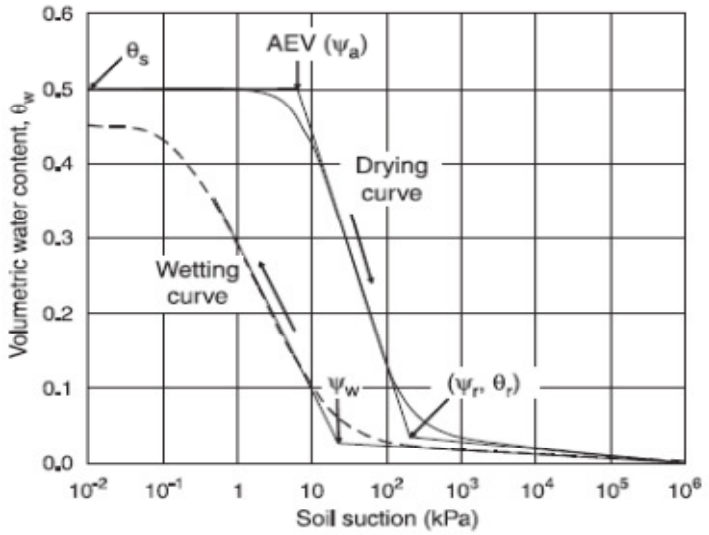

(b)

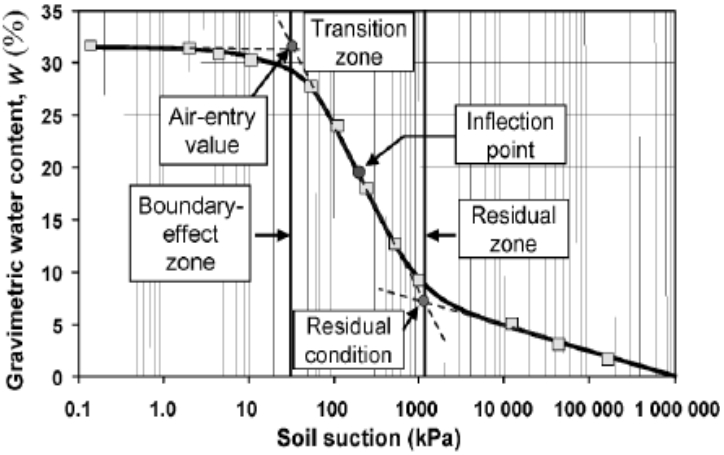

Figure 2.5: Typical soil-water retention curve: (a) features of the curve (Yang et al., 2004; after Fredlund & Rahardjo, 1993); (b) zones of the curve (Fredlund & Houston, 2009)

In the capillary saturation (boundary effect) zone, the pore water is in tension though the soil remains saturated due to capillary forces. This zone within which the air phase is discontinuous ends at the air-entry value where the applied suction overcomes the capillary forces in the soil. The air-entry value, ψ_a, is defined as the suction at which air first enters the largest pores of the soil during a drying process (Fig. 2.5). As suction is increased from zero to the air-entry value, the water content of the soil is nearly constant (e.g. Fredlund et al., 1996; Barbour, 1998; Yang et al., 2004).

The desaturation (transition) zone starts immediately after the capillary saturation zone and the water content steadily decreases to the residual value, θ_r as matric suction increases beyond the air-entry value. The residual water content is the water content at residual state, at which the water phase becomes discontinuous. This marks the end of the desaturation zone and the beginning of the third zone called the residual saturation zone within which water is tightly adsorbed onto the soil particles and any water exchange occurs in the form of vapour. Any water remaining in the soil at the end of this zone is said to be chemically bonded to the soil and could be less important with respect to engineering behaviour (e.g. Fredlund et al., 1996; Barbour, 1998; Yang et al., 2004).

The soil suction corresponding to the residual water content is called the residual soil suction, ψ_r and marks the state at which the mechanism of the removal of water from the soil due to suction increase starts to change from drainage (i.e. liquid flow) to vapour migration (Barbour, 1998). The water-entry value, ψ_w on the wetting curve is defined as the suction at which the soil water content starts to increase significantly during the wetting process (e.g. Yang et al., 2004).

2.3.2 Determination of the WRC

The WRC can be determined either through an experimental programme or empirically. Generally, the experimental measurement of the soil-water retention curve is divided into two parts, namely, the region where the suction is less than approximately 1,500kPa and the region where it is greater (e.g. Fredlund, 2000). Suction in the latter range is commonly established using osmotic and vacuum desiccators. The pressure plate (axis translation technique) is used to establish suction in the range up to 1,500kPa (e.g. Yang et al., 2008; Miguel & Vilar, 2009). As an option to the pressure plate a

pressure membrane (e.g. Nishimura et al., 2010) and Tempe cell (e.g. Yang et al., 2004) are used. Usually a rigid soil skeleton is assumed by ignoring any soil deformations. Wheeler & Karube (1996) argue that such changes in the soil should be taken into account when presenting the WRC. As such there is an increasing tendency to use a triaxial apparatus to determine the WRC. Previous studies in which the triaxial apparatus has been used to establish the WRC can be found in the literature (e.g. Uchaipichat & Khalili, 2009 and Ng et al. 2009). In terms of frequency of use, the pressure plate seems to be the most favoured apparatus for measuring WRC.

The WRC can also be estimated empirically. Some of the empirical equations have been discussed in subsection 2.4.1. In addition, soil classification characteristics and indices have also been proposed to estimate the WRC (Arya & Paris, 1981; Zapata et al., 2000). Fredlund et al. (1997) modified the Fredlund & Xing (1994) WRC mathematical equation to fit the grain size distribution curve. The grain size distribution curve equation (Eq. 2-8) was then used to estimate the WRC. These empirical approaches are however said to be unpopular except in the case of preliminary designs as the accuracy associated with them is low (Fredlund & Houston, 2009). They are inaccurate and can give misleading results if applied to the soils for which they were not validated (e.g. Hoffman & Tarantino, 2008). It therefore means that an experimental programme to generate sufficient data points for the determination of the fitting parameters has to be undertaken each time the equations are used to describe the WRC.

$$P(d)=\frac{1}{\ln\left[\exp(1)+\left(\frac{g_a}{d}\right)^{g_n}\right]^{g_m}}\left\{1-\left[\frac{\ln\left(1+\frac{d_r}{d}\right)}{\ln\left(1+\frac{d_r}{d_m}\right)}\right]^7\right\} \qquad \text{Eq. 2-8}$$

where $P(d)$ is the percent passing a particular grain size, d (mm), g_a is the fitting parameter corresponding to the initial break in the grain size distribution curve, g_n is the fitting parameter corresponding to the maximum slope of the particle size distribution curve, g_m is the fitting parameter corresponding to the curvature of the particle size curve, d_r is the residual particle diameter (mm) and d_m is the minimum particle diameter (mm).

2.3.3 Application of the SWRC

The potential of WRC to play a key role in predicting the behaviour of unsaturated soil has been demonstrated in many studies. It is a measured soil property that has been used to derive other soil functions and provides a common reference to stress state at which other properties are computed (Fredlund et al., 1996). According to Fredlund & Houston (2009), the WRC forms the basis for the implementation of all unsaturated soil mechanics applications (e.g. seepage, shear strength and volume change). They argue that its use to estimate the unsaturated soil property functions is particularly attractive because direct measurement of other unsaturated soil properties (in the laboratory) is too costly for many engineering problems. Using the constitutive relationships of Fredlund & Morgenstern (1976), Barbour (1998) equated the usefulness of WRC in providing the basis for conceptual, interpretative and predictive model to that of the constitutive relationship for volume change of saturated soil i.e. void ratio versus effective stress or consolidation curve.

The fact that both water content and shear strength are a function of matric suction, many researchers (e.g. Fredlund et al., 1996) have attempted to use the WRC together with results from saturated soil testing to estimate shear strength function of an unsaturated soil. Six other equations are given in Garven & Vanapalli (2006) in their study "Evaluation of empirical procedures for predicting the shear strength of unsaturated soils". Vanapalli et al. (2009) presented a method to use the soil-water retention curve and the saturated modulus of elasticity to predict the modulus of elasticity for unsaturated sandy soils. In addition, WRC has also been extensively used to estimate the unsaturated coefficient of permeability function (e.g. Fredlund et al., 1994) and to analyse the transient water flows in unsaturated soils (e.g. Barbour, 1998) as well as to estimate the unsaturated soil volume change functions.

However, it should be emphasised that the WRC does not provide a unique relationship between water content and suction. It is affected by a number of factors as discussed later in subsection 2.3.4. A systematic study of how each of the several factors affects water retention of granular materials seems to be lacking in the literature. Hence even for estimation purposes it can only be used successfully on the materials for which they have been validated. For projects requiring highly accurate data, the necessity to simulate the field conditions during the measurement of the WRC cannot be over emphasised (e.g. Fredlund, 2000; Fredlund & Houston, 2009). The results of Rampino

et al. (1999) evidence the relevancy of paying attention to simulate the field conditions when carrying out laboratory tests. They reported a more increase in specific water volume than specific volume as matric suction is decreased. They explained this behaviour in terms of the higher as-compacted suction compared to the desired initial suction thereby causing samples to change following a wetting path of the WRC.

2.3.4 Factors that Affect the WRC

Conventionally, the water retention curve describes either an adsorption (wetting) or desorption (drying) processes (e.g. Lu & Likos, 2004) without considering the effects of volume changes and stress state (e.g. Ng & Menzies, 2007). Ng & Pang (2000a) experimentally demonstrated the dependence of soil-water retention curve on state and history of the soil. Their results for the tests conducted on a slightly sandy silt-clay volcanic soil of low plasticity are shown in Fig. 2.6. The hysteresis loop of the WRC for the second cycle significantly decreased compared to the one for the first cycle. The drying and wetting paths for the second and third cycles tended to retrace each other. The effect of cycles of wetting and drying on the shear behaviour is discussed later in subsection 2.4.1.3. The results in Fig. 2.6 suggest that the incremental effect of cycles of drying and wetting disappears after a few cycles.

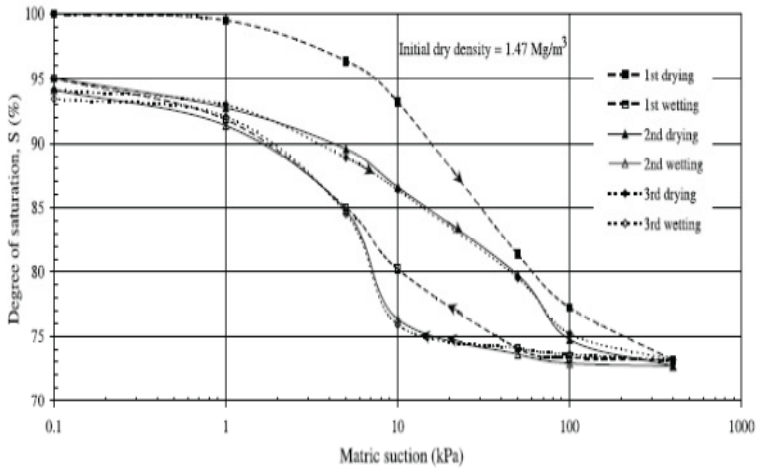

Figure 2.6: Influence of drying and wetting cycles on SWRC (Ng & Pang, 2000a)

With regard to the effect of stress state, the size of the WRC loop for reconstituted samples also reduced with increase in the applied stress, and the higher the applied stress, the larger the air-entry value and the lower the rates of desorption and adsorption. Their results are in support of those of Ng & Pang (2000b) who investigated the effect of stress state on the soil water characteristics and hence introduced the concept of

stress-dependent soil-water retention curve. Further studies showing similar effect of stress state on the WRC include Hoffman & Tarantino (2008) and Ng et al. (2009). Inconsistent with these findings, however, is the observation by Uchaipichat & Khalili (2009) who reported non-effect of stress level on the WRC. In other words, these findings suggest that void ratio is a very important parameter in the determination of WRC. In "none swelling" soils, the effect of applying stress to the sample is to alter the sample void ratio. As a consequence, the properties of the wetting liquid menisci that form in a denser sample are different from those in looser samples.

However, it should be noted that in both studies the tests were done for a low suction range of up to 400kPa (Ng & Pang, 2000a) and up to 200kPa (Ng & Pang, 2000b). This limited their observations to a narrow range of degree of saturation of about 73-100%. These ranges could be surpassed in the field. As can be observed from Fig. 2.6, it is not immediately clear as to how the curves would proceed had matric suction been increased to higher values. It is also noted that such studies on cohesionless materials seems lacking in the literature.

Yang et al. (2004) also studied the factors that affect drying and wetting of WRCs of sandy soils. Their findings show high dependency of the WRC on the grain size distribution and dry density of the soil. Coarse soils had a lower air-entry value, residual matric suction, and water entry value and less hysteresis than a fine grained soil. WRC for uniform soils had steeper slopes and less hysteresis than those of less uniform soils. Lower dry densities also resulted in lower air-entry values and residual matric suctions. In support of these observations, Rassam & Williams (1999) and Hoffman & Tarantino (2008) observed that the primary wetting curve for a coarser soil plotted below a finer soil. Recently, Kawajiri et al. (2010) reported similar dependence of WRC on particle size distribution. It should however be noted that in all these studies the different soils were compared on the basis of particle size distribution ignoring the effect of other properties of the constituent particles that could have also contributed to the observed discrepancies.

The "ink bottle" effect illustrated in Fig. 2.7a explains the effect of non-uniform pore size distribution in the soil on suction evolution. The contact angle and hence the radius of curvature are greater leading to less suction in the case of advancing meniscus (during wetting process) than in the case of receding one even if the global or

macro-scale moisture content is the same. This effect is likely to be more pronounced in soils with large pore size distribution than with small pore size distribution (Ng & Pang, 2000a). However, even if the pore size distribution were uniform the sizes of the menisci would be different depending on whether the soil is drying or wetting (Fig. 2.7b). This is so because of the contact angle effect.

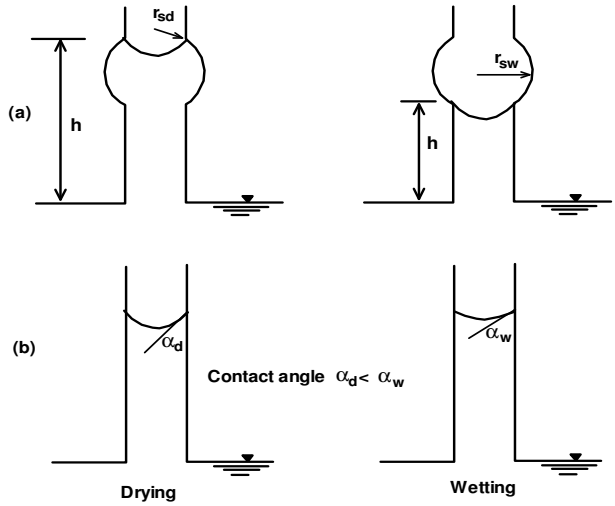

Figure 2.7: The "ink bottle" and contact angle effects: (a) The ink bottle effect; (b) the contact angle effect (modified after Hillel, 1998)

2.4 Mechanical Behaviour and Constitutive Models of Unsaturated Soils

The mechanical behaviour and constitutive models of unsaturated soils reported in the literature are briefly summarised, with particular emphasis on granular soils. The stress state variables and their associated state functions (failure criteria) are presented first, followed by the volumetric behaviour and lastly the elasto-plastic models of unsaturated soils commonly quoted and used in the literature.

2.4.1 Stress State Variables and the Associated State Functions

A successful description of the constitutive behaviour of unsaturated soils depends on the appropriateness of the selected state variables. For such soils, the state of the soil is specified by the stress state, void ratio, degree of saturation and the soil fabric or structure (e.g. Matyas & Radhakrishna, 1968). The stress state variables are considered appropriate only if they are able to adequately account for the influence of the air phase, water phase and the contractile skin in the voids on the behaviour of unsaturated materials. The constitutive behaviour of unsaturated soils is often described using the equations which express the unique relationship between the different state parameters. These equations are termed state functions.

The stress state in a soil can be specified by the total normal (boundary) stress, σ , pore air pressure, u_a and the pore water pressure, u_w (e.g. Coleman, 1962; Bishop & Blight, 1963; Matyas & Radhakrishna, 1968). These quantities can possibly be combined to give the stress state variables: net normal stress as either $(\sigma - u_a)$ or $(\sigma - u_w)$ and the matric suction as either $(u_a - u_w)$ or $(u_w - u_a)$ (e.g. Fredlund & Morgenstern, 1977). Later work (e.g. Fredlund et al., 1978; Wheeler & Karube, 1996) demonstrated $(\sigma - u_a)$ and $(u_a - u_w)$ to be the most suitable combinations for the net normal stress and matric suction respectively. Using these latter combinations, the constitutive behaviour of unsaturated soil has been described either using a single effective stress (e.g. Bishop, 1959), two stress state variables of net normal stress and matric suction (e.g. Fredlund et al., 1978) or the two stress state variables incorporating the influence of degree of saturation (e.g. Toll, 1990). These are comprehensively discussed by Wheeler & Karube (1996) and are further reviewed and discussed below.

2.4.1.1 The single effective stress variable and the associated state functions

For long, shear strength of soil has been modelled using the Terzaghi's equation in which both the strength and volume changes are governed by the effective stress, $\sigma' = (\sigma - u)$ where u is the saturated pore water pressure. This principle of effective stress has been successfully implemented in describing the mechanical behaviour of saturated soil. Its ability to describe the shear behaviour of unsaturated soils is however still a topic of debate, as noted in the following review of the history of some of the attempts that have been made to develop a model that can realistically describe the constitutive behaviour of unsaturated soils.

The earliest attempts to extend the Terzaghi's effective stress concept to unsaturated soils were made in the 1950s (Croney et al., 1958; Bishop, 1959; Jennings, 1961 and Aitchison, 1961). Of these early attempts, however, the one of Bishop (1959) is the mostly quoted and widely used in the literature. It is perhaps the first expression for the effective normal stress in terms of both pore air pressure and the pore water pressure and takes the form of Eq. 2-9.

$$\sigma' = (\sigma - u_a) + \chi(u_a - u_w) \qquad \text{Eq. 2-9}$$

where σ' is the effective stress, σ is total normal stress, u_a is pore air pressure, u_w is the pore water pressure, χ is the material parameter related to the degree of saturation and ranges between one for fully saturated soils to zero for completely dry soil, and $(u_a - u_w)$ is the matric suction in the soil. At the extremes, when $\chi = 1$ and $\chi = 0$, Eq. 2-9 reverts to the classical effective stress parameter. When Eq. 2-9 was substituted in the equation for saturated soils, the unsaturated shear strength was expressed in the form of a modified Mohr-Coulomb strength relationship shown by Eq. 2-10 wherein c' and ϕ' are effective cohesion and effective angle of friction respectively.

$$\tau = c' + \sigma' \tan\phi' = c' + [(\sigma - u_a) + \chi(u_a - u_w)] \tan\phi' \qquad \text{Eq. 2-10}$$

The effective stress equation by Bishop though often quoted and supported by some authors (e.g. Bishop & Blight, 1963; Khalili & Khabbaz, 1998; Khalili et al., 2004) as being capable of describing the shear strength of unsaturated soils has been criticised by many authors (e.g. Jennings & Burland, 1962; Fredlund and Rahardjo, 1993; Wheeler & Karube, 1996) for its inability to satisfactorily describe the mechanical behaviour of unsaturated soils. Khalili & Khabbaz (1998) argued that instead of the degree of saturation there could be some appropriate parameters (suction ratio defined as the ratio of suction to the air-entry value in their study) with which the soil parameter could bear a unique relationship. Coleman (1962) had earlier noted that the parameter χ is strongly related to the soil structure, and therefore it should not be surprising if no unique relationship exists between χ and the degree of saturation. Khalili & Khabbaz (1998) expressed χ as shown in Eq. 2-11.

$$\chi = \left[\frac{(u_a - u_w)}{(u_a - u_w)_b} \right]^{-0.55} \qquad \text{Eq. 2-11}$$

where $(u_a - u_w)_b$ is the bubbling pressure (also known as the air-entry value). However, it should be noted that this relationship is not unique to all the soil types as shown by the scatter in the points according to the soil type. The authors also rightly and explicitly state that the χ values for cohesive and dense materials may be greater than the corresponding values for cohesionless and loose materials at a given value of suction. Moreover the use of air-entry value can be limited by the hysteretic water retention behaviour of soils and its dependence on void ratio.

The validity of the principle of effective stress expression (Eq. 2-9) requires that the soil behaviour is not affected by changes in the net normal stress $(\sigma - u_a)$ and $\chi(u_a - u_w)$ provided their sum remain constant. For many soils this has however been reported to be true only up to a certain critical degree of saturation below which the behaviour disobeys the principle of effective stress. Jennings & Burland (1962) suggested the critical degree of saturation as 50% for coarse soils and 90% for fine (plastic) soils. Limitation of the effective stress principle to 50% degree of saturation in coarse materials implies that it cannot be used in most applications involving such materials as they are likely to exist with a saturation level below this critical.

In their work, Jennings & Burland (1962) observed collapse of the unsaturated silt soil soaked under constant loading contrary to the principle of the effective stress according to which the material should have swollen. They also observed that soaking of silt soil at constant volume required a decrease in applied stress instead of increasing the applied stress by the amount equal to the lost suction component. These findings by Jennings & Burland (1962) were confirmed by Matyas & Radhakrishna (1968) who also observed that wetting of specimens of a clay silt of low plasticity at low applied stress generally caused collapse, a behaviour they explained in terms of the structural rigidity that is induced by suction. This behaviour cannot be explained by the principle of effective stress. Based on the experimental data they demonstrated that the parameter χ could take on negative values greater than unity contrary to the definitive range specified by Bishop or implied by Eq. 2-9. Matyas & Radhakrishna (1968) further observed that a reduction in suction had a two-fold effect on soil structure, namely, a reduction in the inter-granular stress and reduction in the structural rigidity. Above a critical net stress $(\sigma_3 - u_a)$ the volume decrease due to rigidity exceeded the volume increase due to inter-granular stress and the net result was collapse. The reverse resulted in "swelling" below the critical stress.

According to Burland & Ridley (1996), changes in suction give rise to different soil response in terms of mechanical behaviour compared to changes in the applied stress. This is so because while suction acting through the menisci at the contact points between the particles of soil leads to a stabilising effect, applied (boundary) stress causes grain slip. Thus, the two stress systems should not be bundled together into a single effective stress but treated separately.

Another difficulty associated with the Bishop's Eq. 2-9 is related to the determination of the parameter χ. The parameter is different when determined for shear strength compared to when determined for volume change (Fredlund & Rahardjo, 1993). It is argued that the parameter is often estimated by tacitly assuming that the effective stress principle is valid for unsaturated soils (Jennings & Burland, 1962). Moreover the material parameter, χ, is not easy to quantify especially for volume change due to the dominating influence of structural effects (Matyas, 1963 (in Matyas & Radhakrishna, 1968)). Generally, it is recognised that the applicability of the Bishop (1959) effective stress model is impractical.

Given the above limitations in the use of Bishop's effective stress equation, several efforts have been tailored towards a more-than-one stress state variables relationships to describe the mechanical behaviour of unsaturated soils. The following part of this subsection looks at some of the attempts in common use in the literature.

2.4.1.2 State functions based on the two stress-state variables

With the inability of the single effective stress variable to reasonably describe the behaviour of unsaturated soils, notably the volumetric behaviour, several researchers (e.g. Matyas & Radhakrishna, 1968; Fredlund et al., 1978; Peterson, 1988; Vanapalli et al., 1996; Tse & Ng, 2008) have attempted to use two stress state variables. As earlier noted under 2.4.1 the variables in common use are the net normal stress, $(\sigma - u_a)$ and the matric suction, $(u_a - u_w)$. The basis for considering these variables is discussed by many authors (e.g. Fredlund et al., 1978; Fredlund & Rahardjo, 1993; Wheeler & Karube, 1996).

Fredlund et al. (1978) postulated a two independent stress state variables equation of the form of an extended Mohr-Coulomb failure criterion as follows.

$$\tau = c' + (\sigma - u_a)\tan\phi' + (u_a - u_w)\tan\phi^b \qquad \text{Eq. 2-12}$$

where c' and ϕ' are the effective stress parameters, ϕ^b is the angle related to the increase of strength with matric suction $(u_a - u_w)$, and $(\sigma - u_a)$ is the net normal stress acting on the plane of failure. The application of Eq. 2-12 requires the determination of three strength parameters, namely, c', ϕ' and ϕ^b (Fredlund & Rahardjo, 1993).

These parameters can be measured in the laboratory. The c' and ϕ' are determined using the results from saturated sample tests. ϕ^b, on the other hand, is obtained using the results from the tests on unsaturated samples. As the soil approaches saturation condition, the pore water pressure approaches the pore air pressure and matric suction goes to zero. Consequently, Eq. 2-12 reverts to the equation of the saturated soil (Fredlund & Rahardjo, 1993).

Fig. 2.8 shows the surface generated when Eq. 2-12 is plotted in the τ, $(\sigma - u_a)$ and $(u_a - u_w)$ space. In line with the original assumptions by Fredlund et al. (1978) the figure shows a linear relationship between the shear strength, τ and the net normal stress, $(\sigma - u_a)$ as well as between τ and the matric suction, $(u_a - u_w)$. Similar to the implicit proposition of Peterson (1988), in the $\tau : (\sigma - u_a)$ space of this framework the effect of matric suction is to increase the cohesion component of shear strength as the intercepts are shifted upwards by a component equal to a factor $(u_a - u_w)\tan\phi^b$.

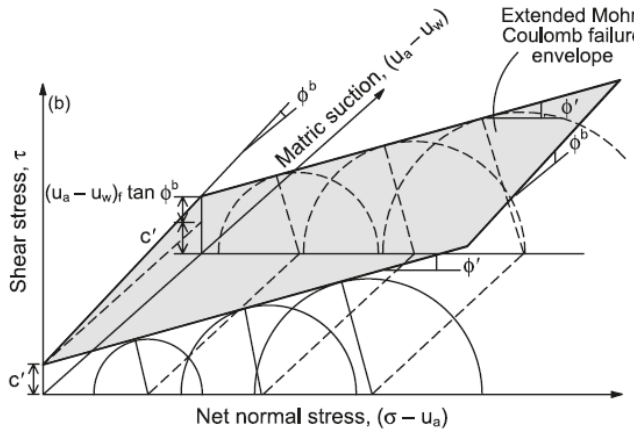

Figure 2.8: The extended Mohr-Coulomb failure envelope (Fredlund & Rahardjo, 1993)

Later work on the subject does not give unidirectional results in regard to the applicability of the Fredlund et al. (1978) postulation. While several studies (e.g. Escario & Saez, 1986; Escario & Juca, 1989; Ng et al., 2000; Lui & Peng, 2008) support the relationship between the shear strength and the net normal stress represented by ϕ' some (e.g. Toll, 1990; Maatouk et al., 1995; Cui & Delage, 1996; Toll & Ong, 2003; Gui & Yu, 2008) argue that ϕ' also depends on suction. In contrast to the observations by Toll (1990) and Toll & Ong (2003) that ϕ' is inversely proportional to

the degree of saturation, Maatouk et al. (1995) and Cui & Delage (1996) reported $\phi^{'}$ to increase with increase in matric suction. It is therefore evident that the dependency of $\phi^{'}$ on suction remains an active area of experimental research.

In the $\tau:(u_a - u_w)$ space of the Fredlund et al. (1978) postulation a nonlinear relationship is generally reported in the subsequent studies (e.g. Escario & Saez, 1986; Rassam & Williams, 1999; Houston et al., 2008; Estabragh & Javadi, 2008), contrary to the original assumption by Fredlund et al. (1978). In this space the effect of net normal stress is bundled in the total cohesion component of shear strength as the intercepts are shifted upwards by a component equal to a factor $(\sigma - u_a)\tan\phi^{'}$ and shear strength increases with increasing suction.

The evolution of shear strength as suction is increased is related to the changes in degree of saturation in the schematic shown in Fig. 2.9. The friction angle due to suction ϕ^b is equal to the internal angle of friction in the suction range between zero and air-entry value, as the soil practically remains saturated with no contractile skin between the soil particles. As suction is increased shear strength increases while ϕ^b gradually decreases eventually becoming zero or even negative at sufficiently high values of suction (e.g. Gan & Fredlund, 1996; Houston et al., 2008). This is attributable to the fact that when air starts to enter in an initially saturated soil the resultant contractile skin between contacting particles generate inter-particle normal force that must be overcome before any inter-particle slip can occur. The number of inter-particle contacts affected by the contractile skin increases as degree of saturation decreases (suction increases) until such a point when the menisci are so localised that the total surface area of the soil particles affected by the contractile skin is small and relatively invariable as suction is further increased. In a highly dilative material negative values of ϕ^b may be observed when the material is sheared at suctions involving highly localised menisci water (e.g. Gan & Fredlund, 1996). Farouk et al. (2004) also observed an apparent increase in strength with suction but only up to some value beyond which the strength decreased. Vilar (2006) explains this behaviour in terms of the perturbation on the capillary meniscus caused by strain and dilation of the materials. In such materials the main source of suction is the capillary phenomenon so that when the material strains and dilates, the points of contact are affected.

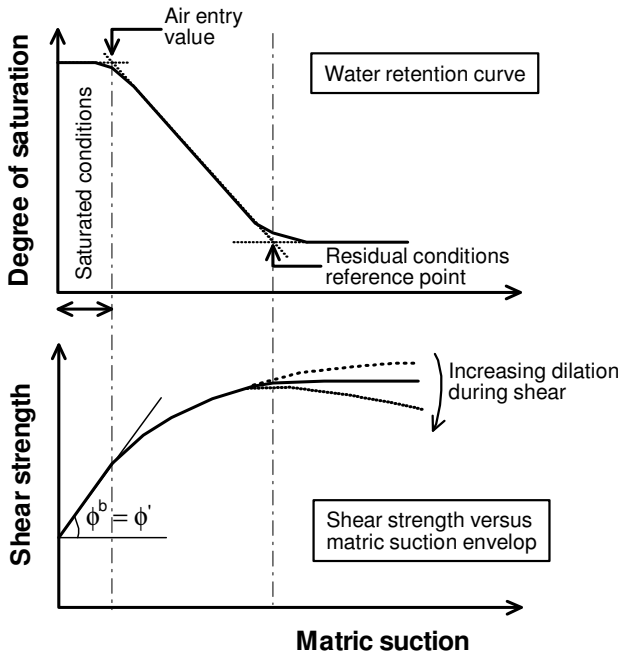

Figure 2.9: Schematic relationship between soil-water retention curve and shear strength versus matric suction envelope (after Gan & Fredlund, 1996)

The nonlinear dependency of ϕ^b on suction makes the Fredlund et al. (1978) equation less appealing. Consequently, several other equations and procedures for estimating the shear strength of unsaturated soils have been proposed by several authors. Toll (2000) proposed that ϕ' in the Fredlund et al. (1978) equation (Eq. 2-12) is replaced by ϕ^a the friction angle with respect to net stress $(\sigma - u_a)$, arguing that the two are not necessarily the same. The value of c' would then be taken as the cohesion when the two stress variables $(\sigma - u_a)$ and $(u_a - u_w)$ are both equal to zero. At critical state (i.e. $c' = 0$) Toll et al. (2008) proposed an equation (Eq. 2-13) for shear strength of unsaturated soils in terms of deviator stress based on the shearing data for an unsaturated artificially bonded soil under constant water content and drained air conditions.

$$q = M_a(p - u_a) + M_b(u_a - u_w) \qquad \text{Eq. 2-13}$$

where q is the deviator stress $(\sigma_1 - \sigma_3)$, p is the mean total stress $(\sigma_1 + \sigma_2 + \sigma_3)/3$, M_a is the critical state stress ratio with respect to net mean stress $(p - u_a)$ and M_b is the critical state stress ratio with respect to matric suction $(u_a - u_w)$. All the other parameters are as defined before. The stress ratios are such that $M_a = f\{q, M_s, (u_a - u_w), (p - u_a)\}$ and $M_b = f\{q, M_a, (u_a - u_w), (p - u_a)\}$. M_s is the

saturated critical state stress ratio. Further details about the procedure for evaluating these parameters can be found in Toll et al. (2008).

Many other researchers have attempted to come up with procedures and formulations to describe the nonlinear shear strength of unsaturated soils (e.g. Vilar, 2006; Houston et al., 2008). Some of the formulations indirectly include features of the water retention curve (e.g. Rassam & Cook, 2002). While maintaining the Fredlund et al. (1978) framework, Houston et al. (2008) focussed on the determination of parameter ϕ^b. They proposed that instead of tangent ϕ^b, secant ϕ^b, evaluated using a hyperbolic model (Eq. 2-14) from the matric suction measurements and the ϕ', should be considered.

$$\phi^b = \phi' - \left[\frac{\psi^*}{a + b\psi^*} \right] \qquad \text{Eq. 2-14}$$

where $\psi^* = (u_a - u_w) - \psi_a$, a is the inverse of the slope of the hyperbolic curve when $\psi^* = 0$ and b is the inverse of ϕ'. Parameters a and b are the intercept and slope of $\frac{\psi^*}{(\phi' - \phi^b)}$ versus ψ^* plot respectively. ψ_a is the air entry value.

It should be noted that the Houston et al. (2008) model requires only one unsaturated material parameter, the air-entry value in addition to the saturated soil strength parameters. Accordingly, the shear strength of unsaturated soil can be estimated if for the soil a WRC and the saturated shear strength parameters are in place. Fig. 2.10a is among the results the authors used to demonstrate the power of the model in fitting the experimental data. However, it should be noted that this model proposed by Houston et al. (2008) may give misleading estimations for plastic soils as it did not satisfactorily fit the experiential data for fine soils (Fig. 2.10b). Also the hyperbolic model may not be suitable for coarse materials at sufficiently high suction values considering that at such suctions, the value of ϕ^b could start decreasing with increase in suction (e.g. Gan & Fredlund, 1996). Moreover it has not yet been validated on a wide range of soils experimental data. A comparison of the performance of the proposed model (Eq. 2-14) in describing the ϕ^b between non-plastic and plastic soils raises an issue of whether or not there are other important factors controlling the increase of shear strength in unsaturated soils aside from matric suction.

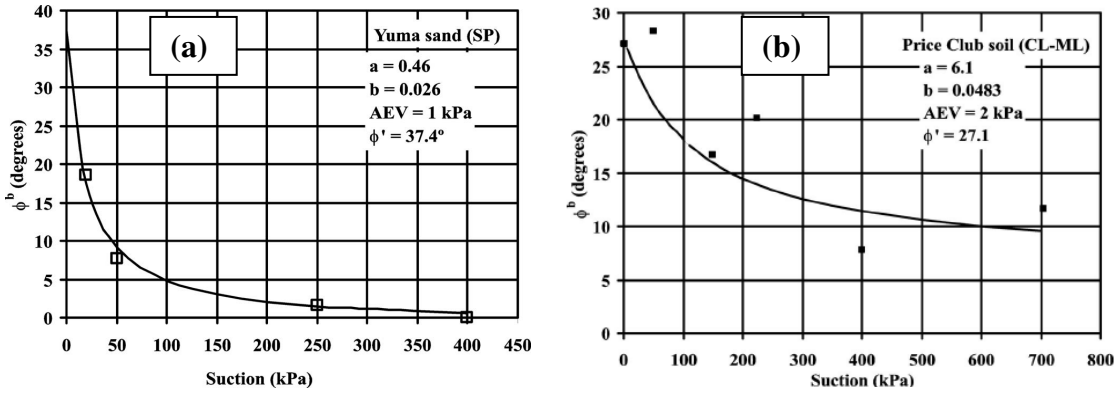

Figure 2.10: Suction versus ϕ^b envelope: (a) Yuma sand and (b) Price club (Houston et al., 2008)

Like the effective stress equations, the ability of the two stress state variables equations to adequately describe the shear strength of unsaturated materials has been questioned by several researchers (e.g. Vanapalli et al., 1996; Wheeler & Karube, 1996; Wheeler et al., 2003; Gallipoli et al., 2003; Toll et al., 2008). Many believe that the hysteretic nature of the water retention behaviour of particulate materials requires that in addition to the net normal stress and matric suction water content is also used directly as an independent variable in the shear strength equations. As such several attempts have been made to incorporate the influence of degree of saturation in the constitutive models of unsaturated soils. These are reviewed in the following part.

2.4.1.3 Two stress state variables state functions incorporating the water content effect

Besides the total stress and pore pressures, water content has also been found to significantly influence the behaviour of unsaturated soils. Toll (1990) observed that for the compacted Kiunyu gravel, lateritic gravel from Kenya, the degree of saturation affected both the suction and total stress contributions to shear strength. Both the critical state total stress ratio and suction ratio were influenced by the degree of saturation. The suction ratio decreased as the degree of saturation reduced. Total stress ratio on the other hand increased as the degree of saturation reduced. These findings were supported by Toll et al. (2008) who observed a coincidence between the changes in degree of saturation and the changes in critical stress ratios.

In section 2.3 of this chapter it has been shown that unsaturated soils can have the same suction but with different water content depending on whether it is at drying or wetting. The influence of this hydraulic hysteresis on the mechanical behaviour of unsaturated

soils and the justification for directly accounting for degree of saturation in the constitutive models for unsaturated soils are discussed by many authors (e.g. Wheeler & Karube, 1996). In addition, several researchers (e.g. Han et al., 1995; Gallage & Uchimura, 2006; Tse & Ng, 2008) have experimentally observed that two identical samples at the same suction but different water content have different shear behaviour. Tse & Ng (2008) reported samples with lower water content to have higher shear strength and stiffness compared to the identical samples with higher water content. They attributed this behaviour to the influence of the water content (degree of saturation); higher degrees of saturation lead to a decrease in the peak shear stress and stiffness and vice versa.

Gallage and Uchimura, however, reported the reverse. They observed that samples with lower water content had lower shear strength and stiffness compared to the identical samples with higher water content. They attributed such a behaviour to the more contractive behaviour exhibited by the specimen at wetting than that at drying. Such discrepancy in the observed behaviour is a manifestation that more experimental work is necessary for a conclusion to be reached as to how the hydraulic hysteresis actually influences unsaturated shear behaviour of materials.

Nonetheless, this hysteretic behaviour of unsaturated materials (soils) has led to the thinking that suction and the degree of saturation should be accounted for independently when formulating a constitutive model to describe the hydro-mechanical behaviour of such materials. It is generally believed that even if other factors (net normal stress, suction and specific volume) were constant, a soil at lower water content would exhibit different mechanical behaviour compared to a soil at higher water content owing to the difference in the inter-particle contact forces. Some of the models incorporating the influence of water content (through the use of water retention curve features) in addition to suction and the net normal stress such as Kato et al. (1995), Karube et al. (1996), Vanapalli et al. (1996), Fredlund et al. (1996), Toll & Ong (2003), Wheeler et al. (2003), and Gallipoli et al. (2003) are reviewed below.

Kato et al. (1995) and Karube et al. (1996) modified the stress state variables to incorporate the effect of the hydraulic hysteresis. They introduced weighting factors for the net normal stress and the matric suction variables. The factor for the net normal stress represents the proportion of total void volume occupied by bulk water while the

suction factor reflects the volume of voids occupied by meniscus water. Wheeler & Karube (1996) comprehensively discussed the procedure for determination of the two weighting factors above. They also observed that such a procedure presents additional experimental complexity.

Vanapalli et al. (1996) proposed that the unsaturated shear strength of soil at a given suction and degree of saturation is given by Eq. 2-15 in which κ_Θ is the fitting parameter. If the parameter κ_Θ is equal to 1.0 as is the case for non-plastic soils, the postulation by Vanapalli et al. (1996) is of the form of the equation proposed by Oberg and Salfors (1997) except that in the latter relationship the degree of saturation is not normalised. These equations were found to approximately fit the experimental data of Tomboy et al. (2009) who conducted unconfined compression tests on unsaturated quaternary loam soil taken from a site at Limelette, Belgium. The tested soil was reported to have a plasticity index value of about 10%.

$$\tau = c' + (\sigma - u_a)\tan\phi' + (u_a - u_w)\Theta^{\kappa_\Theta}\tan\phi' \qquad \text{Eq. 2-15}$$

When the normalised degree of saturation term in Eq. 2-15 is expressed as a function of matric suction then the postulation by Vanapalli et al. (1996) becomes Eq. 2-16 proposed by Fredlund et al. (1996) to describe the shear strength of unsaturated soils using the soil-water retention curve and the saturated shear strength parameters.

$$\tau = c' + (\sigma - u_a)\tan\phi' + (u_a - u_w)[\Theta(u_a - u_w)]^{\kappa_\Theta}\tan\phi' \qquad \text{Eq. 2-16}$$

where $\Theta(u_a - u_w) = \theta(u_a - u_w)/\theta_s$ is the normalised water content given by Eq. 2-6 and $\theta(u_a - u_w)$ is the volumetric water content at any suction. The fitting parameter κ_Θ is a function of plasticity and affects the rate at which the angle ϕ^b decreases as the matric suction exceeds the air-entry value of the soil. The value equal to 1.0 is said to give satisfactory predictions for sands, which could mean that 1.0 is the lower limit for the parameter κ_Θ. However, it should be noted that for better estimates the soil-water retention curve used should be determined for the appropriate confining pressure and the stress history. Secondly, inclusion of degree of saturation is conceptual and more experimental data is needed to validate the model as it has been validated on few experimental data.

Using the results of triaxial tests on sandy clay, Toll & Ong (2003) proposed Eq. 2-17 to describe the shear strength of unsaturated soils at the critical state. This model is generally of the form similar to that proposed by Toll (1990) and Vanapalli et al. (1996).

$$q = M_a(p - u_a) + M_b(u_a - u_w) \qquad \text{Eq. 2-17}$$

with:
$$M_a = M_b = M_s \quad ; \text{for } S_r > S_{r1}$$
$$\frac{M_b}{M_s} = \left(\frac{S_r - S_{r2}}{S_{r1} - S_{r2}}\right)^{k_b} \quad ; \text{for } S_{r2} > S_r > S_{r1}$$
$$\frac{M_a}{M_s} = \left(\frac{M_a}{M_s}\right)_{\max} - \left[\left(\frac{M_a}{M_s}\right)_{\max} - 1\right]\left(\frac{S_r - S_{r2}}{S_{r1} - S_{r2}}\right)^{k_a} \quad ; \text{for } S_{r2} < S_r < S_{r1}$$
$$M_b = 0 \quad ; \text{for } S_r > S_{r2}$$

where p is mean total stress, S_r is the degree of saturation, S_{r1} and S_{r2} are reference degrees of saturation and k_a and k_b are curve fitting parameters relating to the net normal stress and matric suction respectively. The subscripts are added here (different to Toll & Ong) to emphasise the difference between them. The other parameters are as defined before. Further details can be obtained from the original manuscript.

It is noted that if Eq. 2-15 is applied at the critical state of the unsaturated soil then the Toll & Ong (2003) formulation is similar to that by Vanapalli et al. (1996) except that in the former the critical net normal stress ratio, M_a (or ϕ') also varies with the degree of saturation, and hence suction. According to Toll & Ong, the reference states (S_{r1} and S_{r2}) do not coincide with the fully saturated and residual conditions identified from the water retention curve obtained using a pressure plate apparatus with no applied vertical stress as suggested by Vanapalli et al. (1996). This is probably due to the fact that the WRC shifts from its unconfined state owing to the change in pore structure induced during loading and shearing (Rassam & Williams, 1999).

Gallipoli et al. (2003) noted that the degree of saturation affects the area over which water and air pressures act and the number and intensity of capillary-induced inter-particle stresses. This reinforces the argument that suction alone is not sufficient to account for the effect of the presence of both gas and liquid phases in the soil on the

resultant mechanical behaviour of unsaturated soil. In their formulation, Gallipoli et al. (2003) assumed an average inter-particle (skeleton) stress variable of the form of the Bishop's stress except that the parameter χ was replaced by S_r to express the average stress acting in the soil skeleton defined as the difference between the total stress and the average stress of the two fluid phases, with the degree of saturation as the weighting parameter.

In addition to replacing χ with S_r, Gallipoli et al. (2003) introduced a bonding parameter $\xi = f(s)(1-S_r)$ as a measure of the magnitude of the inter-particle bonding due to water menisci so that the second type of suction effect, which is related mainly to (a) the number of water menisci per unit volume of the solid fraction, and (b) the intensity of the stabilising normal stress exerted at the inter-particle contact by a single water meniscus, is properly accounted for. The stabilising normal force exerted at the inter-particle contacts by meniscus lenses of water at negative pressure reduces the relative slippage (irreversible mechanical response) of a granular material at the interface between soil particles (Wheeler & Karube, 1996). The function of suction $f(s)$ in the bonding parameter equation varies between 1 and 1.5 for zero to infinity suction range. As a ratio of the value of stabilising force at a given suction to the value of stabilising force at zero suction, it accounts for the increase with suction of the stabilising inter-particle stress exerted by a single meniscus.

Wheeler et al. (2003) reported on the coupling of hydraulic hysteresis and stress-strain behaviour in unsaturated soil. They linked hydraulic and mechanical behaviour in a single framework to simulate the development of volumetric strains as a result of variation in water content by considering (a) the soil skeleton elastic and plastic (as a result of slippage at inter-particle or inter-packet contacts) strains due to externally applied stress, and (b) the hydraulic process of water inflow and outflow from individual voids, which impact the size and radius of the water menisci. The Wheeler et al. (2003) formulation is similar to that by Gallipoli et al. (2003) except that instead of the bonding parameter, Wheeler et al. used a modified suction given by the product of suction and porosity ($n\psi$) to account for the stabilising effect of the menisci water.

All the models presented hitherto do not account for the possible effects of suction history due to cycles of wetting and drying though several experimental work suggest

the existence of such effects. Tse & Ng (2008) investigated the effects of cycles of drying-wetting on unsaturated shear strength of completely decomposed tuff (inorganic silty clay of low plasticity) from Tung in Hong Kong. They subjected statically compacted samples to cycles of drying-wetting prior to the drained shearing (at constant suction) using a direct shear box capable of independent control of the net normal stress and matric suction. Their results show a high likelihood of the dependency of shear strength on suction history and level, which would mean that some or all of the soil constants in an elasto-plastic model would take on different values depending on drying-wetting cycle. They observed shear strength and stiffness to increase with suction and the shear stress and stiffness associated with the drying path of the primary drying/wetting cycle was greater than one in the second cycle. This was reversed in the case of the wetting specimens. This behaviour is consistent with the measured WRC characteristics presented in subsection 2.3.4. For these samples, the volumetric water content increased during shearing at constant suction; they attributed it to dilation. Based on their findings they thus proposed the equation for shear strength shown in Eq. 2-18. In the equation, υ is the angle of dilation.

$$\tau = c' + (\sigma_n - u_a)\tan(\phi' + \upsilon) + (u_a - u_w)\Theta\tan\phi' \qquad \text{Eq. 2-18}$$

Escario & Saez (1986) had pointed out that the effect of suction on shear strength among many other factors most likely depended on the capillary history of the soil. Consistent with this reasoning is the finding of Koliji et al. (2006) and Pires et al. (2009). Koliji et al. reported a reduction in the soils total porosity due to reduction of mainly the macro-pore volume. Pires et al. observed that wetting and drying cycles affected the pore properties of the tested material. Since pore properties affect the shape and size of the water menisci it is thus prudent and plausible to imagine that the mechanical behaviour is equally affected by drying-wetting cycles. Despite these indicators of the likelihood for unsaturated behaviour to depend on the drying-wetting history it has not, to the best knowledge of the author, been systematically studied except for swelling soils. In practice, soils exposed to prolonged drought could experience nearly complete de-saturation while they could equally re-saturate during the periods of heavy down pour.

2.4.2 Volumetric Behaviour of Unsaturated Soils

As earlier noted (subsection 2.4.1.1), the effective stress concept could not explain the volumetric behaviour of unsaturated soils. Early 1960s, researchers (e.g. Coleman,

1962; Bishop & Blight, 1963) suggested the use of the independent stress state variables namely the net normal stress and matric suction to describe the volumetric behaviour of unsaturated soils. Matyas & Radhakrishna (1968) using the experimental evidence from isotropic and K_o-compression tests on silt-clay mixture proposed the concept of state surfaces to relate void ratio, e and degree of saturation, S_r with the net normal stress, $p-u_a$ and matric suction, ψ to describe the volumetric behaviour of unsaturated soils. According to the state surface concept e and S_r can be expressed as:

$$e = f(p-u_a, q, \psi, e_0, S_{r0}) \qquad \text{Eq. 2-19}$$

$$S_r = f(p-u_a, q, \psi, e_0, S_{r0}) \qquad \text{Eq. 2-20}$$

where $p-u_a$, q and ψ are the stress parameters and, e_o and S_{ro} are the initial void ratio and degree of saturation respectively.

In the above equations (Eq. 2.19 & Eq. 2.20), the effect of soil structure is not included on the assumption that the initial soil state is controlled i.e. does not change. Constant overall volume was controlled to ensure minimum structural disturbance caused by saturation or desaturation on a macroscopic scale. Matyas & Radhakrishna (1968) noted that during volume changes for unsaturated soil the soil structure also undergoes changes. Such changes result in changes in suction (or degree of saturation if suction is controlled) due to structural rearrangement on a microscopic scale. Macroscopically, volume changes influence the stress-deformation behaviour of the soil.

The soil suction influences the soil structure so that as the suction increases soil structure rigidity and the inter-particle stress also increase and therefore the compressibility decreases and vice versa (e.g. Jennings & Burland, 1962). The structural adjustment due to suction decrease may result in collapse or swelling of the soil depending on the net normal stress level, swelling occurring at low stress and collapse taking place at high stress levels. These may not be distinctly pronounced in coarse soils like sands. Matyas & Radhakrishna (1968) further observed that for maintained initial conditions void ratio changes were independent of the path followed. Slopes of the compression curves for tests in which identical stress paths were followed were similar regardless of their stress histories. They concluded that the void ratio-stress relationship is independent of the state history provided that the placement conditions for the

specimens are similar. And that the variation of void ratio with a fixed initial state (e_o, S_{ro}) and compressed under all-round pressure can be represented by a surface in void ratio-stress space. However, when the initial conditions requirement is violated, the hysteresis in the soil structure due to loading and unloading, and drying-wetting, will induce certain non unique characteristics. The degree of saturation was more sensitive to saturation history than void ratio.

Following the work of Matyas & Radhakrishna (1968) among others, various mathematical expressions have been proposed for the state surfaces (e.g. Fredlund 1979; Lloret & Alonso, 1985). All these state surface approaches are unable to provide an integrated framework for a stress-strain characterisation of unsaturated soils. They are only limited to the elastic analysis of soils i.e. soils exhibiting recoverable strains despite the fact that unsaturated soils often undergo irrecoverable (plastic) behaviour (Alonso et al., 1990). Moreover the effect of the hydraulic hysteresis is also not incorporated in the state surface concept. Afterwards, many of these aspects were addressed through elasto-plastic modelling of which the first attempt was made by Alonso et al. (1990). This elasto-plastic model and many others are described further in the following subsection 2.4.3.

2.4.3 Elasto-plastic Models for Unsaturated Soils

A number of elasto-plastic models have been developed over the past few years to account for the possible occurrence of plastic strains and to provide a link between volumetric and shear behaviour of unsaturated soils. In this review, only the models for none expansive soils and which are expressed in terms of the net normal stress and matric suction (or some function of suction) as the stress state variables are considered. The commonly quoted models in the literature include Alonso et al. (1990), Josa et al. (1992), Wheeler & Sivakumar (1995), Wheeler (1996), and Wheeler et al. (2003). These are reviewed and presented below in that order.

Alonso et al. (1990) developed the Alonso et al., (1987) elasto-plastic framework into a full mathematical (constitutive) model to describe the shear and volumetric behaviour of unsaturated soils. This elasto-plastic model which is generally referred to as the Barcelona Basic Model (BBM) reduces to a critical state model when the soil becomes saturated. It was formulated within the framework of hardening plasticity (plastic volumetric strains lead to the expansion of the yield surface) using two independent

stress state variables, namely, the net normal stress and suction. Alonso et al. pointed out that the ψ - p_n space with $p_n = \sigma - u_a$ (net mean stress) is suitable to describe the isotropic behaviour of unsaturated soils. Using the v - $\ln p$ space (Fig. 2.11a), they proposed Eq. 2-21 to define the set of yield stresses p_0 for each associated suction. The corresponding yield curves are known as the loading-collapse (LC) curves (Fig. 2.15b).

$$\left(\frac{p_0}{p^c}\right) = \left(\frac{p_0^*}{p^c}\right)^{[\lambda(0)-\kappa]/[\lambda(s)-\kappa]} \qquad \text{Eq. 2-21}$$

For the relationship (Eq. 2-21), the pre-consolidation mean stress for saturated conditions p_o^* is necessary to isolate a single yield curve. In deriving the relationship and hence the shape and position of the LC yield locus, Alonso et al. (1990) considered an isotropic response of a saturated sample and an unsaturated sample. Whereas a saturated soil sample would yield at a pre-consolidation stress, p_o^* represented by point 3 in Fig. 2.11a, the unsaturated sample would yield at a larger stress p_o at point 1. In general yield stress increases as suction increases. The model considers that for the same material and identical samples, points 1 and 3 belong to the same yield curve in the s - p plane and therefore form the coordinates through which the LC yield curve is drawn (Fig. 2.11b). The relationship (Eq. 2-21) was reached by relating the specific volumes, v at points 1 and 3 through a virtual path which involved an initial unloading at constant suction, from p_o to p_o^*, and a subsequent reduction in suction from ψ to zero, at constant stress p_o^*. The sample initially at point 1 followed the path 1-2-3 in Fig. 2.11, undergoing recoverable swelling. It should be emphasised that this behaviour occurs only inside the elastic zone. However if suction unloading (wetting) takes place outside the elastic zone (zone enclosed by the LC and SI yield curves) irrecoverable strains (collapse) will be experienced with the magnitude of collapse dependent on the type of material. Similarly, a material undergoing suction unloading from inside the elastic zone will first experience recoverable strains before undergoing irrecoverable strains outside the zone.

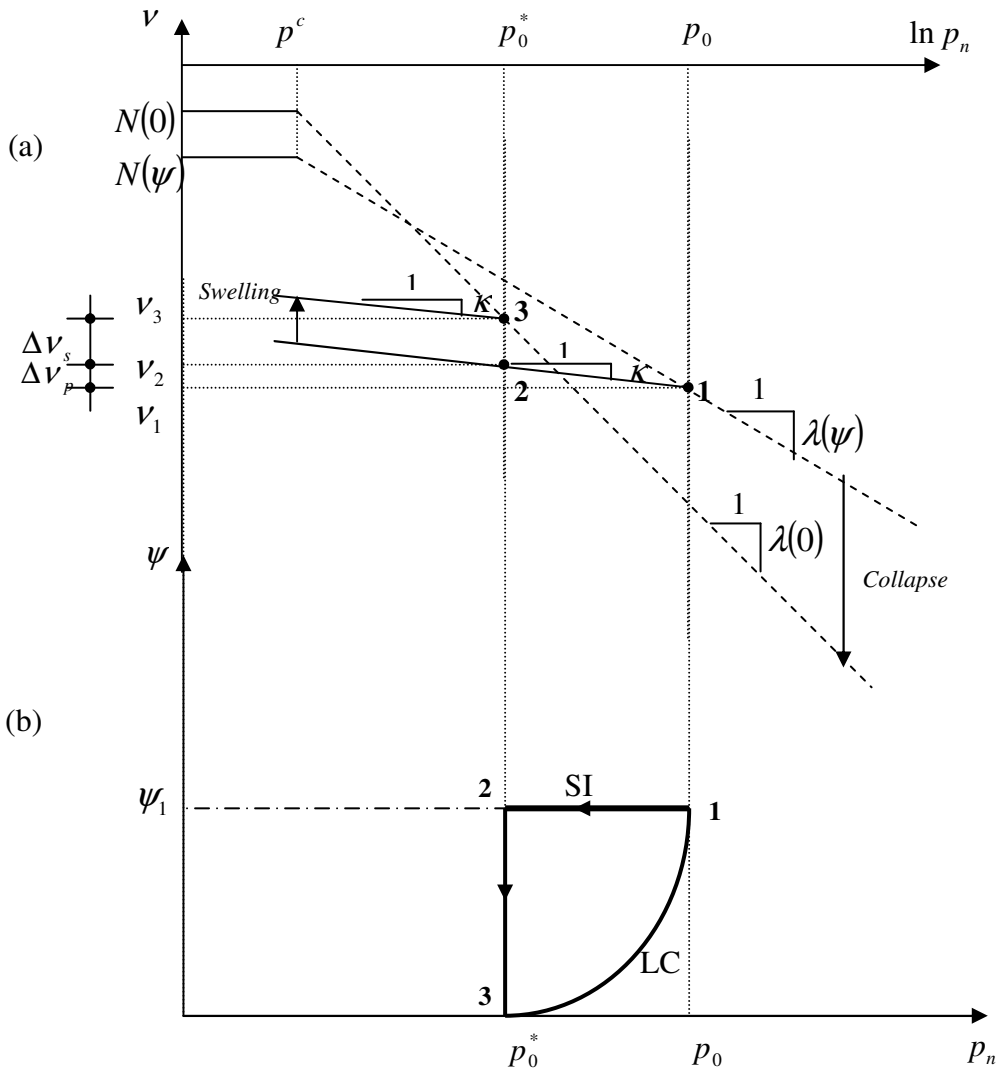

Figure 2.11: Relationship between pre-consolidation stresses p_0 and p_0^*: compression curves for saturated and unsaturated soil; (b) stress path and yield curve in $\psi - p_n$ stress plane (after Alonso et al., 1990)

Fig. 2.12 shows the evolution of the LC yield curve with the hardening parameter p_o^*. Generally, the LC yield curve expands with increase in p_o^*. Inherent to the Alonso et al. model is the assumption that there exists a net mean stress p^c at which one may reach the saturated virgin state through a process of suction unloading that involves only elastic swelling. When p^c coincides with the hardening parameter, p_o^* then the LC is a vertical line i.e. $p^c = p_o$ (Fig. 2.12). It was also assumed that the gradient of the yield curve decreases with increasing suction so that the value of the constant related to the

maximum stiffness of the soil, $r = \lambda(\psi \to \infty)/\lambda(0)$ in Eq. 2-22 was less than one. The constant r establishes the minimum value of the compressibility coefficient for high suction (virgin states) values.

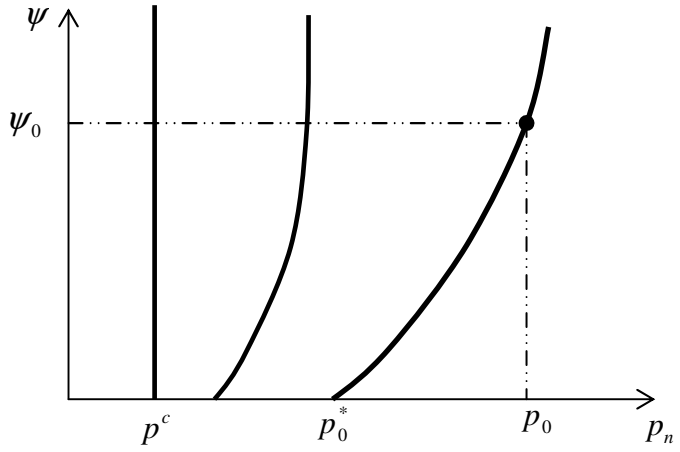

Figure 2.12: Expansion of LC curve (after Alonso et al., 1990)

The compressibility coefficient, $\lambda(\psi)$ for increments of suction across virgin states controls the increase in soil stiffness with suction. Alonso et al. (1990) proposed this coefficient as presented in Eq. 2-22.

$$\lambda(\psi) = \lambda(0)[(1-r)\exp(-\vartheta\psi) + r] \qquad \text{Eq. 2-22}$$

where $\lambda(0)$ is the compressibility coefficient for the saturated state along the virgin loading and ϑ is a parameter that controls the rate of increase of soil stiffness with suction within the virgin state. The compressibility coefficient obtained using Eq. 2-22 decreases with increase in suction but also means that the collapse potential increases indefinitely with increase in the net normal stress.

Besides mechanical actions, suction loading may also induce irrecoverable strains especially when the soil reaches a maximum previously attained value of suction, ψ_0 (Fig. 2.13a). This maximum value of suction interfaces between the elastic state and the virgin state when suction is increased (Fig. 2.13b). The points of yield as suction is increased in the ψ - p_n space define the suction increase (SI) yield locus, and together with the LC enclose the elastic region (Fig. 2.13b). The SI yield curve is more vital in describing the volumetric behaviour of shrinkable materials undergoing suction loading

than granular materials (Alonso et al., 1987). Again a linear relationship between v and $\ln\psi$ is assumed yet this may only be true over a limited range of degree of saturation, as the saturation approaches residual state the relation converges to that of the dry material.

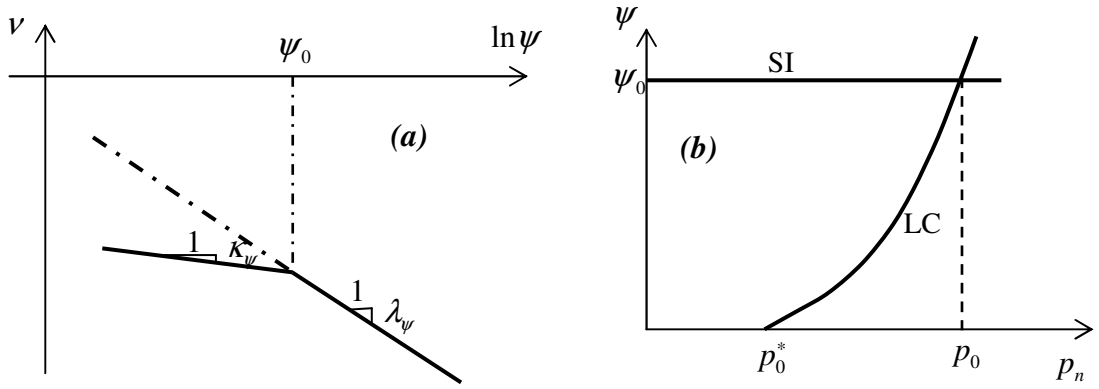

Figure 2.13: Loading-collapse (LC) and suction increase (SI) yield curves (after Alonso et al., 1990)

To account for the effect of shearing stress, the third stress parameter $q=(\sigma_1-\sigma_3)$ was introduced in the model. In this case the strain state becomes $\varepsilon_v(=\varepsilon_1+2\varepsilon_3)$, volumetric strain, and $\varepsilon_s\left[=\frac{2}{3}(\varepsilon_1-\varepsilon_3)\right]$, shear strain. The yield curve at constant suction was thus defined by the equation of the ellipse in Eq. 2-23.

$$q^2=M^2(p_n+p_\psi)(p_0-p_n)=0 \qquad \text{Eq. 2-23}$$

The effect of suction increase was assumed to have no effect on the effective angle of friction, ϕ' (or the critical state stress ratio, M) but the cohesion so that the critical state line (CSL) for the unsaturated sample with suction, ψ would remain parallel to the CSL for the saturated sample (Fig. 2.14). Due to the assumed linear relationship, the ellipse for the unsaturated sample intersects the p_n-axis at $-p_\psi=-k\psi$ where k is the compressibility coefficient along the elastic (unloading-reloading) stress path that controls the increase in cohesion with suction.

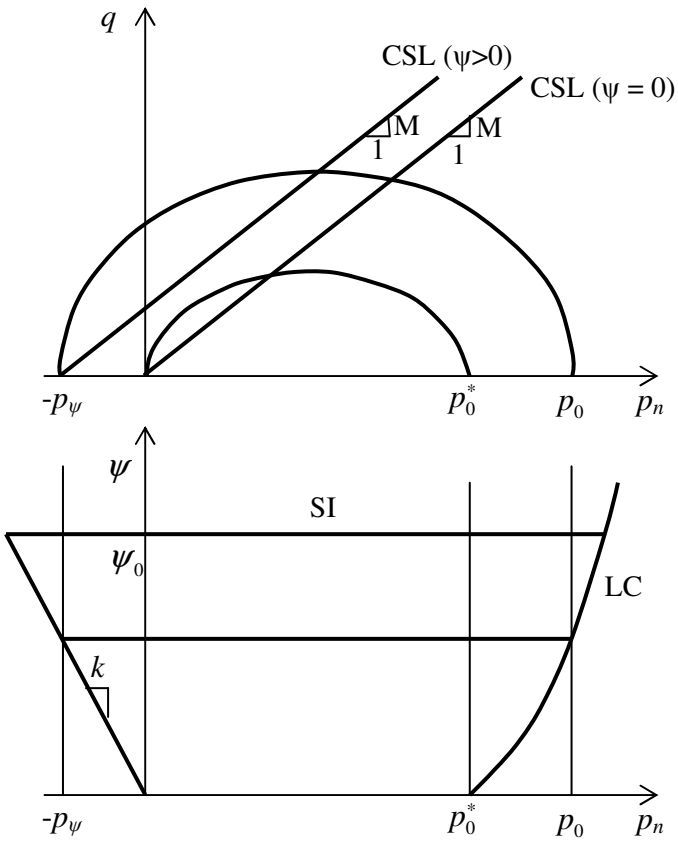

Figure 2.14: Yield surfaces in the (q, p_n, ψ) space (after Alonso et al., 1990)

As shown in Fig. 2.14 the yield curve, SI extends into the region $q > 0$ by a plane parallel to the q -axis. In a three-dimensional view, the yield surfaces in the (q, p_n, ψ) space are as shown in Fig. 2.15.

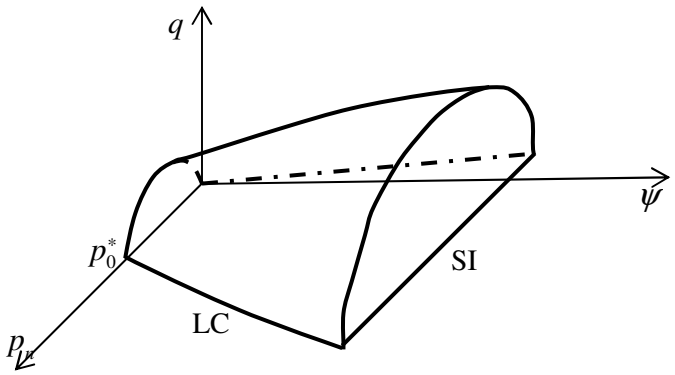

Figure 2.15: Three-dimensional view of the yield surfaces in (q, p_n, ψ) space (after Alonso et al., 1990)

Although several experimental data seem to generally obey the BBM (e.g. Estabragh & Javadi, 2008; Uchaipichat & Khalili, 2009) some deviate (e.g. Estabragh et al., 2004) from the model predictions. Estabragh et al. (2004) observed that contrary to the BBM $\lambda(\psi)$ appeared to decrease sharply as the suction was reduced to zero. These departures of the experimental observations from the BBM have led to several modifications and extensions to the Alonso et al. (1990) model to address its shortcomings.

Josa et al. (1992) extended the Alonso et al. (1990) model to predict the maximum collapse potential on wetting which had been assumed to increase indefinitely with increase in net normal stress. When the collapse approaches its maximum, the unsaturated compression line converges to the fully saturated compression line (e.g. Maswoswe, 1985; Wheeler & Sivakumar, 1995; Sivakumar & Wheeler, 2000). However, the maintenance of the parameter p^c is a restraint to the applicability of these models (Wheeler et al., 2002).

Wheeler (1996) modified the Wheeler & Sivakumar (1995) model to include the specific volume of water ($1+eS_r=1+wG_s$) as the second volumetric state variable, in addition to specific volume. Such a model can be useful for describing the behaviour of unsaturated soils in which water content remains constant. Although the model underestimated the specific water volumes at critical state, normal compression lines for specific water volume at different suction and the specific volume of water during wetting were satisfactorily captured.

Wheeler et al. (2002) commented on the BBM thus: It can be extremely difficult to match correctly the locations of the normal compression lines for different values of suction. According to Wheeler et al. a degree of judgment will be required to select an optimum set of parameter values, and then to decide whether the resulting match between experimental and predicted normal compression lines is sufficiently accurate for the purposes required. Wheeler et al. (2003) then in their constitutive model for isotropic stress states coupled the hydraulic hysteresis and mechanical behaviour to account for the influence of degree of saturation, in addition to that of matric suction, on the stress-strain response of unsaturated soils. According to them, plastic changes of degree of saturation affect the stress-strain behaviour and plastic volumetric strains influence the water retention behaviour. The Wheeler et al. (2003) model is believed to

capture the transition from unsaturated to saturated behaviour as well as the influence of drying-wetting cycle on subsequent behaviour during isotropic compression.

2.5 Laboratory Testing of Unsaturated Particulate Materials

2.5.1 Equipment employed and modifications to the conventional equipment

2.5.1.1 Equipment employed

The laboratory study of unsaturated soils has a long history. Several of such studies have been highlighted in the preceding sections of this chapter. However, no attention has been paid to the equipment used in the testing hitherto. This section is thus devoted to the description of the requirements for the equipment used in the laboratory testing of unsaturated soils. An intensive literature search has revealed that important equipment include direct shear box, oedometer and the triaxial apparatuses. The pressure plate, pressure membrane and Tempe cell are also very important equipment in unsaturated soil testing.

Triaxial apparatus is the most commonly used equipment for shear strength and deformation behaviour testing of soils (Wulfsohn et al., 1998; Gui & Yu, 2008). However, in the testing of unsaturated soils, conventional triaxial apparatus and indeed all other conventional apparatuses requires some modifications (Fredlund & Rahardjo, 1993). The required modifications for the triaxial equipment are described next.

2.5.1.2 Modifications to the conventional triaxial equipment

Conventional triaxial apparatus is modified to accommodate the complexity associated with the testing of unsaturated soils. As the pore fluid consists of both air and water, the modifications must provide for independent control and or measurement of the pore air and water pressures. There should also be a provision in the modifications for minimising the difficulty associated with the measurement of negative pore water pressure in the unsaturated soils (Fredlund & Rahardjo, 1993). Usually an interface known as the high air-entry ceramic disk is used in systems for suction controlled tests. For tests where direct measurement of suction is desired a tensiometer is used in place of the ceramic disk. Additionally, the system has to independently measure the pore water and the total volume changes.

2.5.2 Suction measurement

Measurement of soil suction is either direct or indirect (Ridley & Wray, 1996; Tarantino & Mongiovi, 2001). Direct measurements involve intimate contact between the measuring device and the soil system. Indirect measurements, on the other hand, involve determining the soil suction based on other measured quantity such as relative humidity, soil water content etc. The devices commonly used in the measurement of soil suction include tensiometers for the direct measurements and the psychrometers and filter paper for indirect measurements. These are respectively reviewed below.

2.5.2.1 Direct Measurement (Tensiometers)

Ridley et al. (2003) defined a tensiometer as a piezometer that has been specially designed for measuring pore water tension. It measures directly the negative pore water pressure in the soil system at an atmospheric pore air pressure. Conventionally, the main components of a tensiometer include a water reservoir, a high air-entry interface (usually a saturated porous ceramic filter), and a pressure gauge. The application of conventional tensiometers is hampered by their inability to accurately measure suction in excess of 80kPa (Marinho et al., 2008). At such high suction, cavitation problem stops effective transmission of the suction to the pressure gauge. Ridley & Burland (1993, 1995, and 1999) developed a high capacity tensiometer capable of measuring negative water pressures up to 1,500kPa without cavitation phenomenon. Fig. 2.16 shows the schematic of the Ridley & Burland (1999) tensiometer. The device incorporates a small water reservoir (~3 mm^3 volume) to inhibit cavitation and a high air-entry (1,500kPa) ceramic filter.

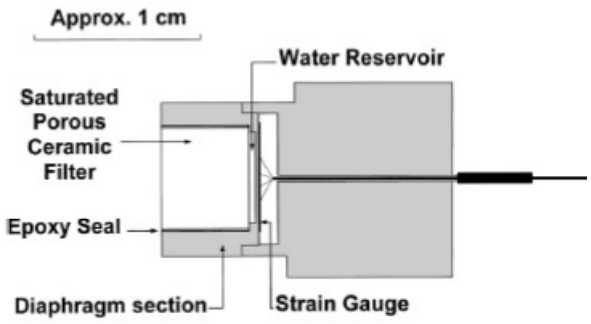

Figure 2.16: Parts of the Imperial College tensiometer (Ridley & Burland, 1999)

However, the most important limitation of the use of tensiometers to measure negative pore water pressure is related to the interpretation and long-term measurement of soil suction. The demarcation between a good and a bad measurement is not straightforward.

In addition, if inadequately saturated, the tensiometer is likely to give very misleading results during its first sets of measurements. This however, improves in the subsequent measurements. The results (Fig. 2.17) of Take & Bolton (2003) in which a tensiometer fitted with 1 bar filter was initially saturated to 0.77 demonstrate these limitations. The tensiometer was subjected to a step wise decrease/increase of pore water pressure within the range of $\pm$100kPa. It recorded correctly the decrease in pore water pressure until a minimum value of -65kPa. Beyond this value, the tensiometer readings become erroneous. Marinho et al. (2008) state that the issue of tensiometer saturation can only be overcome if highly qualified personnel saturate, install and monitor tensiometers.

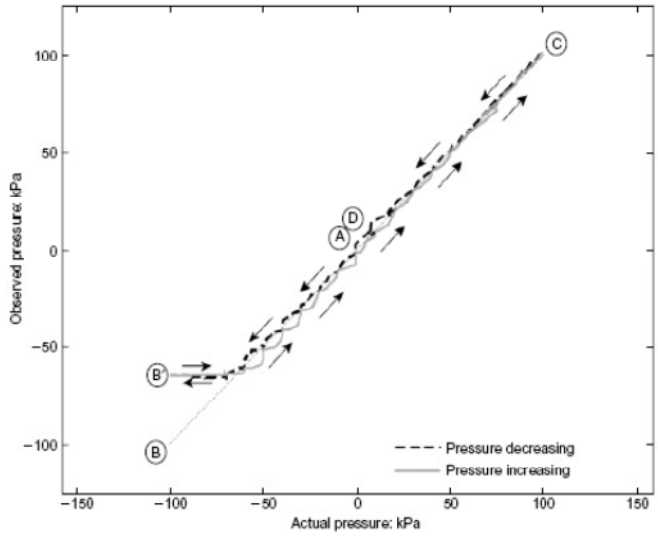

Figure 2.17: Nonlinearity and hysteresis for a poorly saturated tensiometer (After Take & Bolton, 2003)

Delage et al. (2008) emphasised that adequate de-airing and pressurisation are necessary for the proper operation of the Imperial College tensiometer. This was in support of the earlier observations by Tarantino & Mongiovi (2001, 2003) that adequate saturation and preconditioning by subjecting the tensiometer to cycles of cavitation and subsequent pressurisation is essential for their proper and accurate operation. According to Tarantino & Mongiovi (2001), high pressures alone are incapable of dissolving the small gas nuclei in the porous ceramic interstices due to the curvature of the air-water meniscus (Fig. 2.18a). Under high pressures the small gas nuclei remain stable and air is also likely to diffuse towards them (Fig. 2.18b) so that when the water pressure is reduced cavitation is triggered (Fig. 2.18c). When this process is repeated, the number of potential cavitation nuclei is significantly reduced.

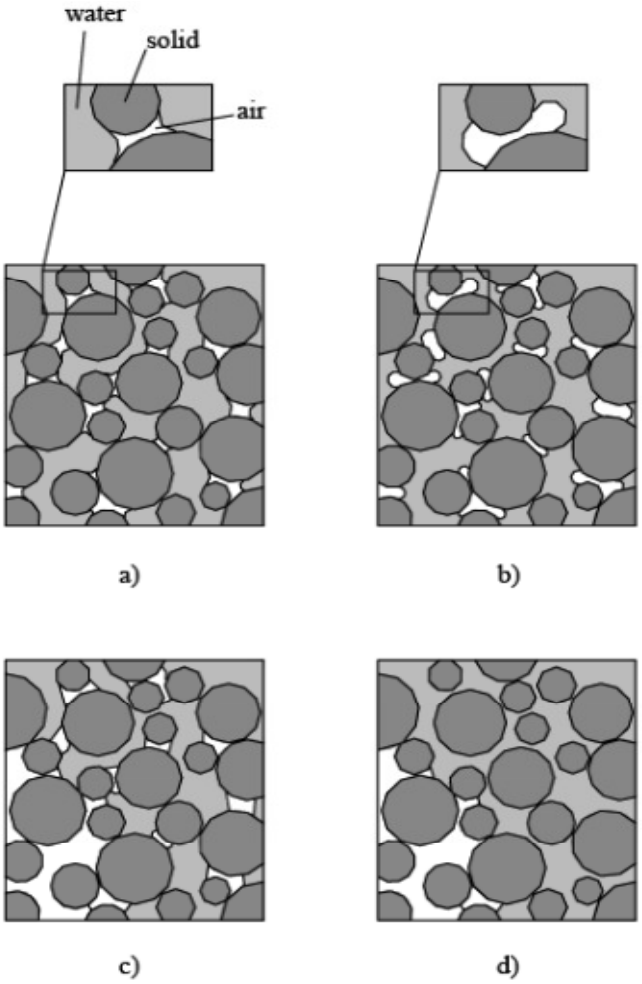

Figure 2.18: Possible cavitation mechanism inside the tensiometer (a) pre-pressurisation; (b) measurement; (c) cavitation; (d) air diffusion (Tarantino & Mongiovi, 2001)

2.5.2.2 Indirect Measurement Techniques

Indirect measurements, on the other hand, involve determining soil suction based on other measured quantities such as relative humidity, soil water content, thermo and electrical conductivity and should therefore be calibrated against known values of suction (Tarantino & Mongiovi, 2001). Bulut & Leong (2008) give a comprehensive review of the techniques of indirect suction measurement. In their review, Bulut & Leong classified indirect suction measurement techniques as primary (e.g. psychrometers) if it measures the vapour pressure, secondary (e.g. the filter paper method) if it measures the moisture content equilibrium condition of another porous medium, and tertiary (e.g. thermo and electrical conductivity sensors) if the quantity actually measured is the physical properties of the other porous medium's moisture equilibrium condition. The capabilities and limitations of these methods are also discussed.

Limitations of the primary techniques, which measure total suction, include unreliability of relative humidity and temperature changes to infer suction. Bulut & Leong (2008) explain that a small change in the relative humidity in the soil air phase leads to a very big change in suction. Similarly, minor temperature changes may lead to large errors in total suction measurements. These limitations compromise the suitability of the psychrometers and any other methods based on relative humidity measurements to measure suction in large pore systems where important suction lies within a low range of relative humidity. This category of methods is thus not recommended for suctions less than 100kPa but can measure suctions up to 30MPa (Bulut & Leong, 2008).

The filter paper (secondary methods) is one of the established techniques to indirectly measure suction (e.g. Gradner, 1937; Chandler & Gutierez, 1986; Chandler et al., 1992; Ridley, 1993; Marinho, 1994; Houston et al., 1994; Oliveira & Marinho, 2006; Haghighi et al., 2012). It has been standardised by the American Society of Testing and Materials as ASTM D 5298 test. Suction is computed using a previous calibration equation and a number of different calibration equations are in place depending on whether it is total or matric suction being measured. The ASTM D 5298 employs a single calibration equation to determine both total and matric suctions and recommends the filter paper to be initially oven dried for 16hours (or overnight) and allowed to cool to room temperature in a dessicator. In the procedure, the filter paper is allowed to come in equilibrium with the soil either through vapour (for total suction measurement) or liquid flow (for matric suction measurement). At equilibrium, the filter paper and the soil have the same suction and after equilibrium is reached the gravimetric water content of the filter paper and the soil are measured. The filter paper water content is then converted into suction using an appropriate calibration equation. According to Bulut & Leong (2008), the filter paper methods require strict adherence to the recommended laboratory protocol otherwise the methods are prone to operator error. In addition, Fredlund & Rahardjo (1993) warned that use of the filter paper technique to measure matric suction could be misleading as it can be difficult to tell whether total or matric suction is being measured, depending on the degree of contact between the soil and the filter paper. This problem is likely to be of great importance when dealing with coarse granular materials and therefore extra care is needed to obtain good results. It has also been reported that a given calibration equation may actually not be unique to all filter paper batches (Lu & Likos, 2002). It therefore means that before adopting any calibration equations one should first validate them for the available filter paper batches

unless the suction being measured does not exceed about 60kPa. In their evaluation of the Chandler et al. (1992) calibration equation, Marinho & Oliveira (2005) found the calibration equation to satisfactorily fit their experimental data below 60kPa suction regardless of the filter paper batch used. At higher suctions, however, many of their experimental points fell below the calibration equation suggesting the necessity to verify the calibration equation at higher suctions (about 200kPa in their study), in confirmation of the observation by Lu & Likos (2002). However, the filter paper method is simple and probably the most affordable indirect method. It can measure suction from nearly zero to about 30,000kPa but long equilibration time is necessary for reliable results. Whereas most of the above quoted calibration equations are limited to relatively high suction, the one of Chandler et al. (1992) is valid for suctions up to 0kPa.

Hysteresis is the critical limitation for the tertiary methods which include thermo and electrical conductivity sensors. Hence their calibration must be correctly carried out for any matric suction measurement to be reliably obtained. The methods are recommended for measurement of matric suctions in the range of 1-1,500kPa.

It should be noted that when investigating the effect of suction changes on the material behaviour, it is necessary to be able to limit such inevitable changes during a particular test. This is not possible with the techniques such as tensiometers, filter paper, psychrometers and the thermo and electric sensors discussed above. These techniques which are comprehensively reviewed by Bulut & Leong (2008) and Marinho et al. (2008) simply measure the suction in the sample and, on their own, are thus inappropriate for the study in which suction control is highly desirable.

The well established methods of controlling suction in the laboratory tests such as oedometer, direct shear box and triaxial tests include the vapour equilibrium technique, osmotic technique and the axis translation technique. Focusing on the principles, applications and limitations, these techniques are pursued further in the following subsection.

2.5.3 Suction Control

2.5.3.1 The vapour equilibrium technique

The vapour equilibrium technique (VET) involves creating an environment of constant suction using the osmotic potential of chemical solutions such as saturated salt solutions and unsaturated acid solutions. Such an environment (vessel containing aqueous solutions) of known potential serves as a reference system. This reference system is placed in a closed chamber in which the test sample is put. Fig. 2.19 show the setup used by Romero (1999) to control suction in an oedometer. Soil water potential is controlled by means of the migration of water molecules through the vapour phase from this reference system to the soil pores, and vice versa depending on the state of the soil, until equilibrium is reached (Ng & Menzies, 2007; Delage et al., 2008). Since the salt solution cannot move through the air from the reference system to the sample and vice versa, only total suction is controlled. At equilibrium, water vapour and hence the relative humidity in the closed chamber are in equilibrium thereby controlling suction. Once equilibrium is reached, the relative humidity of the air inside the chamber is measured using either the hygrometer or the psychrometer and using the Kelvin's equation (Eq. 2.4) the total suction in the sample is quantified.

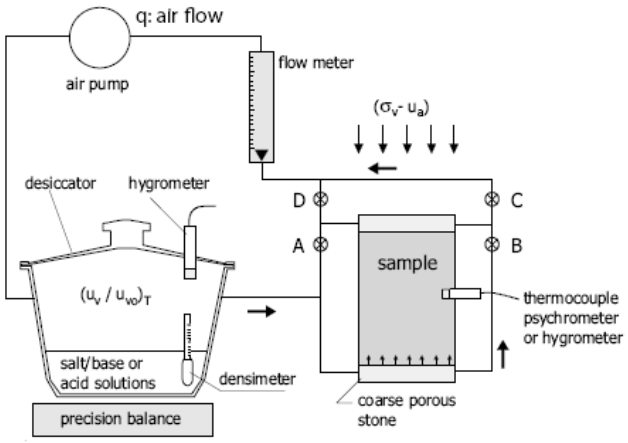

Figure 2.19: Suction-controlled oedometer with vapour equilibrium technique (Romero, 1999)

The main drawback of this technique is related to the extremely long and hence prohibitive time necessary to reach moisture equalisation. Recently, Delage et al. (2008) noted that the equalisation time is of the order of several weeks. The other disadvantages of the vapour equilibrium technique include the difficulty in applying high suctions due to changes in concentration of ionic solution and the need for precise control of the temperature to ensure accurate assessment of the applied suction (Delage

et al., 2008; Blatz, et al., 2008). However, disconnection of the reference system from the sample to inhibit any further moisture transfers (Delage et al., 2008) and circulation of regulated air through the sample or along the boundaries of the sample could reduce the equilibration time (Cunningham, 2000). However, such an approach would require an extensive calibration procedure. To ensure accuracy, independent sensors are necessary to verify the magnitudes and equalisation of the applied suctions (Blatz, et al., 2008).

In addition, the vapour equilibrium method is not suitable for high relative humidity (low suctions). Blatz et al., 2008 reported that at low suctions, the relationship between relative humidity and suction is highly nonlinear which generates difficulties with precise inference of applied suction at low suction levels. Delage et al. (1998 in Koliji, 2008) reported that the reliability of vapour equilibrium technique is dependable only when dealing with suctions in excess of 8Mpa. The technique is capable of applying suctions up to 150MPa.

2.5.3.2 The Osmotic Technique

In the osmotic technique, the sample is placed in contact with a semi-permeable membrane while an aqueous solution containing large-sized soluble polyethylene glycol molecules (PEG) is circulated behind the membrane. The PEG molecules cannot go through the membrane, resulting in an osmotic suction applied to the sample through the membrane. Since the membrane is permeable to water and the salts dissolved in water, the technique controls matric suction, like the axis translation technique which is discussed in the next subsection 2.5.3.3. The value of the imposed suction depends on the concentration of the solution, the higher the concentration the higher the suction and vice versa. The technique is commonly applied within the suction range of 0 - 10MPa (Blatz et al., 2008).

The most important advantage of the osmotic technique lies in its ability to exactly reproduce the real field conditions of the soil suction especially significantly so in the range of high degrees of saturation when air continuity is no longer ensured (Delage et al., 2008). Air diffusion problems are uncommon with the technique as no artificial air pressure is applied to the sample. High levels of suctions up to 10MPa are also possible in the triaxial testing of unsaturated soils with the use of high concentration of PEG solutions, since there is no need to impose high values of confining stress to maintain

constant the net mean stress $(p-u_a)$ at the elevated air pressures needed to impose suction. When dealing with soils with high air-entry value like clays this point needs to be given a considerable attention (Delage et al., 2008). The osmotic method allows liquid water exchanges between the soil and PEG solution; therefore equilibration time is much shorter as compared to the vapour equilibrium technique.

However, even with these good standpoints Delage et al. (2008) noted that the adaptation of the osmotic technique in the triaxial testing is not as straightforward as in oedometer testing, as compared to the axis translation technique. The main setback of the technique is the weakness of the semi-permeable membrane, which limits its applicability. Suction measured by the osmotic technique could be different from the actual suction in the sample. The cellulose acetate membranes which have been most commonly used up to now are particularly highly sensitive to bacteria attack (Delage et al., 2008). Breakdown of the membrane means that the PEG solution can infiltrate the sample and hence suction, especially high suction, can no longer be controlled. Addition of penicillin in PEG solution has been reported to elongate the life span of the membranes but only to about 10 days. Hence for tests involving a testing period in excess of 10 days, the effectiveness of adding penicillin in the PEG solution cannot be guaranteed.

The risk of tear by any traction on the semi permeable membrane is another serious limitation (Blatz et al., 2008). Unlike in the oedometer, this risk is very high in triaxial tests because of the shear stress applied. Moreover the implementation of the undrained triaxial procedures such as constant water content tests using the osmotic technique is very difficult (in Wulfsohn et al., 1998).

2.5.3.3 The Axis Translation Technique

The axis translation technique (Hilf, 1956) is probably the most commonly and widely used (e.g. Matyas & Radhakrishna, 1968; Wulfsohn et al., 1998; Rampino et al., 1999; Toll & Ong, 2003; Farouk et al., 2004; Estabragh et al., 2004; Yang et al., 2008; Toll et al., 2008; Lourenco et al., 2008; Gui & Yu, 2008; Tse & Ng, 2008; Mirzaii et al., 2008; Estabragh & Javadi, 2008; Uchaipichat & Khalili, 2009; Khoury & Miller, 2010) method for controlling matric suction in the laboratory testing of unsaturated soils with relatively high negative pore water pressure. The technique involves placing a specimen of soil on top of a saturated high air-entry ceramic disk below which the pore water

measuring system is connected (e.g. Delage et al., 2008). To avoid entry of the air bubbles into the measuring system, the ceramic disk must have an air-entry value greater than the matric suction in the soil specimen. In practice, the maximum measurable suction using the axis translation technique is a function of the air-entry value of the ceramic disk, and the highest air-entry value of the currently available disks is nominally 1,500kPa (e.g. Fredlund & Rahardjo, 1993; Marinho et al., 2008; Vanapalli et al., 2008; Lourenco et al., 2008).

The technique translates the pore air pressure through an artificial increase of the atmospheric pressure in which the soil is immersed. Consequently, the pore water pressure increases by the same amount but only if the water and soil particles are incompressible or assumed so in which case the curvature of the menisci would not be greatly affected. This assumption seems reasonable in the case of coarse granular materials like sands and glass beads at degrees of saturation in which the air phase is continuous. The range of degree of saturation over which the air and water phases are both continuous is reportedly 20% to 80% (e.g. Fredlund, 2000). The translation of the pore water pressure into the positive range facilitates its control (e.g. Delage et al., 2008).

The application of axis translation technique is illustrated by several researchers (e.g. Fredlund & Rahardjo, 1993; Wulfsohn et al., 1998; Lourenco et al., 2008). Fig. 2.20 shows the illustration by Wulfsohn et al. (1998). The pore water pressure is increased by an amount of 101kPa by applying a value of air pressure of 202kPa to the soil sample. The ceramic disk in this case has an air-entry value of not less than 202kPa. Such an increase in pore water pressure enables its measurement without any risk of cavitation in the measuring system and continuity between the pore water and the water in the measuring system is maintained. In practice, the pore air and pore water pressures can be controlled independently.

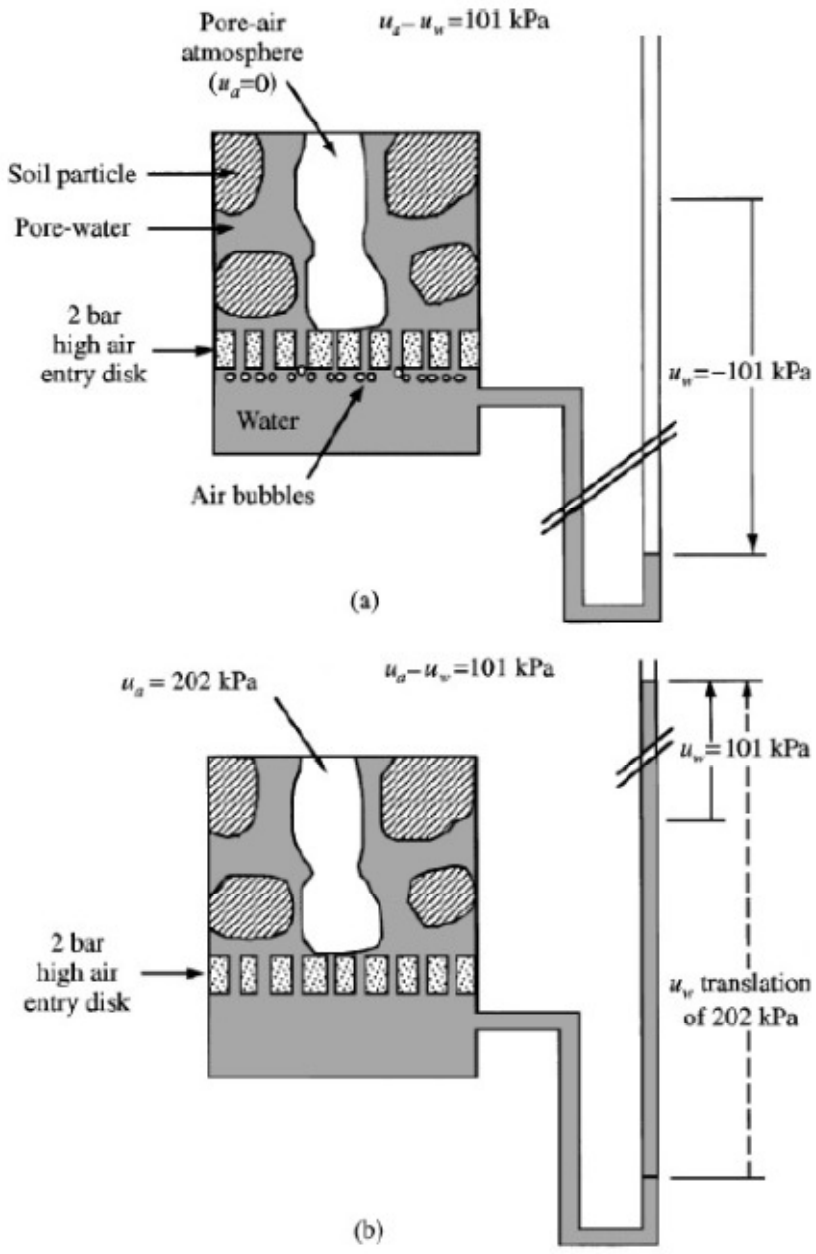

Figure 2.20: Application of the axis translation technique: (a) Direct measurement of pore water pressure showing air diffusion through the high air-entry porous disk and water cavitation in the measuring system; (b) axis translation of 101kPa (Wulfsohn et al., 1998)

The main advantage of the axis translation technique lies in its ability to enable the application of matric suction in excess of 1 atm (or 101.3kPa). Systems that measure matric suction directly in the soil specimen suffer from the problem of water cavitation as the gauge pressure of -1 atm is approached. Conventional tensiometers, for instance, can hardly measure suction in excess of 80kPa (e.g. Marinho et al., 2008) without cavitaion. With the axis translation technique, however, suction up to 1,500kPa can be successfully applied and controlled in the laboratory (e.g. Fredlund & Rahardjo, 1993).

Cavitation, which leads to accumulation of occluded air bubbles in the water compartment below the saturated ceramic disk, induces errors in the pore water pressure and volume measurement, which is limited to -1 atm in direct measurement technique regardless of how high the air-entry value of the disk is. This limitation can be overcome by applying the axis translation technique to the specimen (e.g. Fredlund & Rahardjo, 1993; Ng & Menzies, 2007).

However, the axis translation technique is not free of limitations. Many researchers such as Ridley & Burland (1993) and Burland & Ridley (1996) have described the limitations of the technique. More recently, Lourenco et al. (2008), Delage et al. (2008), Marinho et al. (2008) and Vanapalli et al. (2008) gave a comprehensive review of such limitations and the possible ways to overcome them. The technique creates an artificial atmospheric condition which is not representative of the field conditions where air pressure is atmospheric. As such, though matric suction value is never affected by the translation, it is hypothesised that the translation of pore air pressure affects the way in which the sample drains and consequently behaves mechanically. This point has no sufficient research data to back it up in the literature.

Finally, in terms of the experimental difficulties concerning the application of axis translation technique, Delage et al. (2008) noted that accumulation of diffused air below the saturated porous disk, the control of relative humidity of the air chamber to minimise evaporation and condensation effects on the sample, the application of the pressurisation process at nearly saturated states, and the estimation of the equilibrium time need specific consideration if the technique is to lead to accurate and reliable results. Details about each of the above factors can be got in Delage et al. (2008).

Nonetheless, the axis translation technique is so far the most commonly and widely used experimental technique to control matric suction in the laboratory testing of unsaturated soils. In practice, unlike for the other two techniques previously discussed, its experimental difficulties can readily be overcome. It has proved to provide sufficient, reliable and reasonable results and a good continuity between vapour equilibrium results at elevated suctions and nearly saturated states (Delage et al., 2008). Based on the experimental work of Hoffmann et al. (2005), Delage et al. demonstrated an adequate overlapping in the soil-water retention characteristics results obtained using the three techniques of controlling suction, namely, the axis translation technique, the vapour

equilibrium technique and the high-range transistor psychrometers. In addition, Fredlund & Rahardjo (1993) demonstrated the non-dependence of the accuracy of the technique on the operator.

2.5.4 Summary on the Suction Measurement and Control Techniques

In the preceding subsection, the presently available techniques to control and or measure suction in the laboratory have been reviewed and presented. Table 2-2 summarises the techniques to facilitate easy comparison. In the table one can find the component of suction measured/controlled, suction range, equalisation time and other attributes or comments.

Table 2-2: Comparison of suction control/measurement techniques

Technique	**Suction component**	**Range (MPa)**	**Equalisation time**	**Remarks**
Tesiometer	Matric	0 – 1.5	Days to weeks	Difficulties with cavitation, long-term measurement and detection of bad results.
Psychrometers	Total	0.1 – 30*	Minutes to hours	Very sensitive to temperature and humidity changes.
Filter paper	Total/matric	0 – 30	Days to weeks	Degree of contact highly affects results, method prone to operator errors.
Conductivity sensors	Matric	0.001 – 1.5	Hours to days	Indirect measurement method highly limited by hysteresis and requires high-level calibration.
Vapour equilibrium	Total	0 – 150**	Days to weeks	Sensitive to temperature changes, not suitable for low suctions, the concentration of the osmotic solution may change during up exchanges and equalisation time is long and prohibitive.
Osmotic	Osmotic	0 – 10	Days to weeks	Adaptation to triaxial testing is not straightforward and is limited by bacteria attack of the membrane.
Axis translation	Matric	0 – 1.5	Hours to days	Technique is free of cavitation problems, translates the atmospheric conditions and range of suction control is a function of air-entry value

*Higher values are possible
**Suction range depends on the type and concentration of the solution

2.5.5 Air diffusion in laboratory testing of unsaturated particulate materials

Air diffusion in laboratory testing of unsaturated soils occurs when the axis translation technique is used to control suction. Air moves across the saturated high air entry ceramic disk into the water compartment beneath owing to the air concentration gradient. As discussed in subsection 2.5.3.3, it is a big concern in the unsaturated testing of unsaturated soils. Depending on the value of applied air pressure and period of exposure, it can result in desaturation of the disk and consequently reduced hydraulic conductivity. The end result would be longer equalisation periods and inaccurate volume change measurements.

Fredlund (1975) and Fredlund & Rahardjo (1993) recommended correction for the diffused air whenever the axis translation technique is used in the unsaturated tests running for more than one day. Padilla et al. (2006) investigated, among other things, the frequency of flushing necessary for reliable results. They observed that unlike for 1bar and 3bar disks where diffusion was insignificant, 5bar and 15bar disks required regular flushing. Based on their findings, while only one time flushing in three days of testing would suffice for 1bar and 3bar disks, only once in two days flushing is sufficient for 5bar disks operating at nearly 100% of the rated bubbling pressure value. For 15bar disks one time flushing and twice a day would be necessary when the disk is operating at about 50% and greater than 50% of the bubbling pressure respectively.

To date several devices have been proposed to flush diffused air in axis translation technique. They include the bubble pump technique (Bishop & Donald, 1961), the diffused air volume indicator (Fredlund, 1975), the pressure pulse technique (Lawrence et al., 2005) and the automatic diffused air flushing device (Padilla et al., 2006). All these devices require that after a predetermined period of time the volume change recordings of the transducer both just before and immediately after flushing are taken. The volume of air is then calculated as the difference between the flushed total volume and the "only water" volume. During flushing a pressure difference between the bottom of the ceramic disk and the flushing point is created so that any air accumulated beneath the disk flows out as water takes up its position. All the water collected during the flushing period should be accounted for. It should be noted that the above procedure ignores any fluid flow across the ceramic disk during the time of flushing, which depending on the elapsed time can be significant.

2.6 Application to industrial material handling

Many of the theories used in design of industrial material handling and storage facilities are similar in principle to those used in soil mechanics. For instance, in computing stress distribution in the storage facility e.g. silo, the vertical stresses, wall normal stresses and wall frictional stresses are all evaluated using approaches based on soil mechanics theories. Furthermore, the material properties are often obtained using tests adopted and modified from soil mechanics, particularly the shear tests and unconfined compression tests. The Mohr-Coulomb failure envelope is also extensively used in the determination of the consolidation stress and the unconfined yield strength from which the flow factor is computed (e.g. Schulze, 2008). Relevant to this research project is the flow behaviour of granular materials and the silo design theories, and so only related studies will be pursued further.

2.6.1 Flow behaviour of granular materials

Several studies have been conducted in an attempt to explain the behaviour of granular materials in silos and or bins (e.g. Janssen, 1895; Ooi et al., 1998; Kusinska, 2000; Tixier et al., 2004; Sperl, 2006; Chen et al., 2007; Matchett, 2007). Many of these studies have focussed on explaining flow patterns and pressure distributions in the storage facility during filling, storage and flow stages. From these studies and many more it can be concluded that pressure distribution in a silo depends on the flow pattern and vice versa. These are pursued further in later parts of this section.

Besides the flow pattern and pressure distribution, material flowability has also been extensively studied. Flowability is generally used to refer to the ability of the material to emerge out of the hopper when the outlet is opened. Studies in which the primary objective is material flowability include Fowler & Glastonbury (1959), Beverloo et al. (1961), Johanson (1964), Zhang & Rudolph, 1991; Drescher et al. (1995), Drescher & Ferjani (2004), Fitzpatrick et al. (2004), Grantham & Forsberg (2004), Sperl (2006), Snider (2007), Mankoc et al. (2007), Zhu et al. (2007), Ahn et al. (2008), Datta et al. (2008), Ganesan et al. (2008), Ketterhagen et al. (2009), Persson et al. (2010) and Sheldon & Durian (2010). These studies have identified and explained many important issues relating to material flowability such as characterisation of material flow, factors influencing flowability, measurement of flow and flow prediction. These are presented in the next subsections.

2.6.1.1 Characterisation of material flow in silos

A number of parameters have been identified and used in the characterisation of flow behaviour in silos. The flow rate determined by collecting the discharge material for a given period and then dividing the collected material by the time of collection is perhaps the first and commonly used parameter (e.g. Fowler & Glastonbury, 1959; Beverloo et al., 1961; Verghese & Nedderman, 1995; Hirshfled et al., 1997; Hirshfled & Rapaport, 2001; Mankoc et al., 2007).

Jenike (1960) used flow factor to characterise flow behaviour. It is the ratio of the consolidation stress to the unconfined yield strength (Schulze, 2008). Alternatively, Jenike's design charts are used to estimate the flow factor (Schulze, 2008; Ketterhagen et al., 2009). For any material to flow, its flow factor should be in excess of unity. This means that at the same flow factor a more dense material will flow more easily than a similar loose material as the former is supported by a greater force of gravity. When the effect of bulk density is important, Schulze (2008) suggested using a density-weighted flow factor obtained by multiplying the computed flow factor by the bulk density of the material normalised with the density of liquid water at 0^{o}C and 1bar rounded. The normalisation is intended to ensure the factor remains dimensionless. According to Jenike (1960, in Schulze (2008)) subject to the consolidation stress easy-flowing materials have a flow factor between 4 and 10. A factor in excess of 10 is said to be associated with free-flowing materials e.g. cohesionless bulk solids.

The other factors used in the characterisation of the flow of granular materials include the flow function, outlet opening and the hopper shape and inclination. The flow function of the material is obtained when the unconfined yield strength, σ_c is plotted against the consolidation stress, σ_{con} (Rotter, 2001; Schulze, 2008). If a line passing through the origin with a slope equal to the reciprocal of the flow factor is drawn on a plot of σ_c against σ_{con} an intersection can be defined. The unconfined yield strength given by the intersection point, herein termed the critical unconfined yield strength, σ_{ccrit}, is used together with the hopper half angle, β, the bulk density at critical state, ρ^{crit} and the acceleration due to gravity, g to compute the minimum hopper outlet opening, $D_{\min}$ using Eq. 2-24. Outlets less than the minimum so calculated may cause a stable arch to form when the stress near the outlet drop below the critical unconfined yield strength.

$$D_{\min} = H(\beta)\frac{\sigma_{ccrit}}{\rho^{crit} g} \qquad \text{Eq. 2-24a}$$

$$H(\beta) = 2 + \frac{\beta}{60} \qquad \text{Eq. 2-24b}$$

However, the foregoing approach to $D_{\min}$ determination is more suitable for cohesive materials. In the case of cohesionless materials the minimum hopper outlets are chosen to prevent mechanical arching arising from interlocking of particles. The general consensus is that an outlet diameter in excess of 8 (or 10 where particles are highly angular) times the maximum particle diameter suffices (e.g. Rotter, 2001). A lower factor of 6 may be used for rounded materials. Given the hopper half angle flow of granular materials with known values of wall friction and the effective angle of friction may be characterised as either mass flow, funnel flow or mixed flow.

2.6.1.2 Factors that influence the flow behaviour

The amount of solids emerging out of the outlet when it is opened is dependent on several parameters including bulk solids' properties, size and shape of the outlet and the inclination of the hopper (e.g. Fowler & Glastonbury, 1959; Beverloo et al., 1961; Johanson, 1964; Hirshfled et al., 1997; Hirshfled & Rapaport, 2001; Clearly & Sawley, 2002; Goda & Ebert, 2005). These are the major influential factors for a particular silo design with unaided flow. However, in many applications flow in silos may be aided using specially designed feeders. These were not considered in this study and are therefore not discussed any further.

For a filled silo, the overburden stress increases with depth so that the density of solids at transition is higher than that of solids at lower depths. This is reversed in the hopper wherein stresses decrease towards the outlet. In other words, the air-filled voids decrease with increasing depth. Therefore, if the solids are discharged, less dense material move to higher stress level leading to increased air pressure (greater than zero) in the barrel. The air may thus migrate upwards in response to the pressure gradient. On the contrary, in hoppers the solids move from regions of higher pressure and so they have to dilate in order to flow (e.g. Snider, 2007). The dilation of bulk solids means that air void expands leading to an under-pressure (less than zero) condition. Therefore air flows into the material through the opening due to the resultant pressure gradient. Flow of air from the barrel into the hopper is unlikely as the flow resistance due to bulk solids

above the hopper is larger for sufficiently filled high silos. The amount of air pressure gradient is directly related to the particle size, fine- or coarse-grained. The air pressure gradient in the hopper acts in opposite direction to the gravitation force resulting in a decrease in material flow.

In addition to the bulk density, other material properties such as particle size and shape, cohesion (or internal friction angle) and caking potential also influence flow behaviour in silos. These directly affect the consolidation stress and the unconfined yield strength whose ratio gives the measure of flowability (see subsection 2.6.1.1 for more details). In his design charts for flow, Jenike (1960) related the wall frictional angle and internal angle of friction for a given material to the hopper half angle. In subsection 2.6.1.1 it is stated that within the gravitational field the hopper outlet is directly related to the unconfined yield strength, bulk density at critical state and the hopper half angle. This means that for every material and the silo design, and for a given condition flow is related to the hopper outlet. In fact, there exists a minimum outlet for which flow can take place. For cohesionless materials the minimum hopper outlets are chosen to prevent mechanical arching arising from interlocking of particles (Rotter, 2001). Further details are presented in subsection 2.6.1.1.

The other factors which influence the flow behaviour include the silo wall material properties and the environmental conditions such as the presence of moisture. The presence of wall friction and rigid wall respectively means that the bulk solids are never under the action of only principle stress and that they are never in the active state of stress equivalent to the steady-state flow as the solids are constrained to sufficiently dilate in the horizontal direction. The presence of moisture has been reported in many studies to complicate the flow conditions (e.g. Landi et al., 2011). The general consensus seems to be that moisture increases the total cohesion of the material. Increased cohesion translates into increased unconfined yield strength and hence reduced flow factor. As a result a stable arch forms within the hopper thereby stopping the flow of materials. However, the approaches adopted in all these studies are unable to explain the problem of arching arising from the effect of matric suction. Advances in unsaturated soil mechanics have shown that in describing the mechanical behaviour of unsaturated material the boundary stress, suction and water content should all be accounted for independently (see section 2.4 for more details). Arching in silos

containing granular materials usually occurs when moisture accesses into the stored material and forms "liquid bridges" between the contacting particles.

2.6.1.3 Flow rate prediction models

In bulk solids handling the ability to predict the ensuing flow given the hopper geometry and material properties is necessary for a successful design of hoppers and silos. Many equations can be found in the literature to predict the flow rate of bulk solids under gravity conditions. Fowler & Glastonbury (1959) and Beverloo et al. (1961) present and discuss earlier equations. However the one by Beverloo et al. (1961) seems the oldest that is commonly cited and used in the literature. It is at times referred to as the Beverloo law. For circular outlet openings and coarse-grained bulk solids Beverloo et al. stated that the rate of discharge, W is given by Eq. 2-25:

$$W = C\rho_b \sqrt{g}\left(D_o - k_B d_p\right)^{5/2} \qquad \text{Eq. 2.25}$$

where C and k are fitting parameters. With different bulk solids Beverloo et al. found a range of C as 0.55-0.65 and of k_B as 1.3-2.9; these parameters appeared to be influenced by particle shape; averaging about 0.65 and 2.9 for non spherical (sand) and 0.58 and 1.4 for spherical solids (seed particles) respectively. ρ_b is the bulk density of the solids while D_o and d_p are the outlet and particle diameters. g is the acceleration due to gravity. The dimensionless constant, k_B in Eq. 2-25 was intended to cater for a "dead" zone along the wall perimeter of the outlet.

According to Johanson (1964) the mass flow rate from a conical hopper with an outlet cross section area A and diameter D_o should be estimated using Eq. 2-26. This equation can be written as Eq. 2-27 which is general of the form given by Beverloo et al. (1961) with $k_B = 0$ and $C = \dfrac{0.393}{\sqrt{\tan\beta}}$. The suitability of this equation in estimating the flow rate is limited by use of D_o instead of $D_o - k_B d_p$ which serves to reduce the orifice size to an effective size to cater for the so called 'empty annulus'.

$$W = A\rho_b \sqrt{\frac{D_o g}{4\tan\beta}} \qquad \text{Eq. 2-26}$$

$$W = 0.393\rho_b \frac{\sqrt{g} D_o^{5/2}}{\sqrt{\tan\beta}} \qquad \text{Eq. 2-27}$$

Further studies on the matter have tended to concur with Beverloo's law with others making minor modifications especially of the scaling parameter k_B value (e.g. Zhang & Rudolph, 1991; Garcimartin et al., 2006; Mankoc et al., 2007). The proportionality constant is said to depend on the particle size (e.g. Verghese & Nedderman, 1995) and the hopper half angle (Rose & Tanaka, 1959). Mankoc et al. (2007) citing the inability of the earlier equation to predict flow rate over a wide range of $R^* = D_o / d_p$ with consistent accuracy level proposed, for a single type of material, Eq. 2-28 in an attempt to address the gap. They stress that the relevant control parameter is $R^* = D_o / d_p$.

$$W = C'\left(1 - \frac{1}{2} e^{-b(R^*-1)}\right)(R^* - 1)^{5/2} \qquad \text{Eq. 2-28}$$

Compared to Eq. 2-25, the effect of parameters C, ρ_b and $\sqrt{g}$ is represented by coefficient C'. For different diameter materials $W = W_b m_b \sqrt{d_p}$ with W_b as the number of particles collected per unit time and m_b as the mass of a single particle. The fitting parameter b was reported to be equal to 0.051. A correction term $\left(1 - \frac{1}{2} e^{-b(R^*-1)}\right)$ was introduced in place of using the scaling parameter k_B. The British Materials Handling Board uses $k_B = 1.6$ and $k_B = 2.5$ for spherical and nonspherical particles respectively with the typical C coefficient in Beverloo et al. (1961). The hopper inclination is taken into account by a factor $k_\beta = (\tan\beta)^{-0.35}$ for $\beta < 45^o$. For $\beta \geq 45^o$ the factor is equal to 1.0.

2.6.1.4 Flow pattern observation and measurement techniques

The flow pattern of bulk solids has a strong bearing on the distribution of stresses within hoppers and silos and on how the bulk solids actually flow. Its measurement is thus of great value and relevance in bulk solids handling. Methods of measuring flow pattern in silos are given in several studies in published literature. in laboratory scale model tests flow pattern has been measured using radiographic methods in which flow is first stopped, an X-ray taken and then flow continued before it is stopped again (e.g. Cutress & Pulfer, 1967; Bransby & Blair-Fish, 1975). Unwanted errors may however be

introduced by the intermittent flow of material. An improvement to this technique can be found in the published literature. Grantham & Forsberg (2004), for instance, used the digital speckle radiography to measure flow in a silo. Real time digital measurements of continuous flow were performed using continuous X-ray source and an image intensifier and charge coupled device camera. Photography has also been extensively used in the measurement of particle displacements in transparent-wall silos to track a number of particles as they flow (e.g. Pariseau, 1969). In what seems the first full scale model tests, Ooi et al. (1998) used radio frequency tags to measure flow pattern of gypsum in a 250tonne capacity steel silo. The technique of residence time measurements was adopted. It involved mapping out the locations of the radio tags (markers) after silo filling and the time the markers took to reach the outlet.

The technique adopted to measure the flow pattern of bulk solids is dependent on many factors including wall transparency or ability to make direct visual observations through the walls and size of the models used in testing (in Ooi et al., 1998). In the reported work, flow pattern was measured using both visual observations through the transparent silo wall and photography techniques.

2.6.2 Stresses in silos

2.6.2.1 Stresses in a barrel

Knowledge of stress distribution in silos is very important for their successful design. It influences flow of the stored material. The stress distribution in the silo barrel is different from that in the hopper. Consequently, the distribution of stress in the two parts is described using distinctly different theories. The Janssen's theory (Eq. 2-29) is the most commonly and widely used theory in the literature to design cylindrical silo barrels (e.g. Sperl, 2006; Felice & Scapinello, 2010) and forms the basis of most silo design codes for strength (in Schulze, 2008). In the equation, σ_z and σ_n are the vertical and wall normal stresses respectively while z is the depth of the solids. The rest are as defined before and or used in the next few paragraphs.

$$\sigma_z = \frac{\rho g R_B}{2\mu K}\left(1 - e^{-\frac{2\mu K z}{R_B}}\right) \qquad \text{Eq. 2-29a}$$

$$\sigma_n = \frac{\rho g R_B}{2\mu}\left(1 - e^{-\frac{2\mu K z}{R_B}}\right) \qquad \text{Eq. 2-29b}$$

The lateral pressure coefficient K is usually determined for K_0 condition (Pieper & Wenzel, 1963). Such an assumption seems reasonable from at least two standpoints. The presence of wall friction and rigid wall respectively means that the bulk solids are never under the action of only principle stress and that they are never in the active state of stress equivalent to the steady-state flow as the solids are constrained to sufficiently dilate in the horizontal direction. These assumptions are addressed by considering the wall friction in the analysis (e.g. Walters, 1973). It is also demonstrated that compared to the Rankine's active state approach, use of at-rest condition gives better agreement between calculated and measured values of lateral pressure coefficients (e.g. in Schulze, 2008). Janssen in his work proposed a K value of 0.4 while a range of 0.3-0.6 is specified by Schulze (2008) for estimate of the stresses in the silo barrel.

The coefficient of wall friction, μ, defines the interaction between the solids and the silo wall. It is often determined using angle of friction, ϕ_w obtained for the material using a shear tester in which during shearing the surface of the silo wall material forms the failure surface as solids confined in the upper half and under the normal load move relative to the wall surface.

2.6.2.2 Stresses in a hopper

Due to the effect of wall convergence, the stress condition in the hopper is complex. The major principal stress is gradually oriented vertically along the silo axis and deviates from vertical (as in the barrel) towards the wall. As a result the stress state in this part of the silo is called the active state. Unlike in the barrel where stress increase downwards towards the transition from barrel to hopper, in the hopper the reverse is true. Both vertical and wall normal stresses decrease and approach zero at the hopper apex. Discharge of material from a full mass-flow causes the stress state to transit from active to passive (also called arched or emptying). The bulk solids are compressed horizontally as they flow downwards while it dilates in the vertical direction due to downward flow. As a result the larger stresses act in the horizontal direction and the principal stress is oriented horizontally.

In the emptying state, stresses close to the outlet are independent of the stresses in the upper part of the hopper and, therefore, also independent of the silo's dimensions or level of filling. The deformation of the bulk solids while flowing approximates to the

steady-state flow (constant stresses and bulk density) with compression in the horizontal and dilation in the vertical direction thus:

$$K = \frac{1 - \sin\phi}{1 + \sin\phi} \qquad \text{Eq. 2-30}$$

In the barrel the active state of stress remains during emptying, as long as no local convergence exists: such as due to insertions and dents. From the beginning of discharge, the passive stress state develops in the hopper starting at the outlet and, thus, the change from active to passive travel up towards the transition.

2.7 Concluding Remarks

Literature relevant to the current research project has been reviewed and presented. Emphasis was placed on the review of unsaturated granular materials and suction concepts, hydro-mechanical behaviour including the water retention characteristics, stress state variables and the associated failure criteria, elasto-plastic models and other approaches for the description of volumetric behaviour of unsaturated granular materials. The laboratory testing of unsaturated soils is also reviewed and presented. From the literature review areas of uncertainty in, and the contribution of this research project to, the understanding of the behaviour of unsaturated granular materials can be summarised as below.

The validity of the effective stress principle for unsaturated soils outside the saturated capillary regime remains an active area of research. Whereas some believe in its applicability, most researchers are of the view that beyond air-entry value the principle is not valid as unsaturated soil behaves differently when subjected to changes in boundary stress compared to when subjected to equivalent changes in suction. Generally, it is agreed that relative to saturated parameters suction increases shear strength of a material through increased apparent cohesion; the increase is linear within the saturated capillary regime and highly nonlinear beyond the air-entry value. The rate of increase of strength diminishes as suction increases. However, some experimental results have suggested that suction also affects the angle of friction.

Most relationships describing the shear strength of unsaturated soils are based on an extension of a Mohr-Coulomb type failure envelope to include suction as a second variable. The nonlinearity of the relationships is taken into account empirically in the

models using either degree of saturation as an independent variable or some features of the water retention curve or some other curve fitting procedures. However, the hysteresis involved and its dependence on various factors including soil fabric and the constituent particle properties, void ratio, current stress and stress history makes it one of the most uncertain properties of a soil. These factors especially the constituent particle properties have not yet been systematically studied; this makes a lot of room for improvements. Long history of drying-wetting cycles is another factor not yet considered in the determination of hydro-mechanical behaviour of soils.

The flowability of materials in silos has generally been extensively studied and many influential factors have been identified. However, the effect of moisture continues to be bundled with other factors through the use of total stresses approach. Such approaches are shown to be inadequate in describing the mechanical behaviour of unsaturated soils. It is therefore not surprising that moisture induced arching continues to be a serious problem faced by the industry.

CHAPTER THREE

3 MATERIALS, EXPERIMENTAL TECHNIQUES AND PROCEDURES

3.1 General Overview

The purpose of this chapter is to help the reader have an understanding of the materials, experimental techniques and procedures used in this research project. First, the basic properties of the granular materials used within the experimental programme are described. The chapter then continues with the description of the experimental techniques and test procedures of the different tests including pressure plate tests, triaxial compression tests, silo model tests and filter paper tests. The test apparatuses and the experimental setups are however not described here but in chapter 4. The chapter closes with concluding remarks highlighting the major milestones.

3.2 Materials Used in the Investigation

Two (2) granular materials namely sand and glass beads, and distilled water were used in the investigation. The spherical glass beads were purchased in two different size ranges (i.e. 0.25-0.50mm and 0.09-0.15mm) from Sigmund Lindner. Their roundness which is the ratio of length to width was, according to the supplier, greater than 89%. The nonspherical Leighton buzzard sand (LBS1) was obtained from the Structures Laboratory of the Institute for Infrastructure and Environment, University of Edinburgh, United Kingdom. A fraction of the LBS1 was taken to match the 0.25-0.50mm glass beads grading (shown in the next subsection 3.2.1) and is acronymed as LBS2. The visual impression of the difference between the two materials (LBS1 and LBS2) can be seen from Fig. 3.1 of their microscopic images. From the figure, it is evident that there is more than one qualifying size for each particle and therefore comparing material particle size/grading based on results of sieve analysis alone could lead to misleading conclusions. Since particle shape was a subject of investigation, it was important that the shape factor for each material was obtained. It is the ratio of the equivalent spherical diameter to their average screen size of the particles (e.g. Beverloo et al., 1961) and is also termed form factor (e.g. Verghese & Nedderman, 1995). The equivalent spherical particle diameter is often determined from the specific surface area (SSA) and the void proportion (either porosity or void ratio) of the packed system of materials of known grading.

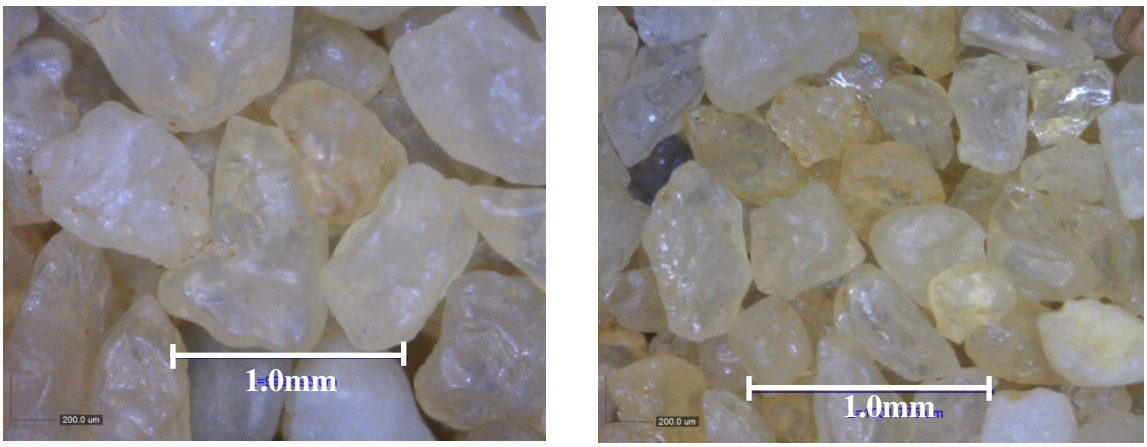

(a) LBS1 (b) LBS2

Figure 3.1: Microscopic images of LBS1 and LBS2 (Taken with magnification X210)

In absence of the directly measured value, the operator-independent approach of Chapuis & Legare (1992) may be used to estimate the SSA of non-plastic granular materials from their grading curve. It was adopted in the current study since it accurately estimates the SSA of non-plastic materials (Chapuis & Aubertin, 2003). The next step was to determine the equivalent mean spherical particle diameter, D_{50eq} of the nonspherical particles. The Kozeny-Carman formula is one common approach used to determine D_{50eq} from the SSA (e.g. Fowler & Glastonbury, 1959; Beverloo et al., 1961; Carrier, 2003). In the formulation, the nonsphericity of the particles is taken into account by introducing a transformation factor F in the SSA equation ($SSA = F/D_{50C}$) to account for the particle shape, roughness and projections (Carrier, 2003). The quantity D_{50C} is the mean particle diameter determined from the particle size distribution curve, say, using the method provided in Carrier (2003). The F factor (and also SSA if needed for comparison with the one obtained using the method of Chapuis & Legare, 1992) can then be back calculated from the experimentally measured permeability coefficient k_{sat} using the Kozeny-Carman equation. Empirical values of F have been proposed by many authors (e.g. Fair & Hatch (1933); Loudon (1952) in Carrier, 2003). With F and indeed D_{50eq} known, the shape factor is obtained. The obtained shape factors are presented in Table 3-1. A comparison is also made between the quantities estimated based on the approach of Chapuis & Legare (1992) with those estimated using the Kozeny-Carman method detailed in Carrier (2003).

Table 3-1: Specific surface area and particle shape factor of glass beads and sand

Material	Measured k_{sat} (cm/s)	Chapuis & Legare (1992)		Kozeny-Carman method		
		SSA (1/cm)	[a]Estimated k_{sat} (cm/s)	Back calculated SSA (1/cm)	Back calculated F (-)	SF (%)
GBS1	0.0596	204.3	0.0541	192.5	6.36	94.3
GBS2	0.0089	469.2[b]	0.0096	489.4	6.02	99.7
LBS1	0.1157	175.0	0.0776	143.4	7.30	82.2
LBS2	0.0673	203.7	0.0734	211.8	7.17	83.3

Notes: [a]After obtaining the SSA permeability is estimated using the Kozeny-Carman method; k_{sat} is the saturated permeability coefficient; SSA is the surface area; F is the transformation factor to take into account the particle shape, roughness and projections; SF is the shape factor and [b]means grading curve was determined using mastersizer.

As shown in Table 3-1, the particle shape factor of 94.3% for the 0.25-0.50mm glass beads and 99.7% for the 0.09-0.15mm glass beads obtained using Kozeny-Carman method satisfies the supplier-provided value of the particle sphericity. The 0.25-0.50mm beads are identified as Type I (acronymed as GBS1) and used as *reference* glass beads while the others are Type II glass beads (GBS2). High sphericity glass beads with distilled water were chosen to give simple and well defined wet granular assemblies where the observed response can be attributed to purely glass-glass and glass-water interaction without the presence of other complex interactions often present in unsaturated soils and other industrial bulk solids.

Compared to glass beads, Leighton Buzzard sand (LBS1) was a low sphericity material; its average sphericity determined using the Kozeny-Carman was 82.2% increasing to about 83.3% for LBS2 (Table 3-1). It is interesting to note that the SSA obtained from the particle size distribution curve based on the work of Chapuis & Legare (1992) agrees well with those estimated using the Kozeny-Carman method. In addition, the Kozeny-Carman method satisfactorily predicted the experimentally measured saturated permeability coefficient with the SSA obtained using the Chapuis & Legare (1992) method. This level of agreement in results obtained with different methods is a manifestation that the obtained shape factors are satisfactorily accurate. They will be used to convert the mean particle diameter determined from sieve analysis (Table 3-2) to their equivalent mean spherical particle diameters when discussing particle size and shape effect on other measured behaviour.

Particle size and distribution is one common approach used to compare and group the behaviour of unsaturated soils (e.g. Yang et al. 2004; Kawajiri et al., 2010). Mixing of distinctly different soils (e.g. Arya & Paris, 1981; Hoffmann & Tarantino, 2008) and splitting one soil sample into groups of samples (e.g. Imre et al., 2006; Somasundaram et al. 2006) are also common in investigating the effect of particle size and distribution on unsaturated behaviour. The dependence of particle sphericity on the particle screen size of Leighton Buzzard sand suggests that such approaches may give misleading results as the tacit assumption of other factors being insignificant is probably unrealistic.

It should be noted that the granular materials used in this study have been some of the major test materials in the study of the behaviour of industrial bulk solids at the University of Edinburgh. In addition, sand has a long history of laboratory study of the behaviour of soils among the geotechnical and petroleum engineering communities. Therefore, in discussing their behaviour reference can be made to the existing information.

The physical and geotechnical properties of the test materials were determined as part of the experimental programme of this research project except where otherwise stated. The following parts of this section are dedicated to the presentation and description of the properties of the two test materials.

3.2.1 Classification/Grading Characteristics

Particle size distribution analyses (BS 1377, 1990) were carried out for a basic understanding of the materials used in the current research project. Fig. 3.2a and Table 3-2 show the particle size distribution curves and a summary of the physical and geotechnical properties, respectively, of the used glass beads and sand. The chemical properties (provided by the supplier) are included in Table 3-2 for clarity and completeness only. In their state the materials were chemically inert and therefore free from any chemical effects.

As the standard method of sieve analysis was unable to give the particle distribution of Type 2 glass beads (GBS2) a mastersizer was used. This provided an opportunity to compare and contrast the results (Fig. 3.2b) from the two methods. The GBS1 grading curve from sieve analysis was expected to be similar to the one obtained using a mastersizer given that the material was spherical. The dry dispersion method was used.

It was noted that whereas the two methods gave similar results for GBS1 in terms of mean particle size the mastersizer tended to overestimate the particle sizes greater than the mean size and to underestimate the sizes less than the mean particle size. As for sand, the mastersizer overestimated all particle sizes thereby shifting the grading curve to the right relative to the sieve analyses results. Considering that output from the mastersizer is highly dependent on the projected face of the particle and that the necessary parameter of refractive angle was simply assumed, the standard method of sieve analysis (BS 1377, 1990) was adopted to provide the particle size distribution of the tested materials except for GBS2 where sieve analysis was not applicable.

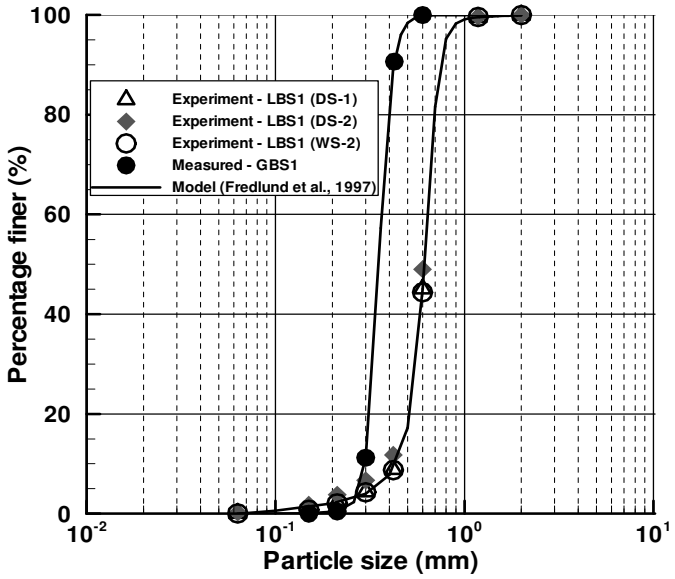

(a) Sieve analysis method

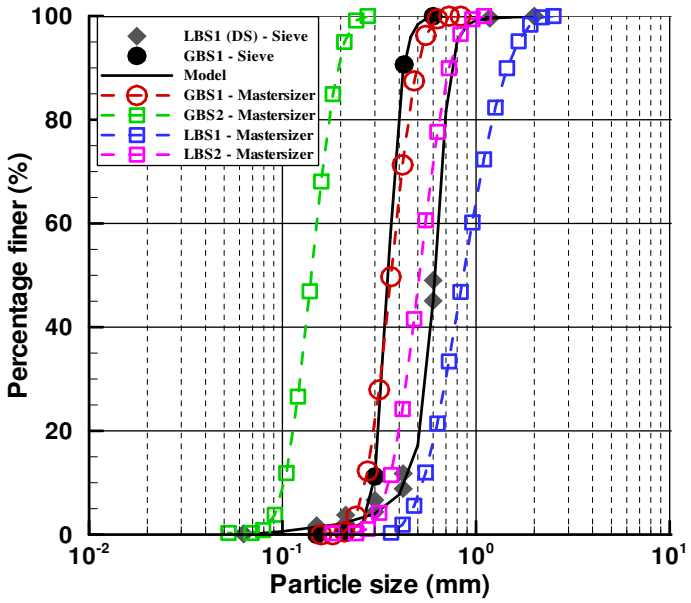

(b) Sieve analysis and mastersizer methods

Figure 3.2: Particle size distribution curves for the materials used in the investigation

Table 3-2: Physical and Grading characteristics of the glass beads and sand

Sample	Sand	Modified sand	Glass beads	
	LBS1	LBS2	Type 1	Type 2[b]
Particle Size Distribution (%)				
Coarse sand sized particles	53	0	0	0
Medium sand sized particles	44	100	100	0
Fine sand sized particles	3	0	0	100
Grading Characteristics				
D_{10} (mm)	0.400	0.29	0.29	0.089
D_{30} (mm)	0.500	0.33	0.33	0.113
D_{50} (mm)	0.610	0.35	0.35	0.123
D_{60} (mm)	0.700	0.36	0.36	0.135
$C_u = D_{60} / D_{10}$	1.75	1.24	1.24	1.517
$C_z = \frac{D_{30}^2}{D_{10}.D_{60}}$	0.893	1.04	1.04	1.063
Specific Gravity, G_s	2.67	2.67	2.50	2.50
Compaction Characteristics				
$\rho_{d\max}$ (Mg/m^3)	1.566	1.476	-	
w_{opt} (%)	9.4	9.4	-	
$\rho_{\max}$ (Mg/m^3)	1.743	1.743	1.630	
$\rho_{\min}$ (Mg/m^3)	1.459	1.459	1.471	
Particles per kilogram ($\times 1000$)	-	-	14,486.6	-
Chemical composition*				
SiO_2		94.6	72.50	
Na_2O		0.66	13.00	
CaO		0.07	9.06	
MgO		0.11	4.22	
Al_2O_3		1.52	0.58	
Others		3.06	0.64	

Notes: D_{10}, D_{30}, D_{50} and D_{60} are particle diameters such that 10%, 30%, 50% and 60% respectively are finer; C_u = coefficient of uniformity; C_z = coefficient of grading; $\rho_{\max}$ = maximum density; $\rho_{\min}$ = minimum density; w_{opt} =optimum moisture content; $\rho_{d\max}$ = maximum dry density; [b]grading characteristics obtained using mastersizer; *chemical composition of sand was obtained from www.garside-sands.com (accessed 25/05/2012)

As can be seen from Table 3-2 and the grading curves (Fig. 3.2), the Type I glass beads are comparable to medium sand in terms of particle size (BS 1377, 1990). This uniformly graded material (C_u = 1.24) which is specified by the supplier as one

comprising particles within the size range of 0.25-0.50mm has an effective size (D_{10}) of 0.29mm. Its mean particle size (D_{50}) is 0.35mm, slightly less than the 0.375mm provided by the supplier. Likewise, the Type II glass beads (having particles within 0.09-0.15mm size range according to the supplier) are comparable to fine sand with 99.7% passing 150μm BS sieve and retained on 63μm BS sieve. The specific gravity, G_s of the glass beads determined at 22°C using the small Pyknometer method (BS 1377, 1990) affirmed the value of 2.5 specified by the supplier.

The Leighton buzzard (light-brown silica) sand comprises 53% coarse sand, 44% medium sand, and 3% fine sand (Table 3-2). It is free of silt, clay and organic matter and has particle sizes between 0.063mm and 1.18mm with the 90% proportion of material in the narrow band of 0.425mm to 1.18mm (Fig. 3.2). It is generally fine-grained cohesionless soil with specific gravity of 2.67, determined at 22°C using the small Pyknometer method (BS 1377, 1990). Its coefficient of uniformity is 1.75 while the effective size is 0.4mm. The material retained on the 2.0mm sieve is 0% and mean particle diameter is 0.61mm. Based on the standard method of soil classification for engineering purposes (USCS), the test material falls in the class of poorly graded (uniform) sandy soil and its USCS symbol is SP.

It should be noted that the experimental data for sand (Fig. 3.2) was obtained from tests on samples taken from different parts of the test material to assess the spatial variability of the particles. The particle size distribution results were found to be independent of spatial location. The particle size distribution results for two of these samples (DS-1 and DS-2) determined by the dry sieving method and that for one of the samples (WS-2) determined by the wet sieving method are evidently the same. Therefore it is plausible to conclude that the particles constituting the sand are individual *clean* particles and not agglomerates of smaller particles, and that practically identical samples were prepared regardless of which portion of the material was used.

Almost similar properties have been reported in previous studies. Lings and Dietz (2004), for instance, reported the specific gravity for this sand as 2.651. In their study, the effective size and mean particle diameter for the fraction of material between Standard sieves No. 14 (1.4mm aperture size) and No. 25 (0.71mm aperture size) was 0.64mm and 0.78mm respectively and the coefficient of uniformity was 1.27. It should

be noted that if the results of the present study are analysed within the proportion considered by Lings and Dietz then the effective size and mean particle diameter would respectively be 0.705mm and 0.75mm. The coefficient of uniformity would be 1.09. The specific gravity does not depend on the proportion of the sand tested and would thus be expected to remain the same unless the tests were performed at changing temperature conditions. Lings and Dietz did not report the temperature at which they did their tests.

The Fredlund et al. (1997) model (Eq. 3-1) was found to satisfactorily describe the experimental points of the particle size distribution curves for the two test materials (Fig. 3.2). The least squares curve fitting parameters are presented in Table 3-3.

$$P(d) = \frac{100}{\ln\left[\exp(1) + \left(\frac{g_a}{d}\right)^{g_n}\right]^{g_m}} \left[1 - \left\{\frac{\ln\left(1 + \frac{d_r}{d}\right)}{\ln\left(1 + \frac{d_r}{d_m}\right)}\right\}^7\right] \qquad 3\text{-}1$$

where $P(d)$ is the percent passing a particular grain size, d (mm), g_a is the fitting parameter corresponding to the initial break in the grain size distribution curve, g_n is the fitting parameter relating to the maximum slope of the particle size distribution curve, g_m is the fitting parameter corresponding to the curvature of the particle size distribution curve, d_r is the residual particle diameter (mm) and d_m is the minimum particle diameter (mm). The particle size distribution curve fitting parameters can be utilised in the estimation of the water retention curves for particulate materials (e.g. Fredlund et al., 1997).

Table 3-3: Least squares curve fitting parameters of the Fredlund et al. (1997) model

Parameter	Glass beads (GBS1)	Glass beads (GBS2)	Leighton Buzzard sand (LBS1)	Modified Leighton Buzzard sand (LBS2)
g_a	0.3428	0.1235	0.6562	0.3428
g_n	11.4012	6.7158	12.8689	11.4012
g_m	3.1884	2.2668	1.3529	3.1884
d_r	0.1468	0.1112	11.3802	0.1468
d_m	0.0236	0.0628	0.0651	0.0233

Many a time materials are grouped and compared based on parameters obtained using different techniques. In an attempt to obtain the grading of GBS2 a mastersizer was used. To make sure that the obtained grading was reliable and representative of the actual part size distribution and similar test was conducted GBS1 whose grading curve had been obtained using sieve analysis. Whereas the mean particle size was almost the same the two methods gave different results of the other grading characteristics (Fig. 3.2b). As it was the mean particle size that was the main parameter the effect of using the mastersizer results was thus inconsequential.

3.2.2 Compaction Characteristics

The compaction tests were performed on Type I glass beads and sand to understand their compaction characteristics. For glass beads, only the maximum and minimum densities were determined (Table 3.2) using the methods for sands whose particles are not susceptible to crushing outlined in the BS 1377 (1990). From the maximum and minimum densities the minimum and maximum void ratios were respectively computed as 0.53 and 0.70.

The standard Proctor tests (BS 1377, 1990) on sand yielded $1.566\,Mg/m^3$ as the maximum dry density, $\rho_{d\max}$ at optimum moisture content, w_{opt} of 9.0%. These compaction characteristics were obtained using the $2.5\,kg$ mechanical rammer method outlined in the BS 1377 (1990). The compaction curve including the 100% degree of saturation (zero-air voids) line is shown in Fig. 3.3a from which the difficulty associated with obtaining considerable compaction through dynamic compaction of this type of sand is evident. Fig. 3.3b shows a zoom-in of the compaction curve. To two decimal places, the results show a large scatter especially so on the dry of optimum. The hand-drawn compaction curve used to fit the experimental data is far from the zero-air voids line implying that with the method used a lot of air remained in the sample voids. These results are perhaps a reflection of the observed behaviour of the sand in the compaction mould during compaction. Dropping the rammer in a particular position caused particles in other positions to displace upwards in a spongy manner.

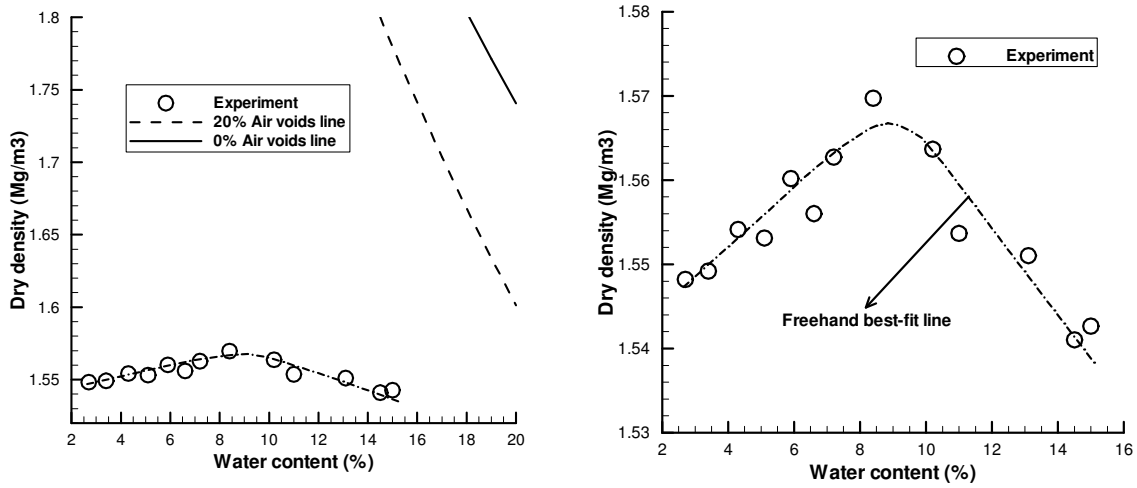

(a) Compaction test results (b) Enlargement of the compaction curve

Figure 3.3: Compaction results for Leighton buzzard sand (LBS1)

Like the Type I glass beads, the range of achievable compaction was assessed by determining the maximum and minimum densities. The methods for sands that are not susceptible to crushing (BS 1377, 1990) were used. Presented in Table 3.2, the maximum and minimum densities were found to be 1.743 and 1.459 respectively corresponding to the minimum and maximum void ratios of 0.53 and 0.83.

3.3 Experimental Techniques and Test Procedures

3.3.1 Pressure plate tests

3.3.1.1 Apparatus and the preliminary operations

The pressure plate extractor used in the determination of water retention curves of the test materials was a 15bar extractor. It was a 1500F1 model supplied by Soilmoisture Equipment Corporation. The imposed air pressure and water pressure were measured using transducers accurate to 1.0kPa. Water pressures less than 1.0kPa were controlled taking advantage of the hydrostatic pressure head in the connecting water tube. Further details of the pressure plate setup are presented in section 4.3, chapter 4. Preliminaries performed ahead of any tests included saturation of the high air-entry ceramic plate, water lines and the GDS pressure/volume controller. These are highlighted in subsection 4.3.1. The pressure plate uses axis-translation technique (Hilf, 1956) to control matric suction. Details of the axis-translation technique are presented next.

3.3.1.2 Experimental Technique

As stated in the preceding subsection, pressure plate uses axis translation technique to impose and control matric suction (Hilf, 1956). Details of the experimental procedures followed are presented later in subsection 3.3.1.4. The technique involves translating the reference conditions for pore water pressure in the sample from atmospheric conditions to an artificially increased pressure environment. Consequently, the pore water pressure increases by the same amount leaving matric suction, which at equilibrium is the difference between the applied air pressure and water pressure, unaffected by the translation. This is however so only if water and the solid particles are incompressible or assumed so in which case the curvature of the menisci would not be affected (e.g. Fredlund & Rahardjo, 1993). This assumption seems reasonable in the case of granular materials such as glass beads and sands. Translation of the pore water pressure into the positive range facilitates its control (e.g. Delage et al., 2008) and the value by which the pressures are translated depends on the desired suction levels. The pressure difference across the ceramic interface is achieved owing to the ability of the saturated high air-entry value ceramic plate to prevent free air phase above the ceramic plate from entering into the liquid phase beneath the plate, and because of water continuity the water pressure in the sample is equal to the water pressure just below the saturated ceramic plate. Exposing the sample surface ensured the necessary continuity between the air in the sample and that from the air compressor through the air pressure regulator.

3.3.1.3 Sample preparation

The pressure plate test samples were prepared directly on a saturated 1500kPa air-entry ceramic plate in 38.6mm diameter and 10.5mm height moulds. All the samples were prepared using oven dried material. Careful tamping was conducted on each sample to achieve the desired initial void ratios and relative densities shown in Table 3-4. The dry mass, measured using a digital balance accurate to 0.01g, was used to ensure that the desired initial sample void ratio was achieved. The samples were then saturated prior to starting the determination of the drying path of the water retention curve (WRC). For all the samples saturation was carried out by carefully supplying distilled water at the contact point between the mould and the ceramic plate using a syringe pipe fitted with a needle. Therefore as water entered into the sample it displaced the air from the voids. It was however not possible to accurately verify the saturation water content owing to the high permeability of the tested materials. Nonetheless, as will be shown in chapter 5, the measured water contents within the capillary bridges zone indicate that a satisfactory

saturation was achieved. The pressure plate vessel was then tightly closed and the pressures imposed as described in the next subsection.

It should be acknowledged that even with the care exercised some of the actual void ratios and hence relative densities achieved slightly departed from the desired values, with all the initial void ratios falling in the range of ±0.01 of the reported values. If this void ratio was insensitive to the errors associated with the accuracy of measured mass and the effective total sample volume then the variation in void ratio with such a narrow range is considered not to have significantly affected the subsequently measured behaviour. An assessment of the sensitivity of void ratio to the possible errors in the measured dry mass and in the effective sample volume is discussed in the next paragraphs.

Table 3-4: Initial void ratios and relative densities of the pressure plate test samples

Material	Initial void ratio (-)	Relative density (%)
Glass beads	0.55	88
Sand	0.62	70
Modified sand	0.56	90

The void ratios reported in Table 3-4 were computed using Eq. 3-2 in which the mass density of water ρ_w, internal volume of the mould, V and the specific gravity, G_s are constant. Any errors in void ratio are thus attributable to the errors in either the measured dry mass, M_d of the material or failure in surfacing the material level with the top of the mould. When preparing the samples care was taken to level the sample surface with the top of the mould. It is therefore plausible to assess the sensitivity of the void ratio to errors in the measured dry mass as well as in the effective total volume of the material. To do this the derivatives of Eq. 3-2 with respect to mass (Eq. 3-3) and volume (Eq. 3-4) were used.

$$e = \frac{VG_s\rho_w}{M_d} - 1 \qquad 3\text{-}2$$

$$\Delta e = -\frac{VG_s\rho_w}{M_d^2}\Delta M_d \qquad 3\text{-}3$$

$$\Delta e = \frac{G_s \rho_w}{M_d} \Delta V \qquad 3\text{-}4$$

where Δe, ΔM_d and ΔV are errors in void ratio, dry mass and total volume respectively.

The sensitivity of void ratio to the measured dry mass and total volume of the sample follows a linear relationship (Eq. 3-3 and Eq. 3-4 respectively). The error limits in the reported initial void ratios are evaluated considering the accuracy of the mass measurements and levelling of the material surface with the top of the mould. The digital balance used to measure mass was accurate to 0.01g thus limiting the errors in void ratio to ±0.0004. This error limit is small compared to that of ±0.0487 arising from the possible errors in the effective sample total volume, determined assuming a maximum error in the effective height corresponding to the mean particle diameter of the reference glass beads. A bigger error would be expected when samples of larger particles are prepared.

Assuming that the errors from the two sources are additive, then the actual range of initial void ratio in this investigation is ±0.0591 of the values reported in Table 3-4. Such a range of the initial void ratio may be sought to bear a significant effect on the measured water retention behaviour. However, as will be shown in chapter 5 the experimental data shows that varying the initial void ratio from 0.55 to 0.62 had only slight effect on the measured water retention curve except within the saturated capillary zone. It is therefore concluded that the unavoidable discrepancies in the initial void ratio did not significantly affect the measured water retention curves especially given that the case examined here is the worst possible that would be highly unlikely. This conclusion is reinforced by the fact that the measured WRCs were remarkably reproducible with the approach used to prepare test samples. Practically the same results were obtained for identical samples prepared with the same initial void ratio (experimental evidence presented in chapter 5).

3.3.1.4 Test Procedure

Pressure plate tests to measure WRC commenced immediately following the completion of sample preparation (see the preceding subsection 3.4.1.3). After imposing the target pore pressures, each sample was allowed sufficient time to achieve

equilibrium. The equilibrating time was carefully investigated using the reference (Type I) glass beads and taken to be when the sample water content change was not more than 0.1% in 24hours. Fig. 3.4a shows the location of the points investigated on the WRC while the results are presented in Fig. 3.4b. The time to reach equilibrium was found to be a function of matric suction. Typically, the samples took about 7 days to approach equilibrium at 2kPa while only about 4 days were necessary at 30kPa. The dependence of equilibrium on matric suction notwithstanding, equilibrium was considered at 7 days in all the tests. After equilibrium, gravimetric water content was determined by oven drying at 105°C.

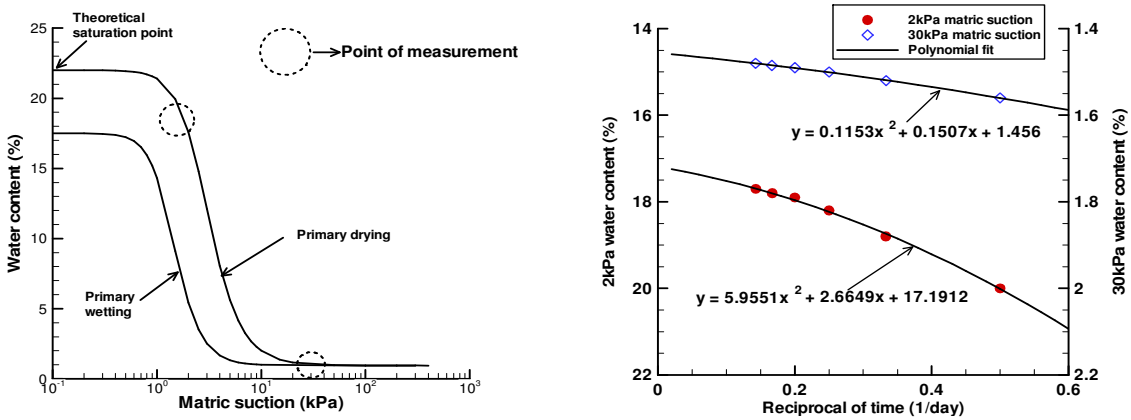

(a) Location of measured points (b) Time history of water content

Figure 3.4: Equilibrium time test results for the reference glass beads

The equilibrium of ≤0.1% water content change in 24hours was chosen arbitrarily to give realistic measurements of water content within reasonable equilibrium time. If however, the samples were allowed more time to equilibrate further change in water content was possible (Fig. 3.4b). Based on the polynomial equations used to best-fit the measured data, extending the equilibrium time to 14days and 56days, the respective additional change in water content would be about 0.3% and 0.5% for the 2kPa matric suction and about 0.1% and 0.2% for the 30kPa matric suction. The effect of such small changes in water content may be ignored without significantly affecting the measured behaviour.

3.3.2 Triaxial compression tests

3.3.2.1 Apparatuses

Two triaxial apparatuses were used to study the mechanical behaviour of granular materials in the current research project. Description of the first one, the conventional

triaxial apparatus and the associated test procedure are omitted here as they are given in many textbooks (e.g. Head, 1986). It was used to determine the saturated and dry behaviour. The other apparatus is the unsaturated triaxial equipment used in the determination of the unsaturated behaviour.

A full description of the unsaturated suction-controlled triaxial apparatus is provided in chapter 4. It was a double-wall triaxial cell instrumented to independently control the pore water pressure and the pore air pressure. In addition, the pore water volume and total volume changes during testing were also measured independently. These quantities are necessary and crucial quantities for the analysis and interpretation of unsaturated triaxial tests results. It was also possible to flush out any diffused air in the course of the test. For more details about the unsaturated triaxial apparatus the reader is referred to subsection 4.2 of chapter 4.

3.3.2.2 Preliminary Operations

(a) System saturation

Each time a test was due, saturation of the high air-entry ceramic disk, water lines, water pressure transducers and volume change transducers was ensured. This was intended to ensure that there was no entrapped air bubbles within the water lines. Air bubble entrapment leads to erroneous volume change measurements. The procedure for the initial saturation of the ceramic disk was based, in part, on the one outlined in Fredlund & Rahardjo (1993) and that proposed by Tarantino & Mongiovi (2001). Details of the procedure followed are presented in subsection 4.2.2 of chapter 4. After initial saturation, the ceramic disk and all the water lines were kept saturated. Nonetheless, it was a routine to resaturate the ceramic disk and to replace all the water used in the previous test.

(b) Setting up the Software for Control and Data Acquisition

The software was setup for control and data acquisition by defining the test stages or sequences and initialising the physical values of all the transducers and the sample dimensions. It was not necessary to enter the calibration factors each time a test was carried out. The calibration factors for all the transducers were entered into the system only once, at the time of calibration. Details are presented in subsection 4.2.3. Data scanning was then run followed by control of the pressures as required.

3.3.2.3 Experimental Technique

In triaxial compression tests, matric suction was imposed and controlled using the axis translation technique (Hilf, 1956), as was in water retention curve tests. Details of this experimental technique are presented in subsection 3.3.1.3. The suitability and justification for the choice of axis translation over the other two available techniques (osmotic and vapour equilibrium) have been presented in subsection 2.5.2 of this thesis, wherein the three (3) well established techniques for imposing and controlling suction in the laboratory testing of unsaturated materials are compared and contrasted.

As noted in subsections 2.5.3.3 and 2.5.5 air diffusion is a serious operational challenge when using axis translation technique to control suction. It affects the accuracy of the measured volumes and may increase the equilibration time. The level of errors in the measured volumes is dependent on the applied air pressure (Padilla et al. 2006). For 10% of the air-entry value of the 15bar disk, air diffusion rates have been reported to range from $0 cm^3/day$ to about $0.2 cm^3/day$ (see Padilla et al., 2006). The values of matric suctions relevant to this part of study were in the range of 0-100kPa. As such air pressure was limited to about 150kPa, a value corresponding to 10% of the 15bar ceramic disk used. With such low values of air pressure the challenges of air diffusion were inconsequential. Nonetheless, for the matric suction of 100kPa flushing was routinely carried out every three days of test running.

3.3.2.4 Sample preparation

(a) Obtaining a cylindrical sample

To obtain a cylindrical test sample for the triaxial compression test, the following steps were observed. Firstly, the pedestal and top cap were cleaned with ethanol before grease was lightly applied to the pedestal. Next, one end of the latex membrane was fastened on the pedestal using two o-rings. The grease provided additional seal between the stainless steel parts and the membrane. Fig. 3.5a shows a clean pedestal (with the glued high air-entry ceramic disk already saturated) before placing the membrane. A two-split mould was then mounted on the pedestal, the membrane adjusted to have its free end folded back over the rim of the mould and fastened with an o-ring (Fig. 3.5b). A vacuum of 1kPa was then applied to the mould so that the membrane was pulled to the mould. The next step was now to prepare and put material in the mould.

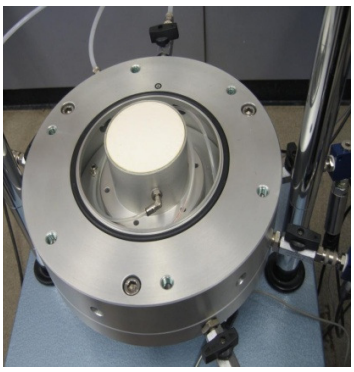

(a) Clean pedestal

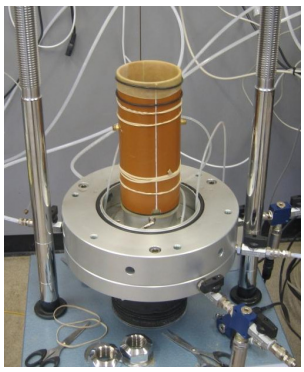

(b) Split mould with membrane folded over

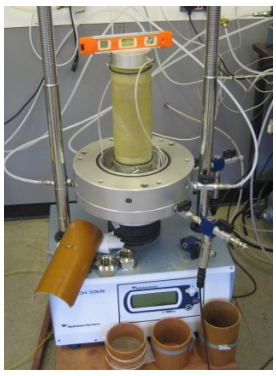

(c) Stiffened self standing sample

Figure 3.5: Steps for the triaxial compression test sample preparation

A known quantity of dry material slightly more than sufficient to make the sample was prepared. Depending on the desired moisture condition, an amount of distilled water was gradually and incrementally sprayed on to the prepared dry material and the two mixed thoroughly until it appeared uniform. To avoid excessive local wetting, water was added in increments of about 1-2% by dry mass and alternated with mixing. The mass of the mixed material was regularly checked by weighing and any water lost due to evaporation was compensated by adding more water. Sample preparation water content was chosen based on the material water retention curve such that when a particular suction was controlled a substantial amount of water moved out of the sample before it approached equilibrium. The material was then put in the forming jacket depending on whether it was dry or moist. The approach adopted in each case is described in the next subsection. Regardless of initial sample moisture condition, the material used to form the sample was measured as it was put in the forming jacket. Care was taken not to lose any particles of the material. Tamping was occasionally conducted on each layer to achieve the desired dry density uniformly distributed along the height of the sample. The material was compacted to a void ratio similar to that in the pressure plate and silo model tests.

After filling the forming jacket to the desired height, a low air-entry porous stone and the top cap were then put in place. The top cap was then lightly greased and the membrane rolled up and fastened on to the top cap using two o-rings. The vertical and horizontal alignments of the mould and the top cap respectively were then confirmed using an appropriate spirit level. As shown in Fig. 3.6, vacuum of about 18kPa was then applied to the sample for about 15-20minutes while keeping the pore water line closed

to enable the sample to stiffen and stand on its own. Note that at this stage the pore air pressure transducer measured the applied vacuum. Closing the pore water line limited transfer of unmeasured water into the sample from water compartment underneath the saturated high air-entry ceramic disk. Water migration into the sample at this stage would alter the initial moisture condition in the bottom part of the sample thereby probably impacting the subsequent behaviour.

The split mould was then removed and the cylindrical sample preparation was complete. Fig. 3.5c shows a stiff self standing sample. The range of initial dry densities for the samples tested in this research project is 1.592 to 1.623Mgm^{-3}. Dry density was computed from the dry mass of the sample and the stiffened self standing sample dimensions.

Finally the cell was put in place and the two cell compartments simultaneously filled with de-aired water prior to gradually applying a confining stress of about 20kPa to the sample (Fig. 3.6). 20kPa is the confining stress commonly used to saturate samples in the standard triaxial testing of cohesionless materials (e.g. Head, 1986). While the confining stress was applied, the vacuum was decreased by almost equal amount so that the net stress holding the sample together remained between 18 and 20kPa (Fig. 3.6). Testing of the sample then followed. Details of how tests were carried out are presented in subsection 3.4.2.6.

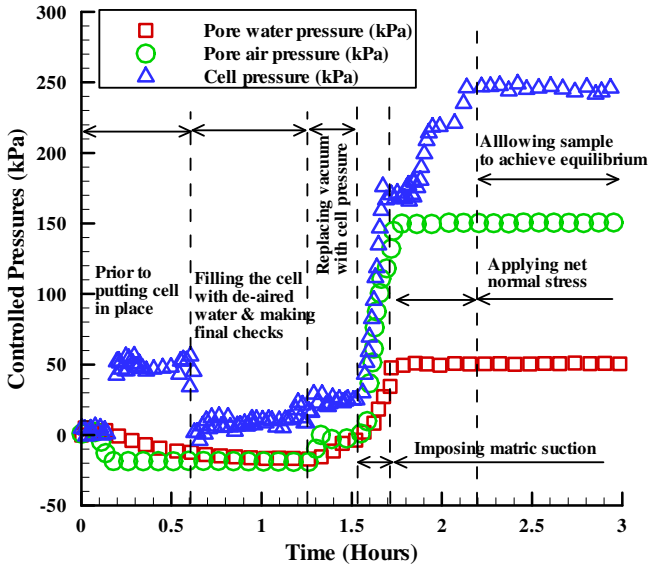

Figure 3.6: Typical pressures applied during triaxial compression sample preparation

3.3.2.5 Density distribution control techniques

In this subsection the procedure employed to ensure that the desired initial sample conditions were achieved is described. Overall two (2) general categories of initial sample conditions were considered in the current study. They are (a) a dry sample with uniform density distribution, and (b) a moist sample with uniform density distribution. These two, described below, were considered in the triaxial compression tests.

(a) Procedure for dry sample with uniform density distribution

Fig. 3.7 shows the procedure employed to come up with the uniform density distribution sample prepared with dry material. This procedure will be referred to as the *tamped air pluviation* technique. It can be considered a modified version of the air pluviation technique used by many researchers (e.g. Yumamuro & Wood, 2004). In the procedure, after applying vacuum between the mould and membrane the smallest aperture-size sieve to pass 100% of the material under consideration was placed on top of the mould (Fig. 3.7). For instance while a 2.0mm BS sieve was used for sand (maximum particle size was retained on the 1.18mm sieve and passed through the 2.0mm sieve) a 600μm BS sieve was used for the *reference* glass beads whose maximum particle size passed the 600μm sieve but was retained on the 425μm sieve. A hard plastic paper disc was then put on top of the sieve to cover in excess the bore of the forming jacket. A 50mm high mould and having same internal diameter as the main sample mould was put on top of the plastic disc. Dry material of predetermined mass was then carefully filled in the 50mm high mould. Carefully pulling out the plastic paper disc allowed the soil to "rain" into the sample mould through the sieve.

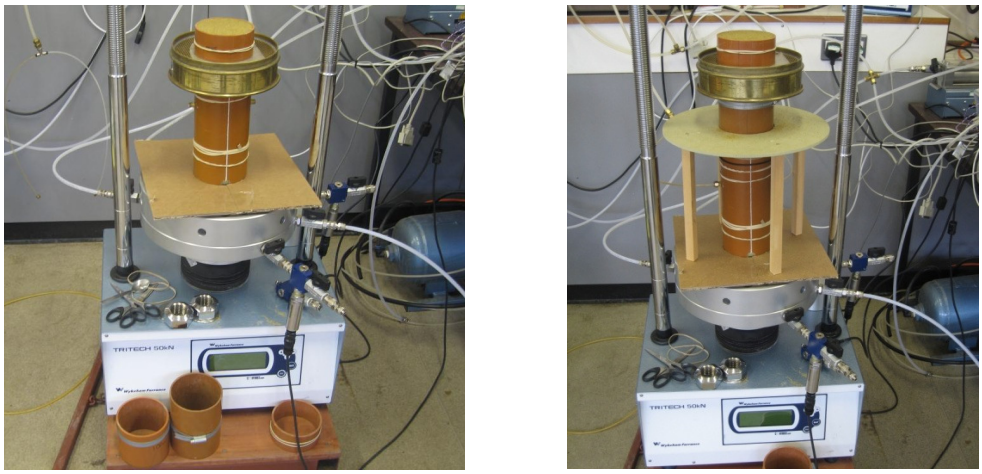

(a) Setup for the first quarter (b) Setup for the final quarter

Figure 3.7: Set up for making a sample with uniform particle and density distribution

To control the falling distance of the particles, the sample was prepared in 4 layers of 50mm each. Through trial and error this number of layers was found to produce relatively uniform density along the sample height. After "raining" the first 50mm of sample, the height of the mould was adjusted by adding a 50mm high mould-spacer between the main sample mould and the sieve. Fig. 3.7b shows a setup for applying the final layer. The platform at the base of the mould helped in recovering any particles that dropped in the process.

(b) Procedure for moist sample with uniform density distribution

In the preparation of a moist sample with uniform density distribution, particles were not rained but rather deposited using a big spoon. This is because unlike with dry material the particles in moist material were not susceptible to segregation as the water kept them held together. Like in the previous procedure, the sample was also prepared in 4 layers of 50mm each. This was to control packing of the particles. In each of the layers, the quantity of material necessary to achieve the desired density was compacted. The continuity between the different layers was ensured by first scarifying (roughening) the surface of the completed layer before adding the next one.

3.3.2.6 Experimental procedure

Unsaturated suction controlled tests were carried out on samples prepared using the method described in subsection 3.3.2.4. The experimental procedure involved testing samples at different suctions. In a typical test, the necessary pressures were controlled to impose suction and the net normal stress. The output from two transducers: pore water volume and total volume transducers were monitored for equilibrium before shearing the samples. With respect to both air and water drainage conditions, only drained tests were performed owing to high permeability of the granular materials. In all the tests samples were sheared at equilibrium having moved from higher water content under particular matric suction. The tests consisted of four (4) distinct stages: initial stage, isotropic compression stage, shearing (deviator) stage and the dismantling stage. These are described one after the other in the following parts of this subsection.

(a) Initial Stage

The initial stage commenced immediately after sample preparation. It helped to move the net normal stress and suction toward their desired initial testing values. The procedure was achieved by gradually and simultaneously raising the pore air and cell

pressures while keeping their difference termed the net normal stress at about 20kPa. This is the confining stress recommended for saturation of conventional triaxial compression test samples of granular materials (e.g. Head, 1986). The increase in pore air pressure was immediately reflected in the pore water pressure output, a confirmation for the continuity between water above the saturated ceramic disk and that in the water compartment beneath it. Once the target pore air pressure was imposed, the pore water pressure controller was set to control the pore water pressure necessary for the desired matric suction while the volume changes were monitored using automatic volume change transducers.

In a typical test, cell pressure and pore air pressure were simultaneously increased to prevent premature compression of the sample. Continuity of pore air space with the pore air pressure was ensured by back pressuring air though the coarse disk on top of the sample. Continuity of the pore water phase between the specimen and the pore water measurement system was ensured by the axis translation technique and the saturated ceramic disk on the pedestal. The specimen at this stage marking the end of the initial stage had a confining pressure $(\sigma_3 - u_a)$ equal to about 20kPa and matric suction of $(u_a - u_w)$ greater than zero.

(b) Isotropic Compression Stage

Once the initial test conditions were reached, the isotropic compression stage was initiated by elevating the cell pressure, σ_3 in excess of the constant-maintained pore air pressure, u_a so that their difference termed the net normal stress, $(\sigma_3 - u_a)$ was equal to the desired value for the deviator stage. During compression, samples were held at desired constant matric suction. Isotropic compression was considered complete when the change in sample volume was less than 0.127% in 24hours. Whereas 2 days were necessary for isotropic compression to complete up to 14 days had to be allowed for sample water to come in equilibrium with the applied suction. Like with pressure plate tests, equilibrium was taken to be when the sample water content change was less than 0.1% in 24hours. The volume of water content and that of the sample were monitored using automatic volume change transducers described in subsection 4.2.1.5. These were later used in the computation of sample water content and the total volumetric strain of the sample. After isotropic compression the samples were subjected to deviatoric stage.

(c) Deviator Stage

Shearing was carried out under strain controlled conditions. It was carried out at a strain rate of 3mm/h or 1.5% strain per hour to the largest level possible which was dictated by the end of the travel of the displacement transducer. The 50mm stroke displacement transducer was used. Therefore the maximum possible axial strain was 25%. All the samples were, however, sheared to about 22% axial strain as an allowance had to be made for the safety of the transducer. This otherwise quasi-static rate of strain is much slower than the average rates used in static tests on saturated materials. Slow rates of strain are believed to facilitate an instantaneous dissipation of the excess pore water pressure so that the sample is drained at all the times (e.g. in Houston et al., 2008). This was however not confirmed in the present study.

(d) Dismantling Stage

The deviator stage was followed by dismantling of the triaxial unit. The pore water pressure line was first closed and the drainage line opened to instantly dissipate the water pressure below the ceramic disk. The cell pressure and the pore air pressure were then simultaneously reduced to zero before closing all the water network valves and draining all the water from the cells. Three samples were then taken; one from nearly 25mm from top of the sample, another from middle and the last one from nearly 25mm above the ceramic disk for determination of the final water content. It was assumed that dissipation of the water pressure beneath the ceramic disk ahead of pore air pressure did not significantly affect the water condition in the sample. The time over which the pore air pressure was reduced to zero was small, typically less than a minute.

3.3.2.7 Analysis of the experimental results

The main variables used in this part of the current research project are deviator stress, total volumetric strain, axial strain, matric suction, void ratio, specific volume, gravimetric water content and degree of saturation. With the equipment used and the calibrations carried out, apart from the deviator stress and total volumetric strain determination of all these variables was straightforward. To determine the deviator stress a 5kN working capacity load cell was used. The load cell however did not output deviator stress directly but force that had to be converted to stress. The cross-sectional area used in conversion of the load to deviator stress is often approximated depending on the observed failure mode (e.g. Wang, 2005).

During drained compression of an originally cylindrical sample in a triaxial cell, the sample cross sectional area often increases. Therefore, its sectional area changes throughout the shearing process resulting in a final area that is totally different from the initial value. By adopting the sign convention: compression is positive and expansion is negative, and denoting the volumetric strain $\varepsilon_v = \Delta V / V_0$ and axial strain $\varepsilon_a = \Delta h / h_0$, then at any time the sample volume V and height h are given by:

$$V = V_0 - \Delta V \qquad \text{Eq. 3-4a}$$

$$h = h_0 - \Delta h \qquad \text{Eq. 3-4b}$$

Dividing Eq. 3-4a by V_0 and Eq. 3-4b by h_0 and combining the results it can be shown that:

$$A = A_0 \left(\frac{1 - \varepsilon_v}{1 - \varepsilon_a} \right) \qquad \text{Eq. 3-5}$$

Where A and A_0 are the instantaneous and initial sample areas respectively. Eq. 3-5 is applicable to situations whereby at any time the sample can be approximated by the perfect cylinder assumption so that any changes in sectional area and volume are purely due to only changes in sample height. In other words, the top cap and pedestal are smooth enough to allow the sample to expand sufficiently and maintain a constant cross sectional area. However, in some cases the sample fails by barrelling so that the perfect cylinder assumption becomes unrealistic. In this case the accuracy of the estimated cross-sectional area is improved by correcting for the barrel shape. Many of the proposed approaches however require on-sample transducers to measure the sample deformations directly on the test sample (e.g. Wang, 2005). Installation of on-sample transducers has not yet been adopted in unsaturated testing, probably due to the complexity involved. In this study therefore Eq. 3-5 was used in converting the measured axial load into deviator stress.

The accuracy of Eq. 3-5 depends on the accuracy and reliability of the measured volumetric and axial strains. The latter is a straightforward variable once a realisable calibration has been obtained, as was the case in this project. Aside from calibrations given in subsection 4.2.3, however, volumetric stains are reported to suffer from the effect of membrane penetration and many theories have been proposed to correct for it

depending on the sample constituent particle size. It is often applied to material with mean particle size of $D_{50} \geq 0.1mm$. According to Baldi & Nova (1984), in addition to the mean particle size the effective confining stress (termed net normal stress $(\sigma - u_a)$ in unsaturated soil testing), the diameter of the sample d_{samp} and the membrane Young's modulus of elasticity E_m and thickness t_m suffice to account for the effect of membrane penetration. They proposed Eq. 3-6 for this purpose.

$$V_m = \frac{D_{50} V_0}{2 d_{samp}} \left(\frac{(\sigma - u_a) D_{50}}{E_m t_m} \right)^{3/2} \qquad \text{Eq. 3-6}$$

Fig. 3.8 shows a comparison of the different theories proposed to account for the effect of membrane penetration in triaxial testing of granular materials. From the figure it is concluded that membrane penetration induced volume change varies nonlinearly with mean particle size and that the equation given by Baldi & Nova (1984) fits the experimental data of many independent studies. A similar conclusion can also be made from the work of Kramer et al. (1990). Eq. 3-6 was thus adopted for use in this research project to correct for the effect of membrane penetration.

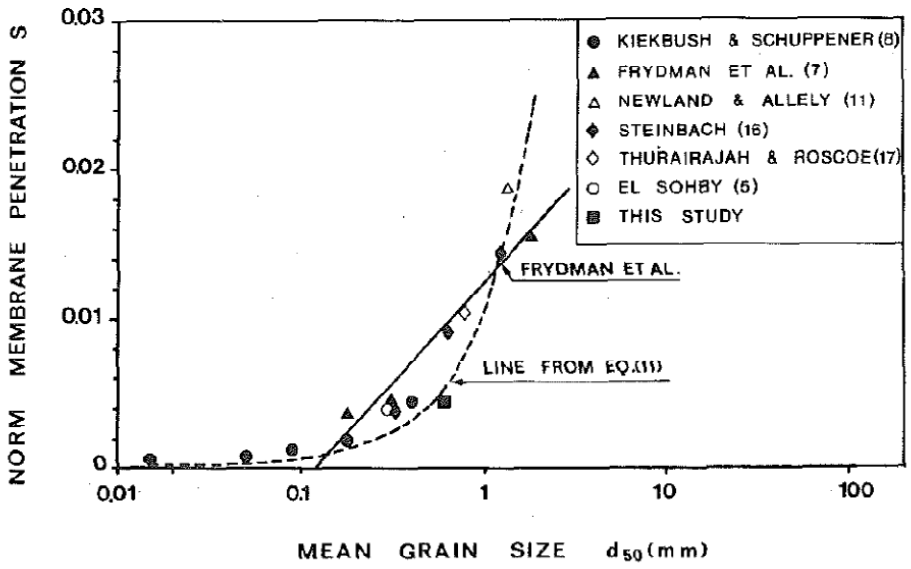

Figure 3.8: Comparison of relationships for normalised membrane penetrations versus mean particle size (Baldi & Nova, 1984)

3.3.3 Silo model Tests

3.3.3.1 Overview

The main objective of the silo model tests was to investigate the effect of suction (moisture) on the flow behaviour of spherical glass beads and Leighton buzzard sand. One of the expected effects was changes in the flow rate. It was therefore necessary that flow rate was determined in every test. Throughout the testing programme distilled water was used so that the observed behaviour was attributable to only material-material and water-material interaction without the presence of other complex interactions often present in most of the materials in real applications.

3.3.3.2 Sample preparation

The preparation of samples for silo model tests had much in common with the preparation of pressure plate test samples and the triaxial compression test samples. The procedure for pressure plate samples is described in the preceding subsection 3.3.1.3 while that of the triaxial compression test samples is presented in subsection 3.3.2.4. In this case the procedure commenced after installation of the relative humidity sensors. Fig. 3.9 depicts the steps followed in preparing samples for the silo model tests.

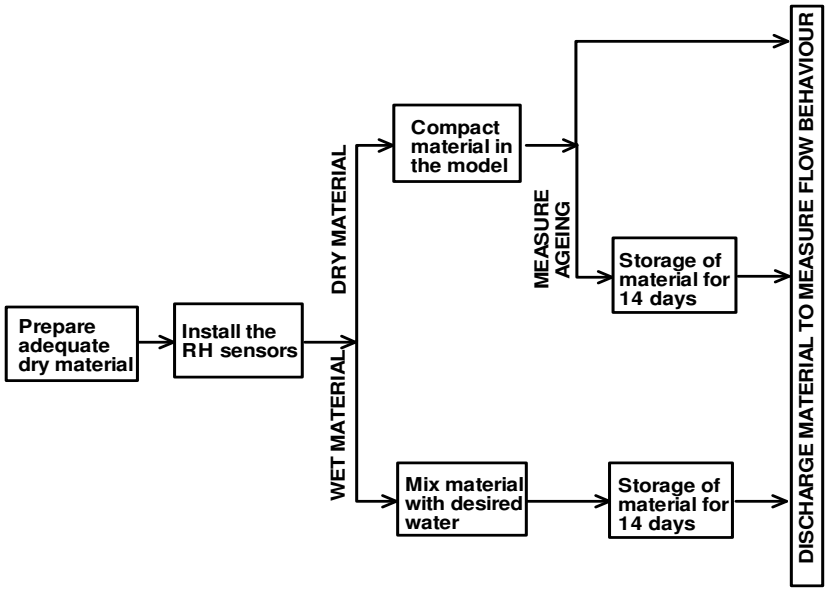

Figure 3.9: Steps followed in preparing the silo model tests samples

The model was marked into layers at an interval of 100mm. The dry material necessary to produce the desired initial void ratio in each of the layers was then prepared. Depending on the desired moisture condition, distilled water was gradually and incrementally sprayed on to the prepared dry material and the two mixed as earlier

described in subsection 3.3.2.4(a). The desired compaction moisture content was based on the water retention curve, determined using a pressure plate. The sand-water mixture was then compacted into the silo model, making sure that all the material is used to fill the layer for which it was intended. The material was compacted to a void ratio similar to that in the pressure plate and triaxial compression tests. The process was repeated in each of the layers until the entire model was filled. Once filled, the silo model was left to stand for 14 days to allow the contents to come to equilibrium with humidity in the compartments for the sensors (Fig. 3.9).

Owing to high permeability of the test materials, the approach just described is suitable for only the samples in which water content was low enough not to flow under the influence of gravity. At water content of about 5% (Fig. 3.10) marginal water redistribution occurred. The data presented in Fig. 3.10b was obtained by compacting moist soil (in the same way it was done in silo models) in a 100mm diameter by 300mm high cylindrical Mylar sheet container and measuring water content in three positions: A, B and C shown in Fig. 3.10a. As long as the water content was less than 5% its dependence on the height of the sample was minimal. This result therefore signifies that above 5% water content compaction of the sample caused some of the water to move downwards, a sign that uniform water content would only be achieved at water contents less than 5%. Above this value, therefore, the reported water content is the one measured near the hopper outlet. It is the material conditions near the outlet that mostly dictate on the formation of a stable arch.

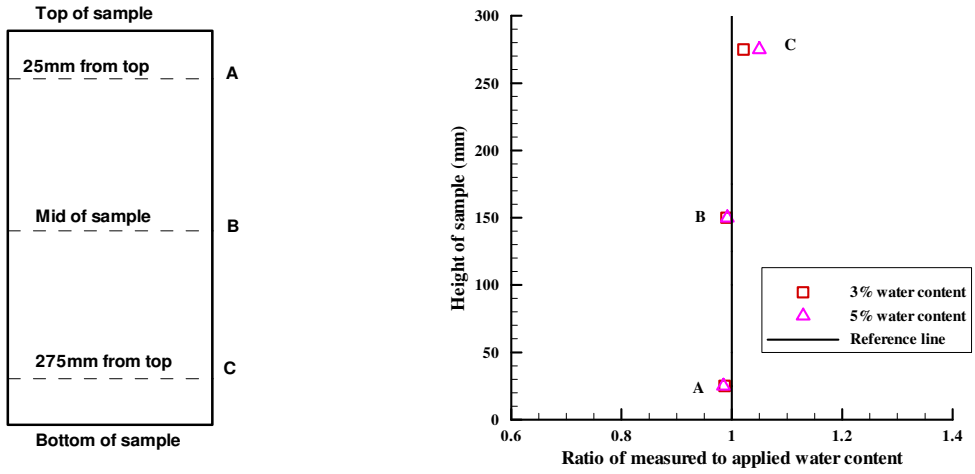

(a) Sampling levels of the sample

(b) Results of water profile

Figure 3.10: Water content profiles in the compacted sample layers

3.3.3.3 Experimental procedure

The flow rate was determined by collecting the discharge material for a given period and then dividing the collected material by the time of collection. This is the method often used for flow rate measurement (e.g. Fowler & Glastonbury, 1959; Beverloo et al., 1961; Hirshfled et al., 1997; Hirshfled & Rapaport, 2001; Mankoc et al., 2007). Care was taken not to interrupt flow during material collection as this would introduce unwanted errors. Once the outlet was opened, it was never closed thereby enabling material to flow continuously. Since the total mass of the material used to fill the silo was known and the flow was never interrupted the flow rate was also obtained by considering the entire mass and the total time taken for it to discharge. The results are presented in terms of flow mass per unit time (second). Particle interaction during flow as well as the wetted proportion of the silo wall in unsaturated tests was recorded using a digital microscope.

Before any tests were conducted, however, the silo model was checked to confirm it was correctly designed otherwise it would be redesigned. The ensuing flow pattern of the dry Leighton Buzzard sand was thus confirmed using visual observations through the transparent silo wall and photographic techniques. These are among the common techniques used in the measurement of flow pattern in transparent wall models. A detailed discussion of the different methods used in laboratory scale model tests is presented in subsection 2.6.1. As can be seen in Fig. 3.11, the initial surface of the material was not affected by flow confirming that the actual flow pattern was mass flow, as intended. In non-mass flow patterns, since flow first takes place in the central core such a flat surface cannot be maintained during flow. In fact an inverted cone would be expected instead (e.g. Snider, 2007).

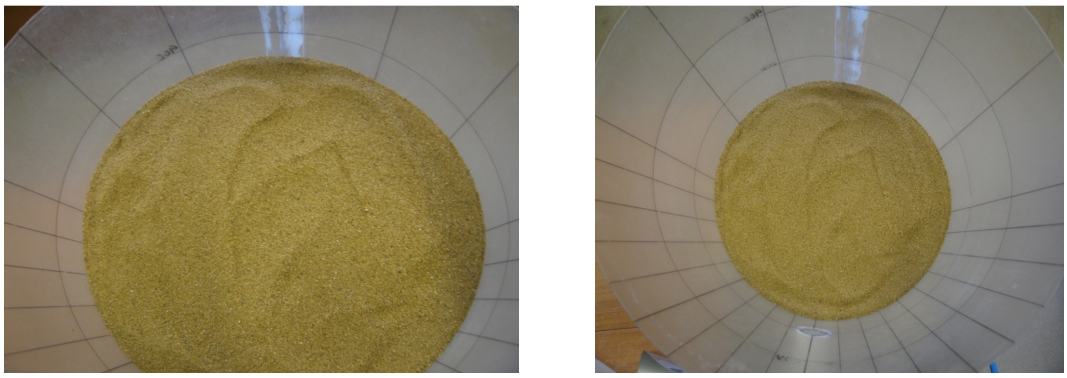

(a) After 6 min. and 8 sec. of flow (b) After 12 min. and 15 sec. of flow

Figure 3.11: Flow pattern observations to confirm the design

As the objective was to investigate the effect of suction (moisture) on the flow behaviour both suction and water content were measured of the flowing material. Suction was inevitably measured using indirect methods as the suitability of the direct method of tensiometers is highly questionable for coarse granular materials given that at low suctions the material desaturates very quickly while at higher suctions the contact between the probe and the material cannot be guaranteed (Jotisankasa, 2005). Indeed suction recorded by the suction probe within the residual condition of water content could be misleading. Further details about suction measurement methods have been presented in subsection 2.5.2. Both the filter paper and the vapour equilibrium methods were simultaneously employed. Filter paper tests were conducted both directly inside the silo model and in small-scale samples specially prepared to represent the model samples. Embedded inside the medium the sandwiched initially dry Whatman No. 42 filter paper measured the matric suction, as it was intimately in contact with the material while total suction was measured using noncontact filter paper method. The calibration equation (Eq. 3-7) by Chandler et al. (1992) was used to convert the measured equilibrium filter paper water content, w_p into suction, ψ. It seems to be the most commonly and widely used and the only calibration equation determined at suctions as low as zero. In fact from amongst the available calibration equations it has been praised by many in the literature to accurately measure suction especially in the low suction range (e.g. Marinho & Oliveira, 2005). Further details about filter paper measurement of suction were presented in subsection 2.5.2.2. As was the case with silo model test samples, the small-scale samples were kept for 14 days to allow the sample to come to equilibrium before measuring the filter paper water content. 14 days was adequate to achieve equilibrium given that the relative humidity of all silo model samples approached equilibrium within that time. Incidentally, it is also taken to be adequate equilibrium time for filter paper measurements of suction (e.g. Marinho & Oliveira, 2005).

$$\log_{10}\psi = 6.05 - 2.48\log_{10} w_p; \qquad \psi < 80kPa \qquad \text{Eq. 3-7a}$$

$$\log_{10}\psi = 4.84 - 0.0622\log_{10} w_p; \qquad 80 \le \psi \le 6000kPa \qquad \text{Eq. 3-7b}$$

Besides, monitoring equilibrium, the relative humidity measurements in conjunction with the Kelvin equation (Eq. 3-8) on the other hand were used to infer total suction within the material. Relative humidity (and temperature and dew point) measurements

were taken from hygrometers retrieved just prior to opening the hopper outlet. To ensure accurate relative humidity and temperature measurements, the sensors were calibrated using NaCl salt solution prepared with distilled water and against known temperature respectively. Given that the fluid thermodynamic properties are affected by temperature changes, in using Eq. 3-8 to compute suction the effect of temperature on molecular volume of water was taken into account.

$$\psi = -\frac{TR}{v_w w_v} \ln R_h \qquad \text{Eq. 3-8}$$

Where the terms are as explained earlier in subsection 2.5.3.

Water content determination was two-fold: (i) the silo model was filled with material mixed with known amount of water and (ii) during discharge portions of the collected material were periodically taken for moisture content determination. In tests where the material failed to flow out of the model water content was taken at different depths during manual emptying of the model from above. This way it was possible to obtain, with confidence, the water content at which each test was carried out. Care was taken to include water contents besides (and at the level of) the relative humidity sensors to identify the sensor readings with the exact water contents. These were related to the measured water retention curves.

For each of the conditions in model tests shear strength parameters were also obtained. Except for tests on dry material, direct shear box tests were carried out on materials retrieved from different locations in the silo model. This was aimed at assessing the dependence of shear strength parameters on the stored sample conditions (density/void ratio and water content). In carrying out the tests, conventional testing method outlined in BS1377 (1990) was used. The samples were sheared until a state of constant shear strength was reached. The results are presented in chapter 7 in terms of total stress parameters.

3.4 Concluding Remarks and Summary of the Executed Tests

In this chapter, the physical and geotechnical properties of the test materials used in this research project have been presented. These properties were carefully measured and are used in the later chapters to discuss how they affect the water retention and shearing behaviour of granular materials as well as the flowability in silo model tests.

Particle size distribution and shape and compaction characteristics have been particularly captured. The appropriateness and reliability of sample preparation and experimental techniques and procedures have also been elaborated in this chapter. Table 3.5 shows a summary of all the tests performed in this research project. In the table the following information is shown: the test performed, the method employed, number of tests carried out in each test category and the purpose of the tests.

Table 3-5: Summary of all the tests performed in this research project

Test	**Test method**	**Number of tests**	**Purpose of the tests**
Particle size distribution	Sieve analysis (BS1377, 1990) and Mastersizer	9 sieve analyses; 4 mastersizer	To determine the particle size distribution of the test materials
Compaction	Standard Proctor (BS1377, 1990)	13	To determine the compaction characteristics of sand
Maximum density	Vibrating rammer method (BS1377, 1990)	4	To determine the maximum densities of the test materials
Minimum density	Graduated cylinder method (BS1377, 1990)	6	To determine the minimum densities of the test materials
Permeability test	Constant head method (BS1377, 1990)	4	To determine the saturated permeability of the test materials
Pressure plate	Axis translation	91	To measure the WRC curves of the test materials
Filter paper	Both contact and noncontact	10	To measure matric and total suctions at different sample water contents
Conventional triaxial compression	Drained tests	2	To determine the stress-strain response and shear strength of the test materials at different effective stresses.
Suction controlled triaxial compression	Drained; suction controlled using axis translation	11	To determine the stress-strain response and shear strength of the test materials at different matric suction and net normal stresses.
Silo model tests	Gravity flow	52	To determine the effect of suction (moisture) on the flowability of the test materials

CHAPTER FOUR

4 EXPERIMENTAL SETUP

4.1 General Overview

Correct and accurate measurement of stresses is a crucial aspect in the analysis and interpretation of laboratory tests. For unsaturated soils, for instance, it has been recognised that to describe the hydro-mechanical behaviour of soil, the stress state functions should be expressed in terms of the total stress, σ, the pore air pressure, u_a and the pore water pressure, u_w. As discussed earlier in subsection 2.4.1.2, the above mentioned variables can be combined in a number of ways (e.g. Fredlund & Morgenstern, 1977). The commonly used combinations are however the net normal stress, $(\sigma - u_a)$ and the matric suction, $(u_a - u_w)$.

These stress variables are measurable and can be measured or controlled in a number of laboratory based unsaturated apparatuses namely the oedometer, direct shear box, triaxial and the pressure plate extractor. Of these, however, triaxial is the most versatile equipment that allows considerable flexibility to control and measure various aspects related to soil properties in nature. In addition, the pressure plate extractor is commonly used to determine the water retention curves for particulate materials.

Wet granular materials present many engineering challenges as their behaviour often tend to be complex with the influence of matric suction arising from interaction between the pore water and pore air. A proper understanding of the extent to which suction and degree of saturation impact the behaviour of such wet materials therefore seems key to addressing the challenges. In unsaturated soil mechanics the test procedure often used to assess the influence of suction and degree of saturation on the subsequent mechanical behaviour of the material involves controlling suction by independently imposing the pore water pressure and pore air pressure (e.g. Houston et al., 2008). In this study, a triaxial apparatus and the pressure plate extractor incorporating the axis translation technique were the major equipment used.

This chapter gives details of the unsaturated triaxial apparatus and the pressure plate extractor used in this study together with the calibrations carried out as part of the study to ensure quality of the data obtained. Details of the silo model used to characterise flow

rate according to moisture content or matric suction are presented last. The other equipment used included the conventional triaxial apparatus and direct shear box. These are well known and are therefore not described herein.

4.2 Unsaturated Triaxial Equipment

4.2.1 Unsaturated Triaxial Equipment Components

The following describes the unsaturated triaxial equipment used in this study. The equipment was Wykeham Farrance International Tritech 50kN, model number 28-WF4005 and serial number 08002742. It was designed and built by Wykeham Farrance International (now Controls Group, Soil Mechanics Division). It will henceforth be referred to as the WFI Tritech 50kN. The schematic representation of the equipment setup is shown in Figs. 4.1 & 4.2. It was a double-wall triaxial cell with six ports for tubing purposes and a rigid loading (reaction) frame. As shown in the figure, one port (port A) was for outer cell pressure control, the second port (port B) was for inner cell pressure control and total volume change measurement, the third port (port C) was for pore water pressure control and measurement and the pore water volume change measurement, the fourth port (port D) was for diffused air flushing and the water network drainage if necessary, the fifth port (port E) was for pore air pressure measurement and the sixth port (port F) for pore air pressure control.

This WFI Tritech 50kN equipment had a control module of which the loading ram was an integral part (Fig. 4.1). The module which utilised AC power had a display screen and control buttons for digital control of the loading and operated by specifying a loading rate. In addition, it had a serial (COM) port for software based control. In this research project it was strain controlled using the integrated control module. The axial (deviator) load to the test specimen was measure by a 5kN submersible load cell attached to the loading rod. The compression of the test specimen was measured by an external 50mm stroke displacement transducer.

Additionally, as remote components connected to the main part of the equipment through horse tubes or electric wires (Fig. 4.1), the system included two 100cm^3 capacity automatic (digital) volume change transducers, two 1000kPa capacity hydromatic (digital) pressure controllers, 1000kPa capacity water pressure (pore water and cell) transducers, 2000kPa capacity pore air pressure transducer, PCI-836 hardware

used to control the hydromatic pressure controllers, an air compressor for pore air supply, two manually controlled Manostats for pore air pressure regulation, MSL data acquisition system and a host computer equipped with TRIAX feedback control software.

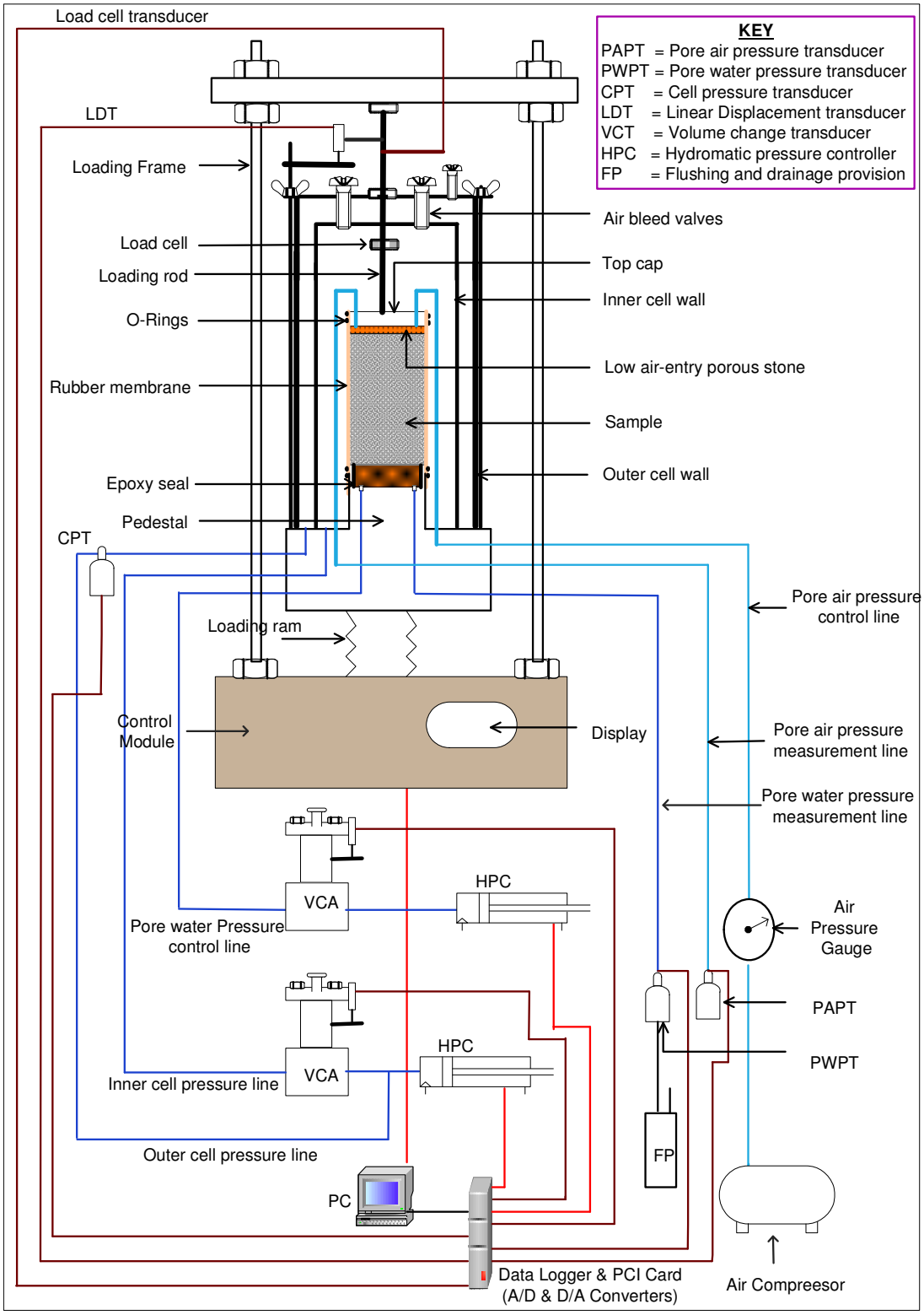

Figure 4.1: Schematic of the setup of unsaturated triaxial equipment used in current study

Given that this is the first time this triaxial equipment was used, having been setup as part of the current study it suffices to provide more information about it. The different parts of the apparatus will now be described in some detail including their functions and any preliminary preparations carried out.

4.2.1.1 Base plate and the Pedestal

As is the case with all triaxial equipment, the base plate provided a platform on to which the rest of the triaxial components were supported. It was provided with ports through which the tubing was made to facilitate the control and measurement of both cell pressure and pore pressures in the sample. Fig. 4.2 shows features of the base plate and the 100mm diameter pedestal. As can be seen in the figure, whereas the base plate had six ports for tubing provision, only two were connected to the pedestal: one for pore water pressure control and volume change measurement, and the other for pore water pressure measurement and flushing of the diffused air if any from the water compartment underneath the high air-entry ceramic disk. The two ports were connected by a circular groove which served as a water channel for flushing any diffused air bubbles that accumulated inside the water compartment during testing. The o-rings were fitted at points of contact between different parts of the stainless steel metals to prevent liquid and pressure leakage.

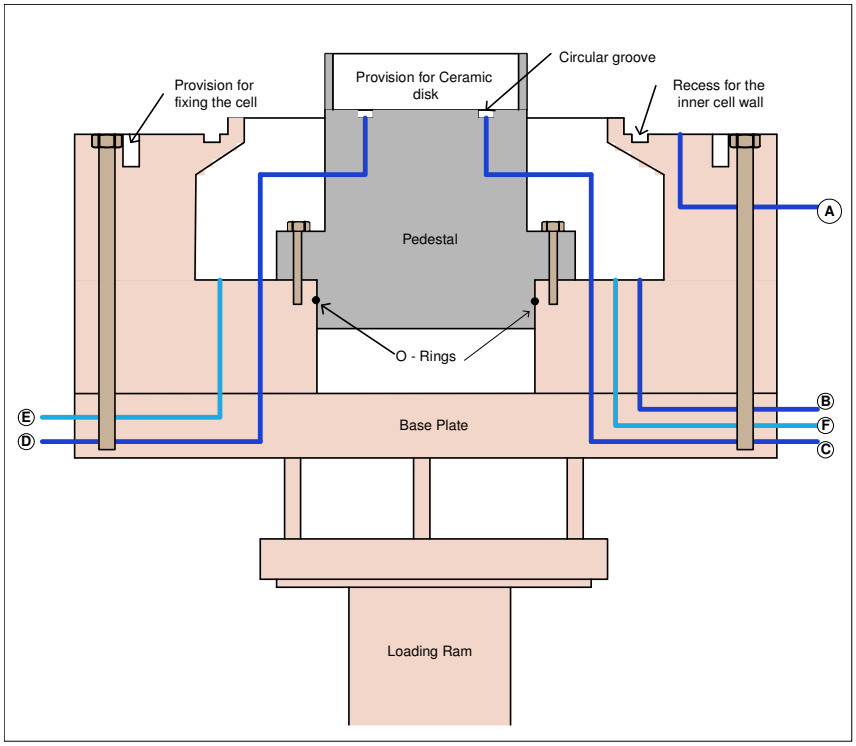

Figure 4.2: Sectional features of the pedestal and the base plate

4.2.1.2 High air-entry ceramic disk

The high air-entry ceramic disk was glued (from the circumferential sides) on top of the pedestal using a special epoxy resin (Fig. 4.3). In addition to holding the disk in place, the rigid impermeable epoxy resin seal helped prevent passage of water around its circumference so that any water exchanges were strictly through the disk. Properties of the epoxy resin which was manufactured by ITW Devcon Ltd are summarised in Table A.1 in Appendix A-1. The high air-entry ceramic disk was used instead of the ordinary (low air-entry) porous stone to prevent free air from crossing to the water underneath and to prevent a sample with high suction from sucking water from the disk. It was 10mm thick and after gluing it flushed level with the top part of the pedestal (Fig. 4.3b).

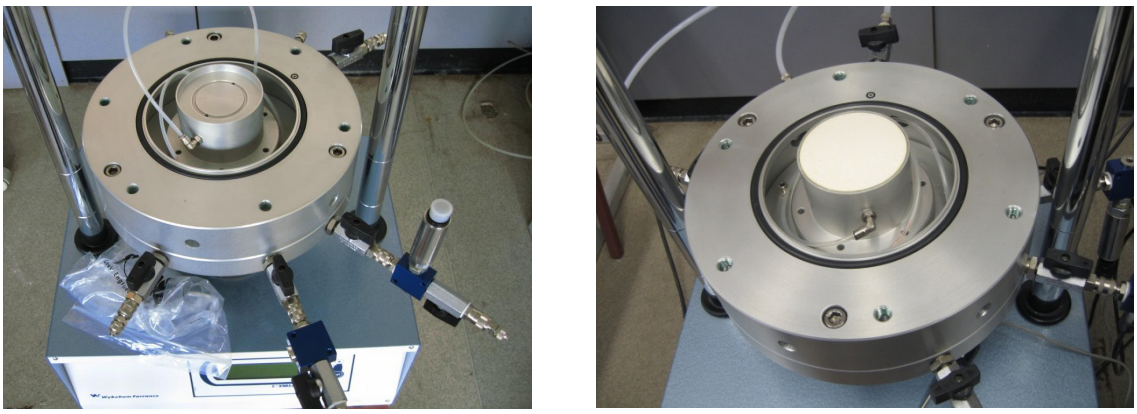

(a) Before sealing (b) After sealing

Figure 4.3: High air-entry ceramic disk cemented on the pedestal

4.2.1.3 The Double-Wall Cell

Due to high pressures and the complexity involved in the testing of unsaturated soils, the triaxial cell was specially designed. Together with the Tritech 50kN reaction frame the cell whose model and serial numbers were 28-WF4171 and 08001522 respectively was supplied by Wykeham Farrance International (now Controls Group). In this study, the cell had two walls to minimise errors due to cell wall deformations (compliance). For safety reasons, the acrylic material outer wall had horizontally running strips to increase its resistance against bursting (Fig. 4.4).

The inner wall was made of glass and so was free of the problems of water absorption. The cell was provided with air bleed valves through which the air displaced as de-aired water was introduced into the cell. The same pressure was applied in both cell compartments thereby subjecting the inner glass cell to zero net pressure. As will be

shown in subsection 4.2.3.2, this helped to eliminate the possibility for it to creep under long-term loading. The cell could withstand pressures up to 2.0MPa, far much greater than the highest pressure levels in the current study.

Figure 4.4: Features of the double-wall cell

4.2.1.4 Load Cell and the Loading Rod

The load cell was attached to the loading rod as indicated in Fig. 4.1. Fig. 4.5a shows the duo in more detail. This submersible load cell, model number STALC3-5kN and serial number 30350, was supplied by Applied Measurements Ltd. Wykeham Farrance International, identified the duo as model 28-WF6353 and serial number 08001973. The load cell whose capacity was 5kN (or 636.3kPa considering a constant sample cross-section area) was never affected by the cell confining pressure. It was located inside the cell to minimise or eliminate any errors that could have been induced due to piston friction effects.

4.2.1.5 The Volume Change Transducer

The apparatus, model number 28-WF4410 and serial number 07001743, comprised a 40.15cm^2 cross sectional area and 25mm stroke piston sealed against a precision-machined calibration chamber, so that the linear movement of the piston was exactly proportional to the volume change of water in the calibration chamber. The piston which was connected to an external measuring medium, a 27mm stroke linear displacement transducer (Novotechnik, type TR 25 and Art No. 023261) connected to the MSL data acquisition system - the DataScan 7220 (Measurement Systems Ltd), allowed volume change of the specimen to be displayed and recorded directly in cubic centimetres. The operational capacity for the apparatus was 100cm^3 with an accuracy of 0.001cm^3. The unit was connected to a control module with change over and bypass valves used for saturation (Fig. 4.5b). consistent with the sign convention used in soil

testing i.e. compression is positive and expansion is negative, the apparatus was adjusted such that once the knob for volume change was turned on, movement of water into the sample resulted in downward displacement of the piston leading to a reduction in water volume within the device and vice versa. This was the same for the inner cell volume change apparatus.

(a) Load cell and the loading rod

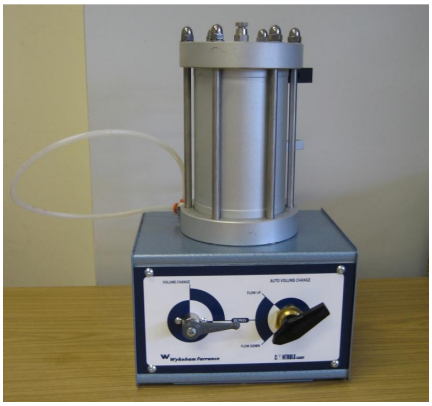

(b) Volume change transducer

Figure 4.5: Load cell and the volume change transducer

4.2.1.6 Control System Hardware

The control system of the unsaturated triaxial apparatus comprised a personal computer, digitally controlled pressure controllers and the data acquisition device. Installed into a slot in the computer, the 1000021305 serial number PCI-836 digital I/O card (Eagle Technology Ltd) drove the hydromatic pressure controllers which were $100\,cm^3$ stepper motor driven piston pumps supplied by Wykeham Farrance International. The controllers (model number 29-WF4502 and serial number 08003196) were capable of executing a step equivalent to $0.0001\,cm^3$ and had a clear Perspex cover allowing the moving parts inside to be viewed (Fig. 4.6). A scale on top side of the Perspex cover helped trace position of the piston. The Tritech 50kN was digitally controlled by the integrated control module to run strain controlled tests.

The data acquisition was by the DataScan 7220 supplied by Measurement Systems Ltd. It was a measurement processor with 16 integral analog input channels with each of the channels configured independently. The data acquisition device was powered by 10V DC and provided 16 bit A/D conversion with sensitivity to voltage changes (resolution) of $0.625\,\mu V$ and local measurement speed of 40 readings/second. The communication was through a serial (COM) port.

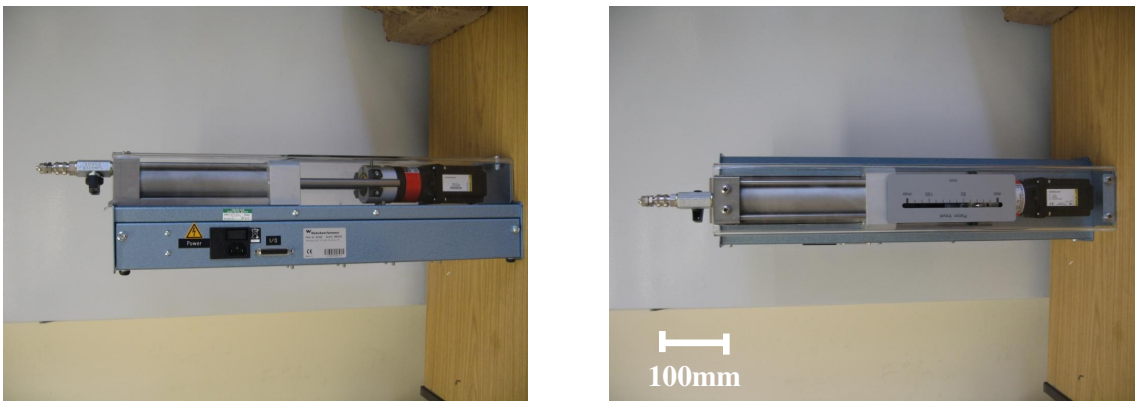

(a) Side view (b) Plan view

Figure 4.6: Hydromatic pressure controller (HPC)

4.2.1.7 Displacement Transducer

Axial displacement of the sample was measured by a displacement transducer (Fig. 4.7a). The transducer model number 30-WF6209 and serial number 09006006 was a linear potentiometric displacement transducer supplied by Wykeham Farrance International (Controls Group) and had a stroke of 50mm. Considering size of the specimen it was capable of measuring up to 25% axial strains. It input 10V DC and output 0-10V and had an accuracy of 0.002mm. It was fixed in place using the mounting block such that it was possible to capture the actual displacement of the test sample. Fig. 4.1 shows the position of the displacement transducer relative to the other components of the triaxial system.

4.2.1.8 Pressure Transducers

Pressure transducers were installed, one on the pore water pressure line, the second on the inner cell line and the other on the pore air pressure line as depicted in Fig. 4.1 to measure and confirm the pressure values subjected to the sample. Fig. 4.7b shows one of the transducers with one of its sides connected to the cable for connection to the data logger. They were the TPS series transducers (model number TPS-4-V-B01D-T and serial number D08070285) manufactured by Gefran Spa. The transducers were unaffected by tightening during installation and two of them measured up to 1000kPa (10bar) pressure while the third measured up to 2000kPa.

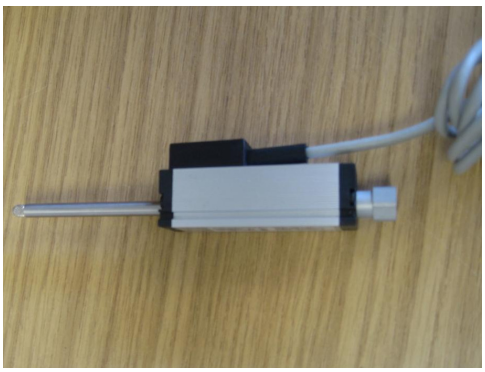

(a) Displacement transducer

(b) Pore pressure transducer

Figure 4.7: Axial displacement and the pressure transducers

4.2.1.9 Connecting Tubes

The ports on the triaxial cell were connected to their respective devices: pressure controllers, volume change transducers and the pressure transducers by the connecting tubes. The connecting tubes (transparent hoses) were $8\times1mm$ PA12 nylon tubes manufactured by ZEC spa and identified by Wykeham Farrance as model 28-WF4191, $6\times8mm$ tubes. According to the manufacturer, the working temperature range for these water and air conduit pipes was negative $20^{o}C$ to positive $80^{o}C$ and their working and burst pressures were respectively 37bar and 59bar at $23^{o}C$. The maximum pressure in the current study was about 400kPa which is far less than the specified (recommended) working pressure. The laboratory working temperature was also maintained at $22^{o}C$ on average. Therefore failure of the connecting tubes was not an issue.

4.2.1.10 The Software

Apart from the ram, the unsaturated triaxial testing system was computer controlled by the TRIAX software version 5.1.7 developed by Toll (Toll, 1993). Using appropriate functions, the control software allowed for monitoring, acquisition (scan) and control of parameters associated with unsaturated material testing including suction control and measurement. These functions which were executable only when the program was running are respectively defined as the monitor, scan, graph and control. They are briefly explained in the following part of this subsection. The other functions which were not used in monitoring the progress of the experiment are not described here. They included the calibrate function, regression function, reset function, initialise function and the zero timer function. More details about the software can be obtained from the appropriate user manual.

In the monitor window values of all the desired and selected variables were displayed on the screen (Fig. 4.8a). This helped in keeping track of the state of all the variables as well as knowing the appropriate times for stage change. The displayed variables included all transducer readings and the system variable of timer. The scan window, on the other hand, displayed the progress of data scanning of the desired and selected variables (Fig. 4.8b). The scanned data was stored in a data file at a predetermined (regular) time interval. The data files were comma separated value text files that were read directly into a spreadsheet package.

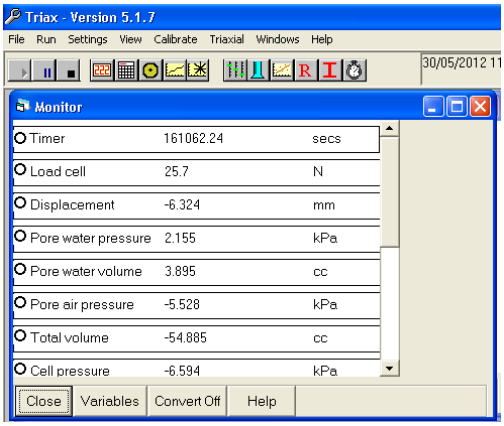

(a): Monitor window

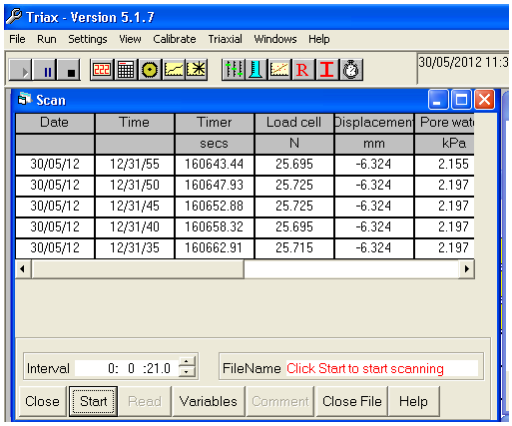

(b): Scan window

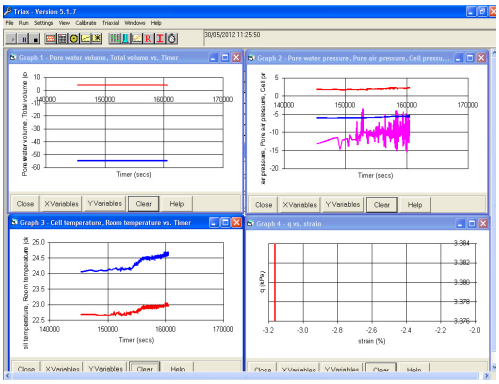

(c): Graph window

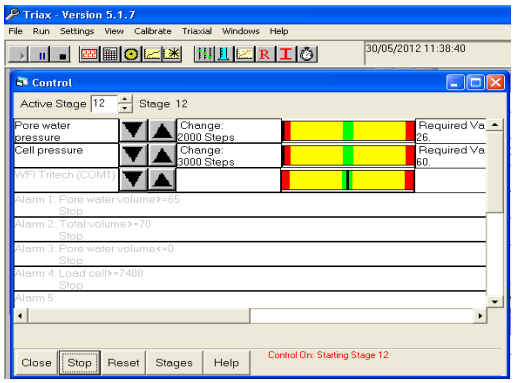

(d): Control window

Figure 4.8: Windows displayed on the screen for monitoring progress of the experiment

Fig. 4.8c and Fig. 4.8d show an example of the display of the Graph and Control windows respectively. Up to four graphs were displayed in separate windows on screen. Within each graph up to six curves were plotted together, each in different colour. All these were used to visualise the progress of the test. The Control function allowed the pressures to be controlled through the control device connected to the computer. The controls were executed depending on the comparison between the number of times the tolerance and the difference between the current and specified hold values.

4.2.2 Initial Saturation of the High Air-entry Ceramic Disk

For accurate measurement of the pore water volume it is necessary that there is continuity between water in the sample and the one in the compartment underneath the high air-entry value ceramic disk. This continuity cannot be established unless the ceramic disk is fully saturated. Being initially a dry new disk, the following procedure was followed to ensure its full initial saturation.

- With the ceramic disk sealed on to the pedestal (Fig. 4.3b), the triaxial cell was put in place. Details regarding sealing of the ceramic disk on the pedestal are presented in subsection 4.2.1.2 of this chapter.
- De-aired water was then introduced into the triaxial cell, and the cell pressure was gradually raised to a value of 600kPa. During the pressurisation process, water was allowed to flow through the disk with the attendant expulsion of some of the air within the ceramic disk. This stage was extended to last for a period of about 6.0hours after full cell pressurisation.
- After 6.0hours, valves connecting the water compartment to the measuring system and flushing line were closed so that the water above, inside, and below the ceramic disk were under the same applied pressure of 600kPa. From this point on the applied pressure was maintained for about 24hours so that any air that could have been in the disk dissolved into the water. After every 24hours, the cell pressure was reduced to 50kPa to allow any entrapped air in the disk to cavitate.
- Flushing was periodically done from below the disk to eliminate any air bubbles.
- The above procedure lasted six (6) days, after which the disk was saturated.
- Complete saturation was confirmed by comparing the amount of water into and out of the ceramic disk. The inflow was equal to outflow at complete saturation.

After the initial saturation, the disk was always submersed in water until a specimen was ready to be placed on it. This helped to always keep the disk nearly saturated and hence to minimise the time required for the subsequent resaturation procedures. This procedure is based, in part, on the work of Fredlund & Rahardjo (1993) and Tarantino & Mongiovi (2001). Tarantino & Mongiovi (2001) reported that pre-pressurisation of the ceramic disk for a tensiometer was not adequate to saturate it. They suggested the

ceramic stone should be subjected to cycles of pressurisation and cavitation in order to remove all the air from it, and discussed the physical significance of this preconditioning procedure to prevent cavitation in the ceramic disk.

4.2.3 Calibration of the Testing Equipment

When the test equipment was in operation, the different components thereof were subjected to different conditions and responded to these conditions differently. The responses were measured and acquired through the data logger in terms of voltage changes other than the physical values. It was thus necessary to calibrate all parts of the test equipment including the assembly as a whole to relate the voltage changes to the physical values. The calibration procedure was analogous with all the different parts of the test apparatus. Suffice therefore to give a detailed procedure for only one (volume change transducers) and a summary of the rest. The detailed description of the calibration each of the transducers not described here is presented in Appendix A-2 in the order shown in Table 4.1. Calibration of the entire system as a whole is presented last.

4.2.3.1 Volume Change Transducers

The automatic volume change transducers (Fig. 4.5b) were used to measure total volume of the sample and volume of water entering or leaving the sample during the test. The water exchanges were then related to the volumetric behaviour of the sample. Therefore the accuracy of the measured volumetric behaviour depended on the accuracy and reliability of the transducers. To make sure that accurate and reliable measurements of volume changes are made, the volume change transducers were calibrated. The following part of this subsection describes how the calibration was carried out. The calibration data is also presented.

With the volume change transducers connected as shown in Fig. 4.9, the system including the transducer cylinder, connecting tubes and the GDS pressure controller (Fig. 4.9) were saturated with de-aired water. The system saturation procedure included alternately passing de-aired water through the transducer and pressurising the entire system to 600kPa for 24hours until there were no signs of air bubbles in the system. The balance and the calibration function in the software were then setup and the calibration of the volume change transducer carried out following a rigorous procedure that included the determination of the calibration factors by plotting the digital readings of

selected channel of the data logger against the physical measurements of volume change through the complete range of the transducer, calculating the regression and saving the software-computed calibration factors in the appropriate directory for future use by the software to convert the voltage readings into physical values and finally verifying the accuracy of the digital measurements of the software/data logger in physical units.

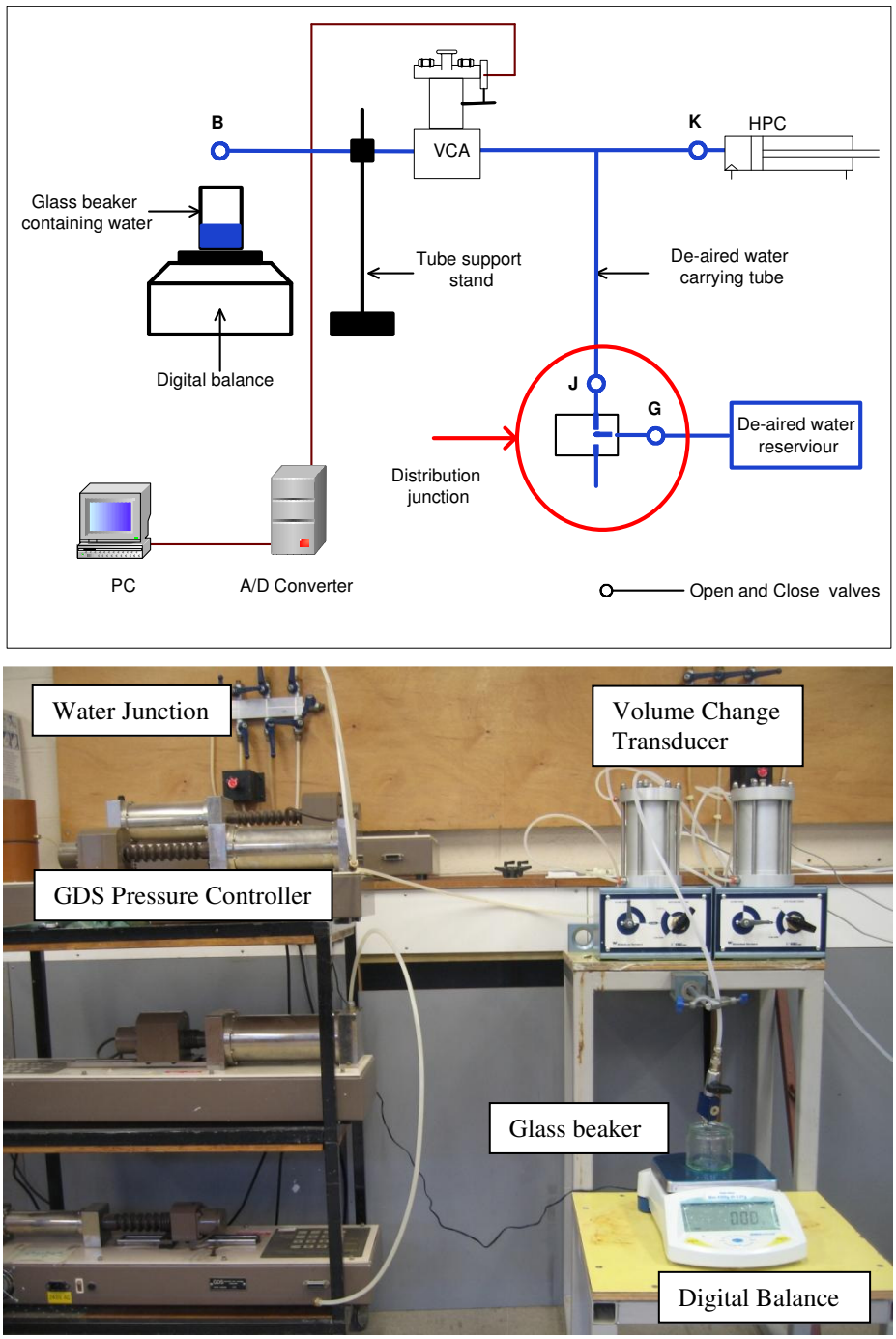

Figure 4.9: Schematic layout and set up for the volume change transducer calibration

A glass beaker of 250ml capacity and a digital balance of 4.5kg capacity and 0.01g sensitivity were used in the determination of calibration factors. With the apparatus correctly setup and completely saturated, de-aired water was allowed to flow through the volume change transducer. As the water flowed through the transducer, the piston to which an external linear potentiometric displacement transducer is connected was accordingly displaced. The voltage changes were directly related to the movement of the external displacement transducer. Measurement of volume change was then performed by collecting and measuring the weight of water that drained from the apparatus as described in the following paragraph. The open and close valve at the end of the tubing on the beaker side helped to ensure accuracy of the measurements as only the water flowing past the transducer was collected and measured at a time. Since the working laboratory temperature was about $22^{o}C$ it was assumed that $1.0g$ was equal to $1.0cm^{3}$ of water.

De-aired water was allowed to flow through the volume change apparatus until the transducer stem was completely compressed. The glass beaker was placed on the balance and the display was set to zero. At the same time this zero value of the balance reading was entered against the voltage reading of the applicable data logger channel (Fig. 4.10a). The flow was reversed to drain about $5cm^3$ of de-aired water into the beaker and its mass recorded into the calibration window of the software against the corresponding voltage reading of the volume change transducer channel. An additional $90cm^3$ of de-aired water was further drained from the apparatus in increments of about $10cm^3$ and for each increment the digital readings of the balance were recorded against the corresponding voltage reading of the transducer. Finally the digital readings of the measurements of volume were plotted against the digital (voltage) readings of the transducer and the linear regression line drawn (Fig. 4.10b). The calibration factor was determined from the equation of the linear regression.

The above rigorous process enabled the determination of the calibration factor. This factor was then verified using the following procedure. Flow through the apparatus was reversed to have the transducer stem again completely compressed. Water was then drained from the apparatus as described before. The resultant data were equally treated as explained in the preceding paragraph. A total of four calibration factors were obtained for each transducer for comparison purposes. It was concluded that since the

calibration factors were experimentally the same then the measurements of volume changes were reproducible and reliable. Fig. 4.10b shows the regression line of the coefficient of regression of 1.000 whose data was stored in the system for use by the TRIAX programme to convert the voltage readings to physical values.

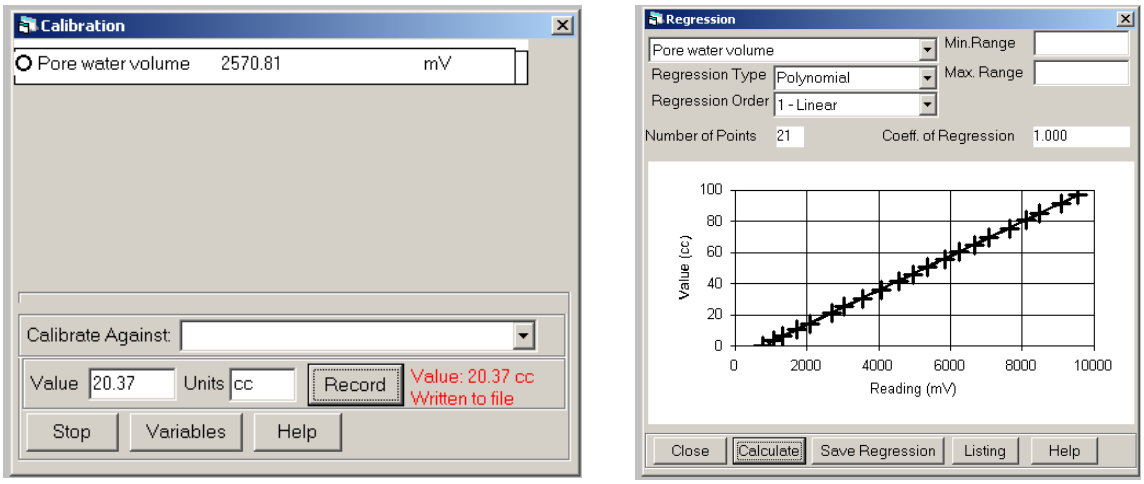

(a): Calibration window (b): Regression window

Figure 4.10: Calibration of the volume change transducer

Table 4-1: Calibration results of the different transducers

Transducer	Calibration method	Calibration equation	Regression coefficient	Number of points	Maximum error (%)
Pore water volume	Water mass measurement	$cm^3 = 0.0110mV - 8.4879$	1.0000	21	0.38
Total volume	Water mass measurement	$cm^3 = 0.0112mV - 3.3542$	1.0000	31	0.26
Pore water pressure	Calibrated transducer	$kPa = 0.0654\mu V - 28.4303$	0.9998	36	0.63
pore air pressure	Calibrated transducer	$kPa = 0.0199\mu V - 5.2311$	1.0000	52	0.38
Cell pressure	Calibrated transducer	$kPa = 0.0653\mu V - 28.3793$	0.9999	37	0.65
Load cell	Dead load	$N = 0.2096\mu V - 1090.7989$	0.9993	42	0.12
Displacement	Micrometer unit	$mm = 0.0051mV - 0.0389$	1.0000	17	0.25

4.2.3.2 System Compliance

The unsaturated triaxial system comprised a number of components connected together. Details of the components and the connections have been described in subsection 4.2.1. Being an assembly of several components, it was hoped that the system compliance

would be in question when subjected to sustained and varying levels of pressure. This would substantially affect the accuracy of the measured values especially the volumetric changes. The following rigorous procedure was thus undertaken to calibrate the entire system for pressure compliance.

A non-deformable dummy specimen was setup sandwiched between the top cap and the pedestal to which a high air-entry ceramic disk was subsequently cemented. The cell was then put in place and water introduced. As water was introduced into the cell, the air bleed valves were open so that any air is displaced by de-aired water. The cell was then pressurised in steps while monitoring the volumetric changes recorded by the transducers. It was observed that for the range of pressure in this study the system was free of creep (Fig. 4.11a). The volume change transducer however recorded a decrease in system water volume as cell pressure was increased. This was probably due to compression to minor expansion of the connecting tubes. A graph of the volumetric changes (cm^3) against cell pressure (kPa) was thus plotted to obtain a correction equation for expansion of the system as given in Fig. 4.11b:

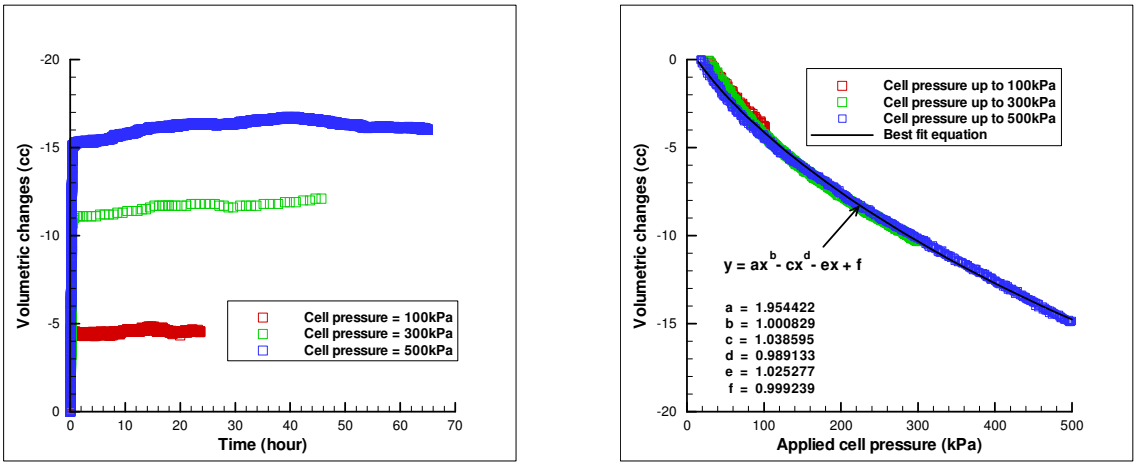

(a): Calibration for creep

(b): Calibration for system expansion

Figure 4.11: Calibration of the entire system for pressure compliance

4.3 Pressure Plate Extractor Setup

The apparatus used to determine water retention curves in this study was a 15bar pressure plate extractor. It was a 1500F1 model supplied by Soilmoisture Equipment Corporation. The schematic of the apparatus setup is shown in Fig. 4.12. The surface of the pressure vessel and that of the lid were painted with Gila coat (asphalt-based paints) so they are resistant to rusting.

To perform the intended purpose, the extractor required additional components. Additionally, the system included a manifold (marked out with dashed line in the figure), GDS pressure/volume controller and the connecting tubes. The manifold consisted of the air filter, two pressure regulators connected in series and a 0.25% accuracy precision pressure gauge.

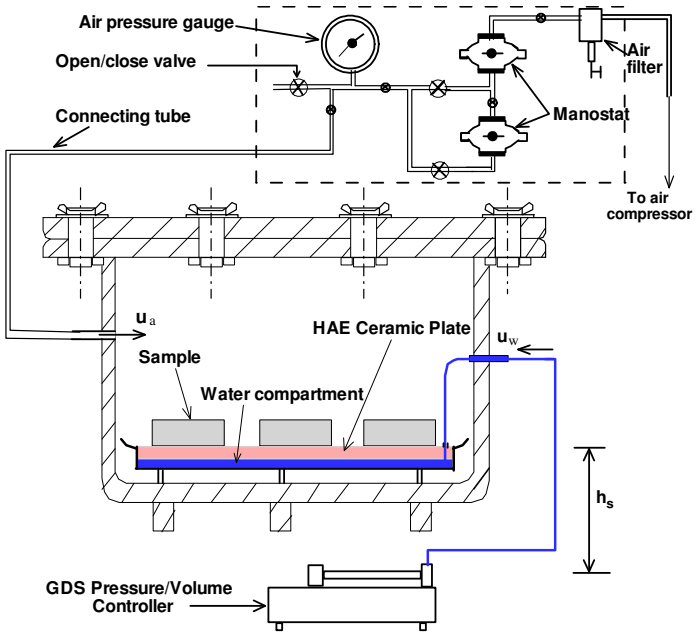

Figure 4.12: Schematic setup of the pressure plate extractor used in the current study

The pressure plate extractor system used was capable of running tests involving matric suction control of up to a maximum of 15bar (1500kPa), a value corresponding to the air-entry value of the ceramic plate. In this study, suction control was limited to 300kPa at which value the change in water content of the test material was reduced to nearly zero.

4.3.1 Initial Saturation of the Pressure Plate Extractor System

The saturation of pressure plate system (see Fig. 4.12) followed in part the procedure detailed in subsection 4.2.3.1 for the calibration of the volume change transducer system. The procedure for saturation of the ceramic plate was also similar to the one for ceramic disk reported in subsection 4.2.2. This saturation procedure was routinely carried out each time a new test was to be performed.

4.3.2 Calibration of the Pressure Plate Extractor System

Like the unsaturated triaxial apparatus, all the pressure plate extractor system transducers were calibrated to ensure accuracy of the measurements. They included air pressure gauge and the GDS pressure/volume controller. Supplied together with the extractor the air pressure gauge was supplied with its calibration certificate. This calibrated air pressure gauge was thus used to check and verify the accuracy of the GDS unit. In the procedure, the two were interconnected and monotonically pressurised with air from the compressor while comparing the pressure readings on them.

4.4 Silo Model used in the Study

4.4.1 Model Design

4.4.1.1 Parameters and assumptions used in the design

The silo model was designed for mass flow of Leighton Buzzard sand (LBS1) taking into consideration, for the dry material, the bulk density, angle of wall friction and the effective angle of internal friction. These are the most important design quantities which unless properly accounted for the designed silo may fall short of the desired operational performance (Schulze, 2008). The cylindrical barrel was based on Janssen's theory (Eq. 2-28, reproduced here as Eq. 4-1). As mentioned earlier in subsection 2.6.2, it is the most commonly and widely used theory in the literature to design cylindrical silo barrels and forms the basis of most silo design codes for strength.

$$\sigma_z = \frac{\rho g R_B}{2\mu K}\left(1 - e^{-\frac{2\mu K z}{R_B}}\right) \qquad \text{Eq. 4-1a}$$

$$\sigma_n = \frac{\rho g R_B}{2\mu}\left(1 - e^{-\frac{2\mu K z}{R_B}}\right) \qquad \text{Eq. 4-1b}$$

In the above equations three quantities: coefficient of wall friction, μ, lateral pressure coefficient (also known as lateral stress ratio), K, and the density of the solids, ρ are known. For any chosen barrel radius, R_B, the vertical stress, σ_z, was determined for different depths, z. The results are shown in Fig. 4.13a. The dependence of stress inside the silo barrel on the barrel radius is evident, as expected. For deep silos the depth is usually such that top solids do not affect pressure at the transition. The Janssen's vertical stress (Eq. 4.1a) is multiplied by the lateral pressure coefficient to obtain the wall normal stress (Eq. 4.1b), shown in Fig. 4.13b.

The lateral pressure coefficient was determined for K_0 condition as 0.455. The basis for choice of this condition has been presented in some detail in subsection 2.6.2. The obtained value is close to 0.4 proposed by Janssen in his work and within the 0.3-0.6 range specified by Schulze (2008) for estimate of stresses in the silo barrel. The angle of internal friction, ϕ used to determine this coefficient was obtained for dry LBS1 using a direct shear box testing machine. The test results are presented in Fig. 4.14b.

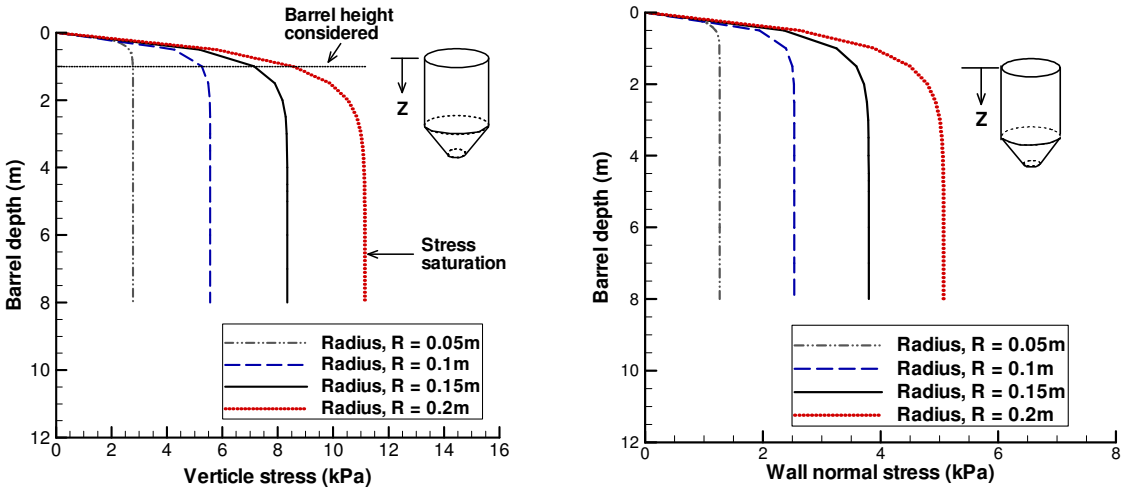

(a) Vertical stress (b) Wall normal stress

Figure 4.13: Stress profile within the cylindrical barrel

The coefficient of wall friction, μ, was determined using angle of friction, ϕ_w obtained for dry material using a direct shear box testing machine in which during shearing the surface of the silo wall formed the failure surface as solids confined in the upper half and under the normal load, N moved relative to the wall surface. Fig. 4.14a shows how the direct shear box was used to determine the wall friction angle. The experimental data is shown in Fig. 4.14b together with the internal angle of friction tests data. Shear testers are said to be the most suitable for determining the internal angle of friction of granular materials for silo design (Schulze, 2008). It should be noted that the density of the solids, ρ used in the direct shear box testing and hence the design reflected the density subsequently used in the model tests.

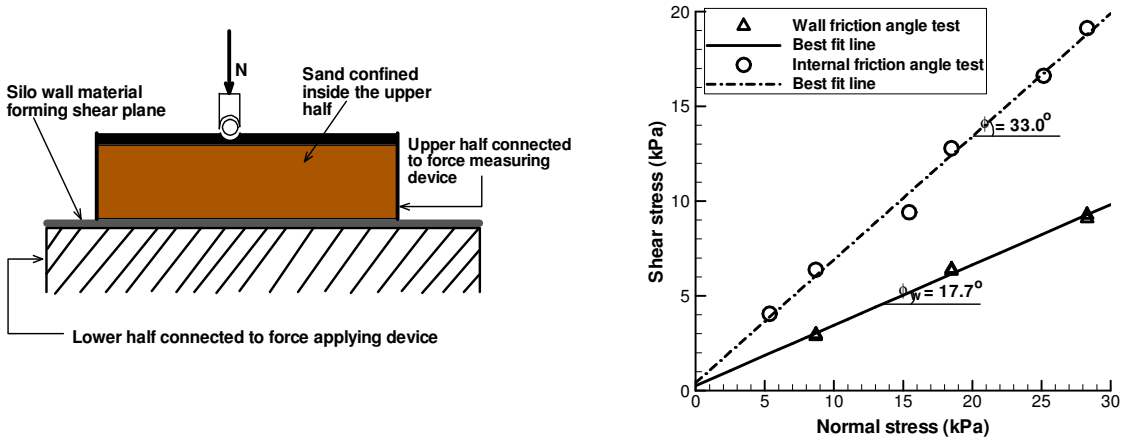

(a) Set up of the direct shear box test

(b) Test results for wall friction angle and internal friction angle

Figure 4.14: Experimental set up and data used in the design of a silo model

4.4.1.2 Hopper half angle and flow factor determination

The hopper half angle was determined using design charts, as is usually the case (Schulze, 2008; Ketterhagen et al., 2009). The design charts relate the hopper half angle to the wall friction angle and internal angle of friction for a given bulk solids. The slope of the hopper wall was decided such that the corresponding flow factor was greater than unit. Flow factor is used as a measure of flowability. The Perspex was selected as silo wall material for visibility reasons and in order to prevent structural failures due to yielding of the wall so as to satisfy the K_0 condition. Table 4-2 presents a summary of the design input and output parameters.

Table 4-2: Silo model design parameters

Selected input data		**Input data from tests**		**Output data**	
Silo barrel height, Z (m)	1.0	Angle of wall friction, ϕ_w (deg)	17.7	Barrel height required, Z (m)	5.7
Angle of repose for top material	0.0	Internal angle of friction, ϕ (deg)	33.0	Hopper angle, β (deg)	30
Barrel radius, R (m)	0.15	Mean particle diameter, d (mm)	0.06	Hopper height, H (cm)	26
Solids density, ρ (Mg/m^3)	1.638	Lateral pressure coefficient, K_0	0.455	Minimum outlet opening, D_{min} (cm)	0.5
				Flow factor, *ff*	1.73

It was hoped that the flow factor would also be computed as the ratio of the consolidation stress to the unconfined yield strength determined from direct shear box test results, as is at times the practice (Schulze, 2008). Such a computed factor would then be compared with that estimated from the design charts and the lesser of the two used to chose the design hopper half angle. An attempt was thus made at obtaining the consolidation stress through a try and error approach. Starting with an underconsolidated material, different but identical samples were sheared under different normal stresses in direct shear box. The idea was to shear each of the samples to critical state and then characterise the resultant critical densities according to the applied normal stress. A critical state in this case is one corresponding to a specimen that has been sheared from its underconsolidation condition to a steady-state condition, defined by conditions of constant shear stress and material volume or density.

From Fig. 4.15a&b it can be seen that critical state was reached in a sample sheared at a normal stress of 8.8kPa. When the normal stress was increased to 18.6kPa and above, it become unclear as to whether or not the samples reached critical state. At these stresses whereas a condition of constant shear stress was achieved (Fig. 4.15a), constant volume was not (Fig. 4.15b). It is not clear whether this is attributable to the nature of the direct shear box test or critical state was truly not reached. The shearing process was executed to the limit of the equipment. On reaching the peak shear stress the top platen of the shear box started to rotate and went on for as long as shearing was continued. As a result it was concluded that the standard direct shear box test was not suitable for the determination of consolidation stress for the material used in this research project; the attempt was considered unsuccessful.

A successful attempt would have meant that the normal and shear stresses giving the critical state with the desired density are identified on the yield locus and a stress circle drawn tangent to the yield locus (also called Mohr-Coulomb failure envelope) at this point (Fig. 4.15d). The major principal stress of the circle passing through the critical point which represents the condition for failure without volume change would then be taken as the characteristic consolidation stress. It is assumed to represent the stress conditions of the material as it flows downwards towards the outlet. The unconfined yield strength σ_c would then be determined from the yield locus, as illustrated in Fig. 4.15d. A circle would be drawn to pass through the origin and tangential to the

failure envelope. The diameter of the resultant circle is the unconfined yield strength (Schulze, 2008).

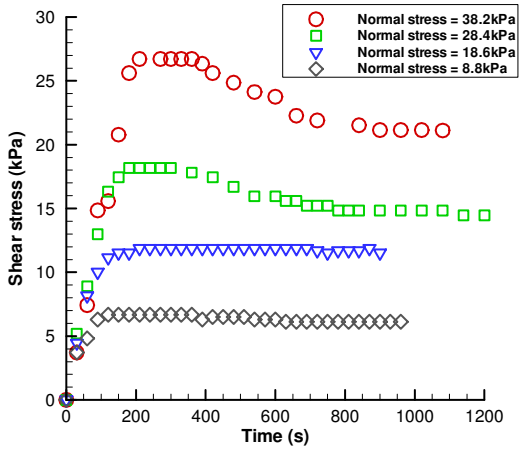

(a) Shear stress

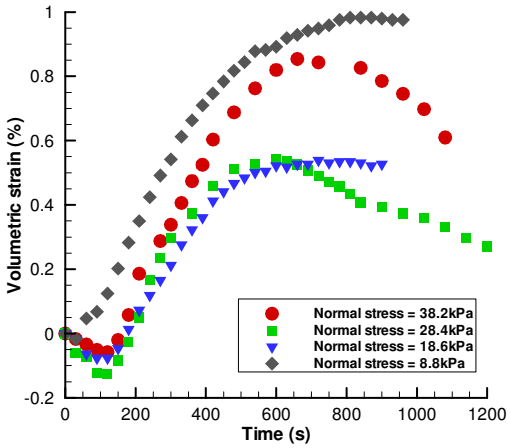

(b) Volumetric strain

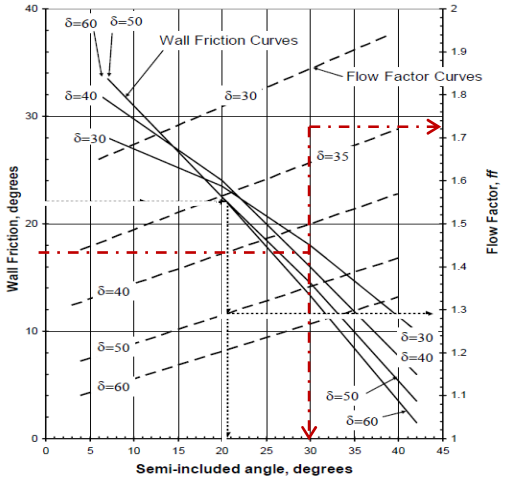

(c) Jenike's chart for conical hopper outlet and flow factor

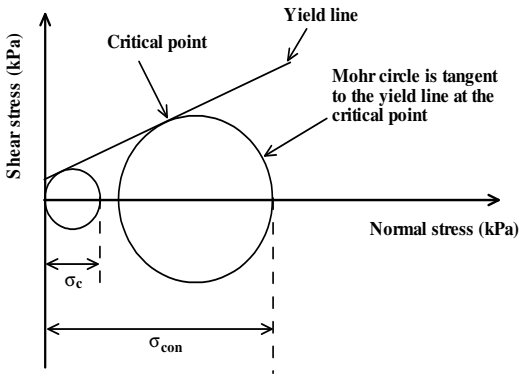

(d) σ_{con} and σ_c determination from Mohr-Coulomb envelope

Figure 4.15: Flow factor determination: Direct shear box test results and Jenike's chart

4.4.1.3 Hopper outlet determination

Next was to determine the hopper outlet diameter. A detailed account of the procedure involved is given in subsection 2.6.1. Using the approach recommended for prevention of mechanical arching arising from interlocking of particles, the minimum hopper outlet was conservatively determined as 5mm. The criterion is to ensure that an outlet diameter in excess of 8 (or 10 where particles are highly angular) times the particle diameter is chosen (Rotter, 2001). Lower factor of about 6 may be used for rounded materials (e.g. Mankoc et al., 2007). The mean particle diameter of the ~82% sphericity Leighton Buzzard sand used in this project was 0.6mm and the maximum particle passed 2.0mm sieve and was retained on 1.18mm sieve.

4.4.2 Model Configuration and Construction

The general configuration of the silo model is shown in Fig. 4.16a. Table 4-2 is a summary of the design parameters. It was made out of Perspex and was axisymmetric. The model consisted of a 30cm diameter cylindrical shell (barrel) and a 26cm height conical hopper. The hopper half angle, β, was 30º. The model was intended to simulate stiff-wall deep silos in which overburden stress increases with depth up to a maximum and the stress due to the weight of the uppermost solids does not contribute to the stresses at the bottom. As indicated in subsection 4.4.1 for a 30cm diameter barrel and wall friction coefficient, μ, of 0.3193 this condition of maximum overburden stress required that the minimum barrel depth is 5.7m. However such a value was not reasonable for a laboratory scale as the required height is in excess of the headroom of the laboratory. Working with such a model would also be difficult in many aspects but emptying the material in the event of no flow. In this model the barrel depth was thus limited to 1.0m. A surcharge was therefore necessary to cater for the extra stress that would be experienced at the transition due to the overburden of the additional top 4.7m of the solids. The surcharge was however not added during the reported tests as the parameters of interest are not dependent on level of material in the barrel (e.g. Fowler & Glastonbury, 1959; Beverloo et al., 1961).

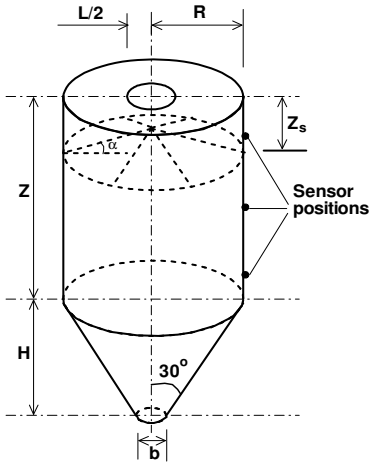

(a) Configuration of the silo model

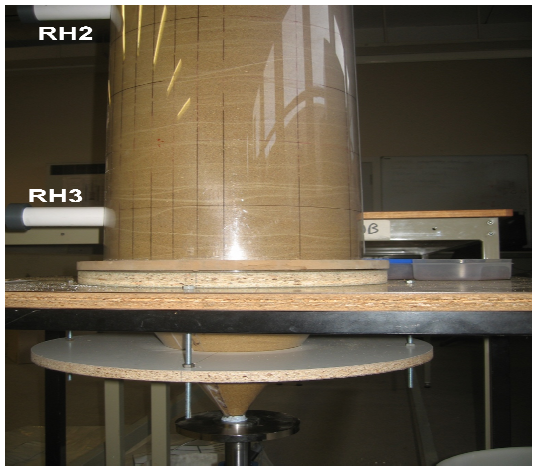

(b) Set up of the silo model test

Figure 4.16: Configuration of the silo model used in the current research project

The discharge point of the hopper was 0.5m off the ground surface. This position allowed for placement of a container underneath the hopper outlet to facilitate easy collection of the solids as they flowed out of the hopper. It was also convenient to fill the silo and to make observations, take photographs, micrographs and micro-video clips

of the solids during the tests. As shown in Fig. 4.16b, the barrel was instrumented with three relative humidity sensors (RH1, RH2 and RH3; numbered from top to bottom). These sensors were strategically located to respectively capture and define the meridional variation of relative humidity in the silo. The water content at corresponding locations was taken during sample preparation and confirmed at the end of the test.

4.5 Concluding Remarks

The major equipment used in the accomplishment of the objectives of this research project was unsaturated triaxial equipment and the pressure plate extractor. A physical silo model was also designed and constructed to study the influence of moisture on material flowability. These have been presented and described in detail in this chapter. The capacities of the equipment and their accuracies have been particularly given considerable attention. The rigorous calibrations of the equipment give confidence and credence to the accuracy of the measured results.

CHAPTER FIVE

5 EXPERIMENTAL CHARACTERISATION OF WATER RETENTION BEHAVIOUR

5.1 Introduction

This chapter presents an experimental characterisation of the water retention behaviour of the tested granular materials. The relationship between water content and matric suction, known as the water retention curve (WRC), was used in the characterisation. These water retention curves were a cornerstone for the determination of the suitability of the selected materials for further testing and the range of suction and hence water content appropriate for the subsequent tests on mechanical behaviour characterisation of the same materials. The chapter is logically organised into five sections. After the experimental programme, experimental results are presented and discussed. The ability of the existing empirical models to describe the water retention behaviour of the tested materials are then discussed before the chapter ends with concluding remarks in terms of the implications of the results to the subsequent parts of the thesis. The experimental equipment and experimental technique and procedures used in this part of the study have been presented in chapter 4 and chapter 3 respectively.

5.2 Experimental Programme

The experimental programme for the water retention curves (WRCs) comprised mainly pressure plate testing of two (2) granular materials namely glass beads and sand. The first (primary) drying paths of the WRCs were followed starting from a saturated sample. After the samples were sufficiently dried by increasing matric suction they were rewetted by decreasing matric suction to define the first (primary) wetting paths. This is the test procedure for determining the primary paths of the WRC. The primary drying and wetting paths enclose the region of possible water content and matric suction combinations for a given material at particular conditions. The combinations in between the enclosed region define scanning curves while the combinations outside the enclosed region are unlikely. Supplementary data points obtained using the filter paper method are also included in the results to check how the results for the as-prepared samples (without any hydraulic history) compare with those measured using the pressure plate (with a hydraulic history).

Table 5-1 presents a summary of all the WRC tests performed. In the table, tests are sequentially named according to the material type and test series, with GBS1 and GBS2 standing for glass beads Type I and II respectively, LBS1 for Leighton buzzard sand and LBS2 for modified Leighton Buzzard sand. Particle size, the initial void ratio, hydraulic path followed (drying or wetting) as well as the number of tests per hydraulic path and total test duration are also included in the table. In the last table column the test method is specified with PP standing for pressure plate and FP for filter paper. Unsuccessful tests are acronymed as UT.

Table 5-1: Water retention curve tests carried out

Material	**Test**		**Particle size range** (mm)	**Initial void ratio,** e_o (-)	**Hydraulic path followed**	**Number of tests**	**Total test duration (week)**	**Test method**
	Series	**ID**						
GLASS BEADS	GBS1	T01	0.25-0.50	0.55	1st Drying	7	7	PP
		T02			1st Wetting	5	5	
		T03			1st Drying	6	6	
		T04			1st Wetting	5	5	
		T05			-	4	2	FP
		T06		0.63	1st Drying	7	7	PP
	GBS2	T07	0.09-0.15	0.55	1st Drying	8	8	
		T08			1st Wetting	7	7	
		T09			2nd Drying	5	5	
LEIGHTON BUZZARD SAND	LBS1	T01	0.063-1.18	0.62	1st Drying	8	8	
		T02			1st Wetting	UT	6	
		T03			-	3	2	FP
		T04		0.56	1st Drying	3	3	PP
		T05			1st Drying	6	6	
	LBS2	T06	0.212-0.50		1st Drying	7	7	
		T07			1st Wetting	6	6	
		T08			2nd Drying	5	5	
		T09			-	3	2	FP

As presented in Table 5-1, a complete WRC for each material is not from a single sample (test) but from a number of practically identical samples. This was inevitable because of the approach adopted i.e. destroying a sample each time the equilibrium water content for a given matric suction was obtained. It is however hoped that using

different but identical samples did not affect the accuracy of the results as they have been evidently demonstrated to be reproducible (see Fig. 5.1).

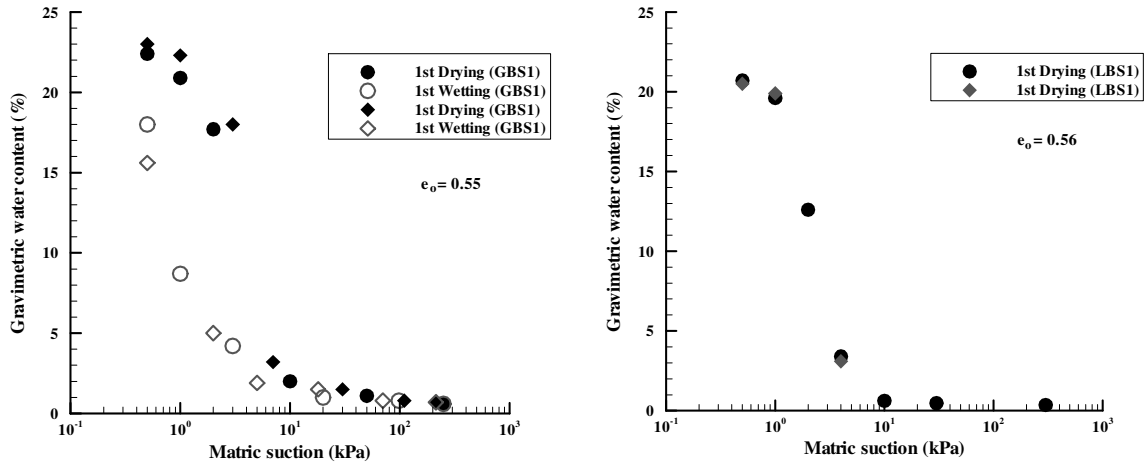

(a) Glass beads (GBS1) (b) Leighton Buzzard sand (LBS1)

Figure 5.1: Test results demonstrating reproducibility of WRCs

With results from the above experimental programme, a number of pertinent factors that influence the water retention characteristics of particulate materials have been assessed. In the following section the experimental results are presented and discussed.

5.3 Water Retention Curves Results and Discussion

In this section the experimental results of the water retention curves and characteristics are presented and discussed according to the variable of interest starting with the primary water retention curves followed by the hysteresis loop. The effect of initial void ratio, cycles of drying-wetting, particle size/grading and particle shape are presented. The results are presented in terms of both gravimetric water content and water ratio vis-à-vis matric suction and they are discussed with reference to the data from previous studies of similar or related materials. The ability of the used deliberately simple materials to capture and explain the features of water retention curves often reported for soils is particularly explored. The robustness of the commonly used mathematical expressions to describe WRC is also checked.

5.3.1 WRC: Primary drying and wetting curves

The primary drying and wetting curves were determined for glass beads of 0.25-0.50mm and 0.09-0.15mm and for Leighton Buzzard sand of 0.063-1.18mm and 0.212-0.50mm particle size ranges. The primary drying path refer to a stepwise gradual

drying of a sample from zero suction (saturated condition) whilst slow wetting of a sample previously dried by increasing suction is termed primary wetting path. Fig. 5.2a shows the primary (first) drying and primary wetting paths for glass beads (tests T01, T02, T03 and T04 of series GBS1 and tests T07 and T08 of series GBS2 in Table 5-1) while those of Leighton Buzzard sand (tests T04 and T05 of series LBS1 and tests T06 and T07 of series LBS2 in Table 5-1) are presented in Fig. 5.2b. The associated retention characteristics are summarised in Table 5-2. As indicated in Table 5-1 and Fig. 5.2, in these tests the initial void ratio of glass beads samples was 0.55 while that of Leighton Buzzard sand samples was 0.56. In the figures the arrows shown parallel to the curves indicate the direction of hydraulic path followed.

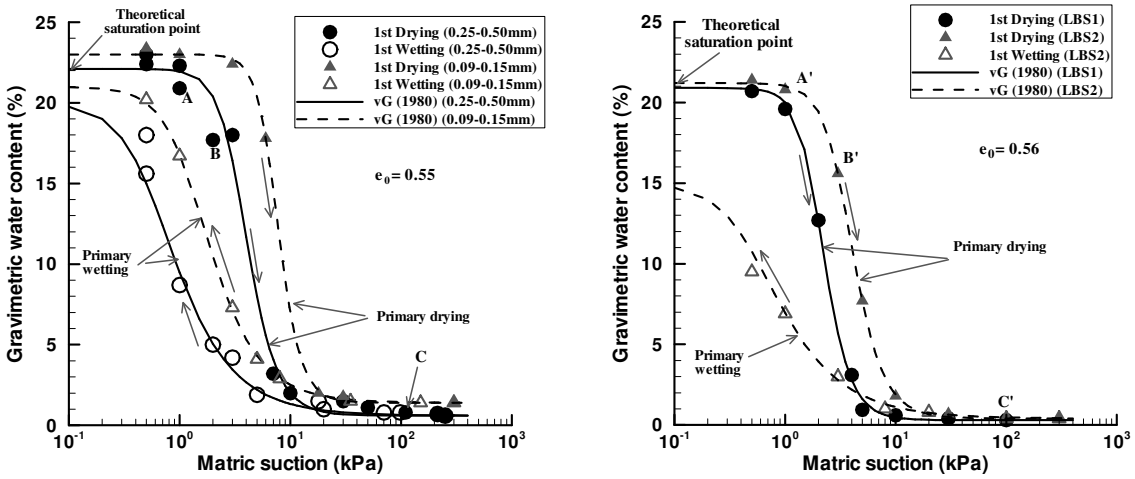

(a) Glass beads (GBS) (b) Leighton Buzzard sand (LBS)

Figure 5.2: Primary WRC results for the tested materials

Table 5-2: Water retention characteristics of the tested materials

Material	**Series**	ψ_a **(kPa)**	w_s **(%)**	**Residual conditions**		**Water entry conditions**		**Slope of tangent line at inflection point**	
				ψ_r (kPa)	w_r (%)	ψ_w (kPa)	w_w (%)	Drying (-)	Wetting (-)
Glass beads	GBS1	2.0	22.1	7.8	1.5	2.8	1.1	34.85	18.17
	GBS2	4.8	23.0	14.0	1.6	5.7	1.5	53.78	20.31
Leighton Buzzard sand	LBS1	1.3	20.9	3.8	0.5	-	-	43.79	-
	LBS2	2.1	21.2	8.0	0.9	3.0	1.0	34.95	12.50

The features of water retention curves often observed in soils have generally been well captured. Regardless of the material type and particle size and shape, increasing matric suction of the sample from zero to about the air-entry value was not accompanied by any significant change in water content. The micrographs (see Fig. 5.3a-d) taken of the sample of Type 1 glass beads and of LBS2 immediately after saturation and at conditions marked "A" and "A[1]" in Fig. 5.2a&b within this saturation regime corroborates with this observation. The images show that while some water redistribution occurred following increase in matric suction to about 1kPa, all the voids remained filled with water with the particles completely submerged at full saturation. It should be noted that the water content of samples immediately after saturation was not measured but based on the measured points before the air-entry value it was slightly higher than the theoretical value calculated using the expression: $w = e_0 / G_s$. These observations indicate that for a given saturated system of particulate material with continuous voids, there exists a minimum potential (force) below which water contained in the voids will not drain. The difference in results (Fig. 5.2 & Table 5-2) is discussed in later parts of this chapter.

This ability of water and indeed any other wetting liquids to hold on to the surface of the system in which it is contained against the forces tending to drain it is long known to many engineers and scientists. It is now widely recognised that when a capillary tube is brought in contact with the free surface of water, the capillary force causes the water to rise in the tube until when the opposing gravitational forces are balanced. The same analogy has been used to explain the formation of *capillary fringe* above the groundwater table (e.g. Childs, 1940) and "to help in the visualisation of the distribution and form of 'capillary' water held in the soil pores as well as to help in providing quantitative interpretation of the form of soil water characteristic curves for various soils" (Barbour, 1998: p. 10). As explained earlier in section 2.1, within the capillary fringe soil is saturated or nearly so. For a given liquid, the height of the capillary rise in soil or the capillary tube and the properties of the air-water interface are, besides environmental factors such as temperature, dependent on the properties of the container surface (i.e. of the constituent particles in case of soil). It therefore means that in investigating and discussing the factors responsible for capillary saturation in different materials attention should be paid to all the surface properties of the materials under consideration.

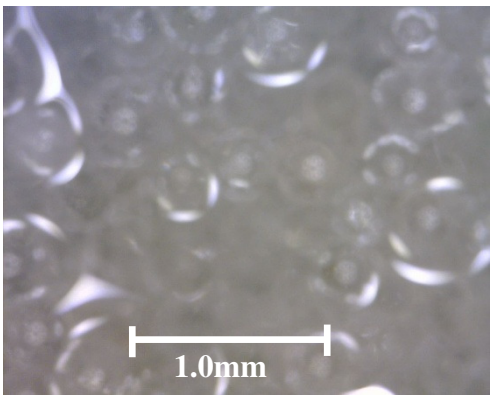

(a) Glass beads (GBS1): Saturated

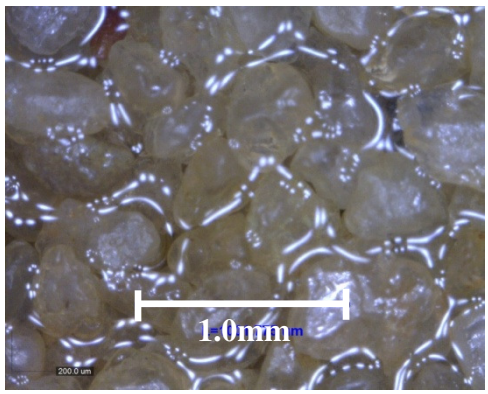

(b) Sand (LBS2): Saturated

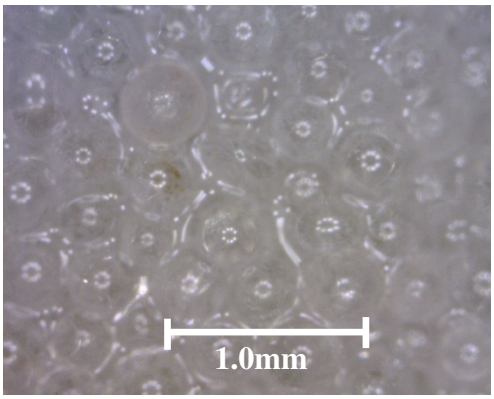

(c) GBS1: 1.0kPa; X205 (point A)

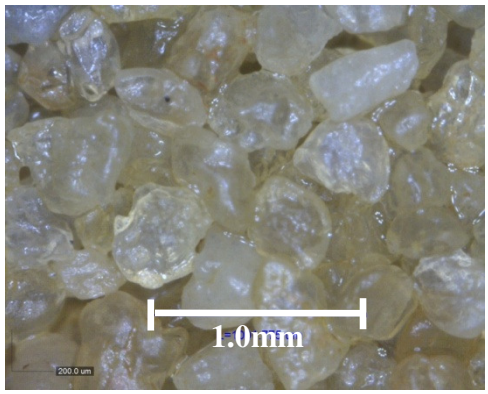

(d) LBS2: 1.0kPa; X210 (point A[l])

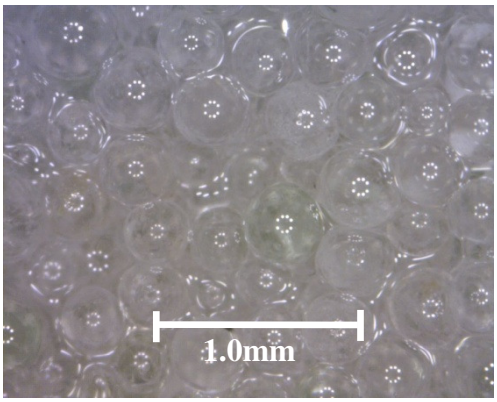

(e) GBS1: 2.0kPa; X205 (point B)

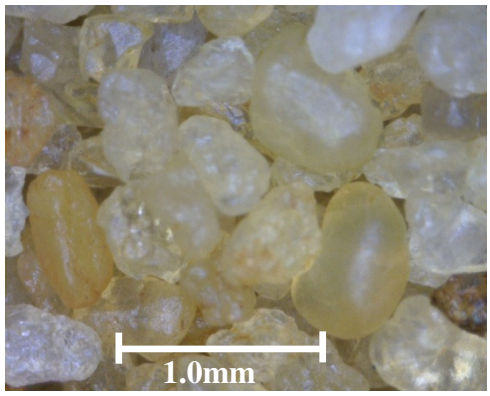

(f) LBS2: 3.0kPa; X210 (point B[l])

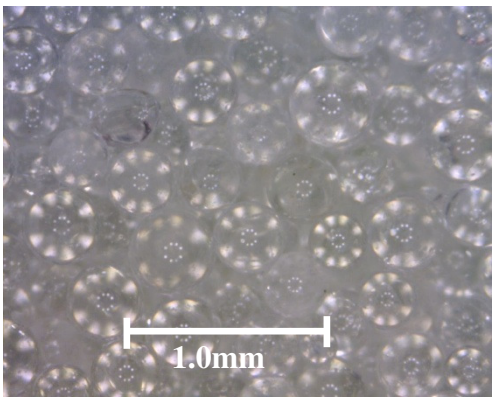

(g) GBS1: 100kPa; X205 (point C)

(h) LBS2: 100kPa; X210 (point C[l])

Figure 5.3: Results of microscopic observations to see the distribution of water

Experimental evidence from soil testing shows that within the saturated capillary regime water content remains nearly constant as suction is increased to the air-entry value (Leverett, 1940; Brooks & Corey, 1964; Fredlund & Rahardjo, 1993; Yang et al., 2004). These authors and many more have attributed this behaviour to the presence of surface tension of water which prevents air from entering into the sample voids. Fig. 5.4 illustrates the involved well known mechanism. When a liquid is introduced between any two spherical particles of diameter D and a distance L apart it gets attracted to each of the particles. With the resultant liquid bridge of say radius R_2, a bonding force F_s due to surface tension T_s of the liquid acting along the section $X-X$, introduces the contact force between the two spherical particles that must be overcome before the liquid is expelled from the particles. The contact force is called the capillary force and is a function of the contact and filling angles (α and φ) and the separation distance. These properties are dependent on the particle surface characteristics. The exact shape of the air-liquid interface is given by the Young-Laplace equation. This is out of scope of this chapter.

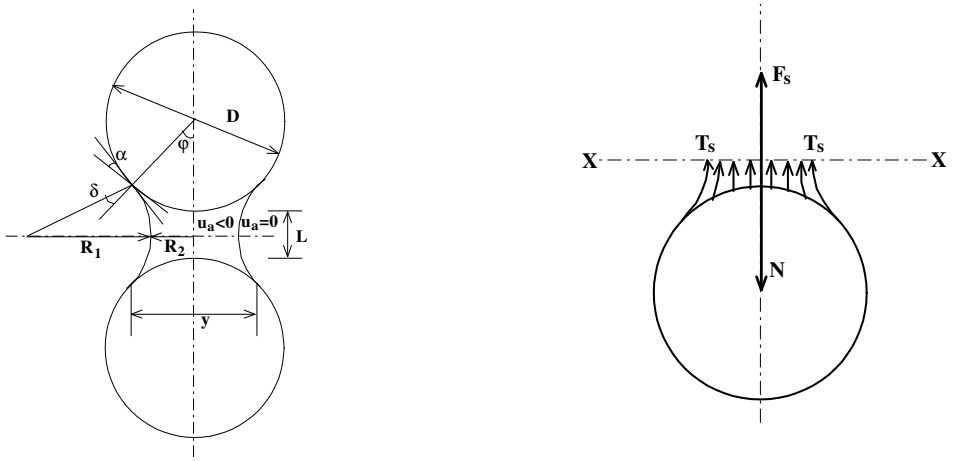

(a) Two spherical particles held together by a liquid bridge

(b) Free body diagram of the bonding forces

Figure 5.4: Capillary mechanism responsible for maintaining water is soil at $\psi_m \prec \psi_a$

It has also been argued that ahead of the air-entry value finer soils present a higher water retention capacity than coarser soils (e.g. Brooks & Corey, 1964; Fredlund & Xing, 1994; Vanapalli, 1994; Zapata et al., 2000; Hodnett & Tomasella, 2002; Miller et al., 2002). Similar deductions can be made by comparing the experimental results in different studies e.g. Buckingham (1907 in Barbour, 1998) and Yang et al. (2004) who worked on fine and or coarse soils respectively. One can also deduce from many of the

studies that finer soils adsorb and imbibe more than coarser soils upon wetting (e.g. Leverett, 1940; Yang et al., 2004). In most of the above studies, however, many of the factors that influence material behaviour have been tacitly assumed to be insignificant. This may be unrealistic especially when comparing the water retention characteristics of noncohesive coarse and cohesive fine soils.

Naturally, soils exist as deposits of particles of different characteristics with finer particles tending to be more rounded and electro-chemically active. Therefore comparing results based on only one factor without controlling all other factors could be misleading. In studying and discussing the factors that influence the water retention behaviour of soils, sieved particle size and or plasticity index (or soil texture) have been used whilst ignoring the other aforementioned influencing factors (e.g. Buckingham, 1907; Brooks & Corey, 1964; Hodnett & Tomasella, 2002; Yang et al., 2004; Houston et al., 2006). The granular materials used in this study were *clean* inert materials free of adhesion forces and with known particle characteristics. It therefore suffices to conclude that within the saturated capillary regime it was purely the capillary forces resulting from surface tension of water that prevented air from entering into the sample voids.

After the air-entry value, further increase in matric suction resulted in significant increase in water content per unit change in suction. The steep slopes of the curves in this funicular bridge zone imply a considerable increase in drainage of water from the samples. Micrographs (see Fig. 5.3e&f) taken of the glass beads of Type 1 and LBS2 samples at the conditions marked "B" and "B^1" in Fig. 5.2a&b show that much of the water drained out of the sample within this zone and the particle edges (outlines) became more clear. It is probable that within the funicular bridge zone matric suction is due to both the adsorbed and menisci water. Typically, similar findings have been reported in the literature (e.g. Brooks & Corey, 1964; Fredlund & Rahardjo, 1993; Yang et al., 2004; Houston et al., 2006; Kawajiri et al., 2010). Fredlund & Rahardjo (1993) argued that in the region of the WRC bound by the air-entry value and the residual suction liquid transport is governed by liquid flow as the effect of matric suction is dominant. As explained earlier in subsection 2.2.1, matric suction is due to both menisci and adsorbed water. The presence of adsorbed water is backed by the fact that liquid continuity within the interconnected voids of the system of packed particles is necessary for it to flow. The results presented in Fig. 5.2 suggest that the menisci and adsorbed water are dependent on the particles properties with the latter becoming dominant as

particle size is reduced. This is consistent with the understanding that adsorbed water is more dominant in clays than sands (e.g. Fredlund & Rahardjo, 1993). The difference is that in the current study the surface properties of the different size particles are the same. This issue is pursued further in subsection 5.3.5.

When water is sufficiently drained from the sample any remaining liquid water becomes disconnected and localized at the inter-particle contacts (e.g. Fredlund & Rahardjo, 1993; Wheeler & Karube, 1996). In this pendular bridge regime, characterized by the residual matric suction ψ_r and residual water content w_r, the matric suction is due to only the menisci water and higher energy is necessary to remove any further liquid from the void. In fact the role of matric suction in causing liquid release progressively diminishes and the dominant mechanism of liquid transfer becomes vapour. Further increase in matric suction beyond the residual value was followed by very small changes in water content (Fig. 5.2). Finally after the matric suction of about 100kPa, negligible water content change was observed in the sample. Images taken of the sample at 100kPa (Fig. 5.3g&h reproduced as Fig. 5.5a&b) were similar in terms of appearance to those of the dry sample (Fig. 5.5c&d) suggesting that within the residual zone very little water existed in the sample.

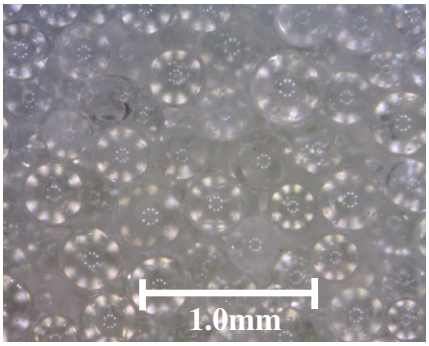

(a) GBS1: 100kPa; X205 (point C)

(b) LBS2: 100kPa; X210 (point C')

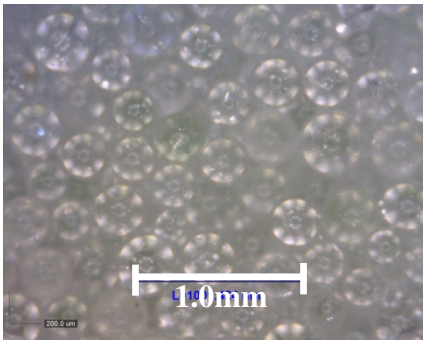

(c) GBS1: Dry; X200

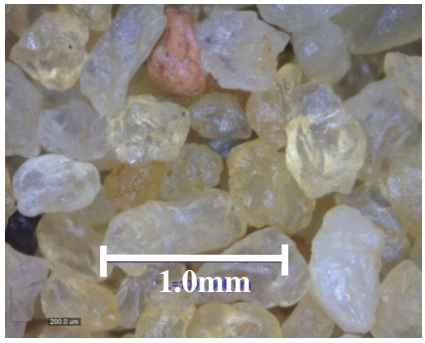

(d) LBS2: Dry; X210

Figure 5.5: Microscopic image of sample at 100kPa suction and of dry sample

It was noted that when the mould containing the sample was lifted, as shown in Fig. 5.6, the particles did not fall apart due to gravitational forces; clearly indicating that there were inter-particle forces holding the sample together. Such forces could have been due to adhesion (probably due to liquid bridges or adhesive nature of the test materials) or pore air suction. However, as the sample did not fall apart for a long period of time (observed for about 3minutes) it is unlikely that pore air suction was the source of the binding forces. Also given that no such forces evidently existed in the dry sample the particle surfaces did not possess any adhesion. It is therefore concluded here that it is the liquid bridge induced adhesive forces that were responsible for holding the sample together. These have been illustrated in Fig. 5.4.

(c) Glass beads (GBS1)

(d) Leighton Buzzard sand (LBS2)

Figure 5.6: Samples held together by liquid bridge induced adhesion

When matric suction for the previously dried sample (through increasing the matric suction to ~300kPa) was decreased the sample rewetted (Fig. 5.2). Until about the water-entry value, water content increased at a rate almost similar to the one for the drying path. Thereafter the change of water content per unit change in suction increased remarkably. The resultant wetting path in this funicular regime was distinctly different from the drying path, giving rise to a hysteresis that has been observed in previous studies of both coarse and fine soils (e.g. Leverett, 1940; Fredlund & Rahardjo, 1993; Yang et al., 2004). Analysis of the observed hysteresis is presented next.

5.3.2 WRC: Hysteresis

The hysteresis of the WRC was studied by subjecting initially saturated samples to a drying-wetting cycle. The WRC results were shown in Fig. 5.2 while the characteristics were summarised in Table 5-2. In carrying out the hysteresis analysis a mathematical equation is necessary. The fitted van Genuchten (1980) equation was used for this purpose and the results are presented in Table 5-3. The hysteresis is bigger for finer GBS2 beads and at low suctions for each sample type. At matric suctions greater than about 20kPa there is evidently no hysteresis in the water retention behaviour of the samples, typical of what is observed in coarse soils (e.g. Yang et al., 2004). In addition, the difference between water content of the sample undergoing drying and that undergoing wetting at extremely low suctions (near saturation) was smaller for finer particles, again typical of what is reported in the literature for soils (e.g. Yang et al., 2004). These results clearly show that glass beads can adequately capture and can be relied on to explain the behaviour of cohesionless soils and other industrial bulk solids. This is very important because then the complex interactions present in many of such materials can be introduced one at a time.

From Fig. 5.2 and Table 5-3 it is obvious that the WRC hysteresis is dependent on the amount of water or suction in the sample. Viewed on a semi-logarithmic scale, the hysteresis generally reduces as water content is decreased following an increase in matric suction. The WRCs for a particular material appear to converge at 20kPa suction suggesting a unique relationship between matric suction and water content regardless of whether the sample is drying or wetting. This observation may be explained in terms of the dependence of the hysteresis on the mechanism of water removal from the sample. At sufficiently low water contents any removal of liquid from the matrix of the sample is through vapour and so matric suction effect is insignificant.

Table 5-3: Hysteresis analysis results of the WRCs for the tested materials

Material	Particle size (mm)	ψ_a (kPa)	Matric suction	Water content on a hydraulic path		Difference in water content
				Drying	Wetting	
			(kPa)	(%)	(%)	(%)
Glass beads	0.25-0.50	2.0	100	0.614	0.620	-0.006
			30	0.797	0.705	0.092
			20	1.086	0.7847	0.301
			10	2.824	1.081	1.743
			5	9.232	1.851	7.381
			1	21.780	10.120	11.661
			0.5	21.976	16.162	5.814
			0.1	22.000	19.889	2.111
	0.09-0.15	4.8	100	1.401	1.441	-0.039
			30	1.517	1.628	-0.111
			20	1.912	1.807	0.105
			10	6.986	2.494	4.492
			5	20.347	4.292	16.055
			1	22.998	16.855	6.143
			0.5	23.000	20.008	2.992
			0.1	23.000	20.979	2.021
Leighton Buzzard sand	0.212-0.50	2.1	100	0.404	0.523	-0.119
			30	0.494	0.748	-0.254
			20	0.663	0.894	-0.231
			10	1.893	1.296	0.597
			5	7.673	2.024	5.649
			1	21.032	6.454	14.578
			0.5	21.185	9.836	11.349
			0.1	21.200	14.499	6.701

5.3.3 WRC: Effect of initial void ratio

The effect of initial void ratio on WRC was evaluated by comparing the results of tests T01 & T03 with T06 of series GBS1 and tests T01 with T04 & T05 of series LBS1 in Table 5-1. The compared results were obtained from tests conducted on similar samples except the initial void ratio. As expected, the results (shown in Fig. 5.7) indicate that higher void ratio meant that more water was taken in by the sample to fill up the larger voids. In the saturated capillary regime, therefore, the experimental points of the samples with higher initial void ratio plotted above those of lower initial void ratio. After the air-entry value, however, the effect of initial void ratio is not as evident especially so for sand. In the transition zone it can be argued that the observed discrepancy in the results (Fig. 5.7) is probably ascribed to the scatter nature of the results rather than the effect of initial void ratio. If this was true then it would mean that as soon as air starts to enter into the largest voids the effect of initial void ratio disappears. The question would then be why all the measured points of the lower initial void ratio sample plot left of those of the sample with higher initial void ratio. With this in mind, it is hereby therefore concluded that the observed discrepancy in results was indeed due to the effect of initial void ratio. In the residual zone, all the experimental data points plotted as if they were obtained from samples of the same initial void ratio. Three hypotheses are most probable here. The first one is that prior to air entry into the sample air pressure had an effect of compressing the sample, similar to the one from boundary applied pressure. Under this hypothesis the samples with higher void ratio would compress more than those with lower void ratio and the effect of initial void ratio would disappear, as it did. If this were to qualify as the reason then the uniqueness in the results would commence right from the onset of the transition zone. Comparison of the results, however, seems to suggest that higher initial void ratio samples have a slightly steeper slope in the funicular zone than the one with lower void ratio.

The second hypothesis is that as matric suction was increased from zero through to the residual value void ratio continuously decreased. The validity of this hypothesis lies in the existence of a progressive disappearance of the effect, which is clearly nonevident. Moreover, no volume change was visually seen in either of the test samples at the end of the test. It is also noted that this theory seems not supported by any experimental evidence in the literature. Variation of the void ratio with increase in suction has been traced to the shrinkage or consolidation behaviour of the material (e.g. Bilgari et al., 2008) and is expected to be insignificant in noncohesive soils especially so when they

are sufficiently dense, as was the case in the current study. In their experimental work, Bilgari et al. (2008) observed that after the shrinkage limit void ratio tended to stabilise as suction was increased further and some clay-sand mixtures did not show any variation in void ratio at all. Hodnett & Tomasella (2002) also observed little scatter in the residual water contents for sandy soils compared to soils with higher silt and clay content. This leaves the third hypothesis as the most probable reason: That for noncompressible materials the WRC in residual zone does not depend on the initial void ratio.

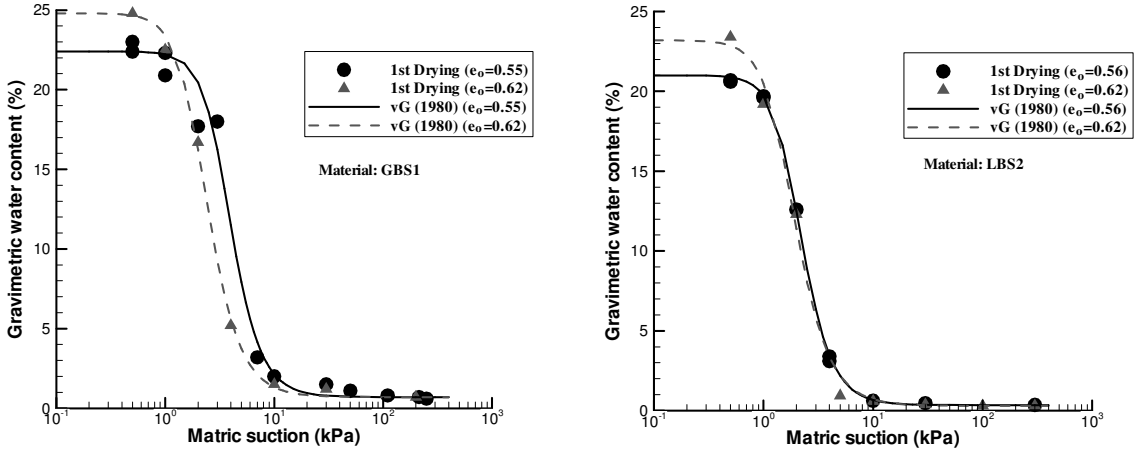

(a) Glass beads (GBS1) (b) Leighton Buzzard sand (LBS1)

Figure 5.7: Results showing effect of initial void ratio on WRCs

Although there is not enough experimental data to draw a strong conclusion on the effect of initial void ratio the third hypothesis is backed by experimental data from previous studies in the literature. It has generally been shown that decrease of initial void ratio results in a forward (and downward within the capillary regime) shift of the WRC (e.g. Yang et al., 2004) and many reasons have been given to explain this behaviour. This was observed in the current study to be very slight following a decrease in the initial void ratio from 0.62 to 0.55, especially for LBS1. According to the experimental data of Biglari et al. (2008), the shift is more for fine (clay) soils than for clay-sand mixtures. Biglari et al. tested Kaolinite clay and a mixture of 60% clay and 40% of medium uniformly graded sand (with fine content of about 1% and specific gravity of 2.69). This behaviour of the drying WRC for cohesive fine soils being more sensitive to initial void ratio and subsequently to changes in void ratio during drying than less or noncohesive soils can be explained from the constituent particles properties point of view.

Owing to the electro-chemical properties of the clay particles, they tend to adsorb more water than the inert noncohesive particles. It is because of this property that clays are susceptible to volumetric changes (i.e. swelling and shrinking) upon wetting and drying respectively (e.g. Kasangaki & Towhata, 2009). In addition, because clayey soils often exist as agglomerates rather than individual particles they present with aggregated structure with both intra-aggregate and inter-aggregate porosity (e.g. Romero & Vaunat, 2000; Koliji, 2008). The level of structural aggregation is a function of the voids in the material. Moreover, depending on the size and strength of the aggregates, the aforementioned features of aggregation may alter the WRC of the material from the one of unaggregated same mineralogy material. Of particular interest to this part of the thesis is the effect of the intra-aggregate porosity. Most of the moisture contained in there does not drain until the one in the inter-aggregates is completed, leading to an apparent residual condition. Once the intra-aggregates water (the adsorbed film of water) starts to drain a further reduction in volume may be registered and overall a bi-modal WRC is obtained. This therefore may explain the discrepancy between the WRCs of samples of clayey soils with different initial void ratio compared to nondeformable coarse granular materials.

5.3.4 WRC: Effect of cycles of drying-wetting

After first drying and wetting cycle, Type 2 glass beads (GBS2 series) and modified Leighton buzzard sand (LBS2 series) were subjected to second drying path in tests T09 and T08 respectively (refer to Table 5-1) to explore the effect of further cycles of drying and wetting on the water retention behaviour (Fig. 5.8). It is interesting to note that the second drying path quickly joined the primary drying path suggesting that at relatively high suctions the observed drying path may be a characteristic path for the material. It was thus considered unnecessary to continue the tests on drying-wetting cycles.

The quick joining of the primary drying path by the second drying path is in contrast with soils containing fines where the subsequent drying path is often distinctly different from the first drying path (e.g. Ng & Pang, 2000a). In reference to the Ng & Pang (2000a) results, the current results indicate that other factors and not the liquid bridge induced forces are responsible for the distinct difference between the primary and subsequent drying paths observed in soils containing fine cohesive soils. There seems to be no existing experimental data on pure cohesionless soils showing the effect of drying-wetting cycles.

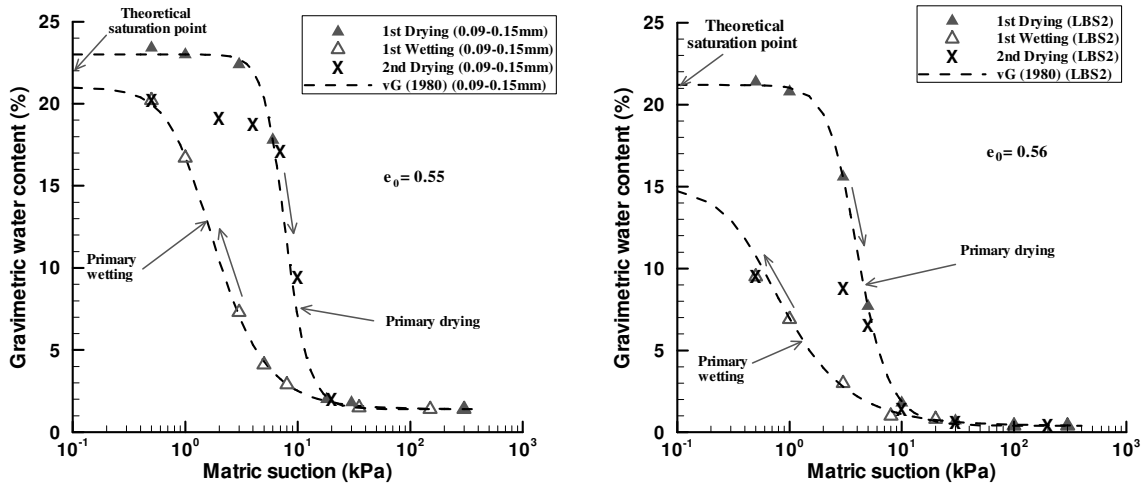

(a) Glass beads (GBS2) (b) Leighton Buzzard sand (LBS2)

Figure 5.8: Effect of cycles of drying-wetting cycles on WRCs

5.3.5 WRC: Effect of particle size/grading

The effect of particle size/grading is remarkably evident when a comparison is made between the results for 0.25-0.50mm and 0.09-0.15mm glass beads. For the matric suction range between 0kPa and the air-entry value, samples of finer beads display higher water retention capacity. The air-entry value is thus greater for smaller particles samples (Table 5-2). The finer material data plot slightly above those of the larger material (Fig. 5.2). As discussed in subsection 5.3.1, this is probably due to the effect of capillary action which is responsible for the prevention of air entrance into the voids. A packed system of smaller particles requires higher air pressure to break the capillary stress presented by the larger menisci than identical larger particles. Other characteristics influenced by the particle size include the hysteresis loop, amount of drainage, residual conditions, water entry conditions and the degree of wetting (Fig. 5.2, Table 5-2 and Table 5-3). The hysteresis has been presented and discussed in subsection 5.3.2. The residual conditions (residual matric suction and residual water content) and the water entry conditions (water-entry value and the corresponding water content) increased with reduction in particle size. The trend was however reversed for the residual air content. It decreased following particle size reduction. As for the rate of drainage and sorption, visual inspection of the WRCs on the semi-logarithmic scale suggests that the rate decreases with reduction in particle size. On a normal scale, however, it appears the trend is dependent on the range of absolute values bounding the transition zone. Typically, both desorption and sorption rates increase with decrease in particle size.

The particle size effects discussed above are also generally applicable to Leighton Buzzard sand. On the face of it however these particle size/grading effects appear to be smaller for Leighton Buzzard sand. This is because the scale factor between the two sizes is smaller for Leighton Buzzard sand than glass beads. The ratio between mean particle diameters is about 1.7 compared to 2.7 for glass beads. Therefore it was logical to compare the results after factoring in/out the sample mean particle size. It appears only two characteristics: air-entry value and the residual water content bear a direct relationship with the mean particle size (see Table 5-2). With other characteristics the particle size effect for glass beads was not the same as for sand. Whether this is because of the shape effect or not it is an issue that needs further analysis. The next subsection 5.3.4 is devoted to the analysis of the particle shape effect. This rather intriguing finding cannot be quantified with most soils and industrial bulk solids as they often present with the difficulty to control other influential factors.

Consistent with the observed effect of particle size/grading are many of the results of experimental studies in the literature. Buckingham (1907 in Barbour, 1998) was probably the first to present WRC of two soils (loam and clay). Suggesting the relationship between water content and capillary potential (suction) be termed as the soil-moisture characteristic curve, Childs (1940) presented results for sand and clay showing the same effect. Yang et al. (2004) carried out an experimental programme on five different soils to determine among other factors the effect of particle size on the WRC. They concluded that reduction in particle size increases the water retention capacity as seen from comparison of the WRC characteristics i.e. the air-entry value, residual suction and the water-entry value. Bilgari et al. (2008) also showed that the drying WRC of clay plots above and to the right of that of sandy clay (obtained by mixing 60% clay and 40% sand). Hodnett & Tomasella (2002) linked the residual water content to the surface area to explain the general increase of the former with increase in clay content. They observed that the distribution of the residual water content tended to spread with increasing silt and clay content. These later observations were in confirmation of those by earlier researchers (e.g. Brooks & Corey, 1964; Fredlund & Xing, 1994). It should be emphasised, however, that unlike in the current study where particle size was the only variable (with all other influential factors sufficiently controlled) in all the above previous studies and many others the contribution of additional unaccounted for influential constituent particle properties to the observed differences in behaviour cannot be ruled out. As shown in Fig. 5.9, in an attempt to

assess the effect of soil texture Vanapalli (1994) presented results comparing the desorption curves of four different soils: sand, Botkin silt, Indian Head till and Regina clay. As emphasised throughout this thesis, such a comparison can be misleading as many factors are bundled together. When particle size is varied by combining and mixing two or more materials then care should be exercised to ensure that other factors such as particle shape are not introduced. Short of that, the difference in behaviour cannot be associated with only one factor, like the case has been in many of the studies (e.g. Yang et al., 2008).

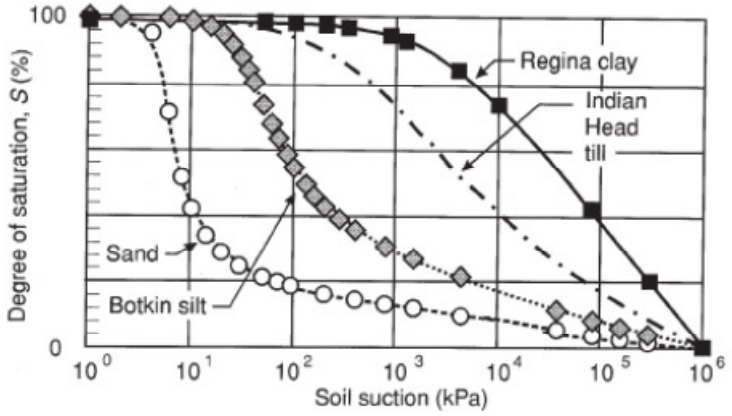

Figure 5.9: Influence of soil texture (after Vanapalli, 1994)

5.3.6 WRC: Effect of particle shape

In an attempt to examine the effect of particle shape on WRCs, LBS1 was modified to match the particle size distribution of GBS1. The resultant nonspherical sand was acrynomed as LBS2. Further details are provided in section 3.2. The WRCs are compared in Fig. 5.10a from which the difference in results is evident. It is however not immediately obvious as to whether or not the difference is due to the particle shape effect alone. Such a conclusion requires satisfying the condition that the LBS2 equivalent mean spherical particle diameter is equal to the mean particle size of GBS1. A shape factor is necessary for this purpose. As stated in section 3.2, it is the ratio of the equivalent mean spherical diameter to the average screen size of the particles (e.g. Beverloo et al., 1961). Details of how it was determined have been presented in section 3.2. As was presented in section 3.2, the shape factor (SF) of LBS2 was found to be 83.3% meaning that the equivalent spherical particle diameter of LBS2 was 0.292mm, slightly less than 0.330mm of GBS1. In line with the particle size effect discussed in the preceding subsection 5.3.5, the WRC of LBS2 would therefore be expected to plot slightly above and to the right of that of GBS1. Whereas this seems to be the case on the

drying path in the saturated capillary regime it is not after the air-entry value as well as on the entire wetting curve. In these parts of the WRC the LBS2 points consistently plot below the GBS1 points.

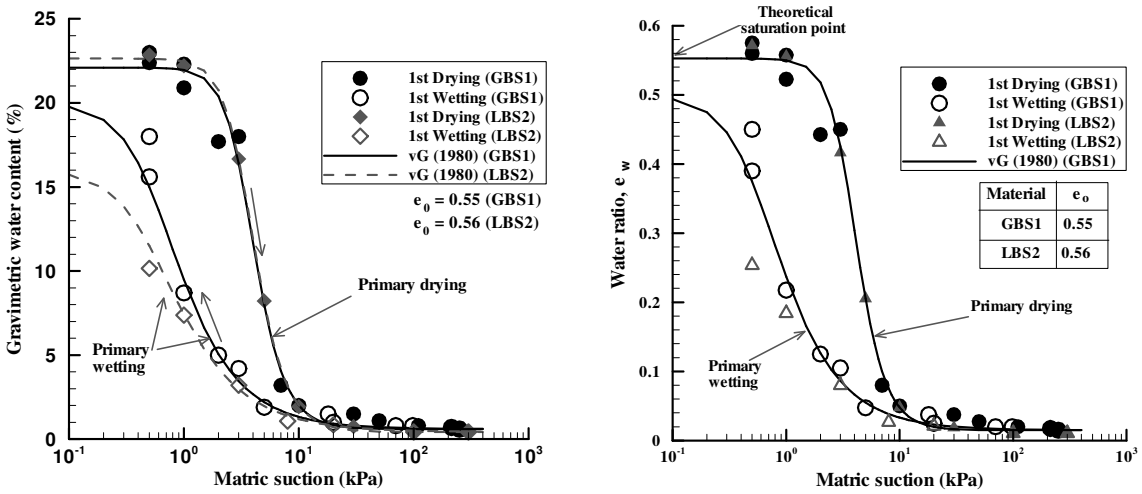

(a) Water content is gravimetric (b) Water content is volumetric

Figure 5.10: Effect of particle shape on WRCs

It is also noted that in comparing results in Fig. 5.10a, the water content is expressed in terms of gravimetric water content. Since the two materials have different particle density, such a comparison would be reasonable only if the capillary forces were directly influenced by the particle density. Instead it is the particle volume (or size of the particle) which directly affects the pore size and hence the meniscus properties that play a central role in influencing the capillary forces in any given system of packed particles. Besides taking into account the influence of changes in void ratio, if any, on the measured data, this is probably the reason why in many of the studies in the literature water content is expressed in terms of either volumetric water content or degree of saturation (e.g. Brooks & Corey, 1964; Vanapalli, 1994; Ng & Pang, 200a&b; Yang, et al., 2004; Ng & Menzies, 2007; Hoffmann & Tarantino, 2008; Bilgari et al., 2008; Ng et al., 2009) or water ratio (e.g. Romero & Vaunat, 2000; Yang et al., 2004). Whereas with both the volumetric water content and degree of saturation it is the system volumes that are compared, the former is believed to be superior. It is equivalent to the product of porosity (or void ratio) and degree of saturation. In fact some experimental evidence suggest that more consistent WRC results are obtainable when water content is expressed in terms of volumetric water content instead of degree of saturation (e.g. Bilgari et al., 2008). In their study Bilgari et al. (2008) observed that discrepancy in

results due to changes in void ratio narrowed especially so for clay-sand mixtures when water content was expressed in terms of volumetric water content instead of degree of saturation. The volumetric water content can be safely interchanged with water ratio, as was the case in the current study, since it is also a comparison of system volumes.

Luckily, it is possible to convert the gravimetric water content to any of the three quantities: volumetric water content, degree of saturation and water ratio. In fact in most of the reported studies it is the gravimetric water content that is actually measured and then converted into the desired parameter (e.g. Romero & Vaunat, 2000; Yang et al., 2004). To convert gravimetric water content to water ratio the former was multiplied by the particle specific gravity, as is usually done. The compared results in Fig. 5.10a are replotted and compared in Fig. 5.10b. Interestingly, when the water content is expressed in terms of water ratio, the different curves "collapse" into a single curve and the similarity in the WRC results of the two materials cannot be over emphasised but only in the saturated capillary and funicular bridge zones of the drying path (Fig. 5.10b). The measured points of LBS2 fall perfectly within the "family" of the experimental data for GBS1. In the residual zone of the drying path and the entire wetting path, however, the difference in results remains with the measured points of LBS2 consistently plotting below the ones of GBS1 contrary to expectation given that the equivalent mean spherical particle size of the former is slightly less than that of the latter. This suggests that for a sample undergoing drying it is in the residual region that the water retention behaviour is affected by the particle shape as no other influential factors are present. If this hypothesis is correct then it means the discrepancy between the wetting paths of the two material WRCs is a consequence of the said effect in the residual zone given that wetting of the material is dependent on its hydraulic history among other factors. It was thus decided to factor the results to harmonise the particle shape. The results are shown in Fig. 5.11 with the residual zone water content of LBS2 divided by its shape factor. Surely, even in the residual zone the similarity in the WRC results of the two materials cannot be over emphasised (Fig. 5.11).

The results in Fig. 5.11 indicate that comparing results of different materials with water content expressed in terms of gravimetric water content can lead to misleading conclusions. This is consistent with, and adds credence to, the fact that capillary pressure is dependent on surface properties and the degree of packing of the particles, as earlier mentioned in subsection 5.3.1. In computing gravimetric water content the

particle weight instead of volume is used. It is therefore remarked here that water ratio (or volumetric water content and degree of saturation) and not gravimetric water content should be used in quantifying and comparing the WRC results of materials of different particle densities. Such a conclusive result cannot be arrived at with most soils and industrial bulk solids due to the influence of other constituent particle properties. Such properties are well controlled in these deliberately simple materials.

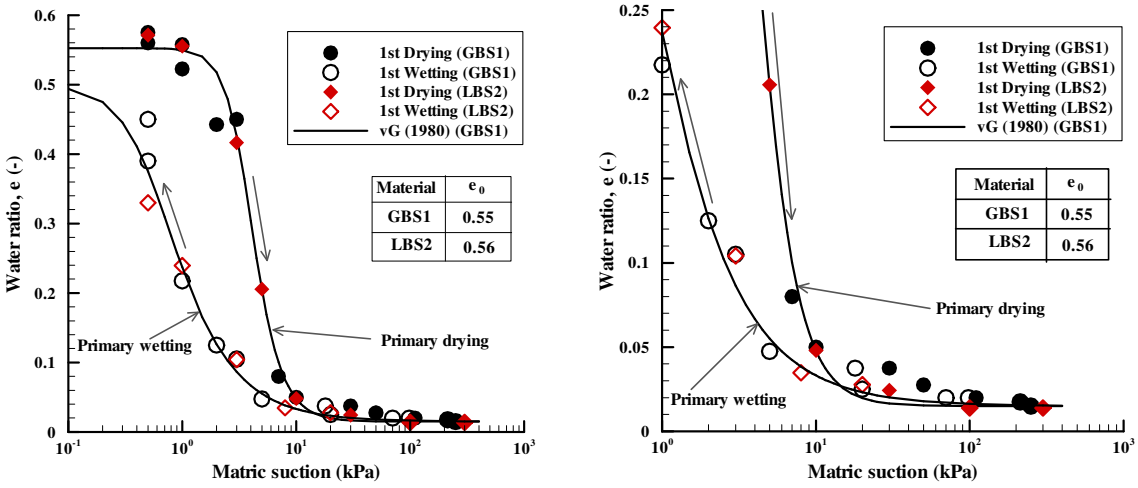

(a) Complete curve (b) Enlargement of the residual zone

Figure 5.11: Effect of particle shape on WRCs

The observed behaviour can be explained using the physical hypothesis depicted in Fig. 5.12. Within the saturated capillary and funicular bridge regimes all the particles will be sufficiently enshrouded in bulk water and none of the available menisci are in contact with the particles (Fig. 12a&c). As such the matric suction which is due to capillary pressure is not influenced by the shape of the particles. Samples of both the spherical and nonspherical particles will retain the same water content at a given matric suction. However, when liquid water is sufficiently drained from the sample it becomes localised only at the inter-particle contact points and matric suction gradually ceases to cause any water release. Instead, water movement becomes dominantly effected by the vapour transfer. At such a point, any available menisci are in contact with the solid phase and so the particle shape starts to play a role in influencing the rate of transfer of water. As shown in Fig. 5.12b&d, some of the particles in LBS2 are not in perfect contact compared to GBS1. This means that whereas the void ratio is the same, the number of contacts in the two samples is different with more contacts in GBS1 than in

LBS2 samples. Owing to its more contacts, GBS1 samples therefore retain more water than LBS2 samples at any given suction within the residual zone.

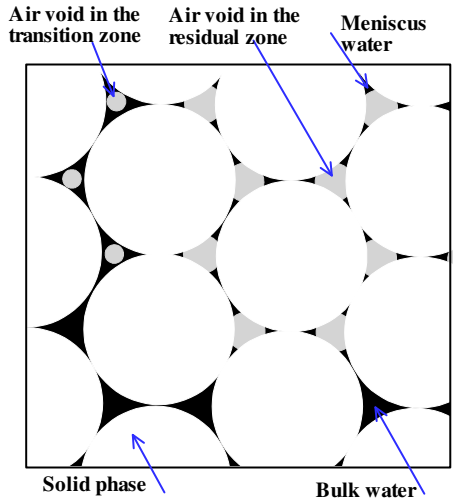

(a) Water in a system of spheres

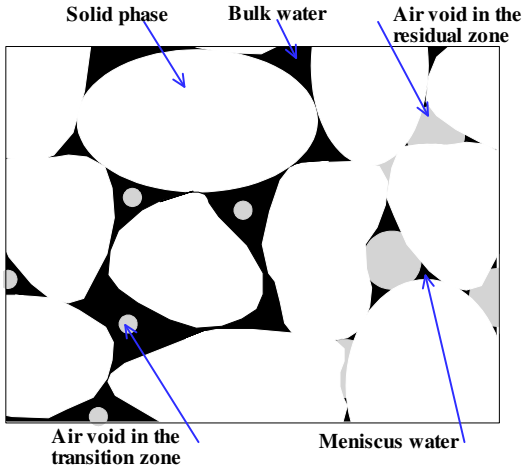

(b) Water in a system of nonspherical particles

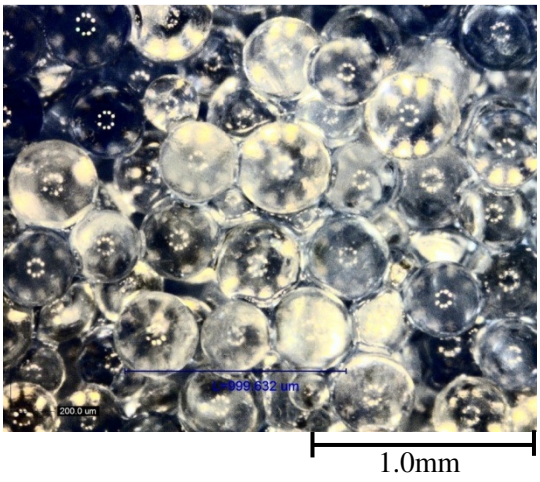

(c) Glass beads (GBS1)

(d) Leighton Buzzard sand (LBS2)

Figure 5.12: Illustration and explanation of the effect of particle shape on WRCs

5.3.7 WRC: Comparison with results from tests using filter paper technique

To assess the location of the as-prepared sample water content and suction combinations relative to the pressure plate measured WRC and to demonstrate the absence or presence of osmotic suction in the test materials, the filter paper technique was used to measure both total and matric suction. Details of the procedure followed were presented in subsection 3.3.3.3. The results are shown in Fig. 5.13 and Table 5-4. As shown in Fig. 5.13, apart from the residual zone the filter paper measured points are enclosed by the pressure plate measured drying and wetting paths. This means that some energy is required to move the as-prepared sample to the higher energy level

primary drying path while energy must be dissipated for the sample to move to the lower energy level primary wetting path, as expected. These results appear to be in agreement with the findings of Zapata et al. (2000) who observed that the points measured by filter paper method outlied with those measured by pressure plate and pressure membrane methods. Next the main purpose of presenting these results in this part (i.e. to demonstrate the absence or presence of osmotic suction) is pursued.

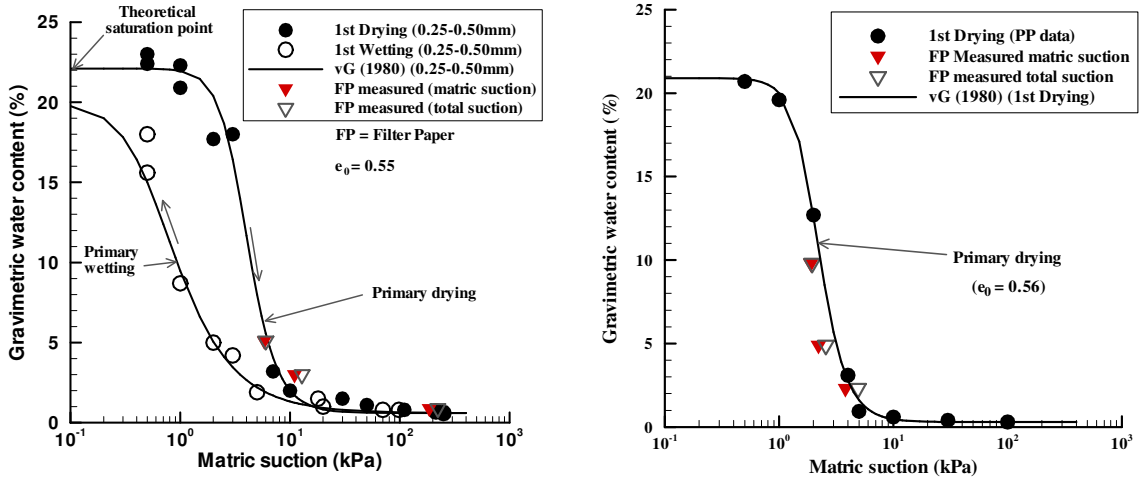

(a) GBS1 (b) LBS1

Figure 5.13: Plot of filter paper measured points relative to the primary WRCs

Table 5-4: Comparison of filter paper measured and pressure plate determined results

Test	Water content		Matric suction ψ_m (kPa)		Total suction ψ (kPa)	$\psi - \psi_m$ (kPa)	$\frac{\psi - \psi_m}{\psi_m} \times 100$ (%)
	w (%)	S_r (%)	Measured	From WRC			
Glass beads (GBS1)							
1	5.1	23.2	5.812	7.140	6.000	0.188	3.2
2	3.0	13.6	11.001	9.663	12.835	1.834	16.7
3	0.9	4.1	185.633	24.862	221.646	36.013	19.4
Leighton Buzzard sand							
1	9.8	46.7	1.897	2.354	1.945	0.048	2.5
2	4.9	23.4	2.208	3.365	2.564	0.356	16.1
3	2.3	11.0	3.806	4.754	4.904	1.098	28.8

Notes: w is gravimetric water content, S_r is degree of saturation, ψ_m is matric suction, ψ is total suction, and WRC is water retention curve; *Measurements conducted directly in the silo model at different levels and the value presented represents an average of three values.

From Fig. 5.13 and Table 5-4, it can be seen that the measured total suctions are marginally higher than the matric suction suggesting that there could be some osmotic suction in the material. The osmotic suction values increase with suction contrary to what is reported in the literature (Krahn & Fredlund, 1972). Krahn & Fredlund observed that changes in matric suction were equal to changes in total suction implying that osmotic suction did not change with water content. It is therefore most probable that the observed discrepancy between the matric suction and total suction is due to other factors other than osmotic suction. This will be pursued further in subsection 7.3.2.2 where the filter paper test results are applied to explain the unsaturated flow behaviour in silo model tests. The error margin of the filter paper method is also reported to be ±25% (e.g. Chandler et al., 1992). If this is taken into consideration then all the measured points (both total and matric suctions) belong to the same "family". It was thus concluded that there was no measurable osmotic suction in the test materials.

5.4 Mathematical description of the measured WRCs

For its application in deriving other unsaturated soil property functions, notably the permeability function (e.g. Mualem, 1976) and shear strength function (e.g. Vanapalli et al., 1996) considerable attention has been given to obtaining a mathematical equation that adequately describes the WRC. Such an equation, or set of equations, allows for continuous representation of the WRC and easy derivation of other functions. Over the years a number of equations have been proposed. In their work "review of soil-water characteristic curve equations", Leong & Rahardjo (1997) observed that out of the many equations the one by Fredlund & Xing (1994) is the best in describing the WRC for all the soil types. It was followed by the van Genuchten (1980) equation. Similar conclusions have been made in other studies, as presented in subsection 2.3.1. If only sandy soils were considered, however, the van Genuchten emerged the best. It appears that the correction factor, $C(\psi)$, in the Fredlund & Xing (1994) equation to force the WRC to terminate at a suction of 1000MPa at zero water content is not applicable to coarse granular materials given that in their dry state, these materials possess no binding force. In some studies (e.g. Sillers & Fredlund, 2001) it is completely omitted and the water content parameters adjusted to include the residual water content (Fredlund & Xing, 1994). Identification and common usage of the best performing equation(s) facilitates easy establishment of useful databases on unsaturated parameters for practical applications of unsaturated soil mechanics.

In parallel to obtaining the mathematical equations have been efforts to estimate the WRC fitting parameters from the physical and or basic index properties of the soil (e.g. Arya & Paris, 1981; Fredlund et al., 1997; Zapata et al., 2000; Aubertin et al., 2003; Yang et al., 2004) as well as from fewer experimental points and the index properties (e.g. Houston et al., 2006; Chin et al., 2010). The proponents of this approach argue that it is particularly important because the direct measurement of a complete WRC is still a time consuming and costly task. However, like many of the proposed equations derivation of the fitting parameters from the physical and or basic index properties of the soil is still unable to give satisfactory results for all the materials. It tends to work for the materials for which they were generated and validated. This is probably due to the fact that many of the constituent particle properties are ignored in these considerations. This is backed by the fact that in most of the above studies it is observed that better estimations are associated with noncohesive soils. The complexity introduced by particle properties is less in noncohesive than cohesive soils. In fact, where clay particles are dominant, the clay mineralogy has been used to explain the significant differences in behaviour with montmorillinite and kaolinite showing remarkably different WRCs (e.g. Hodnett & Tomasella, 2002). Therefore, by accounting for most of the influential particle properties it may be possible to satisfactorily estimate WRCs from physical and index properties without having to undertake the time consuming direct measurements. To confirm this, statistically adequate data from experiments on materials with sufficiently controlled (measured) particle properties is needed. Determination and presentation of the fitting parameters to the measured WRCs in this study and evaluation of some of the proposed approaches therefore contributes to the database.

5.4.1 Determination of the fitting parameters from experimental data

It was not the intent of this thesis to evaluate the ability of all the various WRC mathematical formulations to describe the measured water retention curves. Only the two commonly used equations to describe the water retention curves: the van Genuchten (1980), Eq. 5-1 and the Fredlund & Xing (1994), Eq. 5-2 are considered here. A general review of these equations and many others has been given in section 2.3, Chapter 2. Here, therefore, focus is on their proposed application.

$$w = w_r + \frac{(w_s - w_r)}{\left[1 + (\alpha_{vG}\psi)^n\right]^m} \qquad \text{Eq. 5-1}$$

$$\Theta = \left\{ \frac{1}{\ln\left[e + \left(\frac{\psi}{a} \right)^{n} \right]} \right\}^{m} \qquad \text{Eq. 5-2a}$$

$$C(\psi) = \left[1 - \frac{\ln\left(1 + \frac{\psi}{\psi_r} \right)}{1 + \frac{1000000}{\psi_r}} \right] \qquad \text{Eq. 5-2b}$$

In their work, both van Genuchten (1980) and Fredlund & Xing (1994) assumed that the saturated and residual water contents are known, since they are easy to measure. The unknown curve fitting parameters that have to be determined therefore include α_{vG} and n for van Genuchten's equation and a, n and m in the case of Fredlund & Xing's equation. These fitting parameters can be estimated graphically or more accurately determined through the least squares curve fitting procedures. A detailed description of the procedure for graphical estimation of the fitting parameters is given by the respective authors. In order to obtain a closed-form empirical model for hydraulic conductivity, van Genuchten related n and m through an equation $m = 1 - 1/n$. The use of n to obtain m reduces the flexibility of the van Genuchten's equation. In line with the objectives of this part of the thesis graphical estimation of the fitting parameters was not assessed.

Following the original author considerations, the residual water content was taken to be the water content at which the desorption path becomes constant with increase in suction (van Genuchten, 1980) and zero at a suction value of 1,000,000kPa (Fredlund & Xing, 1994). These are different to the adopted definition in geotechnical engineering (see subsection 2.3.1). The choice of the suction value of 1,000,000kPa by Fredlund & Xing was based on experimental evidence that water content of soil approaches zero as the suction tends to 1,000,000kPa (e.g. Coleman & Croney, 1961). It is also supported by the thermodynamic consideration that the maximum suction value corresponding to zero relative humidity in any porous material is about the same value. According to van Genuchten, if the residual water content cannot be measured experimentally as may be the case with clays it should be treated as an independent fitting parameter.

Both the van Genuchten (1980) and Fredlund & Xing (1994) empirical equations were found to provide a relatively acceptable fit ($R^2 > 99\%$) to all the hysteretic drying-wetting experimental data, as shown in Fig. 5.14a&b and Fig. 5.14c&d respectively with the former giving more satisfactory fitting. The least squares curve fitting parameters are shown in Table 5-5 while the regression coefficients are given in Table 5-6. Noting that the two models are of the same generic form, Leong et al. (1997) also through extensive comparisons concluded that the van Genuchten (1980) model gave more accurate descriptions of the water retention curves for cohesionless materials than other models including the Fredlund & Xing (1994) model that came second. For both equations the fit is more satisfactory in the saturated capillary and funicular bridge zones than in the residual zone. This is probably because in developing these equations much of the measured data was from the two zones but also probably because much of the attention in developing unsaturated soil mechanics has been mainly focused on the transition from saturated to unsaturated behaviour. Therefore if the focus lies in describing the transition from saturated to unsaturated behaviour then the equations offer satisfactory fit to the experimental data.

For use in industrial bulk solids handling, however, focus would be in the residual zone as the moisture contents are likely to remain significantly low. Therefore, in this study attention was more on the residual conditions than the saturated capillary and funicular bridge zones. It is shown that in the residual zone for glass beads the curve fitting equations are not as good (Fig. 5.15a). The equations underestimate the water content especially so with the Fredlund & Xing equation that forces the curve to terminate at 1000000kPa suction value. Consistent with many of the previous researchers' experiences and probably not surprising because pure sand was among the materials used in its development, Fig. 5.15b evidently shows that the van Genuchten equation is better than the Fredlund & Xing equation in describing the WRC of sand in the residual zone (e.g. Leong et al., 1997). Inconsistent with this observation, however, are the results of (Yang et al., 2004) who reported the Fredlund & Xing equation to be superior. The reason for this is not clear. It has been shown that the superiority of the Fredlund & Xing equation increases with increase in the fines content (e.g. Leong et al., 1997). It is further shown that the fitted wetting paths overestimate the water contents in the residual zone. As can be seen in Fig. 5.15, further improvements of the parameter m (it controls the position of the fitting curve in the residual zone) is likely to narrow the gap

between the measured and fitted WRCs in the residual zone. This will ensure the safe use of the mathematical equations in the handling of industrial bulk solids.

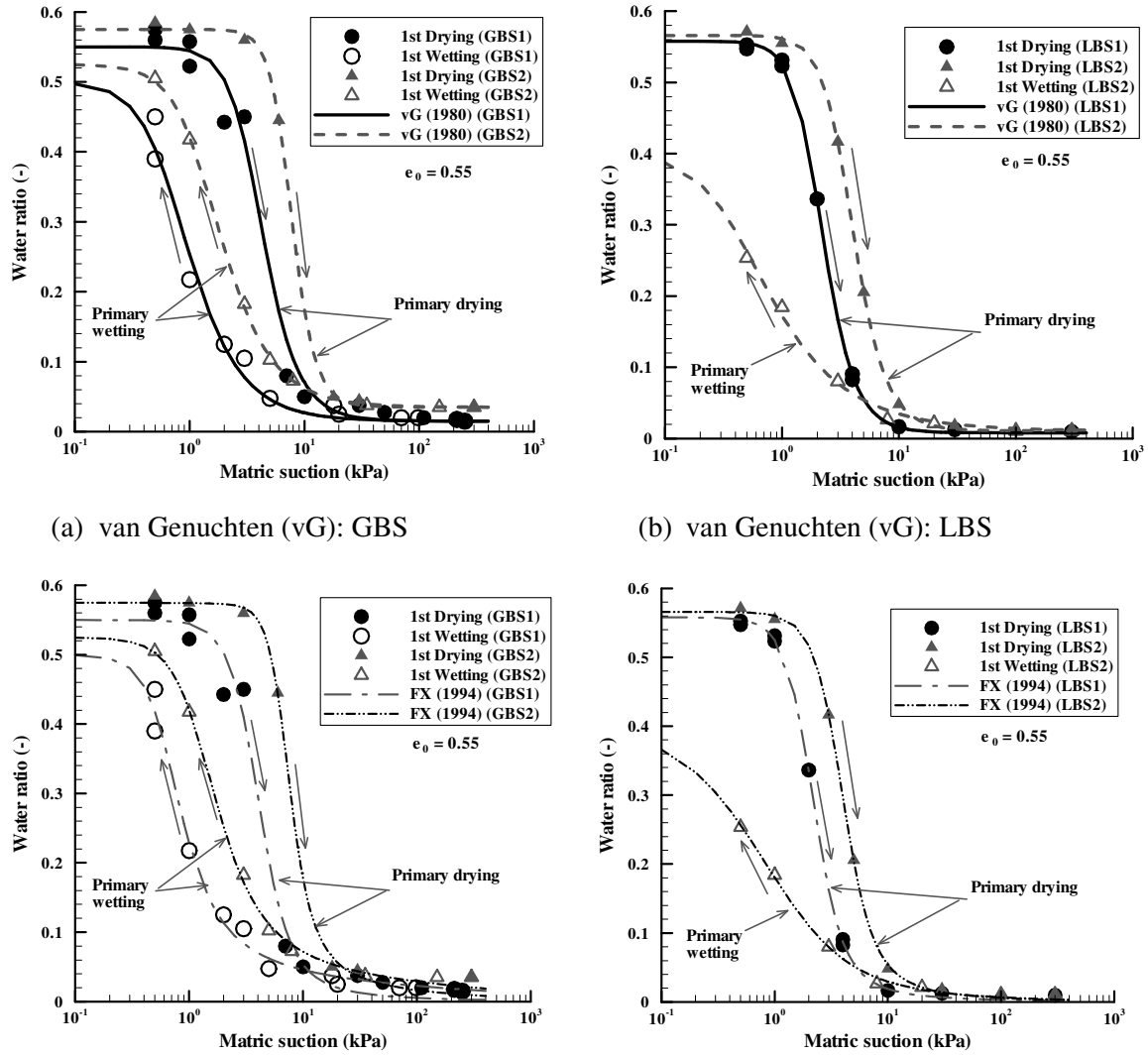

(a) van Genuchten (vG): GBS

(b) van Genuchten (vG): LBS

(c) Fredlund & Xing (FX): GBS

(d) Fredlund & Xing (FX): LBS

Figure 5.14: Comparison of fittability of van Genuchten and Fredlund & Xing equations to the measured WRCs through least squares curve fitting procedure

Table 5-5: FX (1994) and vG (1980) curve fitting parameters

Material	FX (1994) curve fitting parameters						vG (1980) curve fitting parameters				
	Drying			Wetting			w_{rvG}	Drying		Wetting	
	a	n	m	a	n	m		α_{vG}	n	α_{vG}	n
	(kPa)	-		(kPa)	-		(%)	(kPa)	-	(kPa)	-
GBS1	3.754	3.292	1.932	0.602	3.271	1.073	0.015	0.273	3.230	1.446	2.383
GBS2	6.575	5.000	1.342	1.192	2.592	1.158	0.035	0.139	4.661	0.750	2.430
LBS1	2.052	3.437	1.987	-	-	-	0.008	0.509	3.606	-	-
LBS2	3.655	3.339	1.882	0.784	1.093	2.410	0.011	0.281	3.529	2.547	1.862

Table 5-6: R^2 values of the fitting equations

Material	FX (1994) R^2 values (%)		vG (1980) R^2 values (%)	
	Drying path	Wetting path	Drying path	Wetting path
GBS1	98.97	98.89	98.94	98.32
GBS2	99.81	99.76	99.95	99.97
LBS1	99.77	-	99.89	-
LBS2	99.97	99.75	99.98	99.22

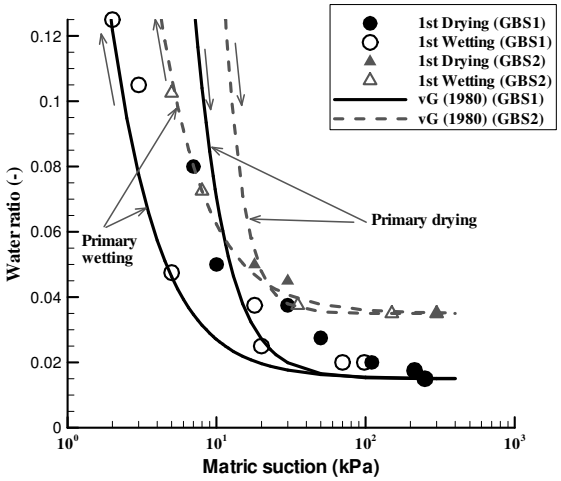

(a) van Genuchten: GBS1 & GBS2

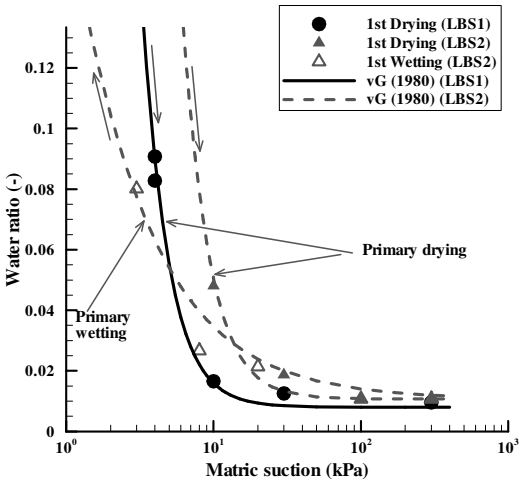

(b) van Genuchten: LBS1 & LBS2

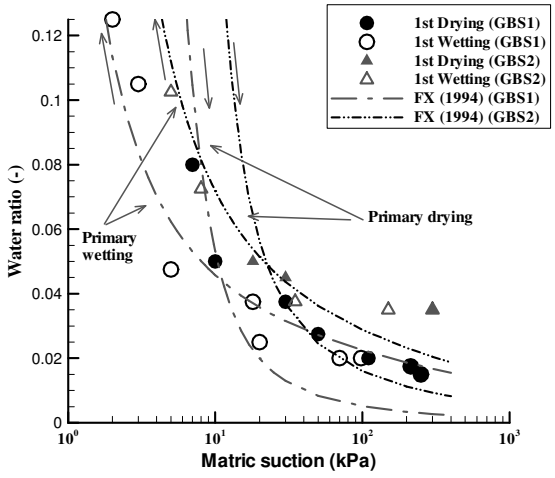

(c) Fredlund & Xing: GBS1 & GBS2

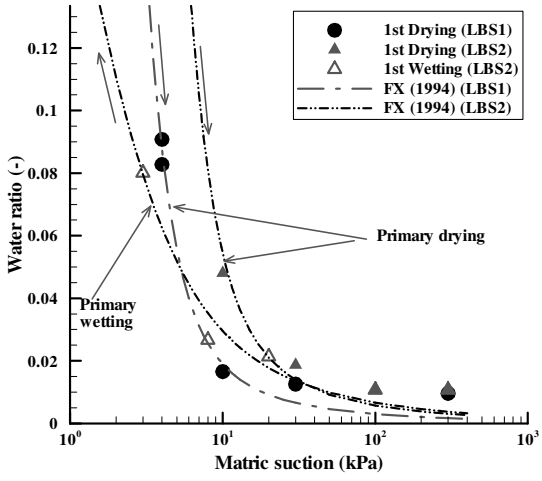

(d) Fredlund & Xing: LBS1 & LBS2

Figure 5.15: Enlargement in of the WRCs in Fig. 5.14

5.4.2 Determination of the fitting parameters from physical parameters

In comparing his equation to that of Brooks & Corey (1964), van Genuchten (1980) observed that α_{vG} is inversely proportional to the air-entry value, which Brooks & Corey

used in their formulation. Fredlund & Xing (1994) noted that in general a is greater than the air-entry value though for small values of m it can be taken to equal to the air-entry value. Small values of m are associated with fine materials, implying that a shifts the position of the desorption curve with downward increasing particle size. With this, many attempts have been made to correlate the parameter α_{vG} (or a) with the air-entry value ψ_a (e.g. Yang et al., 2004). The disadvantage of this approach lies in the fact that the measured WRC or part of it is a pre-requisite to its application. Taking advantage of the similarity between the WRC and the particle size distribution, many believe that α_{vG} (or a) should be directly dependent on D_{60}, the particle size such that 60% are finer. This basic soil index is favoured because it is obtained from easy, routine laboratory tests. As shown in Fig. 5.16a, the use of D_{60} to empirically determine α_{vG} (or a) may indeed be trusted with coarse soils. Once α_{vG} is obtained the air-entry value can be determined from the relationship shown in Fig. 5.16b. The task now remains to get either parameter n or m whichever is best estimated from the simple test basic index parameters. These two parameters are related through the equation $m = 1 - 1/n$.

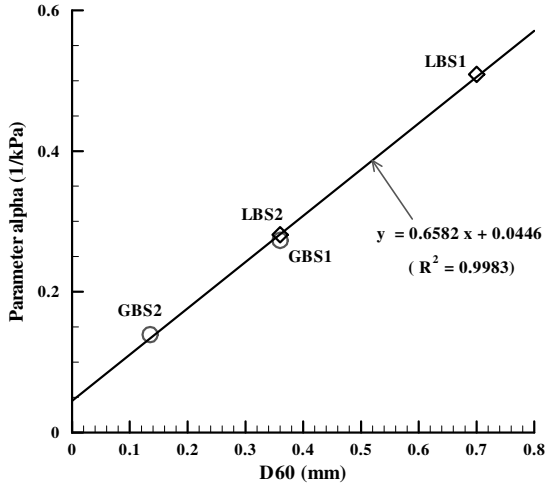

(a) Relationship between α_{vG} and D_{60}

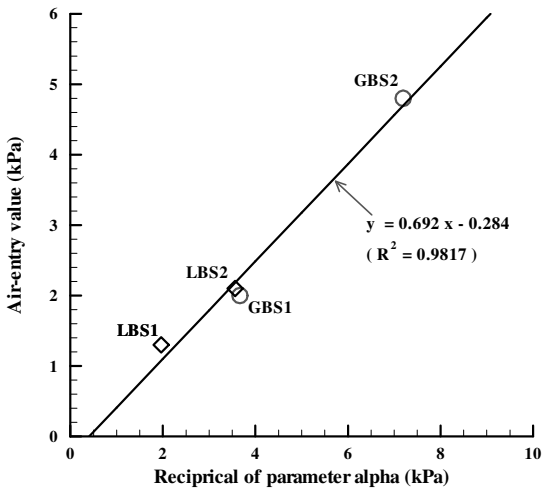

(b) Relationship between ψ_a and α_{vG}

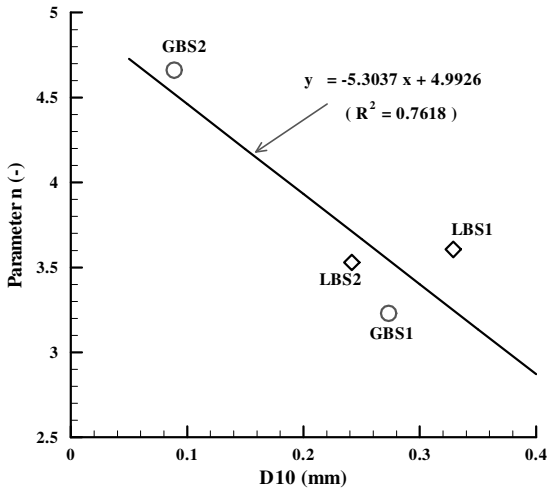

(c) Relationship between n and D_{10}

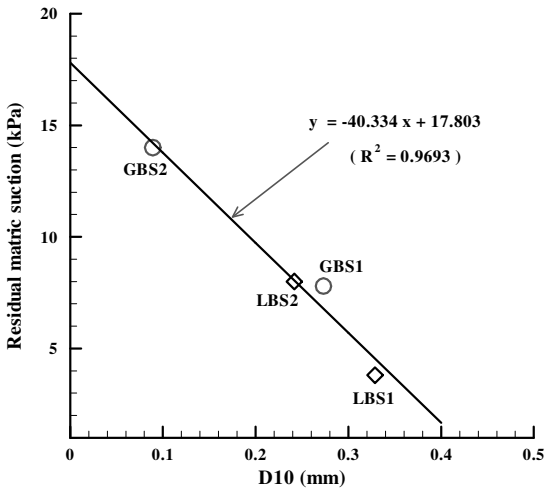

(d) Relationship between ψ_r and D_{10}

Figure 5.16: Relationship between index properties and van Genuchten fitting parameters and retention characteristics

While the parameter m did not correlate well with any of the basic index properties, Fig. 5.16c shows that n can be estimated from the effective size D_{10} just like the residual suction (Fig. 5.16d). The n value is an increasing function of the slope of WRC which is a result of the sample having a narrow pore-size distribution. It generally increases with particle size and uniform grading. For the similarity between the WRC and the particle size distribution it has been correlated with the slope of the particle size distribution as well (e.g. Zapata et al., 2000; Yang et al., 2004). After estimating n the parameter m is then known. It appears that the inability of mathematical equations to satisfactorily describe the WRC in the residual zone is responsible for the inability of m to correlate with the basic index properties. More experimental data are, however, needed to reach statistically acceptable conclusions. For fixed values of α_{vG} and n, m controls the residual portion of the curve. Low values result in mild transitions from the funicular bridge zone and the value of unity gives the sharpest transition with the van Genuchten equation.

5.5 Concluding Remarks

The water retention curves (WRCs) for two types each of glass beads and Leighton Buzzard sand in terms of particle size-ranges have been presented. From the results the influence of particle size and shape as well as the cycles of drying and wetting and initial void ratio on the water retention characteristics has been assessed and discussed with reference to results of the related materials in the literature. The robustness of the

two most popular mathematical equations of van Genuchten (1980) and Fredlund & Xing (1994) for the description of the hysteretic water retention curves have been assessed; the one by van Genuchten (1980) gave the more satisfactory description of the hysteretic behaviour of the water retention curves though it too fell short of giving acceptable descriptions in the residual zone. Attempts at correlating the WRC fitting parameters to the physical properties of the material suggest that provided the influential particle properties are controlled WRCs may be satisfactorily estimated from the material basic index properties. It has been shown that particle-water interaction through liquid bridges alone can produce the typical unsaturated behaviour which affects the bulk hydro-mechanical response of the material. Consequently, the selected test materials were found to be suitable for further testing of the hydro-mechanical behaviour, and the relevant range of matric suction, and hence water content, was established. The test materials were free of osmotic suction and within the relevant suction range they exhibited a unique relationship between water content and matric suction.

CHAPTER SIX

6 EXPERIMENTAL CHARACTERISATION OF SHEAR BEHAVIOUR

6.1 Introduction

This chapter characterises the mechanical behaviour of the tested granular materials. One of the core objectives of this research project was to investigate the unsaturated mechanical behaviour of spherical glass beads using a suction-controlled triaxial apparatus. The experimental programme was thus designed to explore the stress-strain, shear strength and volumetric behaviour of compacted samples of glass beads at different values of matric suction and net normal stress. The matric suction was controlled using the axis translation technique. The results are used (in chapter 7) to explain the observed flow behaviour in silo model tests. Synonymous with shearing in soils, resistance to relative movement between particles in the storage facility is a mechanical property. Characterisation of such a property is based on studies of the shearing behaviour of the test materials.

To identify the saturated and dry material behaviour, conventional triaxial compression tests were also carried out on fully saturated and oven dry samples of the compacted test materials. The chapter is logically organised as follows. First, the experimental programme is presented. The test results are then presented and discussed. The chapter then continues with a more in-depth interpretation and discussion of the experimental results using various existing frameworks. The chapter ends with summary and concluding remarks to highlight the implications of the observed behaviour to the arching of stored granular materials in silos. The experimental equipment and experimental technique and procedures used in this part of the research project have been presented in chapters 4 and 3 respectively.

6.2 Experimental Programme

Triaxial compression tests were carried out on two types of spherical glass beads in terms of particle size range. The materials were tested in oven dry, saturated and wet but unsaturated conditions. The dry and saturated results provided the reference behaviour to the unsaturated behaviour. All the tests were performed on samples prepared using the procedure described in subsection 3.3.3. The as-compacted conditions are shown in Table 6.1. As will be seen in Chapter 7, the test samples prepared at different water

contents were compared. It was feared that comparing results from such samples could be illogical considering that the initial sample structure was probably not the same. It was thus decided to check the presence of the effect of this initial sample structure due to the discrepancy in initial water content on the shear strength of the test material. The results are presented in subsection 6.3.4.

A total of thirteen (13) tests were successfully accomplished. In all the tests, samples were first isotropically compressed to different net normal stresses (or effective confining stress for saturated and dry tests) before shearing to about 21% axial strain. Overall three net normal stresses (i.e. 100kPa, 150kPa and 200kPa) were considered. Accordingly, the results have been grouped into three (3) depending on the net normal stress to which the sample was compressed. Of the tests, one (1) involved testing saturated material whereas another one was performed on oven dry material. After isotropic compression the saturated and dry tests were sheared drained with respect to both the pore air and pore water, owing to high permeability of the test materials. The suction controlled tests were conducted at matric suction values of 10, 50 and 100kPa. These suctions were based on the water retention characteristics for the material in consideration of the most likely extent of wetting in real applications. The water retention characteristics are presented in chapter 5. It was thus possible to quantitatively assess the effect of suction on both the isotropic compression and shear behaviour of the material according to the level of applied net normal stress. In section 6.3 the behaviour of the samples during isotropic compression and shearing is explained in detail.

Table 6-1: Sample and testing conditions for triaxial compression tests

Test Material	**Test Series**	**Test ID**	**Particle size (mm)**	e_0 * **(-)**	w_0 **(%)**	S_{r0} * **(%)**	$\sigma_3 - u_a$ **(kPa)**	$u_a - u_w$ **(kPa)**	**Test duration (days)**	**Hydraulic path**	**Remarks**
GLASS BEADS	GBS1	T01	0.25-0.50	0.55	0	0	100	-	1	-	T01-Dry test, T02-saturated test; conventional apparatus used
		T02						0	3		
		T03			8	36		10	14	Drying	Unsaturated test; advanced unsaturated apparatus used
		T04			2	9		50			
		T05			8	36		100			
		T06						50			
		T07						50			
		T08					150	10			
		T09						50			
		T10						100			
		T11					200	50			
		T12						100			
	GBS2	T13	0.09-0.15				100	50	14	Drying	

Notes: *The quoted value was the target void ratio; actual void ratios varied within the range of ±0.1 as will be shown together with the results; e_0 = initial void ratio; w_0 = initial water content; S_{r0} = initial degree of saturation; $\sigma_3 - u_a$ = net normal stress; $u_a - u_w$ = matric suction

6.3 Experimental Results

This section presents and discusses the results of triaxial compression tests carried out in this study. Both conventional and suction-controlled triaxial apparatuses were used in carrying out the tests. Table 6.1 categorises the tests according to the applied net normal stress. In the subsequent parts of this subsection, the results are presented according to the different topics of investigation. The isotropic compression behaviour at different matric suctions is discussed first; in particular the $e - p_n$ space is used to assess any effects of matric suction on the Normal Compression Lines (NCLs). The shearing behaviour at different matric suctions is then presented together with its discussion.

6.3.1 Isotropic compression behaviour

The behaviour of compacted glass beads during isotropic compression at different matric suction was investigated in 11 tests of series GBS1 and 1 test of series GBS2. As shown in Table 6.1, the GBS1 series tests included T02 through to T12 while the GBS2 series test was T13. Prepared with the same initial water content of 8%, samples of four tests (T03, T05, T06 and T07) of GBS1 series and T13 were compressed to the maximum net normal stress of 100kPa at different imposed matric suctions. Another test (T04) belonging to this category of net normal stress was prepared with water content of 2%. The other 3 (i.e. T08, T09 and T10) and 2 tests (T11 and T12) were compressed to the maximum net normal stress of 150kPa and 200kPa respectively. In order to have a reference, one test (T02) was performed following the well known conventional triaxial compression test procedure while one other test (T01) was conducted on the dry glass beads of series GBS1. It should however be noted that with these latter two tests (T01 and T02) it was not possible to record the volumetric response of the samples owing to the labour intensive nature of the test. Therefore the initial area was used in deviator stress calculation.

In all the suction controlled tests, immediately after sample preparation, the pore air pressure (u_a) and the pore water pressure (u_w) were simultaneously raised and subsequently maintained at $\psi_m + 20\text{kPa}$ and 20kPa respectively, to impose the desired matric suction $\psi_m = u_a - u_w$. As an example, Fig. 6.1a shows the pressures controlled in test T05 involving matric suction $\psi_m = 100\text{kPa}$. As the pore pressures were applied, cell pressure, σ_3 was equally increased so that the process of imposing matric suction

to the sample was executed at a net normal stress of $\sigma_3 - u_a = 20\text{kPa}$, which is equal to the confining stress used when back pressurising in the conventional saturated triaxial tests on coarse soils (e.g. Head, 1986). As the net normal stress at this stage of testing was more or less equal to the vacuum used in the preparation of the sample, volumetric strains were inconsequential (e.g. as shown in Fig. 6.1b for test T05). Once the matric suction of interest was imposed, the net normal stress was immediately increased to the desired value, and the sample monitored for equilibrium in terms of both water content and volume change. It should be noted that in this study matric suction values of 10kPa, 50kPa and 100kPa were considered.

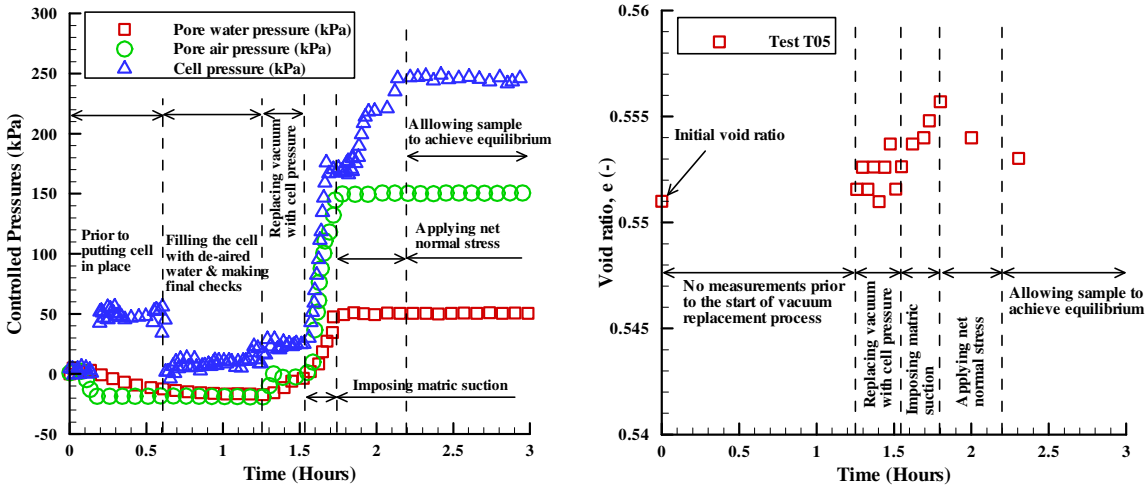

(a) Test T05 controlled pressures: σ_3, u_a & u_w

(b) Volumetric response of the sample during the process of imposing suction

Figure 6.1: Controlled pressures and sample response during the process of imposing suction and net normal stress

It is seen in Fig. 6.2a that degree of saturation started decreasing in response to the applied pore pressures or indeed imposed matric suction and the applied net normal stress. As shown in the figure, in the case of test T05, degree of saturation reduced from the as-compacted value of 36.4% to 6.8% at equilibrium corresponding to a change in water content from 8.0% to 1.4%. At the onset of load application, however, the degree of saturation tended to first increase due to sample volume reduction without a proportionate decrease in water content. The corresponding volumetric response of the sample is shown in Fig. 6.2b. The time taken for the sample to achieve equilibrium varied from about 7days to 13days depending on the imposed suction and particle size. As in pressure plate tests, equilibrium was taken to be when the sample water content change was not more than 0.1% in 24hours. It took longer for samples with lower

values of suction, higher water content and smaller particle size to attain equilibrium. Typically, for GBS1 with initial water content of 8% about 7days were necessary for 100kPa suction, 9days for 50kPa suction and about 11days for 10kPa while for the GBS2 glass beads with 50kPa suction about 13days were necessary for the sample prepared with 8% water content to attain equilibrium. Decreasing water content from 8% to 2% resulted in reduction in equilibrium time for the sample at 50kPa suction from 11days to about 6days. Owing to the variation in the time required for the samples with different suctions, initial water content and particle size to attain equilibrium a value of 14days was adopted as a single time for equalisation of the sample. Therefore any time dependent effects were minimised and at least adequate time was allowed for each sample to move to its characteristic drying path of the water retention curve (WRC). In chapter 5 it was shown that the tested glass beads possessed a characteristic drying path so that any wetter sample would quickly move to its characteristic path upon drying. It is evident from Fig. 6.2 that at the end of the isotropic compression stage in each of the tests volumetric equilibrium was allowed and came ahead of the moisture equilibrium.

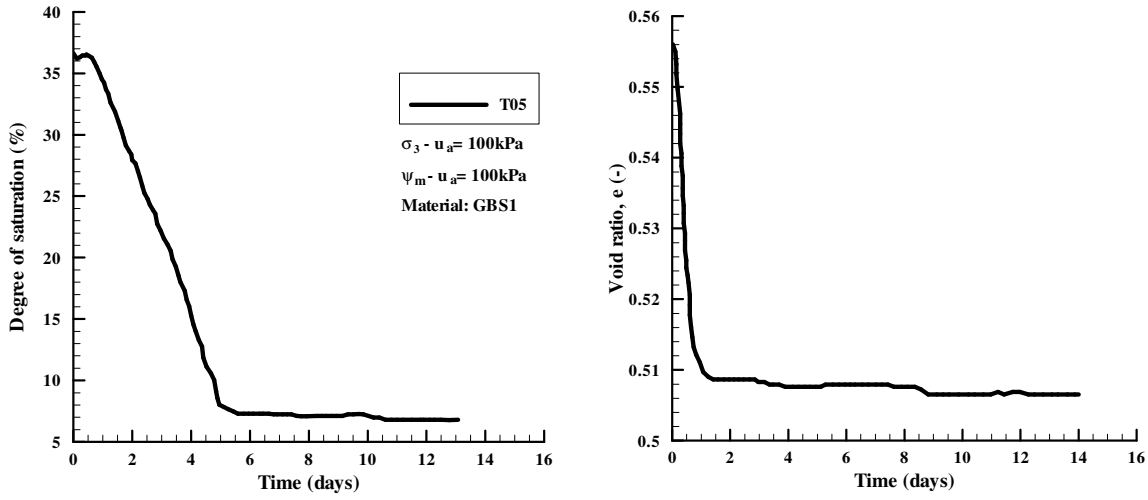

(a) Instantaneous sample degree of saturation (b) Instantaneous sample void ratio

Figure 6.2: Time history of test T05 sample response during equilibration

Owing to the fact that water retention measurement is less costly in terms of time and resources compared to the direct measurement of other unsaturated properties, its features have quite often been used together with the saturated parameters in the estimation of the more costly unsaturated properties including shear strength (e.g. Fredlund et al., 1996), permeability (e.g. Fredlund et al., 1994), transient flow (e.g. Barbour, 1998) to mention a few. This approach to estimation of other unsaturated

properties from the features of the water retention curve and saturated parameters suffers from one major setback: correct estimates can only be realised when the retention curve is applied at conditions it was measured. It therefore means that before this approach can be adopted the sample condition must be checked for harmony.

In Fig. 6.3 the data points measured from the triaxial apparatus are superimposed on to the fitting curves to the pressure plate measured points. Clearly, the triaxial points plot slightly above those of the pressure plate. This can be explained in terms of the effect of void ratio on the water storage capacity of the material as observed in chapter 5. Lower void ratio samples were found to have higher water storage capacity. As will be seen from the volumetric behaviour presented in the next few paragraphs, although the triaxial samples were prepared with the same initial void ratio as the pressure plate samples, their void ratio at equilibrium (and at peak deviator stress) were somewhat lower. The results in Fig. 6.3 therefore confirm that in using the WRCs to constitutively estimate other unsaturated properties, as the practice has often been (e.g. Khalili & Khabbaz, 1998; Rassam & Cook, 2002), care should indeed be exercised to take into account this effect of void ratio.

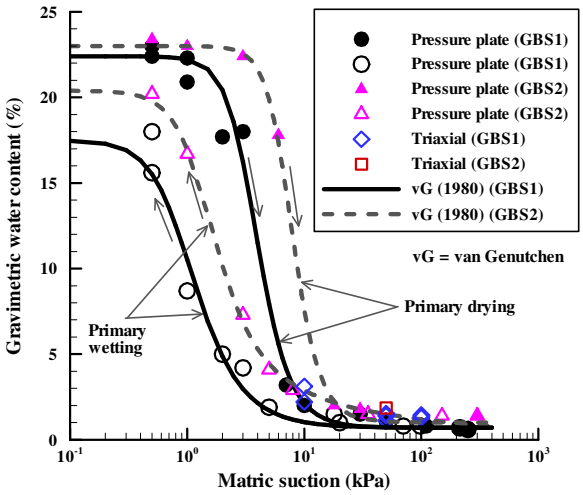

Figure 6.3: Superposition of triaxial measured points on to pressure plate measured WRCs

Ordinarily, engineers and scientists are aware of the probable volumetric response of either saturated or dry cohesionless granular material upon load application. The compression and or consolidation are immediate in the sense that air and or water are almost instantly expelled as the load is applied owing to its high permeability. In clayey soils due to the low permeability these processes can last quite long. When it comes to

unsaturated material however the situation tends to be complicated with the presence of matric suction. Whereas a lot of experimental work on clayey soils can be found in the literature nothing is available on cohesionless granular materials, at least to the best knowledge of the author. Therefore the question of whether suction would affect the volumetric behaviour of granular materials remains to be answered with some experimental evidence. This is given in the following paragraph for the tested glass beads.

The changes in total volumetric strain of the sample during isotropic compression at different net normal stresses and different matric suctions are shown in Fig. 6.4a. Following the application of the net normal stress the samples reduced in volume with the amount of reduction increasing with the applied confinement. On other hand, the results appear to indicate that provided equilibrium is allowed matric suction will have no measurable effect on the changes in volume of noncohesive granular materials due to the applied stress. It should be recalled that the effect of temperature on the measurements was minimised by keeping fluctuations in temperature very low, typically within ±1°C.

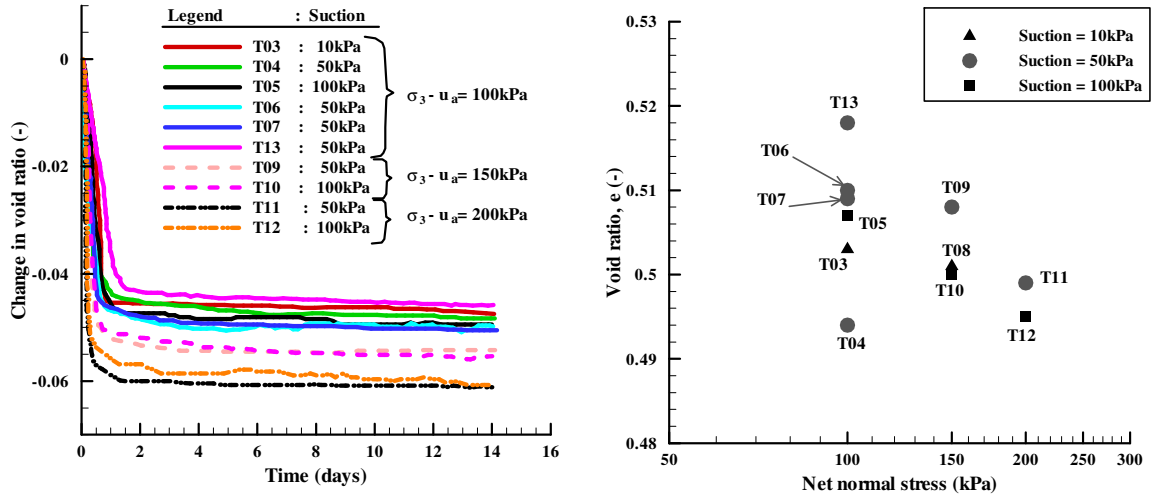

(a) History of change in void ratio

(b) Results in the $e - p_n$ space

Figure 6.4: Results of the volumetric behaviour during isotropic compression

In order to identify the Normal compression lines at different matric suctions, if any, the results of the isotropic compression tests at different matric suctions were also analysed using the $e - p_n$ space. The results are shown in Fig. 6.4b. Overall, the results show that the sample void ratio decreased with increase in the net normal stress and a normal

compression line can be identified within the scatter of the results. Comparison of the test results on the basis of imposed suction, however, falls short of giving conclusive evidence of the dependence of the normal compression lines on the material suction. Whereas distinct normal compression lines can be identified for each matric suction it is not clear as to whether the difference in the initial water content of the test T04 sample is responsible for its overly outlying with all other data points of its "family" even though as will be shown later it did not affect the shear behaviour. Whereas the initial water content of all the other test samples was 8%, it was 2% for the test T04 sample. Even if it is argued that the T04 results can be ignored on the basis of comparing results over a narrow range of void ratio and net normal stress, this thesis could not offer an explanation as to why the line for matric suction of 100kPa lies in between the lines for 10kPa and 50kPa. The results in Fig. 6.4b further show that the yield stress often observed in unsaturated clayey soils cannot be identified for the tested glass beads. It is not readily clear as to whether this is attributable to the absence of the yield stress in granular materials or to the fact that stresses considered in the current study were far much in excess of the yield stress of the material. Further experimental work in the lower range of net normal stress is necessary to draw a conclusion. No experimental evidence exists in the literature backup either the presence or absence of the yield stress.

6.3.2 Shear behaviour

Following the isotropic compression in all the triaxial tests presented and discussed in the preceding part of this section samples were sheared at constant matric suction and net normal stress in an attempt to assess their influence on the shear behaviour of the tested glass beads. Shearing was carried out to an axial strain of about 21%, measured using a global potentiometric displacement transducer. The stress-strain response of the tested glass beads in $q-\varepsilon_a$ space is shown in Fig. 6.5a with the corresponding volumetric response in the $\varepsilon_v-\varepsilon_a$ space shown in Fig. 6.5b. From the figure it is remarkably evident that the effect of matric suction was to increase the stiffness and peak deviator stress of the tested glass beads. In terms of volumetric change the samples first underwent slight contraction before dilating into a barrel shape at the end of the test, typically. Beyond the axial strain of about 10% the effect of suction on the shear behaviour appears to start dwindling given that the stress-strain relationships at different matric suctions tended to begin converging towards a common point. Whereas this kind of behaviour can be ascribed to the dilation induced perturbation of water menisci, the

actual behaviour was also found to be influenced by the failure mode. As will be discussed in subsection 6.3.4 sample failure mode varied from mild barrelling to barrelling and rotation with a tendency to shear either in the lower or upper one-third of the sample. The measured shear quantifiers were therefore accordingly affected and so it was considered unfit to examine the critical state parameters.

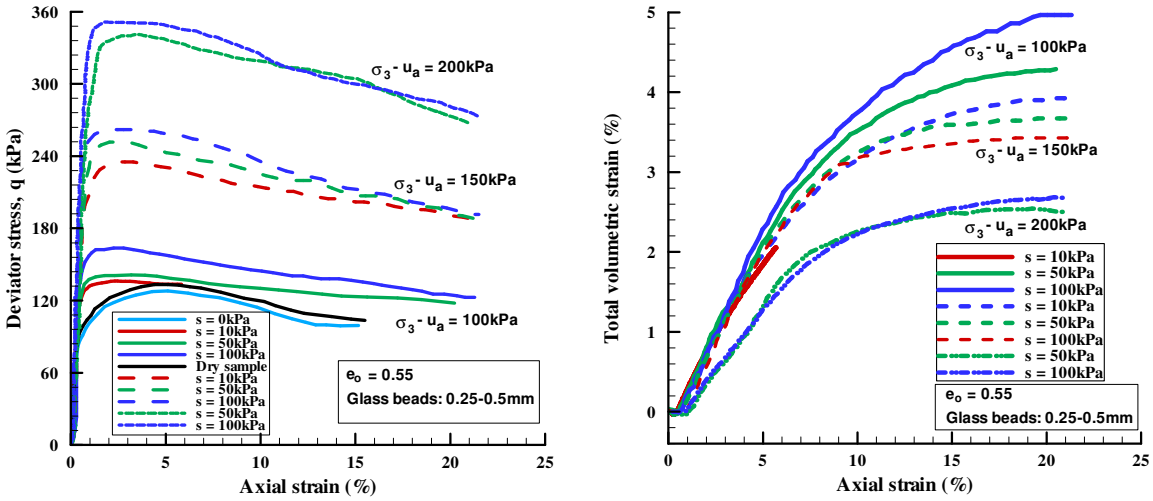

(a) q versus ε_a at different matric suctions (b) ε_v versus ε_a at different matric suctions

Figure 6.5: Results of the shear behaviour in suction controlled triaxial compression tests

Many previous studies have reported the mechanical behaviour of particulate materials to depend on among others the sample conditions and every stage of test. In fact, many constitutive approaches for predicting or describing the shear strength envelope of unsaturated soils have been developed taking into consideration the influence of sample conditions in addition to the prevailing stresses. One such condition is the number of water lenses or wetted surface of the solid phase in form of degree of saturation (Gallipoli et al., 2003) or some function of degree of saturation (Bishop, 1959) and modified suction to take into account the porosity of the sample (e.g. Wheeler et al., 2003). With this in mind, various conditions and properties of the sample were recorded at various stages of the test as shown in Table 6.2 including the as-prepared and after isotropic compression void ratio, water content and degree of saturation. The applied net normal stress, imposed matric suction, and the measured shear strength and the axial strain corresponding to peak deviator stress are also included in the table. From Fig. 6.4b it can also be seen that samples at higher degree of saturation tended to exhibit more volumetric stability.

Table 6-2: Test conditions and properties of the tested glass beads

Test Series	Test ID	Net normal stress $\sigma_3 - u_a$ (kPa)	Imposed Matric suction ψ_m (kPa)	Initial void ratio e_0 (-)	Initial degree of saturation S_{r0} (%)	Void ratio after isotropic compression e_{ic} (-)	Degree of saturation after isotropic compression S_{ric} (%)	Void ratio at peak deviator stress e_{peak} (-)	Degree of saturation at peak deviator stress S_{rpeak} (%)	Shear strength $\tau = q/2$ (kPa)	Axial strain at peak deviator stress (%)
GBS1	T01	100	-	0.54	0	0	0	0	0	67.0	4.0
	T02		0	0.55	0	-	100	-	100	64.5	4.0
	T03	100	10	0.55	36.36	0.503	15.52	0.538	14.51	68.0	2.0
	T04		50	0.54	9.26	0.494	5.67	0.532	5.27	72.0	1.5
	T05		100	0.56	35.71	0.507	6.79	0.559	6.16	80.0	1.2
	T06		50	0.56	35.71	0.510	6.89	0.557	6.31	70.0	1.2
	T07		50	0.56	35.71	0.509	7.37	0.555	6.76	71.5	1.3
	T08	150	10	0.54	37.04	0.501	11.03	0.526	10.51	119	2.5
	T09		50	0.56	35.71	0.509	7.57	0.550	7.01	125	2.0
	T10		100	0.55	36.36	0.500	7.19	0.548	6.56	131	1.2
	T11	200	50	0.56	35.71	0.499	7.30	0.550	6.62	170	3.0
	T12		100	0.55	36.36	0.495	7.28	0.548	6.58	175	1.2
GBS2	T13	100	50	0.57	35.09	0.518	8.96	0.564	8.24	64	2.0

Notes: *Matric suction taken at water content corresponding to the average water content after isotropic compression and moisture equalisation.

In order to appreciate how matric suction and net normal stress influence shear strength the results presented in Fig. 6.5a and Table 6.2 are often presented in the $q-\psi_m$ space and $q-(\sigma_3-u_a)$ space. This was done too and the results are shown in Fig. 6.6a and Fig. 6.6b respectively. As can be seen from Fig. 6.6a, the results indicate that as matric suction was increased the material's shear strength also increased. The increase was nonlinear in the sense that the rate of increase of shear strength appears to diminish as suction increases. In fact, it appears that if suction was increased further the shear strength would eventually attain a maximum. Following this argument, it is expected that the angle of friction with respect matric suction should decrease as matric suction is increased. It was found that ϕ^b varied marginally, that is within the range of less than 1.0 degree. This suggests that within the residual zone ϕ^b may attain a minimum value. On the contrary, Fig. 6.6b shows that the effect of increasing net normal stress was to linearly increase the shear strength. The angle of friction with respect to the net normal stress ϕ' was found to be 27° and was independent of the imposed matric suction.

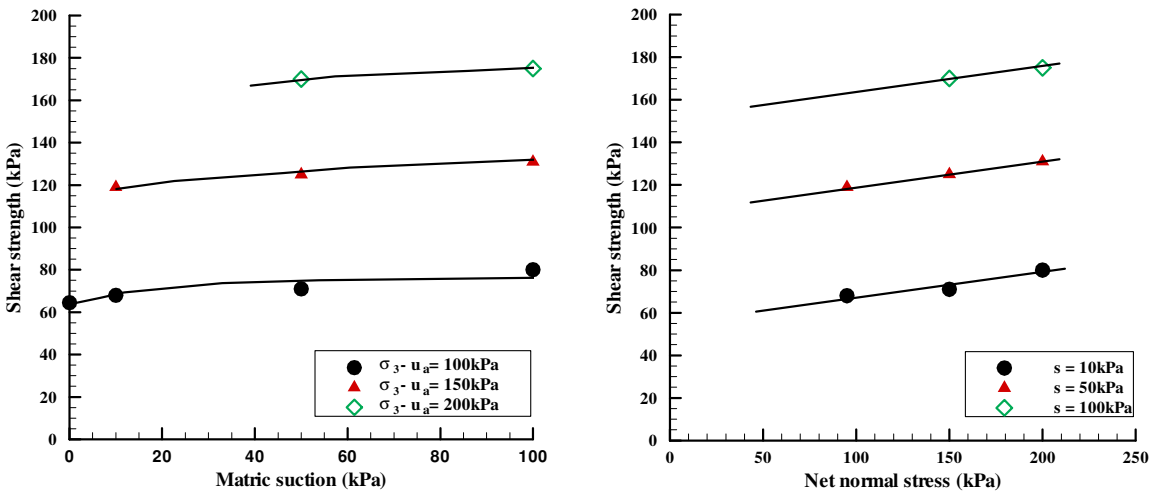

(c) τ versus ψ_m at different σ_3-u_a values (d) τ versus σ_3-u_a at different ψ_m values

Figure 6.6: Results of variation in shear strength with matric suction and net normal stress

The observed increase in the stiffness and peak deviator stress as well as the increase in shear strength and volumetric stability with increase in matric suction of the tested glass beads can be explained in terms of the additional inter-particle bonding force introduced through the liquid bridges maintained by the matric suction in the sample. This is consistent with what was observed in Chapter 5 with unbound wet noncohesive particles sticking together against the gravitational force. It will also be shown in

Chapter 7 that this additional inter-particle bonding force was strong enough to prohibit dilation of the material within the gravitational field alone.

Similar experimental results can be found in the literature including the works of Gan & Fredlund (1996), Farouk et al. (2004), Estabragh & Javadi (2008) and Houston et al. (2008). However, compared to all these studies, and many others, the current study presents results in which the observed behaviour is attributable to only the liquid bridge induced inter-particle bonding. All other influential parameters were controlled through the use of inert spherical glass beads with distilled water. This is not easy to achieve in most of the naturally occurring materials such as soils.

As reviewed and presented in Chapter 2, it remains to be seen as to what will eventually be an agreed position in terms of how shear strength should be constitutively modelled in the application of unsaturated soil mechanics. What appears certain is that theories supported by experimental evidence and involving parameters that are easily obtainable constitutively and, or, through less costly experimental programmes in terms of both time and resources will be favoured. With this in mind, it was found logical to assess the robustness of some of the commonly and widely used constitutive model for estimating unsaturated shear strength. This was done in section 6.4 after discussing the observed effect of particle size and microstructure on the shear behaviour.

6.3.3 Effect of particle size on the unsaturated shear behaviour

The effect of particle size on the shear behaviour of cohesionless granular materials is appreciated when the results of tests T06 and T07 of series GBS1 are compared with those of test T13 of series GBS2. The comparison is shown in Fig. 6.7. In these tests, apart from the particle size all the particle properties of the sample and test conditions were the same within the accuracy levels presented in chapters 3 and 4. The samples of tests T06 and T07 constituted particles of 0.25-0.50mm size range with its mean particle size as 0.354mm being 2.9 times the mean particle diameter of the sample of test T13 that comprised 0.09-0.15mm particle size range. The results indicate that the shear strength of large sized particles is greater than that of similar but small sized particles. The stiffness, and the volumetric response within 10% axial strain, on the other hand seems to be independent of the particle size. Beyond 10% axial strain the volumetric response was partly influenced by the failure mode of the sample implying that the discrepancy between the results at higher strain levels cannot be ascribed to the particle

size alone. The failure mode varied from barrelling to a combination of barrelling and rotational shear as depicted in the photos of failed samples in Fig. 6.8. Since the failure mode was not anticipated to significantly vary from test to test the photos were not identified with their corresponding tests and are thus for illustrative purposes only.

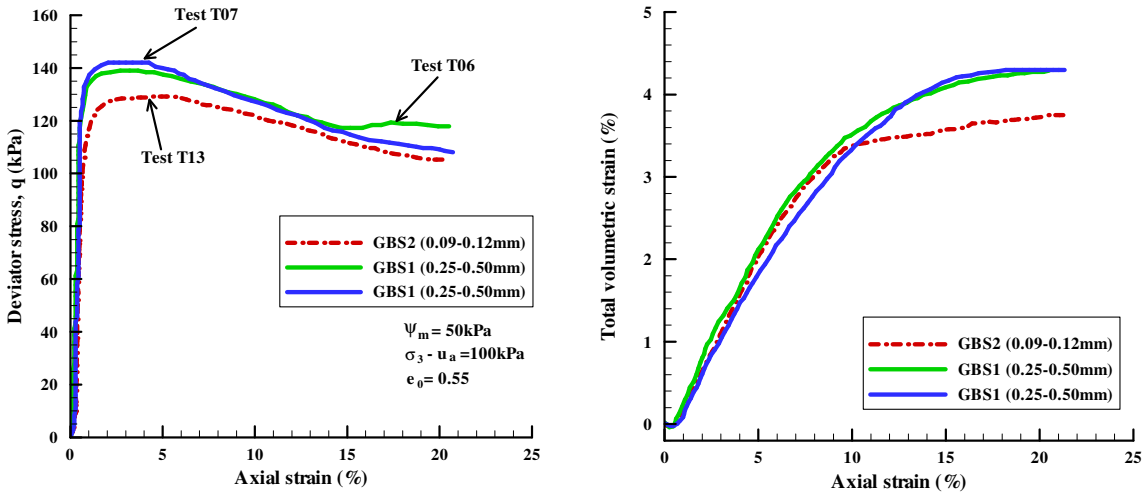

(a) Stress-strain response (b) Total volumetric-axial strain response

Figure 6.7: Effect of particle size on the shear behaviour of the tested glass beads

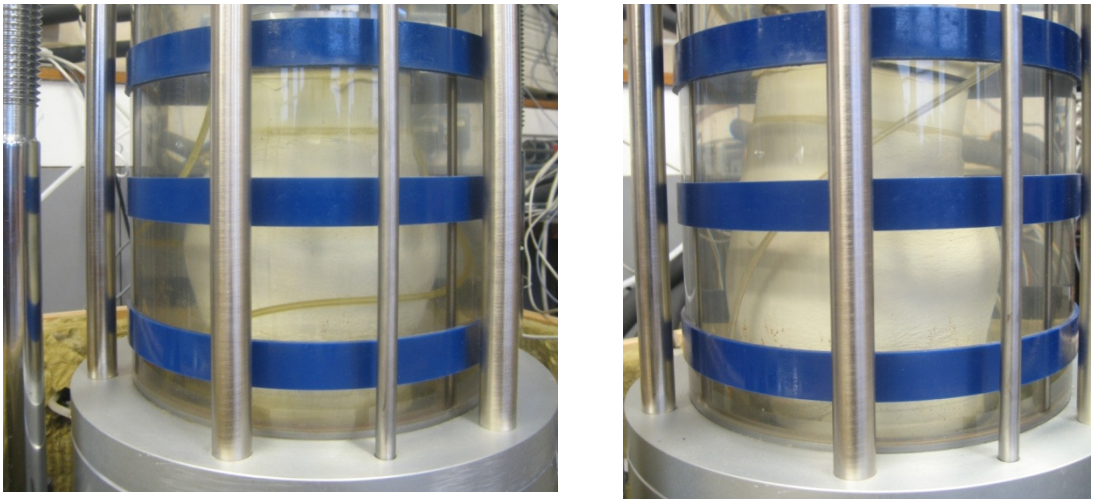

(c) Mild barrelling failure mode (d) Barrelling and rotational failure mode

Figure 6.8: Examples of failure mode of triaxial compression tests

The above results are contrary to expectations and this thesis could not find a conclusive reason for the observed behaviour. Logically, it appears that provided the material and testing conditions are the same the particle size should not have any effect on the material response. The initial void ratio, initial water content, net normal stress and the

imposed suction were all the same in the compared tests. Therefore based on the initial conditions the compared results should have been the same.

In Fig. 6.9, a comparison is made of the time history of change in void ratio (Fig. 6.9a) and degree of saturation (Fig. 6.9b) of the sample during isotropic compression and suction equalisation in an attempt to trace for any discrepancies that could have lead to the difference in observed behaviour. It is evident that smaller particles sample exhibited more volumetric stability and was thus sheared at relatively higher void ratio than the larger particles samples. Other factors constant it would be expected that at the start of shearing test T13 sample was at a lower degree of saturation compared to tests T06 and T07 samples. As it turned out however, the reverse was true and the difference in degree of saturation was about 2%. To explain this, the results of water retention behaviour presented in chapter 5 were examined. It is concluded that the observed higher degree of saturation in test T13 sample than tests T06 and T07 samples is due to the fact that the smaller particles samples possess higher water retention capacity than the larger particles samples. In chapter 5 it was shown that a reduction in particle size increases the water storage capacity of the test samples. The question is whether or not the observed difference in shear strength is a coupled result of higher void ratio and degree of saturation of the test T13 sample at the commencement of shearing.

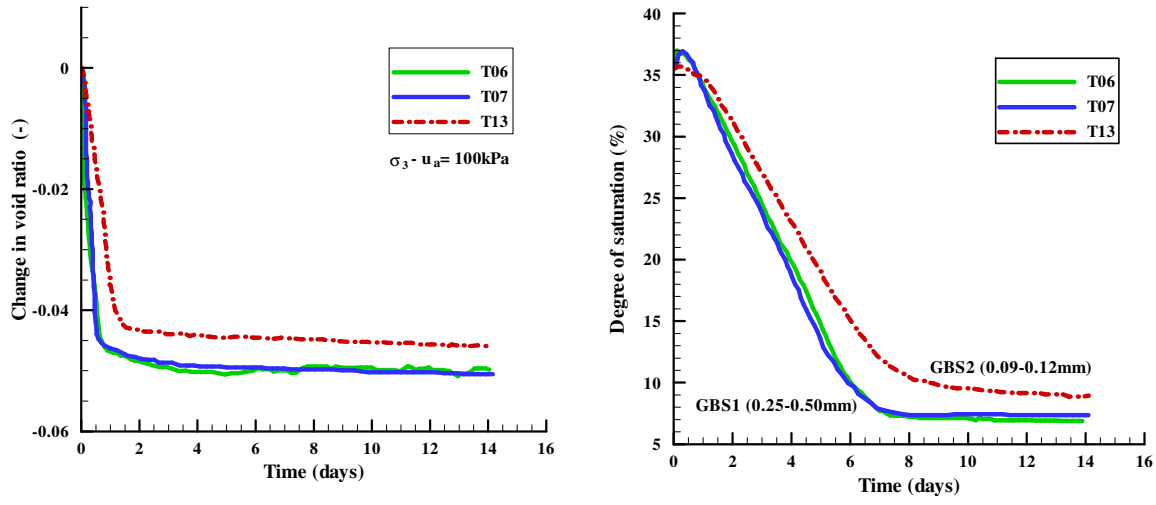

(a) Change in sample void ratio (b) Degree of saturation of the sample

Figure 6.9: Time history of sample conditions of tests T06, T07 and T13

The results of volumetric response during shearing suggest that degree of saturation could not have affected the behaviour of the test samples. Although the initial void ratio of test T13 sample was 0.01 higher than the initial void ratio of test T06 and test T07

samples, the three samples presented with almost the same volumetric response (see Fig. 6.7b). Since volumetric stability is a direct reflection of the samples resistance to deformation it is expected that samples displaying similar volumetric behaviour should have the same shear strength. The question is whether or not the observed difference in shear strength is a coupled result of higher void ratio and degree of saturation of the test T13 sample at the commencement of shearing.

Based on the existing knowledge in the literature, suction monotonically decreases with increase in degree of saturation. This can also be seen from the water retention curves presented in chapter 5. It is also shown from the previous section 6.3.2 that the coupled effect of suction and degree of saturation is to monotonically increase the shear strength of the tested glass beads. It appears therefore that the observed difference between test T13 sample and tests T06 and T07 samples is a result of higher degree of saturation in the former than in the latter two tests. More experimental evidence is however needed to reach a realistic conclusion.

6.3.4 Effect of initial water content on the unsaturated shear behaviour

Structure is said to significantly affect the mechanical behaviour of the material, cohesive and noncohesive materials alike (e.g. Matyas & Radhakrishna, 1968; Romero & Vaunat, 2000; Miura & Toki, 1982; Yumamuro & Wood, 2004; Yumamuro et al., 2008). In clayey soils for instance, particles can exist as aggregates of individual particles giving rise to what is called aggregated structure with both intra-aggregate and inter-aggregate porosities (Romero & Vaunat, 2000). Depending on the aggregation level and the moisture condition, therefore, clayey soils may present with differing mechanical behaviour. Aggregation is, however, not a material characteristic of predominantly sandy soils. Instead, different structures are ascribed to the difference in orientation of particles in the samples. Research has shown that depending on the method and the amount of water used to prepare samples of noncohesive granular materials a different mechanical response may be observed (e.g. Miura & Toki, 1982; Yumamuro & Wood, 2004; Yumamuro et al., 2008). It is not clear as to whether such a difference in behaviour can be observed in inert spherical granular materials. This aspect was investigated in this study and the following paragraph discusses the results.

In order to assess the effect of structure in terms of initial water content or degree of saturation on the shear behaviour of cohesionless granular materials, tests were conducted on samples of GBS1 series glass beads prepared with different water

contents. Fig. 6.10 gives a comparison of the results of test T04 sample prepared with water content of 2% and test T07 sample prepared with 8% water content. Evidently, the results are remarkably the same implying that initial water content induced sample structure had no effect on the mechanical response of the tested spherical glass beads. It therefore means that the difference in behaviour often ascribed to initial water content in sands is not actually due to moisture induced structure but rather particle shape and/or any other factors.

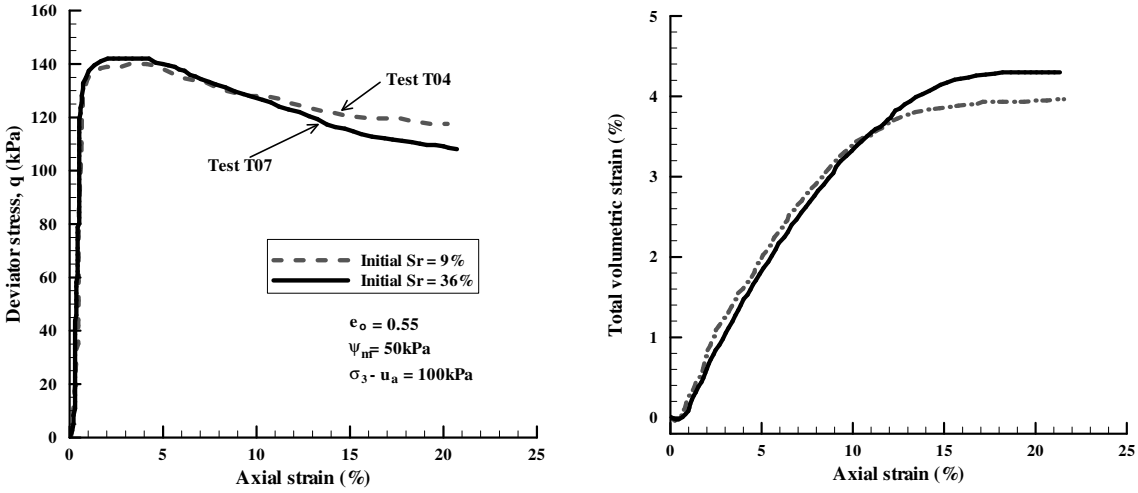

(e) Stress-strain response (f) Total volumetric-axial strain response

Figure 6.10: Result of shear behaviour of samples prepared with different water content

6.4 Robustness of selected constitutive unsaturated shear strength models

6.3.3.1 Effective stress based formulations

In section 2.4 the most common and widely used constitutive formulations in the literature to describe the shear strength of unsaturated soils have been compared and contrasted. It was concluded that the validity of the effective stress principle for unsaturated materials outside the saturation capillary regime remains an active area of research. It recently formed the theme for Colloquium 539 by the European Mechanics Society titled "Mechanics of Unsaturated Porous Media: Effective stress principle; from micromechanics to thermodynamics" at Utrecht University, The Netherlands. Following successive criticism to the Bishop (1959) formulation, Khalili & Khabbaz (1998) proposed that the Bishop's effective stress equation is valid but only when the parameter χ is expressed as the ratio of suction to the air-entry value raised to the power of -0.55. It, however, appears that this proposition by Khalili & Khabbaz (1998) has not been validated for a wide range of materials especially so for coarse granular materials. Khalili et al. (2004) gives its performance in estimating the contribution of

suction to shear strength of some fine soils. In this study therefore it was assessed for inert spherical glass beads and its performance is discussed in the following paragraph.

Fig. 6.11a shows a comparison between the measured incremental values of shear strength and those predicted using the Bishop (1959) effective stress principle with the parameter χ expressed as proposed by Khalili & Khabbaz (1998). Incremental shear strength is considered because of the need to do away with any effects that could be attributed to errors in conventional triaxial results. It should be remembered that unlike with unsaturated test results, with conventional tests it was not possible to take into account changes in sample area when computing the deviator stress due to lack of the volumetric response of the sample. From the figure, we see that up to 40% error can be expected when the approach proposed by Khalili & Kabbaz (1998) is used to predict the shear strength of noncohesive granular materials. Whereas it can be argued that use of the air-entry value determined under zero net normal stress is the reason for such a low accuracy of Khalili & Khabbaz approach, results in Fig. 6.11b show that even when the air-entry value is varied upwards by 100%, the approach still perform poorly. Based on the results presented in Chapter 5, a reduction in void ratio from about 0.55 to about 0.53 at peak deviator stress could not increase the air-entry value beyond this value.

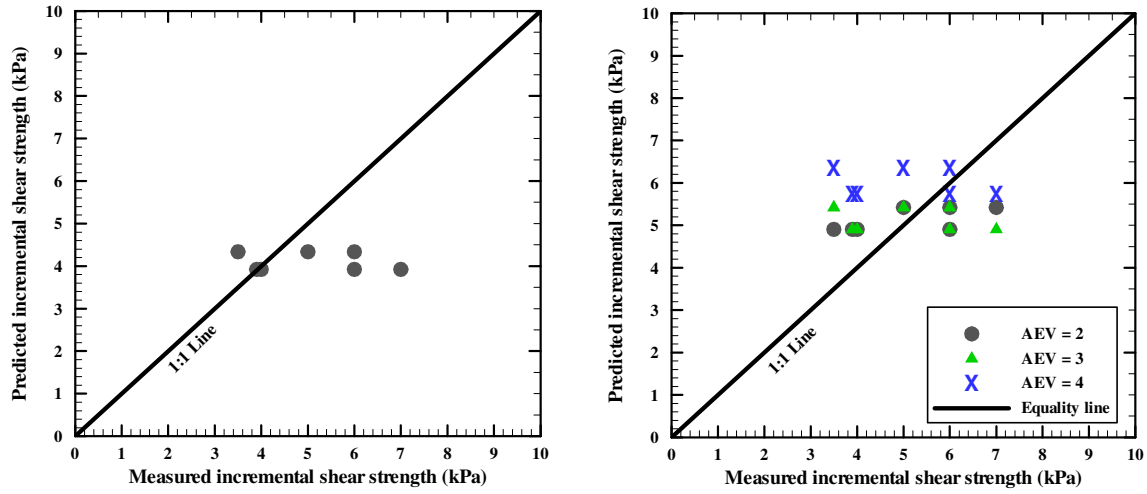

(a) Air-entry value from pressure plate tests (b) Varied air-entry values

Figure 6.11: Prediction of shear strength using Khalili & Khabbaz (1998) approach

6.3.3.2 Two stress state variables based formulations

Among the several two stress state variables based equations that exist in the literature to describe the shear strength of unsaturated soils, only the one by Vanapalli et al.

(1996) is considered. Besides its common use in the literature, this equation was chosen because all the parameters necessary for its use were directly measured in the experiments. Therefore any deviations from the measured values cannot be blamed on the inaccuracy of derived parameters. Moreover it is similar to many others in the literature as presented and discussed in Chapter 2 (e.g. Fredlund et al., 1996). A comparison of the predicted incremental shear strength and the measured incremental shear strength is shown in Fig. 6.12a.

Like the Khalili & Khabbaz (1998) approach, the Vanapalli et al. (1996) equation was also found to predict the shear strength of the tested spherical glass beads with an error margin of up to about 43%. This level of performance was achieved with the fitting parameter $\kappa_{\Theta} = -0.823$ and not the value of 1.0 which gave grossly erroneous predictions. These findings raise a number of questions about the predictability of shear strength using many of the approaches proposed in the literature. One such question is whether or not the fitting parameters depend on the constituent particles properties of the test materials. In this study all the influential particle properties were eliminated through the use of inert spherical glass beads and distilled water. It may also be argued that matric suction is actually not the suitable parameter to characterise the shear strength of unsaturated granular materials in the residual zone. This study focussed on the residual zone to assess the effect of matric suction.

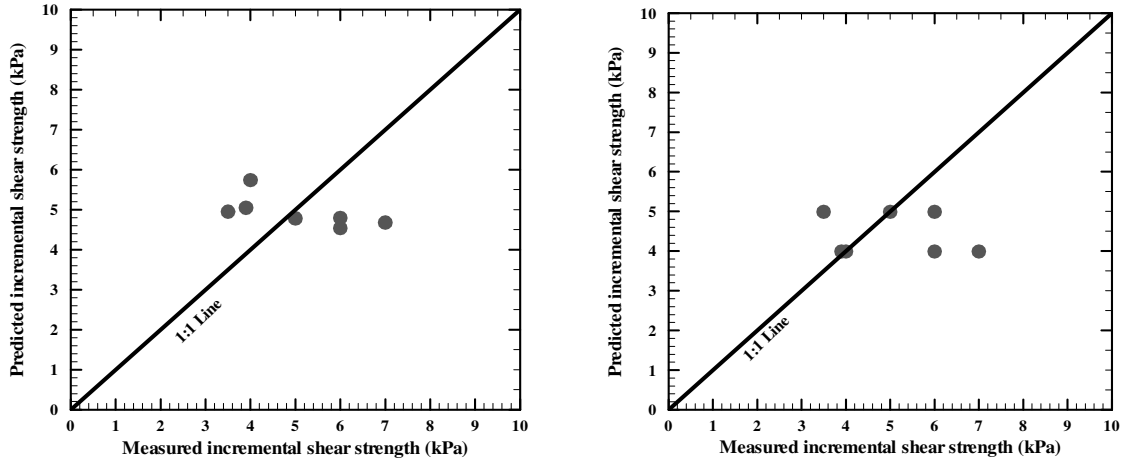

(a) Vanapalli et al. (1996) equation (b) Fredlund et al. (1978) equation

Figure 6.12: Prediction of shear strength using (a) Vanapalli et al. (1996) and (b) Fredlund et al. (1978) equations

To validate the first question it was decided to revert to the original Fredlund et al. (1978) equation bearing in mind that the relationship between shear strength and matric suction is a nonlinear one. From Fig. 6.12b we see that some points move on to the 1:1 line while others still lie far from it. It was noted that the points that plotted on the 1:1 line corresponded to experimental results obtained at lower matric suctions and net normal stress. This is consistent with the results presented earlier in subsection 6.3.2. It appears therefore that the weighting parameters often introduced in the equations for estimating the shear strength of unsaturated porous media account for factors other than matric suction and wetted area of the samples and that matric suction alone is indeed not an appropriate parameter for describing the shear strength of unsaturated porous media. The second question could not be validated given that shear strength at lower suctions was unavailable.

6.5 Concluding Remarks

The stress-strain, shear strength and volumetric behaviour of spherical glass beads have been presented and shown to be typical of the behaviour of unsaturated soils reported in the literature. In particular using the $q-\varepsilon_a$ space the stiffness and peak deviator stress of samples of glass beads was found to increase with increase in matric suction. Interpretation of the results using the $q-\psi_m$ space, $q-(\sigma_3-u_a)$ and the $\varepsilon_v-\varepsilon_a$ space revealed that shear strength and volumetric stability also increased with increase in matric suction and the net normal stress. More details will be given in Chapter 8.

CHAPTER SEVEN

7 EXPERIMENTAL CHARACTERISATION OF FLOW BEHAVIOUR

7.1 General Overview

Silos are the most commonly and widely used facilities for storing industrial bulk solids. Preferred for their versatility, silos constitute a significant proportion of the industrial infrastructure. They can be configured to allow different flow patterns and do not require a lot of land to install. They however suffer from two common failures, namely, structural and operational failures. The structural failures are related to the discrepancy between anticipated and the actual wall pressures. Operational failures, on the other hand, are when the bulk solids fail to emerge from the storage facility as desired due to phenomena such as arching, segregation, rat-holing or dead storage. These failures are said to be highly and closely related to the solids flow pattern and properties of the solids in the storage facility. They can be minimised if an appropriate design criterion - taking into consideration all the important influential parameters - is adopted. Therefore a good understanding of these important influential parameters is paramount to a successful storage facility design.

It was shown in Chapter 5 that the presence of both air and water in the stored granular materials generates matric suction. The resultant matric suction serves to bind the granular solids together, thereby increasing the shear strength of the material as shown in Chapter 6. Considering the solids handling processes, the most relevant suction lies within the residual zone. This is because the amount of moisture ingress into the solids during transportation, placement, and storage is relatively small. It is, however, not claimed that funicular and capillary bridges cannot form. The pendular bridges are associated with suction levels that may be high enough to cause arching. This part of the thesis studied this arching phenomenon. Silo model flow tests were carried out on spherical glass beads and nonspherical Leighton Buzzard sand. The main objective was to assess the effect of suction on the flow behaviour of granular materials in silos. Flow tests were carried out on these materials at different compaction (filling) water contents.

In this chapter, characterisation of the flow behaviour of the tested materials at different water contents and hence suctions is presented. As shown in the next section 7.2 and subsection 7.3.2 the measured suction and water content combinations are comparable

to those obtained in pressure plate and controlled in triaxial tests. This chapter is logically organised in the following parts. First, the experimental programme is presented. The experimental results of the different tests, their interpretation and discussion are then presented. The suitability of some of the most commonly cited and most recent equations to predict the flow rate of the tested materials are then explored. Finally, concluding remarks are presented to highlight the implications of the observed behaviour in consideration of the previously presented test results, notably pressure plate and triaxial compression tests. The silo model and experimental methods including suction and water content measurement, silo filling, and test procedures are described in detail in chapter 4 and chapter 3 respectively.

7.2 Experimental Programme

The experimental programme of the flow behaviour tests comprised silo model tests on spherical glass beads (GBS1 and GBS2) and nonspherical Leighton Buzzard sand (LBS1). Both dry and unsaturated tests were carried out. After samples were prepared using the method detailed in subsection 3.3.2, tests were immediately executed or equalisation time of 14days was allowed before the model outlet was opened for the material to discharge. The equalisation time was to enable the system to come to equilibrium itself and with the relative humidity sensors. Any ageing effects were also assessed by comparing results of dry tests executed immediately with those carried out after the storage time. Ageing is of interest in materials that undergo behaviour change as a function of time. It should be noted that all the tests were carried out at $22 \pm 2^{o} C$ temperature.

The unsaturated tests were performed on material with the preparation nominal water contents of 0.5%, 1.0%, 3.0% and 5.0%. The corresponding measured suctions are shown in Tables 7-1&7-2 and later in subsection 7.3.2. A detailed account of the testing procedures and the measurements made has been presented in subsection 3.3.3. Table 7-1 presents a summary of all the silo model tests performed on glass beads and their testing conditions while a similar summary is given in Table 7-2 for sand. In the tables, tests are grouped according to the test series. In each series dry tests are presented prior to unsaturated tests. The dry tests totalled to 21 with 1 on the GBS2 series, 8 on GBS1 series (see Table 7-1) and 12 on LBS1 series (see Table 7-2), while the unsaturated ones amounted to 21. Of the unsaturated tests, 10 were conducted on GBS1 series whereas the remaining 11 were performed on the LBS1 series. For each of the water contents,

the hopper outlet diameter D_o was varied in an attempt to determine the minimum diameter necessary for the material to flow. The initial void ratio, e_0 (or bulk density, ρ_b) was also varied in the tests involving dry materials to examine its effect on the discharge rate.

Table 7-1: Silo model tests carried out on glass beads and their testing conditions

Material	Test		w	w_{ratio}	D_o	R^*	ρ_b	e_0	ψ_m	Remarks
	Series	ID	(%)	(-)	(cm)	(-)	(g/cm^3)	(-)	(kPa)	
GLASS BEADS	GBS1	D-01	0	0	0.370	10.5	1.603	0.56	-	Tests carried out using only the hopper
		D-02			0.600	16.9				
		D-03			0.800	22.6				
		D-04			1.016	28.7				
		D-05			1.450	41.0				
		D-06			1.831	51.7				
		D-07			3.188	90.1				
		D-08			5.400	152.5				
		W-01	0.5	0.0125	1.450	41.0	1.611		-	
		W-02	1.0	0.0250			1.619		185	
		W-03	3.0	0.0750			1.651		11.0	
		W-04	5.0	0.1250			1.683		5.8	
		W-05	0.5	0.0125	5.400	152.5	1.611		-	
		W-06	1.0	0.0250			1.619		185	
		W-07	3.0	0.0750			1.651		11.0	
		W-08	5.0	0.1250			1.683		5.8	
		W-09	0.5	0.0125	9.850	278.2	1.611		-	
		W-10	1.0	0.0250			1.619		185	
	GBS2	D-01	0	0	1.450	117.9	1.592	0.57	-	

Notes: w = gravimetric water content; w_{ratio} = water ratio; $R^* = D_0 / d_p$; d_p = equivalent mean spherical particle diameter; ψ_m = matric suction.

Table 7-2: Silo model tests carried out on LBS1 and their testing conditions

Material	Test		w	w_{ratio}	D_o	R^*	ρ_b	e_0	ψ_m	Remarks
	Series	ID	(%)	(-)	(cm)	(-)	(g/cm3)	(-)	(kPa)	
LEIGHTON BUZZARD SAND	LBS1	D-01	0	0	0.370	8.9	1.638	0.63	-	Tests carried out with the entire silo model filled up
		D-02			0.600	14.4				
		D-03			0.800	19.1				
		D-04			1.016	24.3				
		D-05			1.450	34.7				
		D-06								
		D-07								
		D-08					1.669	0.60		
		D-09			1.831	43.8	1.638	0.63		
		D-10			3.188	76.3				
		D-11			5.400	129.2				
		D-12			9.850	235.6				
		W-01	0.5	0.0134	1.450	34.7	1.646		16.0	
		W-02	0.5	0.0134			1.646		16.0	
		W-03	1.3	0.0347			1.659		4.2	
		W-04	3.0	0.0801			1.687		2.9	
		W-05	5.0	0.1335			1.720		2.2	
		W-06	0.5	0.0134	5.400	129.2	1.646		16.0	Carried out with 30.0cm of materials above the transition
		W-07	1.0	0.0347			1.659		4.2	
		W-08	3.0	0.0801			1.687		2.9	
		W-09	5.0	0.1335			1.720		2.2	
		W-10	0.5	0.0134	9.850	235.6	1.646		16.0	
		W-11	1.0	0.0347			1.659		4.2	

In the following section the results for all the above tests are presented and discussed, starting with the dry test results. The effect of moisture and hence suction is presented next. The experimental results are discussed with reference to data from the preceding two chapters and from the previous studies about similar or related materials.

7.3 Silo Model Tests Results

The flow behaviour of spherical glass beads (GBS1 & GBS2) and nonspherical Leighton Buzzard sand (LBS1) was investigated by means of hopper and silo model tests respectively. Both the dry and wet but unsaturated behaviour have been investigated. The much known dry behaviour was used as a reference for the poorly known unsaturated behaviour. The experimental programme has been presented in the preceding section 7.2. The experimental results are presented in terms of discharge rate, W_{obs} directly measured in the course of the tests. The reported measurements are based on an average of at least two measurements.

7.3.1 Experimental Results with Dry Material

The flowability tests on dry material were carried out both immediately and 14days after sample preparation. The test results are presented and discussed in the following subsections. From the results, the following pertinent factors that control the discharge rate (W) of dry granular materials from silo hopper outlets have been discussed: initial void ratio (e_0), particle size (d_p), bed height above the outlet (H_h) and the outlet diameter (D_o). However, in order to confidently and meaningfully compare the results to discuss how each of the above affects the discharge rate it was necessary to ascertain the reproducibility of the test results.

7.3.1.1 Reproducibility of the results

Reproducibility of the results was ascertained by comparing test results of two separate but identical tests (D-05 and D-06) on Leighton Buzzard sand ($D_{50} = 0.61mm$ and equivalent spherical mean particle diameter $D_{50eq} = 0.418mm$). For each of these tests, measurements were taken at different bed heights. The outlet diameter was 1.45cm. The measured discharge rate fell within a narrow range of $47.194 \pm 0.741 g/s$ (Table 7.3). The samples for these two tests (D-05 and D-06) were prepared to the same initial conditions, as shown in Table 7-2 and Table 7-3 and the tests were executed immediately. The maximum error of about 1.6% in the measured discharge rates should have been introduced by the inability to collect the discharged material over exactly the same period. It should be remembered that the discharge rate was obtained using the commonly employed method of averaging the discharged material over the collection period (e.g. Fowler & Glastonbury, 1959; Beverloo et al., 1961; Hirshfled et al., 1997; Hirshfled & Rapaport, 2001; Mankoc et al., 2007). Therefore minor errors are expected

in starting and stopping the clock vis-à-vis starting and stopping material collection. Even then the measurements are sufficiently reproducible. Such a remarkable repeatability of the results implies that the reported comparisons of the test results are meaningful and that any discrepancies in results are attributable to the difference in the sample and testing conditions other than lack of reproducibility of the measurements.

Table 7-3: Reproducibility and dependence of W_{obs} of Leighton Buzzard sand on H_h

Material	Test		D_0	ρ_b	e_0	H_h	W_{obs}
	Series	ID	(cm)	(g/cm3)	(-)	(cm)	(g/s)
LEIGHTON BUZZARD SAND	LBS1	D-05	1.45	1.638	0.63	116	47.935
						76	47.885
						56	47.320
						26	46.713
		D-06	1.45	1.638	0.63	116	47.591
						76	47.182
						56	47.020
						26	46.907

7.3.1.2 Dependence of discharge rate on the free surface level of material above outlet

The results in Table 7-3 further demonstrate that in its dry state Leighton Buzzard sand is a free flowing material. It should be noted that the outlet size satisfies the minimum required for continuous flow. Particles emerging from the discharge outlet were not characterised by jamming and the mass discharge rate was found to be independent of the level of the free surface of the material H_h above the outlet, up to the transition level (Table 7-3). Below the transition (i.e. within the hopper) a slightly lower rate was consistently obtained. However, since its departure from the mean value remained within 1.6% error the difference was considered insignificant. Similar conclusions can be found in the literature (e.g. Fowler & Glastonbury, 1959; Beverloo et al., 1961). This nondependence of the discharge rate on the bed height is due to the fact that particles are not forced out of the bottom of the hopper by a hydrostatic "head" (Snider, 2007) but rather accelerate from a nearly zero velocity under the action of gravity. This is in contradiction to the belief that denser materials will flow faster owing to greater gravitational drag (e.g. in Schulze, 2008).

In Table 7-3, $H_h = 26cm$ means the flow rate measurement was taken with the free surface of the material at the transition level. This value is 0.87 of the barrel diameter D_B of the silo model. Yet the measured flow rate is comparable to the one obtained with the silo model nearly full. Therefore the observation that the material should be kept at least 1.2 times the barrel diameter was not applicable in the current study involving mass flow. This is contrary to the funnel flow where the bed height is required to be at least $1.2D_B$ for the flow rate to remain independent of the bed height (Hirshfled et al., 1997; Hirshfled & Rapaport, 2001). This result can be explained in terms of the effect of the inverted cone that forms in funnel flow. With the cone fully formed, most of the material is on the sides of the outlet must, therefore, first slide towards the centre before flowing out while this is not the case in mass flow.

The nondependence of discharge rate on the bed height meant that it was not necessary to fill the silo model each time a test was carried out. In fact all the tests on glass beads were carried out using only the hopper as the beads were not adequate to fill the entire silo model. Typically, discharge rate was obtained by averaging material collected over a discharge period of not less than 30s. However, for increased hopper outlet size the available glass beads were insufficient to achieve this. For this reason, with outlet sizes larger than 3.188cm flow rate of dry glass beads was obtained by considering the total mass of the material used to fill the hopper and the total time taken for all the particles to discharge.

7.3.1.3 Ageing effects on mass discharge rate

As will be shown in subsection 7.3.2, a time lag of 14days between sample preparation and unsaturated flow test execution was necessary to bring the stored moist material to equilibrium in terms of relative humidity. It was thus decided to conduct a replicate test (test D-07 of series LBS1) with dry material. The test results are compared in Table 7-4 with those of identical test (test D-05 of series LBS1) executed immediately after sample preparation. The results show that allowing a time lag between sample preparation and discharge of the material had no measurable effect on the dry discharge rate. This independence of the discharge rate of dry LBS1 on the storage time means that ageing is not a material characteristic of the dry LBS1, as expected given that the material is noncohesive inert sand. Therefore comparisons made in subsection 7.3.2 between dry and moist material behaviour do not suffer from any ageing effects.

Table 7-4: Effect of ageing on the flow rate of Leighton Buzzard sand

Material	Test		D_o	ρ_b	e_0	H_h	W_{obs}
	Series	ID	(cm)	(g/cm3)	(-)	(cm)	(g/s)
LEIGHTON BUZZARD SAND	LBS1	D-05	1.45	1.638	0.63	116	47.935
						76	47.885
						56	47.320
						26	46.713
		D-07	1.45	1.638	0.63	76	47.117
						56	47.687
						26	46.649

7.3.1.4 Initial void ratio effect on mass discharge rate

The dependence of the discharge rate of dry LBS1 on initial void ratio (or bulk density) was examined by comparing the results of, say, test D-05 and those of test D-08 in which a higher value of initial bulk density was used. From Table 7-5 it can be seen that increasing density from 1.638Mg/m^3 to 1.669Mg/m^3 was accompanied by a very slight change in mass flow rate; the discharge rate only decreased from 47.194g/s to 46.100g/s corresponding to a change in flow rate of 2.3%. This marginal dependence of flow rate on the density within the range reported can be explained using the well known changes in density on initiation of flow. According to Fickie et al. (1989) the emptying density in the vicinity of the orifice can be up to 30% less than in the upper parts of the system. A similar observation can be found in Cleaver & Nedderman (1993) who reported density changes of up to 10% on initiation of shear. It therefore means that particles had to dilate in order to flow thereby having its density reduced to the emptying density. An analysis of the video clips taken during emptying does add credence to the fact that filling density was higher than emptying density. As depicted in Fig. 7.1, inter-particle interaction was dominated by sliding and collisions for larger particles (Fig. 7.1a&b) while smaller particles predominantly rolled over other particles and collided within the system (Fig. 7.1c&d). Such inter-particle interactions can only take place in “loosely” packed system of particles. This corroborates well with the consensus that for any granular material to flow there exist a characteristic critical density (in Schulze, 2008) and with the observation by Weir (2004) and Verghese & Nedderman (1995) that emptying density should be used instead of filling density when predicting flow rate using the Beverloo et al. (1961) semi-empirical model. The filling density in excess of

the critical density means the material is too dense to flow without dilating first. It is this dilation process that is therefore responsible for the observed reduction in the discharge rate.

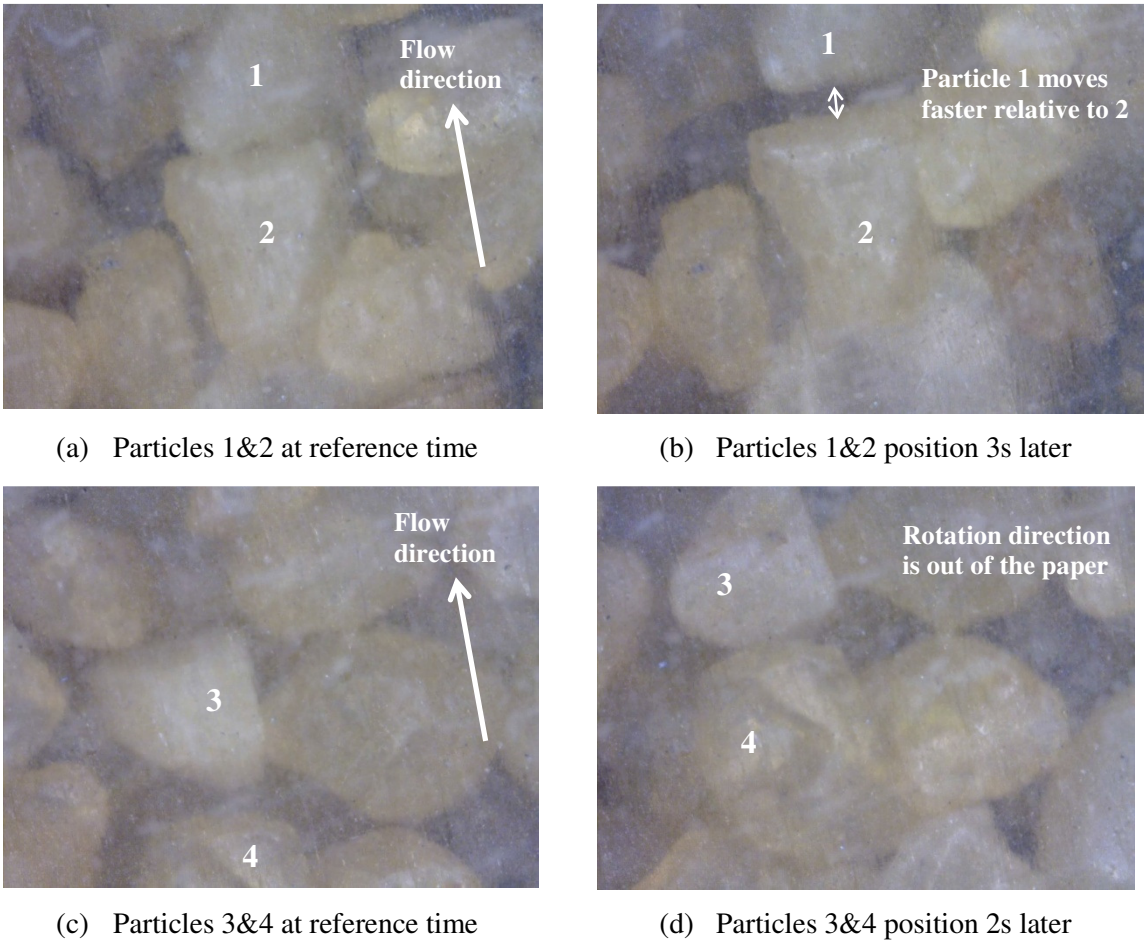

(a) Particles 1&2 at reference time

(b) Particles 1&2 position 3s later

(c) Particles 3&4 at reference time

(d) Particles 3&4 position 2s later

Figure 7.1: Microscopic images showing relative position of LBS1 particles during flow: (a) & (b) relative sliding and (c) & (d) rotation

Attempts to rationally obtain the characteristic critical density as a function of the normal stresses proved futile as the appropriate equipment was unavailable. As shown in Fig. 4.15a&b subsection 4.4.1.2, using a direct shear box test the critical density was obtained only at normal stress of 8.8kPa. It is believed that this value is on the higher side given the stress levels in the vicinity of the hopper outlet. Yet it corresponds to the minimum normal stress that can be applied in a standard direct shear box test. According to Schulze (2008), for general application with free flowing solids the normal stresses should be chosen to give the characteristic consolidation stress in the range of 3.0kPa to 12.0kPa. For a specific application, the vertical stress at the outlet of a mass flow conical hopper may be given by $\sigma_{zo} = 0.2 g \rho_b D_o$ and the horizontal stress is

obtained by multiplying the vertical stress by the active coefficient of lateral pressure. The stresses so calculated could be much less than the ones specified for general applications depending on the outlet size. Nonetheless, the obtained critical density of $1.473\,Mg/m^3$ at the normal stress of 8.8kPa gives a basis for discussing the measured results. Compared to the filling densities, the critical density is lower. Therefore if lower normal stresses were used as recommended in Schulze (2008), even lower critical densities would be obtained in which case it is clear that in both tests (D-05 & D-08) the material was initially in a denser state than could be supported during flow through relatively small orifice diameters. Note that in the test to determine the critical density the material dilated throughout the shearing process. Consequently, the effect of filling density was inconsequential as it had to reduce in response to the dilation of the material upon flow.

7.3.1.5 Outlet size effect on mass discharge rate

The experimental programme required that the hopper outlet size is varied. This enabled its influence on the discharge rate to be assessed. Not surprisingly, the results (Table 7-5) show that increasing the hopper outlet size tremendously increases the mass discharge rate. For instance increasing the outlet size from 0.6 to 0.8cm was followed by an increase in discharge rate of LBS1 from 3.178 to 9.350g/s and of GBS1 from 4.780g/s to 14.499g/s. A similar trend has been reported in the literature (e.g. Glastonbury, 1959; Beverloo et al, 1961; Mankoc et al., 2007). Logically, more material is expected to flow out of larger outlets over the same period of time. In fact this is well depicted in the semi-empirical equations (i.e. $W \propto \rho_b \sqrt{g}\left(D_0 - k_B d_p\right)^{5/2}$) for predicting the mass flow rate of granular materials presented earlier in subsection 2.6.1. The ability of selected equations to predict the mass flow rate of the tested materials is discussed in section 7.4. It has been shown that for a given material particle size and shape there exist a critical size of the outlet below which the flow may be pulsating or nonexistence unless poked owing to the formation of a stable mechanical arch (e.g. Mankoc et al., 2007). Typically, steady discharge of material is realised when the outlet size is such that $R^* \leq 6$ where R^* is the ratio of the outlet size to the particle size. Slightly higher values of the minimum ratio $R^*_{\min}$ are obtained with highly angular particles (Rotter, 2001) while for spherical particles lower values are possible. In this study too, the threshold value of $R^* = 6$ did not give steady discharge of the nonspherical LBS1 and even after poking it took only about 5s for a stable arch to form again. Precise

determination of the threshold value of the outlet opening was not the intent of this study but the results indicate that it lies between 6 and 10.

Table 7-5: Effect of D_o on flow rate of dry Glass beads and Leighton Buzzard sand

Material	Test		D_o (cm)	$R^* = D_0 / d_p$ (-)	ρ_b (g/cm^3)	e_0 (-)	W_{obs} (g/s)
	Series	ID					
GLASS BEADS	GBS1	D-01	0.370	10.5	1.534	0.56	1.101
		D-02	0.600	16.9			4.780
		D-03	0.800	22.6			14.499
		D-04	1.016	28.7			24.538
		D-05	1.45	41.0			64.457
		D-06	1.831	51.7			134.936
		D-07	3.188	90.1			586.420
		D-08	5.400	152.5			2375.036
	GBS2	D-01	1.45	117.9			68.425
LEIGHTON BUZZARD SAND	LBS1	D-01	0.370	8.9	1.638	0.63	-
		D-02	0.600	14.4			3.178
		D-03	0.800	19.1			9.350
		D-04	1.016	24.3			16.888
		D-05	1.450	34.7			47.194
		D-06					47.465
		D-07					47.078
		D-08			1.669	0.60	46.100
		D-09	1.831	43.8	1.638	0.63	87.371
		D-10	3.188	76.3			488.201
		D-11	5.400	129.2			1789.001
		D-12	9.850	235.6			7725.152

7.3.1.6 Particle size effect on mass discharge rate

The particle size effect on mass discharge rate is appreciated when the test results on two different spherical glass beads in terms of particle size are compared. The results indicate that for the given model configuration and sample conditions, the mass discharge rate of the dry materials is dependent on the particle size/grading. Whereas the discharge rate of 64.457g/s was obtained in test D-05 on glass beads of mean particle diameter, $D_{50} = 0.354$mm (series GBS1 in Table 7-1 & 7-5) a rate of 68.425g/s was recorded in test D-01 on glass beads with mean particle diameter, $D_{50} = 0.123$mm

(series GBS2 in Table 7-1 & 7-5). Referenced to the $D_{50} = 0.354\text{mm}$ glass beads discharge rate, the difference in flow rate between these two same material composition and shape beads is about 6.2%. It should be emphasised that other than size, all other particle properties and the test conditions were the same in the compared tests.

The above observation is consistent with the general agreement that the effect of increasing particle size is to decrease the flow rate (e.g. Fowler & Glastonbury, 1959; Zhang & Rudolph, 1991; Mankoc et al., 2007). This effect is reflected in many of the proposed equations for predicting the gravity discharge rate through orifices whereby effective discharge diameter is used. The effective discharge diameter is expressed as the difference between the orifice diameter and a factored particle diameter (i.e. $D_0 - k_B d_p$). The value of k_B often used is generally in the range of 1-3 depending on the material type and particle size and shape. This factor is often determined through an experimental programme and so it reduces to a fitting parameter. Further details about the k_B value are given later in section 7.4.

7.3.2 Experimental Results with Unsaturated Material

7.3.2.1 Flowability of unsaturated material

In this part of the thesis, results of the tests carried out to assess the effect of moisture (or suction) on the flowability of granular materials are presented and discussed. Details of the tests carried out were presented in section 7.2. Table 7-6 presents the results. For the given model configuration and sample conditions the mass discharge rate of the wet unsaturated glass beads (GBS1) and Leighton Buzzard sand (LBS1) was found to be highly dependent on water content and hence suction. When water content of 0.5% was introduced into the material, the particles did not discharge immediately on opening the outlet due to the formation of a stable arch. It should be remembered that for the range of hopper outlet diameters studied these inert materials in their dry state discharged without any jamming (see subsection 7.3.1). Therefore the resultant liquid bridges must have been responsible for the formation of the stable arch. Further increase of water content to about 1%, 3% and then to 5% did not change the status quo as the discharge of the material remained nonexistent on opening the outlet. Whether or not these materials would finally discharge after leaving them for some time is discussed later. If water content was probably increased further a condition would be reached when the material would flow. It was however considered unnecessary to investigate this condition in this study as such a condition is very unlikely in practical applications.

Instead uncontrolled but slow spraying of water to the material in the silo was carried out to examine the extent of wetting at which the formed stable arch would collapse for the flow of material to take place under the influence of gravitational drag alone. It was until the water droplets started to emerge from the hopper outlet that the material started to flow but only intermittently. It was thus not possible to accurately measure the water content corresponding to this condition. From the few attempts made at measuring it, water content appeared to be slightly higher than the saturated water content suggesting that unless the bulk water in the material aided the material to flow (in this case in form of lumps) it would not flow.

The observation just described was made with a hopper outlet diameter of 1.45cm - the minimum considered in the unsaturated tests. This outlet diameter was more than 10 times the maximum screen particle diameter of the nonspherical LBS1 and far much more than 6 times the mean screen particle diameter of the spherical GBS1 (see Table 7-5). These ratios of outlet diameter to particle diameter have been shown to be satisfactory in allowing steady flow of noncohesive granular materials (without any jamming due to mechanical arching) (e.g. Rotter, 2001; Mankoc et al., 2007). It might be thought that slightly increasing the outlet size would cause the wet material to flow. This was investigated and it was found that for the water content of 0.5% flow would not immediately take place on opening the discharge outlet until the outlet diameter was about 220 particle diameters for $D_{50} = 0.61\text{mm}$ mean particle diameter LBS1 and more than about 425 particle diameters for $D_{50} = 0.354\text{mm}$ mean particle diameter GBS1. The minimum outlet diameter at which no stable arch due to liquid bridges would form is hereinafter termed the critical outlet diameter with respect to liquid bridge induced arch (D_{crit_lb}). As can be seen in Table 7-6 and Fig. 7.2 for given water content flow was only possible above the critical diameter. Slightly greater outlet diameter to particle diameter ratios were necessary for the material with higher water content (within the range of water contents investigated) to discharge immediately upon outlet opening suggesting that stronger binding forces were associated with higher water contents. It should be noted that when the outlet diameter was equal to D_{crit_lb} the material suddenly slumped that any attempts to measure the flow rate were futile as the critical diameters were so large that it took a very short time for the silo to empty. As such, in Table 7-6 the flowability results are presented in terms of flow or no flow.

Table 7-6: Flowability of wet Leighton Buzzard sand (LBS1)

Material	Test series	Water content			Normalised outlet diameter	Bulk density	Void ratio	Matric suction[a]	Flowability
		w_g (%)	w_{ratio} (-)	S_r (-)	R^* (-)	ρ_b (Mg/m^3)	e_o (-)	ψ_m (kPa)	W_{obs} (g/s)
LEIGHTON BUZZARD SAND	LBS1	0.5	0.0134	0.021	≤ 260	1.644	0.63	16.020	No flow
		0.5			≥ 320				Flow
		1.0	0.027	0.043	≤ 380	1.654		4.196	No flow
		1.0			≥ 457				Flow
		3.0	0.081	0.129	≤ 457	1.687		2.899	No flow
		3.0			≥ 495				Flow
		5.0	0.1335	0.212	≤ 495	1.720		2.208	No flow
		5.0			≥ 524				Flow
		8.0	0.214	0.340	≤ 524	1.769		-	No flow
		8.0			≥ 570				Flow

[a]*Data obtained using the filter paper method*

In Table 7-6 and Fig. 7.2, the outlet diameter was normalised using the equivalent mean spherical particle diameter computed from the results of sieve analysis and the particle shape factor, as is often the case (e.g. Beverloo et al., 1961). Both the experimental data of the maximum normalised outlet diameters for which no flow was observed at each water content (curve 1) and the minimum outlet diameters for which a stable arch would not form (curve 2) were recorded (Table 7-6) and plotted on the same graph (Fig. 7.2). From the figure we see that the gravimetric water content (Fig. 7.2a) and degree of saturation (Fig. 7.2b) of LBS1 at which liquid bridge induced arch cannot form varies nonlinearly with the normalised outlet diameter. The resultant relationship was found, through the nonlinear curve fitting procedure, to follow a power law (see Eq. 7-1 with water content in terms of degree of saturation) and is herein termed the *wet flowability curve*. In the equation, a and b are fitting parameters whose values are dependent on the form of water content used as shown in Fig 7.2. The region to the left of the wet flowability curve defines a no flow zone while the one to the right of the curve indicate

sudden discharge zone. The region enclosed by the two curves is therefore the region of uncertainty. It is not clear whether or not a stable arch would form in the uncertainty region. Independent of the form of water content used however the parameter b is a constant and is equal to 0.0105 implying that the actual wet flowability curve could be an average of the two curves.

$$S_r = ae^{bR^*} \qquad \text{Eq. 7-1}$$

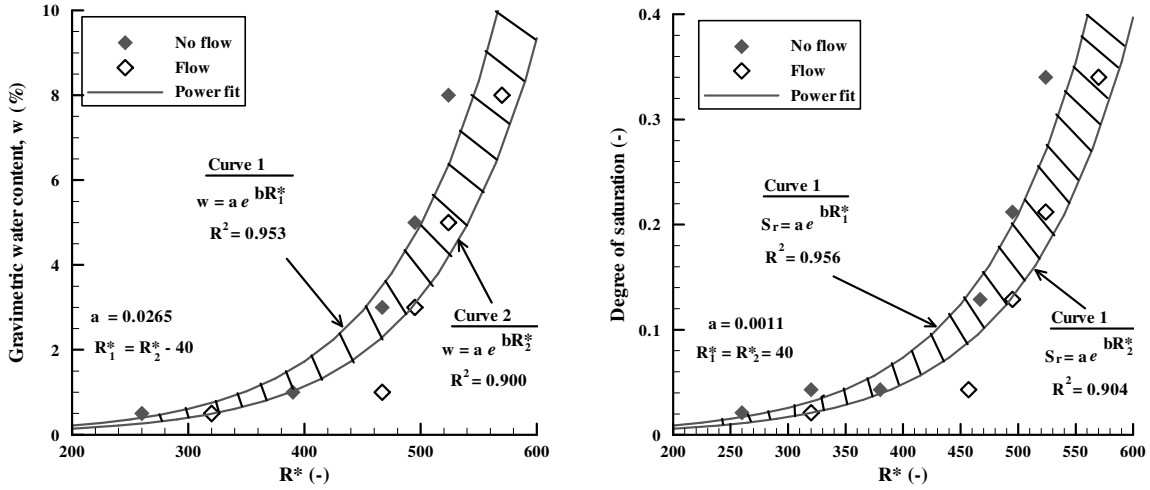

(a) In terms of gravimetric water content

(b) In terms of degree of saturation, S_r

Figure 7.2: Flowability of LBS1 on a plot of water content versus normalised outlet diameter

Previous studies of the effect of moisture on the flowability of bulk solids from silos and hoppers have focused on cohesive powders and materials with particles that absorb water and hence increase in volume (e.g. Fitzpatrick et al., 2004; Iqbal & Fitzpatrick, 2006; Ganesan et al. 2008) as well as very fine glass powders (e.g. Landi et al., 2011). In most of these indirect studies (indirect in the sense that flowability was derived from other measured properties), however, the observed behaviour cannot be attributed to moisture alone as several other particle properties were not sufficiently controlled. Nonetheless, from these studies and many more a general conclusion is that increasing moisture content decreases flowability owing to the enhanced cohesion component of the material strength. This conclusion together with lack of the experimental data for wet *clean* noncohesive granular materials seem to cloud the impression that such granular materials would not sustain a stable arch unless it is very fine with electrostatic forces and or capable of absorbing moisture. The results of this study reveal otherwise as elucidated in the preceding paragraphs.

It should be noted that the tested glass beads and sand were inert, noncohesive materials and that water content was generated using distilled water. Therefore the observed formation of a stable arch can only be attributed to the liquid bridge induced adhesion forces. According to the work of Kim & Hwang (2003), a sample of clean sand with $e_0 = 0.65$ can sustain up to about 1.2kPa in tension within the range of water contents considered in this study. Therefore the bulk solids must first overcome the apparent cohesion associated with this tensile strength before accelerating from zero velocity under the influence of gravity alone. This is consistent with the observations made in Chapters 5 & 6 of water retention and shear behaviour respectively. It makes sense therefore to look at the appearance of the material and the corresponding matric suctions in furtherance of the understanding of the problem. These observations further show that the finer the particles and the more the degree of saturation the more efforts needed in causing the material to flow.

7.3.2.2 Suction and liquid bridges in silo model tests

It had been hoped that the hygrometer-measured relative humidity and temperature in conjunction with the Kelvin's thermodynamic equation would be suitable for giving the total suction of the unsaturated model test materials. It turned out that the sensitivity of 0.5% of the used hygrometers was insufficient to give reasonable suction values within the range of water content relevant to, and indeed considered in the current study. This is because the variation in relative humidity due to changes in water content was marginal. Yet within the range of measured relative humidity, suction is very sensitive to changes in relative humidity and temperature. For instance a change in relative humidity of 0.001% from 99.5% at a constant temperature of 22^{o}C would induce a change in suction of about 13.660kPa, which is quite significant. It therefore means that reasonable measurements would only be realised using hygrometers accurate to 0.000001%. With this, the purpose of the hygrometers was thus reduced to qualitatively assessing the adequacy of 14days in attaining equilibrium in the samples.

As an example, Fig. 7.3a&b show the entire time history of relative humidity and temperature, respectively for test W-01 of the LBS1 series. The corresponding data for tests W-02 and W-03 of the same series are shown in Fig. 7.3c&d and e&f respectively. The bottom sensor was located at 10cm, while the middle and top sensors were respectively located at 50cm and 80cm above the transition level. It is observed that within 14days all the water content samples had come to equilibrium in terms of relative

humidity and temperature and that these quantities were fairly and satisfactorily maintained constant at least two days to opening of the hopper outlet for material to discharge. From Fig. 7.3 we further see that relative humidity and temperature was constant along the meridional axis. Therefore the filter paper measured matric suctions were made after the samples had reached equilibrium and it did not matter where the measurement was taken from.

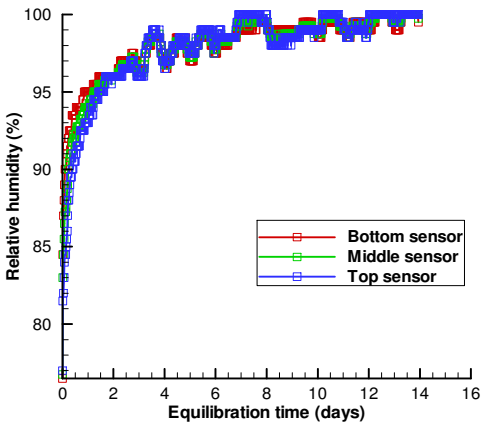

(a) Gravimetric water content of 0.5%

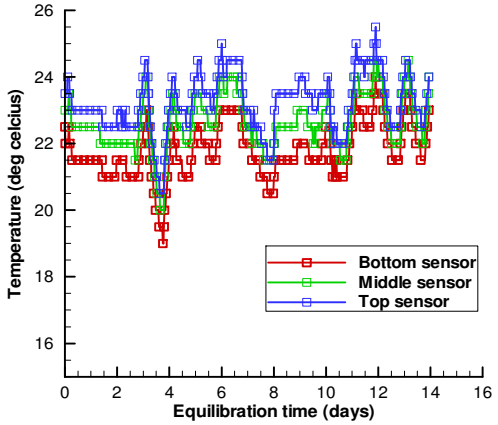

(b) Gravimetric water content of 0.5%

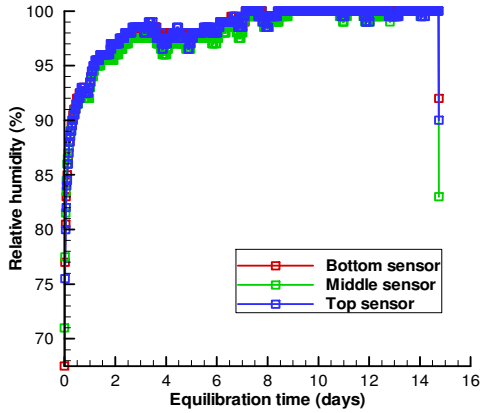

(c) Gravimetric water content of 1.3%

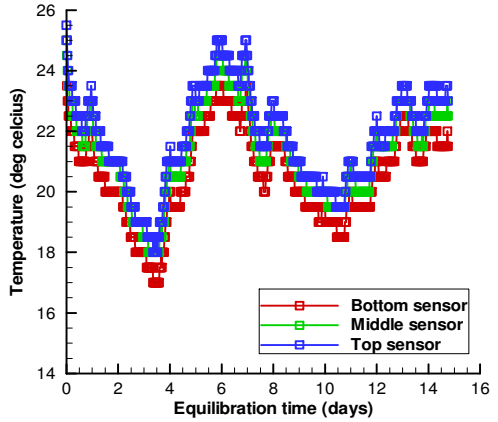

(d) Gravimetric water content of 1.3%

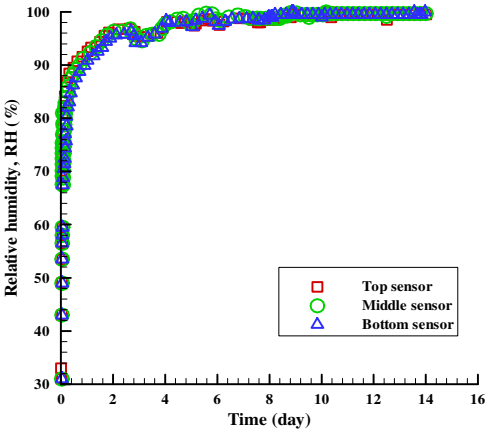

(e) Gravimetric water content of 3%

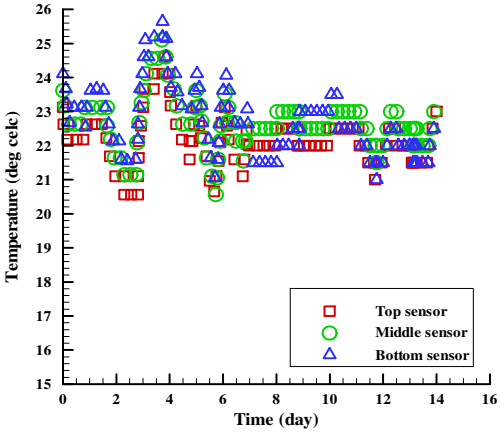

(f) Gravimetric water content of 3%

Figure 7.3: Time history of relative humidity and temperature for the specified water content tests

The results of filter paper tests on GBS1 and LBS1 are presented against the water contents in Table 7-7 from which it is clear that higher values of matric suction were obtained at lower water contents, as expected. Whether or not the filter paper method is suitable for measuring matric suction in coarse granular materials is a controversial issue yet to be resolved. It is feared that while intimate contact is a requirement for a successful application of the method, the relatively large voids present in a packed system of coarse granular materials makes it difficult to establish this intimate contact. This is especially so at sufficiently low water contents so that the measured matric suction is somewhat between the true matric suction and total suction. To allay this fear both matric and total suctions were carefully measured in this study following the established procedure as follows. To measure matric suction, an initially dry sandwiched filter paper was placed in between the sample ensuring intimate contact to facilitate moisture exchange between the sample and filter through liquid flow. The opposite was true with the measurement of total suction. The filter paper was placed to have no direct contact with sample in a closed environment so that any moisture exchanges between the two media were solely through vapour transfer.

The results indicate that for all the water contents total suction is higher than matric suction. Whether the difference is due to lack of intimate contact or something else requires further analysis. If the lack of intimate contact is the reason then it means that the tested materials had some osmotic suction in them. However, it should be remembered that the tested materials especially GBS1 were inert and therefore given that distilled water was used osmotic suction cannot be the reason for the difference. As shown in Table 7-7, the difference falls within about 25%. According to Chandler et al. (1992) whose calibration equation was used in converting the filter paper water content to suction, the filter paper method is accurate to about 75%. Therefore the difference could have been a result of the scatter nature of the measurements. The question that remains to be answered is about the observed consistence in the difference. This is probably due to the fact that 14days could have been insufficient to achieve equilibrium given that moisture transfer in the range of water content considered is predominantly through vapour. The 14days equilibrium is based on calibration tests involving use of acid and or salt solutions.

Table 7-7: Results of filter paper tests on glass beads (GBS1) and sand (LBS1)

Test	Water content		Matric suction ψ_m (kPa)		Total suction ψ (kPa)	$\psi - \psi_m$ (kPa)	$\frac{\psi - \psi_m}{\psi_m} \times 100$ (%)
	w (%)	S_r (%)	Measured	From WRC			
Glass beads (GBS1)							
1	5.1	23.2	5.812	7.140	6.000	0.188	3.2
2	3.0	13.6	11.001	9.663	12.835	1.834	16.7
3	0.9	4.1	185.633	24.862	221.646	36.013	19.4
Leighton Buzzard sand							
1	9.8	46.7	1.897	2.354	1.945	0.048	2.5
2	4.9	23.4	2.208	3.365	2.564	0.356	16.1
3*	3.0	12.7	2.899	4.212	-	-	-
4	2.3	11.0	3.806	4.754	4.904	1.098	28.8
5*	1.3	5.5	4.196	6.245	-	-	-
6*	0.5	2.1	16.020	11.619	-	-	-

Notes: w is gravimetric water content, S_r is degree of saturation, ψ_m is matric suction, ψ is total suction, and WRC is water retention curve; *Measurements conducted directly in the silo model at different levels and the value presented represents an average of three values.

In Fig. 7.4, the filter paper measured suctions are plotted together with the van Genuchten (1980) fitted pressure plate experimental data to examine how these suctions measured without any hydraulic history compare with those with a hydraulic history. Overall, the results show that samples that have not experienced any hydraulic history are at a lower potential compared to those undergoing drying with some hydraulic history, and at a higher potential compared those undergoing wetting. Seen on a semi-logarithmic plot, the difference in potential is more pronounced at higher water contents. This is probably due to the role plaid by moisture transfer mechanism; at higher water contents it is through liquid flow while it is through vapour transfer at lower water contents. Therefore the rearrangement of water at very low water contents is minimal. In fact at very low water contents it can be concluded that the hydraulic history does not affect the water retention curve of the tested granular materials. Therefore as shown in Table 7-7 the filter paper measured matric suctions can be used in place of the pressure plate suctions and vice versa.

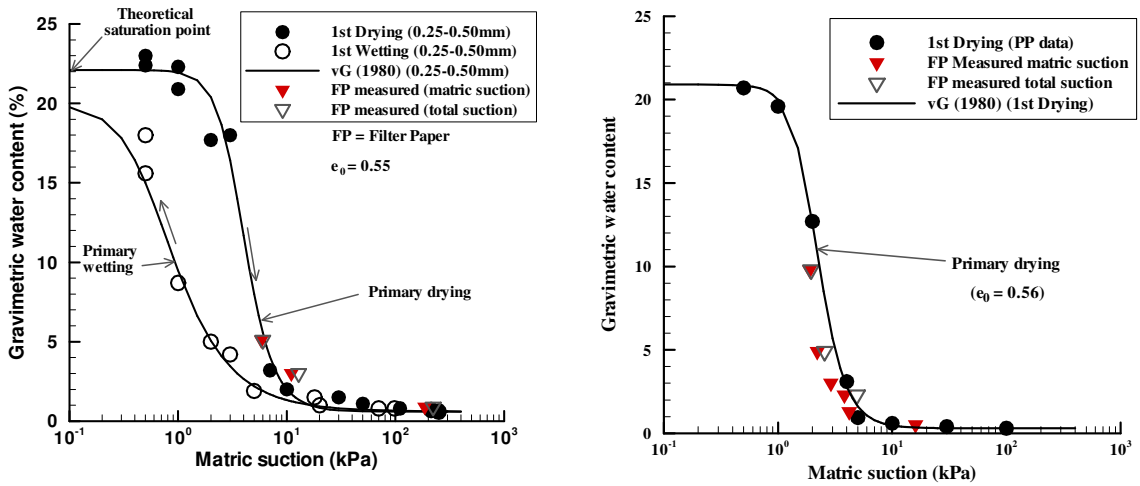

(a) Glass beads (GBS1) (b) Leighton Buzzard sand (LBS1)

Figure 7.4: Comparison of suction with and without hydraulic history

Aside from relative humidity and temperature, microscopic images of the wet unsaturated LBS1 as seen through the transparent wall were taken. It had been expected that for hopper outlets satisfying the existing sizing criterion of the horizontal hopper outlet for free flowing solids, especially at low water contents, the test materials would flow, at least at a reduced rate. The microscopic images would then be used to quantitatively relate the flow rate to the proportion of the wetted surface of the silo wall in addition to the water content or suction and its effect on the various flow influencing properties. As it turned out, however, flow of unsaturated material was not immediately possible. It would probably have happened if water contents lower than 0.5% had been considered. However, these were not considered in the current study owing to the difficulty in achieving uniform distribution of water within the material at such extremely low water contents. Moreover since within such a low range of water content, moisture exchange is dominated by vapour transfer rather than liquid flow it would take prohibitively longer to achieve equilibrium. Nonetheless, the microscopic images provide useful particle level information including uniform distribution of water in the material.

As shown in Fig. 7.5, all particles were moist and as the water content was low significant proportion of the voids remained occupied with air. Therefore only the parts of the silo model wall in contact with the wet particles were wetted. As expected, the extent of wetting increased with increase in water content. Experimental evidence has shown that coexistence of gas and liquid phases in solid phase generates matric suction

that serves to bind the contacting solids together. This has also been shown in Chapter 5 and Chapter 6 of this thesis. It therefore makes sense to examine the sustainability of the stable arch associated with the different water contents or suctions and the mechanism responsible for its formation.

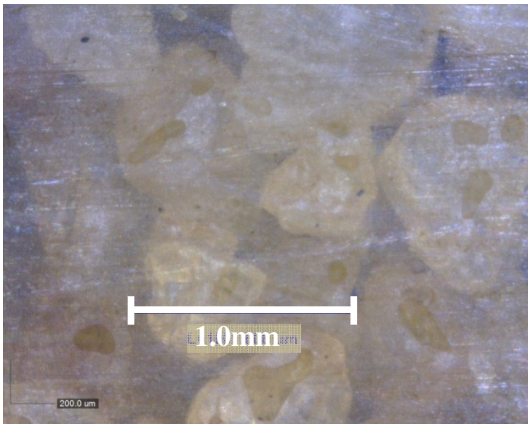

(a) Gravimetric water content of 0.5%

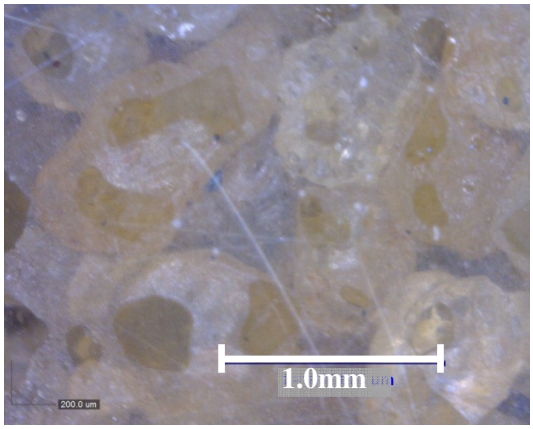

(b) Gravimetric water content of 0.5%

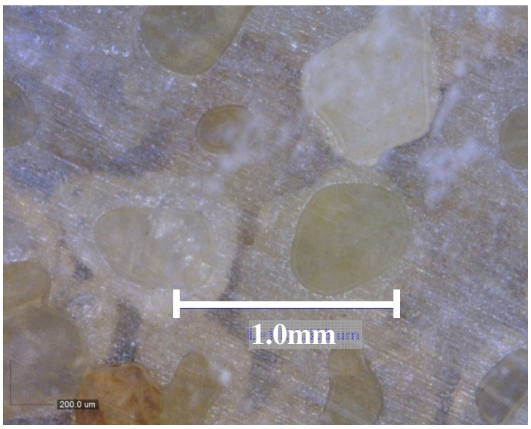

(c) Gravimetric water content of 1.3%

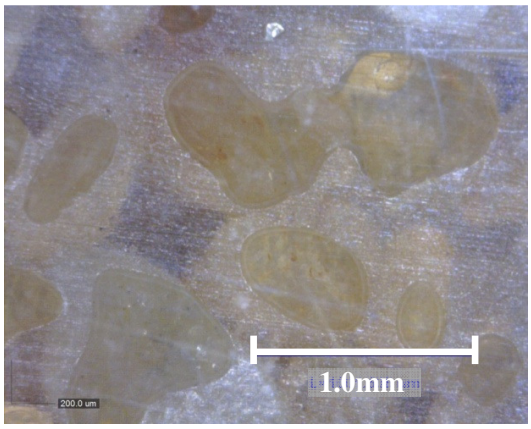

(d) Gravimetric water content of 1.3%

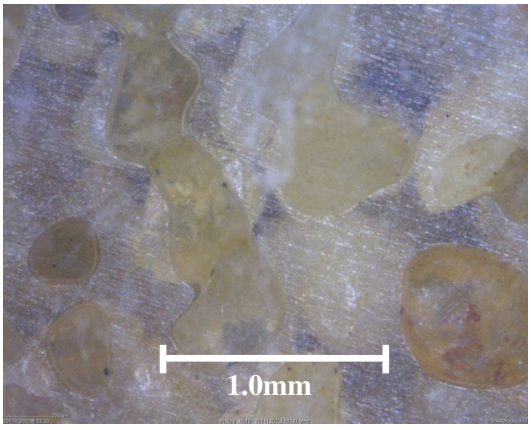

(e) Gravimetric water content of 3%

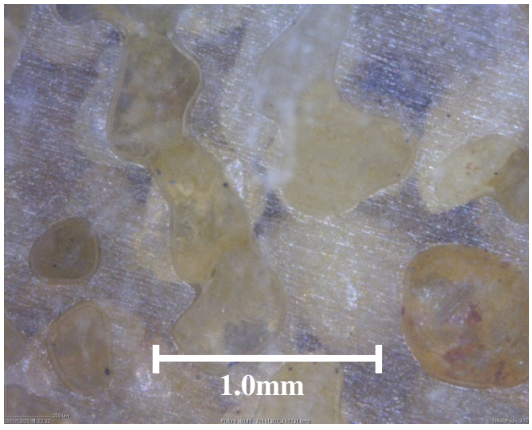

(f) Gravimetric water content of 3%

Figure 7.5: Microscopic images showing proportion of the wetted surface of the silo wall at different water contents: a, c & e taken next to the relative humidity sensors, and b, d & f taken opposite of the relative humidity sensors

7.3.2.3 Sustainability of the stable arch in unsaturated silo model test materials

Throughout the preceding part of this section it is emphasised that the wet unsaturated glass beads and Leighton Buzzard sand did not immediately flow following opening of the hopper outlet. This is because a liquid bridge induced stable arch formed in the vicinity of the outlet. The question was how long it would take for the material to finally flow. It was therefore decided to leave the material exposed to atmosphere from both top and the outlet side so that moisture would transfer to the laboratory atmosphere. For outlet size of 1.45cm and all water contents considered, material did not flow even when it was left for one week. In fact at 3% water content, the sample was left for one month but still the stable arch remained. This is because at room conditions ($22 \pm 2^{o}C$) this time was not adequate to have all the moisture lost from the sample. Increasing the hopper outlet size reduced the time needed for the stable arch to collapse. For the outlet size of 9.85cm and 0.5% water content only about 45minutes was required for the material to discharge. However, as the opening was significantly large, it was not possible to accurately measure the time taken to empty the model. This is because unlike in dry tests where the start of discharge was known in wet unsaturated tests it was not easy to tell exactly when the material is due to discharge. With this size of the outlet however more time was necessary for the stable arch to collapse in material at higher water content, explored for 3% and 5% water content. The exact time was not precisely determined owing to the fact that flow happened at night when no one was available to take note of the time.

These observations indicate that use of warm air to dry wet unsaturated materials can take prohibitively long period of time depending on the amount of moisture and while widening of the discharge outlet reduces the time it may not be practical. At discharge outlets large enough to prohibit the formation a stable arch, the discharge rate can be too high for most of the industrial processes requiring controlled discharge of the material. The observations further suggest that matric suction alone is not a suitable parameter for characterising the flowability of wet unsaturated granular materials. Whereas suction increases with decrease in water content, the stability of the observed arch reduces with decrease in water content. It is thus either a combination of both water content and suction or some other parameter related to water content that contribute to the forces responsible for the formation of a stable arch in clean noncohesive granular materials. This is explored further in the following subsection.

7.3.2.4 Mechanism responsible for the formation of the observed stable arch

Jenike (1964) postulated a theory of arching based on the stresses in hoppers. Although several other theories have subsequently been proposed (e.g. Walters, 1973; Enstad, 1975; Morozov et al., 2002), Jenike's approach remains the most applied and therefore is considered in here. A comprehensive review of some of the theories is presented elsewhere (e.g. Ooi & Rotter, 1991). Consider an infinitesimal element of volume ΔV of arched bulk solids in the hopper shown in Fig. 7.6a. Consider also that the arch has a constant thickness and supports its own height. Jenike made simplifying assumptions with respect to material properties and the flow conditions to arrive at Eq. 7-2 defining the stress σ_{hw} transferred to the conical hopper walls in order to determine the minimum hopper outlet to avoid arching. He considered that for the emptying conditions the effective angle of internal friction is given by the ratio of the major to minor principal stresses and that the yield locus gives the material characteristics for the incipient flow. The latter case is of much interest here. The bulk density ρ_b was also assumed to be independent of r, the radial distance from the hopper virtual apex. The parameter β is the hopper half angle. The distribution of σ_{hw} along the silo height during emptying is indicated in Fig. 7.6b.

$$\sigma_{hw} = \rho_b g r_0 \sin\beta \qquad \text{Eq. 7-2}$$

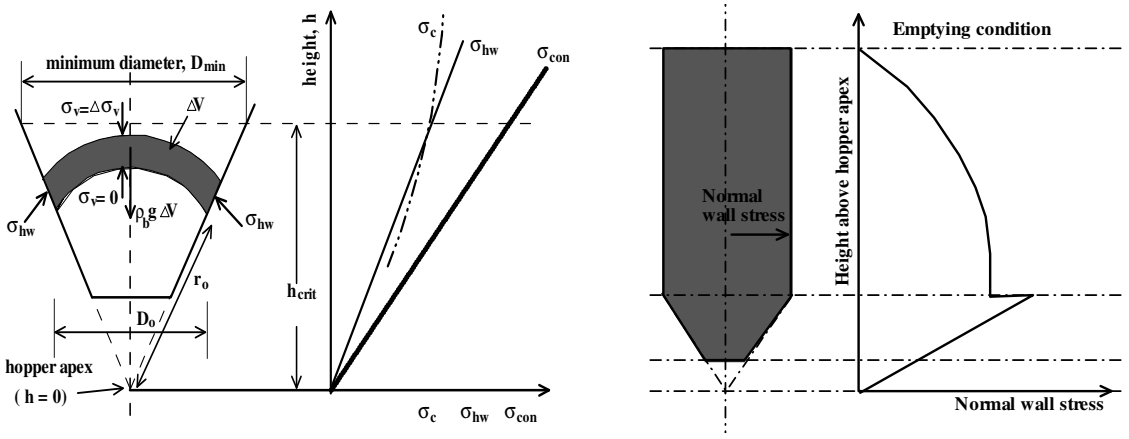

(a) Stress acting on a stable arch in hopper (b) Emptying normal wall stress in silo

Figure 7.6: Forces responsible for the formation of a stable arch in wet granular materials

The stress obtained using Eq. 7-2 represents the principal stress needed to support the weight of the stable bulk solid arch; it acts at the 'abutment' of any arch that tends to form. It follows that the principal stress in conical hopper is proportional to the local

hopper diameter which itself is proportional to the radial distance of the arch along the hopper wall from the virtual hopper apex. The principal stress dictates the local properties of the bulk solids in the hopper including the unconfined yield strength that must be overcome by the stress given by Eq. 7-2 for the solids to flow. For dry noncohesive bulk solids the unconfined yield strength is negligibly zero so that no cohesive arch is possible. Any arching is therefore due to mechanical interlocking of the solids. Therefore provided the hopper outlet satisfies the minimum size requirements arching would never be a problem in such materials. Empirically, the minimum hopper outlet diameter is taken to be six times the spherical particle diameter or ten times the nonspherical particle diameter. This is however only so if the material remains dry. As soon as moisture ingresses into the material the situation changes.

The results of this study have shown that moisture and hence suction introduces a bonding force between the particles that must be overcome for the material to flow, just like the unconfined yield strength of cohesive solids must be overcome first before the material can discharge. For cohesive materials with nonzero unconfined yield strength, σ_c the value of the unconfined yield strength below which arching would occur is termed the critical unconfined yield strength σ_{ccrit}. This critical value of strength is used to obtain the minimum outlet diameter $D_{\min}$ for which a stable arch would not form. Eq. 2-24 (reproduced here as Eq. 7-3) is used for this purpose with ρ^{crit} as the critical density of the bulk solids. The term $H(\beta)$ accounts for any variation in the arch thickness, hopper type and hopper half angle.

$$D_{\min} = H(\beta)\frac{\sigma_{ccrit}}{\rho^{crit} g} \qquad \text{Eq. 7-3a}$$

$$H(\beta) = 2 + \frac{\beta}{60} \qquad \text{Eq. 7-3b}$$

It appears that the apparent unconfined yield strength associated with the tensile strength of the wet noncohesive bulk solids can be substituted for the term for critical unconfined yield strength in Eq. 7-3 to obtain the corresponding minimum outlet diameter. This is explored next. Previous studies have shown that the wet unsaturated noncohesive granular materials possess an apparent cohesion ascribed to the influence of matric suction (e.g. Fredlund & Rahardjo, 1993). As shown in chapter 6, this leads to increased shear strength. In some studies suction stress (conceptualised as the resultant

of inter-particle physicochemical stress attributable to cementation, van der Waals attraction, double layer repulsion, capillary stress arising from surface tension, and the negative pore water pressure) has been used in place of matric suction (e.g. Lu & Likos, 2006). From all these studies and the results of the current study, it can be concluded that the effect of matric suction or the apparent shear strength ascribed to the material tensile strength is relatively more pronounced at relatively low values of the net normal stress. From the foregoing (see Fig. 7.6b) it is obvious that in the neighbourhood of the hopper outlet the normal wall stresses are so small that any forces tending to bond the solids together can significantly affect the flowability of the solids. In fact the particles exposed to the atmosphere are under zero vertical stress so that without the bonding force or some kind of strength to overcome, they would quickly accelerate under the influence of gravity.

Whereas the results in Table 7-7 suggest that matric suction progressively becomes significant as water content reduces, the silo model test results indicate that the most significant effect of matric suction is not associated with the highest suction. Within the range of water content studied, the highest water content gave the strongest resistance to flow. This is consistent with the findings of the previous studies (e.g. Kim & Hwang, 2003; Kim & Sture, 2004; Houston et al., 2008). In their study, Kim & Sture (2004) observed the tensile strength of wet unsaturated sand to increase nonlinearly as water content was increased up to about 15%. Thereafter it was apparent that any further increase in water content would serve to decrease the tensile strength. The presence of tensile strength in noncohesive granular materials implies apparent shear strength and hence an apparent unconfined yield strength.

In the area of industrial bulk solids handling the effect of cohesion is taken into consideration by including the unconfined yield strength in the equation for the minimum hopper outlet diameter (see Eq. 7-3). The unconfined yield strength is often determined experimentally using shear testers such as the Jenike tester which is essentially a modified version of the standard shear box test. With the modification, it is possible to strain the sample to the necessary critical condition. However, issues remain with the accuracy of the results within the stresses associated with the unconfined yield strength of noncohesive granular materials. Moreover, extrapolation from the high stress levels may also give misleading results.

In absence of the experimentally measured unconfined yield strength, however, for each of the water contents an indirect value can be obtained from the tensile strength σ_t of the material and the corresponding internal angle of friction obtained using the standard shear box test. This is especially possible given the angle of internal friction is not dependent on water content or suction (e.g. Fredlund & Rahardjo, 1993; Landi et al., 2011), as has also been shown in Chapter 6. Based on the Mohr-Coulomb concept, the procedure is as follows: First, using Eq. 7-4 the apparent cohesion c is computed. A line is then drawn from the point defining the tensile strength on the normal stress axis to pass through the apparent cohesion coordinate on the vertical axis. For noncohesive granular materials, equating the slope of this line to the tangent of the internal angle of friction may not introduce significant errors. Thirdly, a circle is drawn passing through the origin and touching the line drawn in the preceding step. The radius of the circle so drawn gives the shear strength of the material while the unconfined yield strength σ_c is given by the diameter of the circle.

$$c = \sigma_t \tan\phi' \qquad \text{Eq. 7-4}$$

Whereas the internal angle of friction was experimentally determined in this study, the tensile strength, shear strength and the unconfined yield strength were not. However, numerous theories exist in the literature from which they can be estimated. One such theory is the one presented by Kim & Hwang (2003) to estimate the tensile strength of sand from the material physical properties. These are shown in Fig. 7.7a for coarse sand (F-75-C) and sand containing 2% fines (F-75-F). In this study, using this theory the estimated tensile strength was then used to infer the values of shear strength and unconfined yield strength σ_c based on the Mohr-Coulomb theory. The two results were then related to the stresses transmitted to the hopper wall (computed using Eq. 7-2) for the openings that allowed flow to check how they compare and the results are shown in Fig. 7.7b. From the figure, we see that for all water contents the shear strength was lower while the unconfined yield strength was higher than the stress transmitted to the hopper wall. From the design point of view these results suggest that the unconfined yield strength is more useful than the shear strength in estimating the minimum hopper outlet for wet noncohesive granular materials. It may be expected that since the considered outlet sizes are the minimum for flow to take place the plotted points in Fig. 7.7b should plot along the 1:1 line. As can be seen in the figure, this is nearly so but only up to 1% water content. Higher values of water content give higher unconfined

yield strength compared to the stress transmitted to the hopper wall σ_{hw}. The shear strengths are lower than the σ_{hw} for all water contents. The higher unconfined yield strength compared to σ_{hw} may be ascribed to the effect of particle size on the tensile strength of sand. The sand used in this study was coarser than that used by Kim & Hwang (2003) in developing their equation yet from Fig. 7.7a the tensile strength of sand decreases with increase in particle size. Any decrease in tensile strength serves to move the plotted points of σ_{hw} against σ_c closer to the 1:1 line. Further experimental work on the subject will therefore offer further evidence to the applicability of the Kim & Hwang (2003) equation in determining the σ_c as herein proposed.

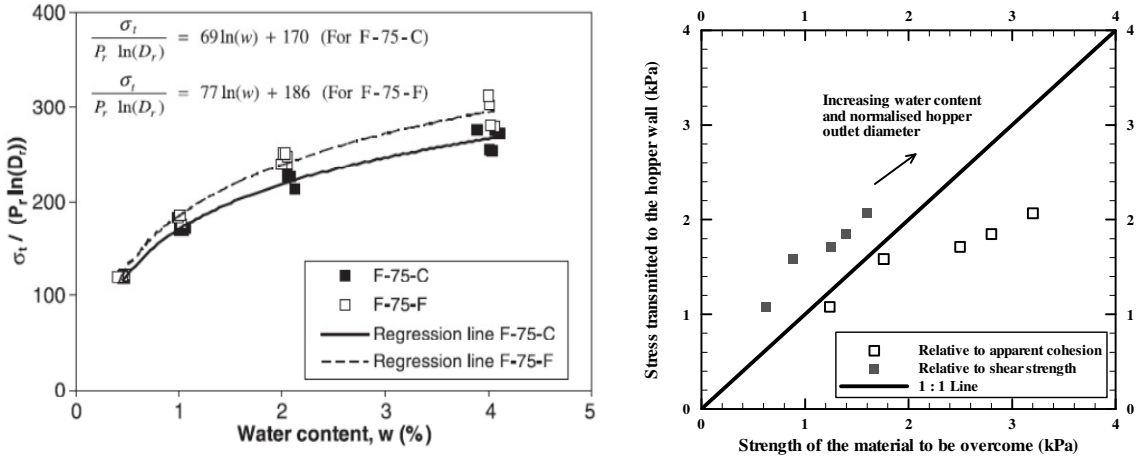

(a) (b)

Figure 7.7: (a) Comparison of stress transmitted to the hopper wall and the strength responsible for stable arch formation, (b) Kim & Hwang (2003) data for tensile strength of sand

It should be emphasised that the stress σ_{hw} is directly proportional to the hopper outlet diameter. Since the hopper outlet diameter for which the wet unsaturated material will flow increases nonlinearly with increase in moisture content as does the unconfined yield strength then σ_c and σ_{ccrit} in Eq. 7-3 for estimating the minimum hopper outlet diameter can be used interchangeably. The accuracy of the predicted hopper outlet diameters will depend on the correctness of tensile strength used. It is therefore recommended here that for accurate predictions the tensile strength used to estimate the unconfined yield strength should be determined experimentally instead of using the Kim & Hwang (2003) equation. Alternatively the Kim & Hwang (2003) equation should first be validated for the material at hand.

7.4 Predictability of the mass flow rates from silos

In bulk solids handling, the ability to predict the ensuing flow given the hopper geometry and material properties is necessary for a successful design of hoppers and silos. Many equations can be found in the literature to predict the flow rate of bulk solids under gravity conditions. However, the one by Beverloo et al. (1961) seems the oldest that is commonly cited and used in the literature. It is at times referred to as the Beverloo law. Since its development, several attempts have been made to evaluate the robustness of this widely accepted equation (e.g. Nedderman et al., 1982; Zhang & Rudolph, 1991; Hirshfled et al., 1997; Hirshfled & Rapaport, 2001; Mankoc et al., 2007; Datta et al., 2008). The general agreement is that provided that $D_B > 2.5D_o$ and $(D_B - D_o) > 30d_p$ with D_B as the silo barrel diameter (or width in the case of rectangular hoppers) then the Beverloo law is valid. In addition, the discharge rate depends on the shape of the hopper (Clearly & Sawley, 2002; Goda & Ebert, 2005).

However, it appears that in most of the above attempts to validate Beverloo law over a wide range of conditions only experimental results from flat-bottomed cylinders have been used. In such cylinders, flow near the orifice is strongly influenced by the shear resistance between the flowing and nonflowing particles at the base of the cylinder, typical of what happens in the funnel and or mixed flow patterns where the core material discharges first yet the relationship seems applicable to mass flow as well (e.g. Datta et al., 2008). As such, some numerical simulations have been carried out with the stationary particles replacing the container wall (e.g. Zhang & Rudolph, 1991). The choice of flat-bottomed cylinders is probably motivated by the need to be consistent with the original experimental setup by Beverloo and the co-workers as well as to reduce the computation efforts in numerical simulations. The question is whether relationships obtained by replacing the container wall with nonflowing particles are applicable to situations where the container wall is essentially the sliding surface, as is the case in pure mass flow. Unless the wall friction is the same as the internal friction angle of the material this is highly unlikely. The angle of wall friction is the major property for mass flow hopper design (Jenike, 1960).

The Beverloo law can be obtained through dimensional analysis. For a given hopper geometry and material, experimental results indicate that the flow rate, W is dependent

on the material bulk density ρ_b, acceleration due to gravity, g and the orifice size, D_o (e.g. Beverloo et al., 1961). By carrying out dimensional analysis it can be shown that:

$$W \propto \rho_b \sqrt{g} (D_0)^{5/2} \qquad \text{Eq. 7.5}$$

The proportionality constant, C has been found to be related to the coefficient of friction between the sliding and stationary surfaces. Similar results can be obtained by assuming that flow is proportional to the product of the velocity of particles freely falling from just above the orifice and the cross-sectional area, analogous to the outflow of liquids under gravity conditions. It should however be noted that this is only strictly true if there exists a nearly stable arch zone whose size is proportional to the radius of the orifice and above which the particles are almost stationary. However, with Eq. 7-5 exponents greater than 2.5 have been consistently obtained from experimental results, particularly with larger particle diameters (e.g. Beverloo et al., 1961). This has been attributed to the possible existence of an 'empty annulus' in the outlet with its size taken to be proportional to the particle diameter and dependent on particle shape and the hopper slope. The parameter k_B is often used as the proportionality constant. Consequently, for circular outlet openings and noncohesive coarse-grained bulk solids Beverloo et al. (1961) modified Eq. 7-5 to state that the rate of mass discharge W is given by Eq. 7-6:

$$W = C\rho_b \sqrt{g} \left(D_0 - k_B d_p\right)^{5/2} \qquad \text{Eq. 7-6}$$

The constants C and k_B are essentially fitting parameters and this makes the Beverloo law a semi-empirical relationship as they have to be determined experimentally for every given material and container properties. With different bulk solids Beverloo et al. (1961) found a range of C as 0.55-0.65 and of k_B as 1.3-2.9; averaging about 0.583 and 1.5 for spherical solids. The values of 0.65 and 2.9 were associated with sand. The parameter k_B is generally taken to be between 1 and 3.

The meaning of the parameter k_B however remains unresolved. As already mentioned, Beverloo et al. (1961) assumed that "along the margin of the orifice a zone is useless or less fit for use for the flow". This zone was taken to be proportional to the particle diameter. Brown & Richards (1970) then gave probably the most and widely quoted interpretation. They argued that the centres of the particles cannot approach the edge of

the orifice through a distance $k_B d_p / 2$. According to Zhang & Rudolph (1991) however the only plausible value of k_B is 1.0 and instead a factor dependent on the orifice diameter and representing the effect of shear friction between flowing and nonflowing particles at the edges of the orifice is needed. Mankoc et al. (2007) have concurred with Zhang & Rudolph (1991) that indeed a value of $k_B = 1.0$ should be used but with another term which is a function of D_0 / d_p replacing the frictional coefficient. The robustness of these modifications to, and the Beverloo law itself are however yet to be examined for mass flow over a wide range of $R^* = D_0 / d_p$ values and material with nonspherical particles having a range of different sizes. The following paragraphs of this section thus assess the suitability of the Beverloo et al. (1961), Zhang & Rudolph (1991), and Mankoc et al. (2007) in predicting the mass flow rate of spherical glass beads (GBS1) and nonspherical Leighton Buzzard sand (LBS1) over a range of R^* values from about 9 to 236.

In Table 7-8, a comparison is made of the observed (W_{obs}) and calculated (W_{calc}) mass flow rates of dry GBS1. The corresponding comparison for dry LBS1 is made in Table 7-9. The calculated flow rates were obtained using C and k_B values proposed in the authors' original work. It is observed that for GBS1 the Beverloo et al. (1961) equation's original 90% accuracy is obtained within only a section of the range of R^* values they considered. Outside this range the equation progressively becomes unsuitable. The results show that the coefficients in the Beverloo law are indeed fitting parameters and ought to be determined experimentally for each type of material and container properties. Otherwise, grossly misleading results can be obtained, in this case in the neighbourhood of $\mathrm{R}^* = 10$.

Table 7-8: Comparison between measured and calculated gravity discharge rates

Author	Material properties	D_o (cm)	R^* (-)	W_{obs} (g/s)	W_{calc} (g/s)	$W_{(err)}$ (%)[a]
Beverloo et al. (1961)	Glass beads (GBS1)					
	d_p (cm) = 0.0354 ρ_s (g/cm^3) = 2.5 ρ_b (gcm^{-3}) = 1.603 ϕ (deg) = 26.8	0.370	10.5	1.101	1.654	-50.2
		0.600	16.9	4.780	6.473	-35.4
		0.800	22.6	14.499	14.108	+2.7
		1.016	28.7	24.538	26.624	-8.5
		1.450	41.0	64.457	67.489	-4.7
		1.831	51.7	134.936	123.335	+8.6
		3.188	90.1	586.420	509.187	+13.2
		5.40	152.5	2375.036	1934.522	+18.5
Zhang & Rudolph (1991)	Glass beads (GBS1)					
	d_p (cm) = 0.0354 ρ_s (g/cm^3) = 2.5 ρ_b (gcm^{-3}) = 1.603 ϕ (deg) = 26.8	0.370	10.5	1.101	0.990	+10.1
		0.600	16.9	4.780	4.137	+13.5
		0.800	22.6	14.499	9.625	+33.6
		1.016	28.7	24.538	19.400	+20.9
		1.450	41.0	64.457	55.145	+14.4
		1.831	51.7	134.936	109.618	+18.8
		3.188	90.1	586.420	488.309	+16.7
		5.40	152.5	2375.036	1844.444	+22.3
Mankoc et al. (2007)	Glass beads (GBS1)					
	d_p (cm) = 0.0354 ρ_s (g/cm^3) = 2.5 ρ_b (gcm^{-3}) = 1.603 ϕ (deg) = 26.8	0.370	10.5	1.101	1.262	-14.6
		0.600	16.9	4.780	5.255	-9.9
		0.800	22.6	14.499	12.015	+17.1
		1.016	28.7	24.538	23.572	+3.9
		1.450	41.0	64.457	62.716	+2.7
		1.831	51.7	134.936	117.197	+13.1
		3.188	90.1	586.420	494.769	+15.6
		5.400	152.5	2375.036	1878.442	+20.9

[a] $W_{(err)} = \dfrac{(W_{obs} - W_{calc})}{W_{obs}} \times 100$

Table 7-9: Comparison between measured and calculated gravity discharge rates

Author	Material properties	D_o (cm)	R^* (-)	W_{obs} (g/s)	W_{calc} (g/s)	$W_{(err)}$ (%)
Beverloo et al. (1961)	Leighton Buzzard sand (LBS1)					
	d_p (cm) = 0.0418 ρ_s (g/cm^3) = 2.67 ρ_b (gcm^{-3}) = 1.638 ϕ (deg) = 33.0 ϕ_w (deg) = 18.0	0.370	8.9	-	1.025	-
		0.600	14.4	3.178	5.265	-65.7
		0.800	19.1	9.350	12.600	-34.8
		1.016	24.3	16.888	25.139	-48.9
		1.450	34.7	47.194	67.561	-43.2
		1.831	43.8	87.371	123.573	-41.4
		3.188	76.3	446.768	546.725	-22.4
		5.40	129.2	1789.001	2125.183	-18.8
		9.85	235.6	7725.152	9799.601	-26.9
Zhang & Rudolph (1991)	Leighton Buzzard sand					
	d_p (cm) = 0.0418 ρ_s (g/cm^3) = 2.67 ρ_b (gcm^{-3}) = 1.638 ϕ (deg) = 33.0 ϕ_w (deg) = 18.0	0.370	8.9	-	1.308	-
		0.600	14.4	3.178	5.179	-63.0
		0.800	19.1	9.350	11.574	-23.8
		1.016	24.3	16.888	22.509	-33.3
		1.450	34.7	47.194	60.608	-28.4
		1.831	43.8	87.371	116.389	-33.2
		3.188	76.3	446.768	528.483	-18.3
		5.40	129.2	1789.001	2000.380	-11.8
		9.85	235.6	7725.152	9068.561	-17.4
Mankoc et al. (2007)	Leighton Buzzard sand					
	d_p (cm) = 0.0418 ρ_s (g/cm^3) = 2.67 ρ_b (gcm^{-3}) = 1.638 ϕ (deg) = 33.0 ϕ_w (deg) = 18.0	0.370	8.9	-	1.235	-
		0.600	14.4	3.178	5.235	-64.7
		0.800	19.1	9.350	12.081	-29.2
		1.016	24.3	16.888	23.904	-41.5
		1.450	34.7	47.194	64.486	-36.6
		1.831	43.8	87.371	121.641	-39.2
		3.188	76.3	446.768	522.863	-17.0
		5.40	129.2	1789.001	1999.189	-11.7
		9.85	235.6	7725.152	9069.703	-17.4

The use of parameter $k_B > 1.0$ to account for the possible existence of the "empty annulus" in the outlet for all values of R^* and all flow patterns remains unresolved. In the studies where it has been found to be applicable the value of R^* has been small and within a narrow range and it seems only spherical particles have been used. In doing so both flat-bottomed cylinders (e.g. Hirshfled et al., 1997; Hirshfled & Rapaport, 2001) and hopper silos have been used (e.g. Datta et al., 2008). Whereas the effect of the so-called empty annulus may be significant at low values of R^* its significance at high values of R^* is unresolved. Following the recommendation by Zhang & Rudolph (1991) that the only plausible value of k_B is 1.0 Mankoc et al. (2007) using flat-bottomed cylinder experimentally demonstrated that values of $k_B > 1.0$ underestimates the flow rate for very large R^*. In fact k_B simply shifts the fit along the horizontal axis. The logarithmic scale, however, causes the shift to appear as a rotation about the upper part of the curve. The results of flow rate of GBS1 in Table 7-8 and Fig 7.8 (curve 1) are in agreement with this observation. The flow rate is progressively underestimated for $\mathrm{R}^* > 60$. For $20 \le \mathrm{R}^* \le 60$ the flow rate agrees well with the Beverloo law. The law then overestimates the flow rate for $\mathrm{R}^* < 20$. Similar observation has been made by Mankoc et al. (2007) who also observed a switch over from overestimation to underestimation of flow rate as the value of R^* was increased passed the window $10 < \mathrm{R}^* < 20$ with $k_B = 1.16$ instead of $k_B = 1.5$ often used with the Beverloo law. A close look at the Hirshfled & Rapaport (2001) results also reveals that the Beverloo law overestimates flow for $R^* < 13$ and underestimate it for $R^* > 13$. It should be noted that in their numerical simulations Hirshfled & Rapaport (2001) used $k_B = 2.6$. Larger values of k_B serve to shift the neatly fitted part of the curve to the left (toward smaller values of R^*) and vice versa.

Whereas the results of GBS1 agree with the previous findings, those of LBS1 do not. As shown in Table 7-9 and Fig. 7.8, using the typical fitting parameters the Beverloo law overestimated the flow rate for all values of R^* considered. As shown graphically in Fig. 7.8a, the overestimation reduces nonlinearly with increase in the R^* value suggesting the need for checking both the scaling parameter k_B and the discharge rate coefficient C proposed for sand by Beverloo et al. (1961). However, the value of $k_B = 3$ obtained from experimental data (Fig. 7.8b) for both sand and glass beads indicate that use of $k_B = 2.9$ for sand could be justified provided that a suitable value of

C is used. The value of C is evidently dependent on the material and density as expected. It should be recalled that the bulk density of glass beads was lower than that of sand and that the former was smoother that the latter. Therefore a lower value of C is not surprising. What is surprising, however, is the value of $k_B = 3$ for glass beads. It is believed to be about 1.5. This value was found to work for only a limited range of R^*, from about 20 to 60. Moreover, when both GBS1 and LBS1 were fitted together different fitting parameters were obtained, as shown in Fig. 7.8c. It appears therefore that once a wide range of R^* is considered $k_B = 1.5$ is no longer valid and that for such ranges only one value of $k_B = 2.9$ is valid.

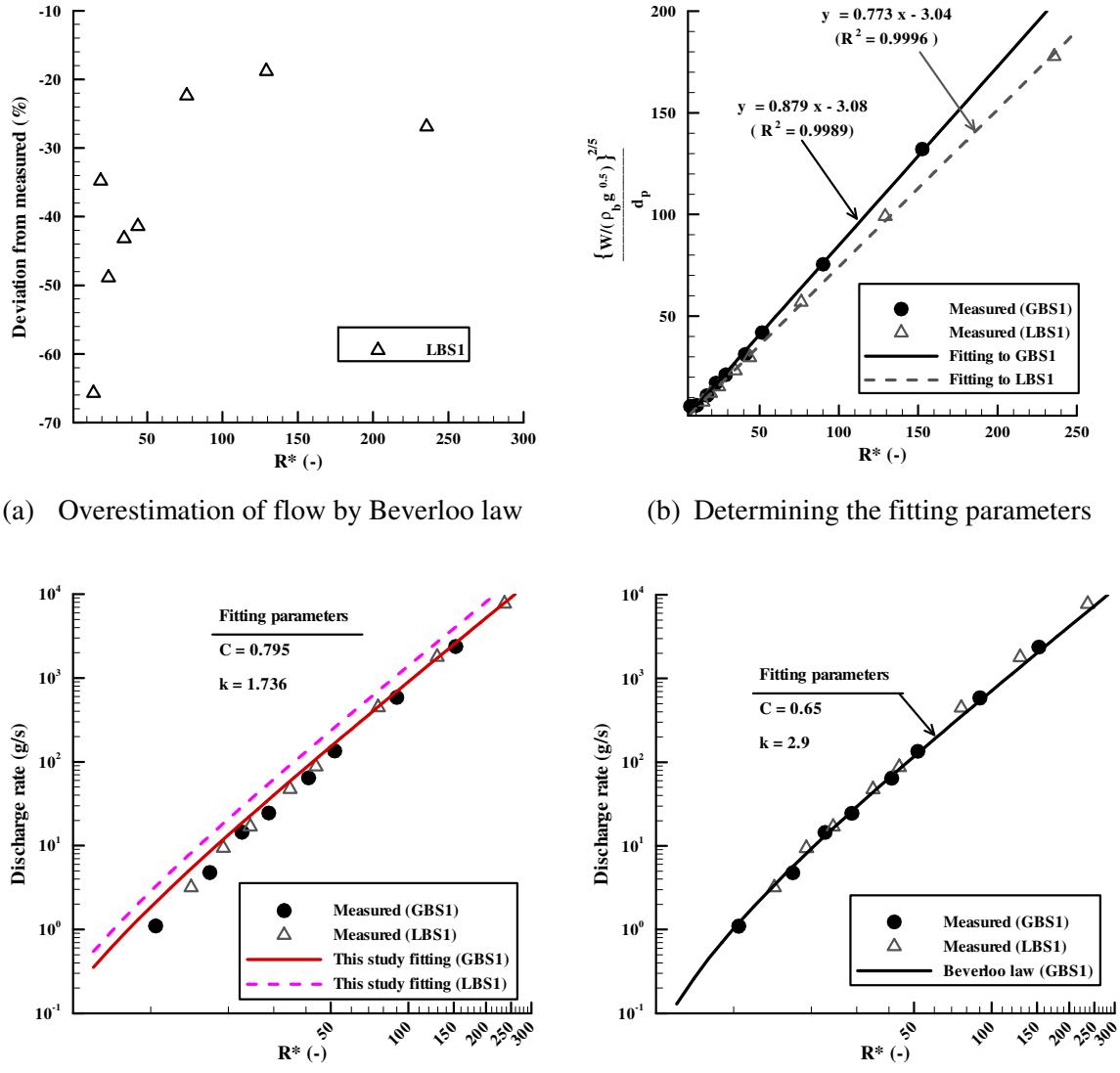

(a) Overestimation of flow by Beverloo law

(b) Determining the fitting parameters

(c) Fitting to individual material

(d) Fitting to all materials

Figure 7.8: Comparison of the observed and predicted flow rates in the silo model tests

In Fig. 7.8c, the experimental results were also fitted using the fitting parameters $C = 0.795$ and $k_B = 1.736$ obtained as the average fitting to both GBS1 and LBS1 together. Clearly with these parameters the experimental results are grossly overestimated especially for LBS1. However, the slopes of the fitted curves in Fig. 7.8c suggest that the value of C is overestimated while that of k_B is underestimated. The remarkably evident difference between the fitting curves for the two materials whose experimental data plot to more or less the same "family" seems to add credence to the argument that bulk density is indeed not an appropriate parameter for use with the Beverloo law. In this study the bulk density of GBS1 was lower than that of LBS1. It was thus decided to carry out nonlinear curve fitting procedures to the experimental data of GBS1. Finally as shown in Fig. 7.8d, the Beverloo et al. (1961) proposed fitting parameters for sand were found to give a satisfactory fitting. These results further affirm the validity of the Beverloo law even over a wide range of R^* independent of the particle shape. In fact what is never explicitly said is that the value of $k_B = 2.9$ for sand is because Beverloo et al. (1961) investigated a wide range of R^* for sand than the other materials that gave $k_B = 1.5$ value. The question therefore is whether or not the later modifications of the Beverloo law offer better results. This is addressed next.

According to Zhang & Rudolph (1991) $k_B = 1.0$ should be used with another factor C_τ introduced to account for the effect of material shear resistance. The role of C_τ as given by Eq. 7-7 is to essentially reduce the flow rate for $R^* < 64$; for larger values of R^* it has no effect on flow rate and is equal to 1.0. In the equation, β is the slide angle between the flowing and nonflowing particles and is given by $\beta = 45 + \phi/2$ in which ϕ is the angle of internal friction of the material. As can be seen in Table 7-8, the Zhang & Rudolph's equation underestimates flow rate of glass beads with the deviation averaging to about 19% of the measured flow rate. These results which are shown graphically in Fig. 7.9a suggest that use the internal angle of friction to estimate C_τ for mass flow may be inappropriate. It is most likely that the parameter is overestimated as the wall friction is less than the internal angle of friction in the current study. However for Leighton Buzzard sand the flow rate is consistently overestimated, ideally in the same way they are by the Beverloo law. This may be because the parameter C_τ is underestimated for nonspherical particles. It seems Eq. 7-7 is yet to be validated for nonspherical particles with a wide range of hopper materials.

$$C_\tau = \left(\frac{3}{2} - \frac{2}{\tan\beta}\right) + \left(\frac{2}{\tan\beta} - \frac{1}{2}\right)\frac{D_o/d_p}{(D_o/d_p)_{\min}}; \quad R^* < 64 \qquad \text{Eq. 7-7a}$$

$$C_\tau = 1.0 \qquad ; \quad R^* \geq 64 \qquad \text{Eq. 7-7b}$$

It can be argued that using Eq. 7-7 to estimate C_τ for purposes of assessing its validity is not doing justice to Zhang & Rudolph (1991). In their work Zhang & Rudolph stressed that for better estimates the parameter should be determined experimentally. However, if the problem lies with the use of inaccurate C_τ then this can be seen from the predictions for values of R^* for which it is equal to 1.0. From Tables 7-8&7-9 and Fig. 7.9, however, the performance of the Zhang & Rudolph equation seems independent of the value of R^* considered suggesting that whether or not the parameter C_τ is experimentally obtained the predicted flow rate over a wide range of R^* will more or less remain comparable to the one obtained by the Beverloo law.

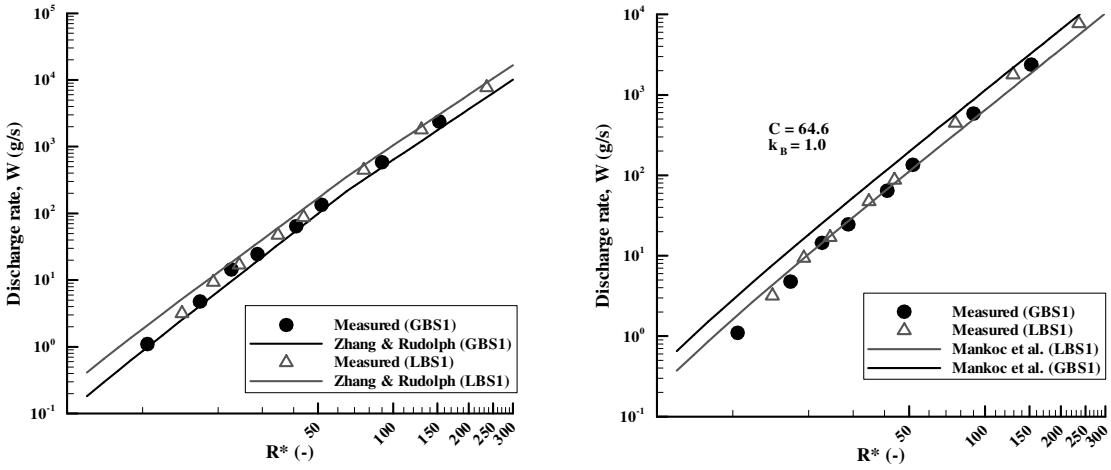

(a) Zhang & Rudolph fit to GBS1 & LBS1 (b) Mankoc et al. fit to GBS1 & LBS1

Figure 7.9: Comparison of the observed and predicted flow rates in the silo model tests

Compared to the Beverloo law, Mankoc et al. (2007) equation was not found to offer a better alternative to the former. In fact the two equations gave almost similar predictions for both glass beads and Leighton Buzzard sand (Tables 7-8&7-9). The graphical representation of the results is shown in Fig. 7.9b. These results suggest that the effect of the two fitting parameters is a coupled one in the sense that several combinations may be used to give essentially the same results. In such a situation the option with few parameters would be preferred as the price of using many parameter equations is increased complexity and hence computational efforts. It was therefore not considered

necessary to attempt to re-evaluate the parameter in the Zhang & Rudolph (1991) and Mankoc et al. (2007) equations.

7.5 Concluding Remarks

The influence of matric suction and water content on the flowability of glass beads (GBS1) and Leighton Buzzard Sand (LBS1) was studied in this part of the thesis using a silo model designed for mass flow. The dependence of flowability of the tested sand on the water content is particularly captured with zones of flowability identified in the space of water content versus the outlet diameter normalised by the equivalent mean spherical particle diameter. The unconfined yield strength derived from the tensile strength of the material has been found to be promising in predicting the minimum outlet diameters for which the wet material will flow. Besides the wet unsaturated flowability, discharge rate of the two test materials in their oven dry state have been studied with a view of examining the robustness of the most popular and most recent predictive equations. The observed flow behaviour has been explained using the data obtained from other tests notably the pressure plate, filter paper and the unsaturated triaxial compression tests.

CHAPTER EIGHT

8 CONCLUSIONS AND OUTLOOK FOR FUTURE WORK

8.1 Conclusions

The present research project was conducted in order to improve the understanding of the hydro-mechanical behaviour of granular materials. Laboratory tests were conducted on both spherical glass beads and nonspherical Leighton Buzzard sand in two distinct size ranges each. Water retention, shear and flow behaviour were investigated with particular emphasis on how the particle-water interaction through the liquid bridges alone influence the bulk hydro-mechanical behaviour and how this influence depends on the constituent particle properties. Water retention curves were measured using both pressure plate apparatus and the filter paper technique. The shear behaviour on the other hand was investigated using both conventional and the advanced unsaturated triaxial apparatuses with suction controlled using the axis translation technique while silo model tests were run to measure the flowability of the test materials at different moisture contents and hence matric suctions. The major conclusions drawn from the study are described below according to the different topics of investigations, namely, the water retention behaviour, shear behaviour and the flow behaviour.

8.1.1 Water retention behaviour

- Particle-water interaction through the liquid bridges alone can produce the hysteretic behaviour which affects the bulk hydro-mechanical response of the material. The features of water retention curve often observed for soils were well captured with simpler spherical glass beads.
- Particle size was found to highly influence the water retention capacity of both spherical glass beads and the nonspherical Leighton Buzzard sand. Reducing the particle size increased the material air-entry value, residual matric suction, and the water-entry value and their corresponding water contents, and also the primary wetting maximum water content.
- The hysteresis of water retention curve (WRC) with suction expressed in terms of matric suction is a function of suction and hence water content. The hysteresis of the tested granular materials reduced as water content decreased following an increase in matric suction. The drying and wetting paths of the curve tended to converge at about 20kPa matric suction suggesting a unique relationship

between water content and matric suction regardless of whether the sample is drying or wetting.

- The initial void ratio affects the WRC in the saturated capillary and funicular bridges zones with no effect in the residual zone where the water is localised at the inter-particle contacts. Increasing the initial void ratio of the tested granular materials resulted in reduced water storage capacity as the curve plotted to the left and above the lower initial void ratio sample.
- The water retention behaviour of noncohesive granular materials is not affected by drying and wetting cycles. Further drying and wetting cycles did not alter the WRCs as is often observed in clayey soils suggesting that factors other than the particle-water interaction are responsible for the alteration of the WRCs of clayey soils up on subsequent drying and wetting cycles.
- The granular material particle shape effect on the material's water retention behaviour depends on the hydraulic path and amount of water present in the material. Particle shape was found to affect the water retention behaviour but only in the residual zone of the drying path and the entire wetting path. Ahead of the residual zone of the drying path, the measured points of the nonspherical Leighton Buzzard sand plotted within the scatter of the points of glass beads with the same particle size range and same mean particle size and well below the entire wetting path. The deviation in results was adequately explained by the shape factor and a method has been proposed for this purpose.
- Although the popular van Genuchten (1980) equation performed better than the Fredlund & Xing (1994) equation in describing the hysteretic WRCs both fell short of satisfactorily describing the curves of the spherical glass beads in the residual zone.
- Using the van Genuchten (1980) equation it has been shown that the water retention curves can be reliably estimated from the basic index material parameters without having to undertake the WRC experimental programme. In particular, the following strong correlations were found between the listed parameters: $R^2 = 0.998$ between α_{vG} and D_{60}; $R^2 = 0.982$ between α_{vG} and ψ_a; $R^2 = 0.762$ between n and D_{10}; $R^2 = 0.969$ between ψ_r and D_{10}.

8.1.2 Shear behaviour

- Shear strength increases nonlinearly with matric suction. As matric suction was increased, the shear strength of the tested glass beads increased at a decreasing

rate with a tendency to reach a maximum value. This finding supports the argument that matric suction alone cannot account for the observed increase in shear strength within the residual zone.

- Shear strength increases linearly with net normal stress. Following an increase in the applied net normal stress, shear strength was found to increase proportionately independent of the imposed matric suction suggesting that the internal angle of friction is independent of suction.
- The water induced structure does not affect the shear behaviour of noncohesive granular materials. Preparing samples with different water content did not affect the shear behaviour of the tested glass beads suggesting that factors other than the water bridge induced structure are responsible for the discrepancy in shear behaviour often observed in samples of soil prepared with different water content.

8.1.3 Flow behaviour

- The flowability of dry glass beads and Leighton buzzard sand over a wide range of hopper outlet to mean particle diameter ratio (R^*) was found to follow the Beverloo law with the value of $k_B = 2.9$ applying to both sand and the glass beads. This result suggests that the various values of k_B often reported in the literature depends on the range of R_B and that provided a wide enough range is considered a single value of k_B applies to all the materials. The best fitting was obtained with density lower than the filling density for sand implying that it the emptying density instead of filling density that is a suitable parameter.
- The presence of moisture within the range of 0.5% to 8.0% by dry weight was found to have a significant effect on the flowability of glass beads and Leighton Buzzard sand depending on the size of the outlet relative to mean particle size. This effect was reflected in the formation of stable arch essentially preventing material from flowing.
- A criterion was suggested for predicting the flowability of wet granular materials in form of a wet flowability curve defining flow or no flow zones in the space of water ratio versus R^*. Combinations of water content and R^* left of the curve result in the formation of a stable arch while those at the right give rise to sudden flow.

- The unconfined yield strength derived from the tensile strength using the Mohr-Coulomb concept has been shown to be a promising parameter to estimate the minimum hopper outlet diameters for which no stable liquid bridge induced arch can form, in the same way it is done for cohesive materials.

8.2 Recommendations for Further Research

Whereas the current research project managed to achieve its objectives a number of pertinent issues came up in the course of the study that this study on its own or in conjunction with the existing knowledge in the literature could not provide an explanation. These are hereby recommended for further study as described in the following subsections as per the subject area of investigation.

8.2.1 Water retention behaviour

- It had been anticipated that it would be possible to come up with correlations between the various water retention characteristics and the mean particle size of the material. As it turned out, however, only the air-entry value appeared to be strongly correlated to the mean particle diameter. It was not clear as to whether or not few experimental data were responsible for the apparent lack of correlation between the mean particle size and the other water retention characteristics. It is therefore recommended that this work is extended in form of further experimental work on various other materials with particle size as the only variable to be able to reach a definite conclusion.
- The effect of initial void ratio was investigated for only the drying path and so it is not clear how the wetting path would be affected by the same. It is thus recommended that the study is extended to investigate the effect of initial void ratio on the wetting path of the retention curve.
- The study results have shown that the particle shape factor can be used in estimating the WRC of nonspherical materials provided that the curve for the spherical particle material with similar particle size range and mean size has been measured. This was, however, not applied to many independently measure WRCs and so further experimental work will help validate the hypothesis.
- The most popular mathematical equations of van Genuchten (1980) and Fredlund & Xing (1994) for describing the WRCs were found to fall short of giving a satisfactory description of the WRCs of spherical glass beads in the residual zone. For use in industrial bulk solids application it is the residual zone

that is most relevant as the solids' moisture content is predominantly low so an appropriate equation would be required. This can be obtained through an extensive study which this thesis recommends.

- In order to demonstrate the reliability of the basic index material parameters in estimating the WRC without having to undertake a time consuming and costly experimental programme, it is necessary to demonstrate the reliability of the proposed correlations over a wide range of materials. This can be achieved through an experimental investigation, similar to the one described in this thesis on, materials with well defined particle properties. This is recommended by this study.

8.2.2 Shear behaviour

- This study was unable to offer a conclusive explanation for the observed effect of particle size on the shear behaviour. Whereas it was expected that the unsaturated sample with small particles would give stronger mechanical response than a sample with larger particles of the same material type, it turned out to be the reverse. Whether the observed behaviour is characteristic to the tested glass beads can only be confirmed by undertaking further experimental work. This is recommended by this study.
- The shear behaviour after sample failure was found to be partly dependent on the mode of failure which varied from mild barrelling to barrelling and rotation. It therefore became meaningless to attempt to evaluate the critical state behaviour. Such an evaluation calls for strictly ensuring that all samples fail in the same way. As such, a recommendation is made accordingly.

8.2.3 Flow behaviour

- The flowability curve of the wet granular materials has been shown to be nonlinear with the range of water content from 0.5% to 8.0% by dry weight. Whereas based on the measurement near complete saturation it is possible to extend the measured curve, it would make much sense to have the curve experimentally measured. It is therefore recommended for further study.
- The flowability of the wet material exposed to the atmosphere was seen to depend on the time of exposure. It was, however, not possible as part of the current study to characterise the material flowability according to the time of exposure. This is thus one of the items that can be pursued further.

- This study finally recommends a numerical analysis of the wet flowability of granular materials.

APPENDICES

APPENDICES

APPENDIX A-1: Properties of the Epoxy Resin

Table A- 1: Properties of epoxy resin

Physical properties of the uncured product	
Colour	Clear
Viscosity (cps)	9,000
Functional cure time at $25^{o}C$ $(\min)$	45
Full bond strength time $(hours)$	16
Specific volume (m^3/kg)	833
Percentage solids by volume $(\%)$	100
Performance characteristics when cured for 7days at $24^{o}C$	
ASTM D1002 Adhesive tensile shear strength (N/mm^2)	9.7
Operating temperature, dry (^{o}C)	-40 – 93
ASTM D792 Cured density (g/cm^3)	1.10
ASTM D2240 Cured hardness (D)	85
ASTM D149 Dielectric strength $(volts/mil)$	490
Chemical resistance (7days room temperature cure; 30days immersion at $24^{o}C$	
Kerosene	Very good
Hydrochloric acid and 10% Sulphuric acid	Very good
Chlorinated solvent and Methanol	Fair
Toluene and Ammonia	Very good
10% Sodium Hydroxide	Very good

Source: *ITW DEVCON Ltd*

APPENDIX A-2: Calibration of the Different Triaxial Equipment Components

A-2.1 Water Pressure Transducers

The water pressure transducers (pore water pressure and the cell pressure) were calibrated against the calibrated GDS pressure unit. They were connected in series and calibrated all at once (in one setting). This section describes how the calibration was carried out. The calibration data are also presented. The procedure involved sufficiently saturating the water conduits between the transducers and the GDS unit, setting up the calibration window (Fig. A. 1a) in the software and then pressurising the water line to which the transducer is connected at prescribed intervals. The calibration window displayed the voltage values for the respective data logger channels to which the transducers were connected. The GDS pressure (kPa) readings were then recorded against the corresponding voltage readings into the calibration window of the software and saved to the calibration file.

The GDS pressure was applied in increments of about 100kPa to about 95% full capacity of the transducers and was applied for four cycles to assess the repeatability and the hysteresis. For each increment the digital readings of the GDS were recorded against the corresponding voltage reading of the transducer. Finally the digital readings of the measurements of pressure (kPa) were plotted against the digital (voltage) readings of the transducer and the linear regression line drawn (Fig. A. 1b). The calibration factor was determined as the slope of the linear regression. As can be observed from Fig. A.1b, the measurements of pressure changes are highly reproducible and reliable. Fig. A.1b shows, as an example, the regression line for the pore water pressure transducer whose data was stored in the system for use by the TRIAX programme to convert the voltage readings to physical values.

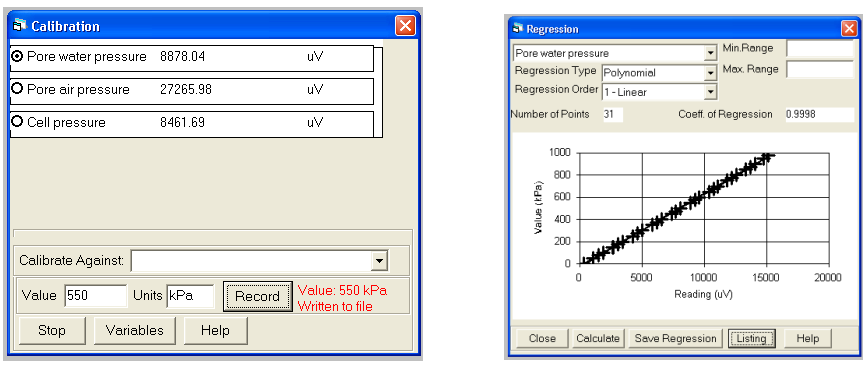

(a): Calibration window (b): Regression window

Figure A. 1: Calibration of the water pressure transducer

A-2.2 Pore Air Pressure Transducer

Like the water pressure transducers, pore air pressure transducer was also calibrated against the GDS pressure unit. The calibration system set up and the pressurisation procedure were exactly as for the water pressure transducers except that instead of conduit between the transducer and the GDS being filled with water it was filled with air from the compressor supplied through a regulator. The calibration window is shown in Fig. A. 1a, together with water pressure transducers. Fig. A.2 shows the calibration data (regression line) which was stored in the calibration directory for future use by the programme to convert the voltage readings into pore air pressure values.

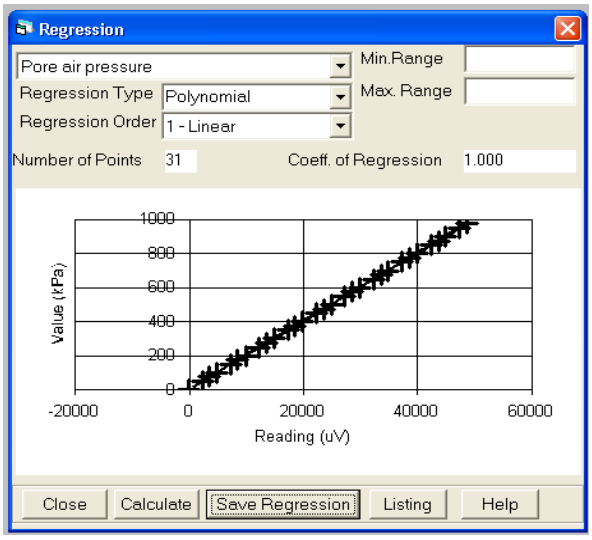

Figure A. 2: Calibration data for pore air pressure transducer

A-2.3 Load Cell Transducer

The load cell transducer calibration involved loading it with dead loads and measuring the corresponding voltage changes (Fig. A.3a). The dead loads were applied up to 50% of the maximum working capacity of the transducer, which is 5kN. The transducer over load value is 7.5kN. Three cycles of loading and unloading were applied before the actual calibration to minimise the hysteresis. Fig. A.3b shows the calibration data (regression line) which was stored in the calibration directory for future use by the programme to convert the voltage readings into the axial load values.

(a): Dead load application

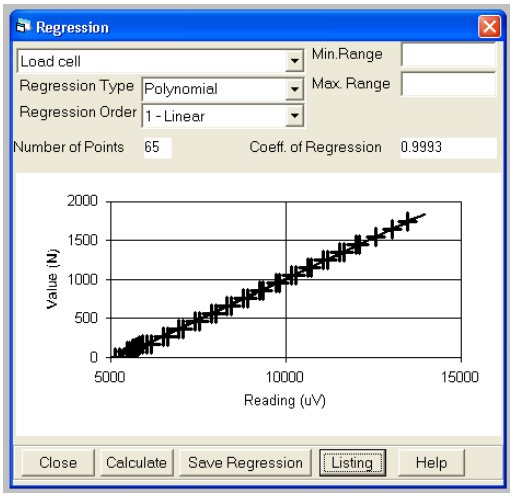

(b): Regression window

Figure A. 3: Calibration of the load cell

A-2.4 Linear Potentiometric Displacement Transducer

The linear potentiometric displacement transducer used to measure the axial displacement of the test specimen was calibrated using the micrometer calibration unit. Fig. A.4 shows the calibration window and data for the transducer.

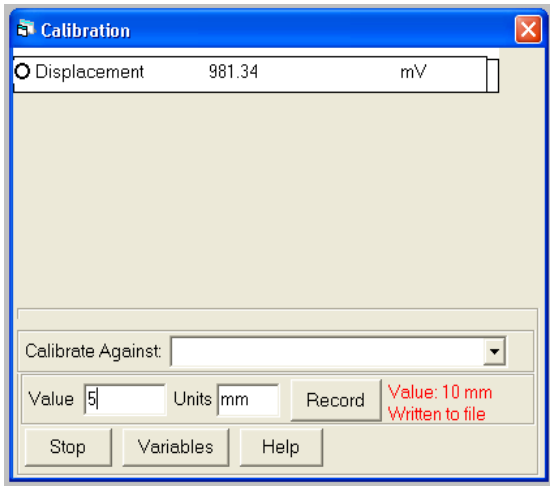

(a): Calibration window

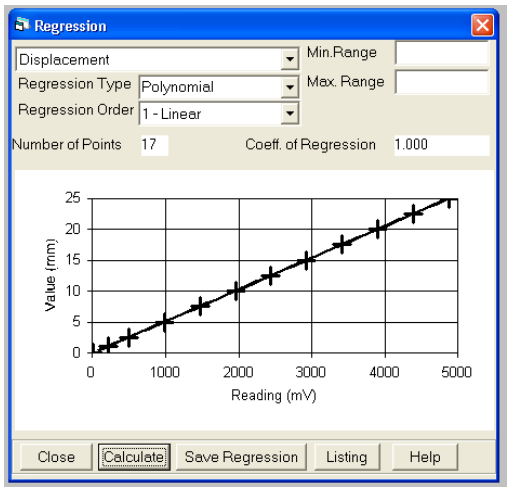

(b): Regression window

Figure A. 4: Calibration of the linear potentiometric displacement transducer

References

Aitchison G.D., 1961, *Relationships of moisture stress and effective stress functions in unsaturated soils*, Pore Pressure and Suction in Soils, Butterworths, London, 47-52

Alonso E.E., Gens A., Josa A., 1990, *A constitutive model for partially saturated soils*, Geotechnique, **40(3)**, 405-430

Alonso E.E., Gens A., Might D.W., 1987, *Special problem soils: General report*, Proceedings of 9th European Conference on Soil Mechanics and Foundation Engineering, Dublin, **3**, 1087-1146

Anh H., Basaranoglu Z., Yilmaz M., Bugutekin A., Gul M.Z., 2008, *Experimental investigation of granular flow through an orifice*, Powder Technology, **186**, 65-71

Arya L.M., Paris J.F., 1981, *A physicoempirical model to predict the soil moisture characteristic from particle-size distribution and bulk density data*, Soil Science Society of America Journal, **45(6)**, 1023-1030

Aubertin M., Mbonimpa M., Bussiere B., Chapuis R.P., 2003, *A model to predict the water retention curve from basic geotechnical properties*, Canadian Geotechnical Journal, **40(6)**, 1104-1122

Baldi G., Nova R., 1984, *Membrane penetration effects in triaxial testing*, Journal of Geotechnical Engineering, **110(3)**, 403-420

Barbour S.L., 1998, *Nineteenth Canadian Geotechnical Colloquium: The soil-water characteristic curve: a historical perspective*, Canadian Geotechnical Journal, **35(5)**, 873-894

Beverloo W.A., Leniger H.A., van de Velde J., 1961, *The flow of granular solids through orifices*, Chemical Engineering Science, **15**, 260-269

Biglari M., Shafiee A., Asheyeri I., 2008, *Determination of soil suction state surface*, Toll et al. (Eds), Unsaturated Soils: Advances in Geo-Engineering, Taylor and Francis Group, London, 235-242

Bilgari M., Shafiee A., Ashayeri I., 2008, *Determination of soil suction state surface in pure and composite clays by filter paper method*, Toll et al. (Eds), Unsaturated Soils: Advances in Geo-Engineering, Taylor and Francis Group, London, 235-242.

Bishop A.W., 1959, *The principle of effective stress*, Teknisk Ukeblad, **106(39)**, 859-863

Bishop A.W., Blight G.E., 1963, *Some aspects of effective stress in saturated and partly saturated soils*, Geotechnique, **13(3)**, 177-197

Bishop A., Donald I., 1961, *The experimental study of partly saturated soil in the triaxial apparatus*, 5th International Conference on Soil Mechanics and Foundation Engineering, Paris, 13-21

Blatz J.A., Cui Y., Oldecop L., 2008, *Vapour equilibrium and osmotic technique for suction control*, Journal of Geotechnical and Geological Engineering, Springer, 661-673

Bransby P.L., Blair-Fish P.M., 1975, *Initial deformations during mass flow from a bunker: Observation and idealizations*, Powder Technology, **11**, 273-288

British Standard, 1990, *Methods of tests for soils for civil engineering purposes*, British Standard Institution, London, UK

Brooks R.H., Corey A.T., 1964, *Hydraulic properties of porous medial*, Hydrology Paper 3, Colorado State University

Bulut R., Leong E.C., 2008, *Indirect measurement of suction*, Journal of Geotechnical and Geological Engineering, Springer, **26(6)**, 633-644

Burland J.B., Ridley A.M., 1996, *The importance of suction in soil mechanics*, Keynote address, Proceedings of 12th Southeast Asian Geotechnical Conference, **2**, 27-49

Carrier W.D., 2003, *Goodbye, Hazen; Hello, Kozeny-Carman*, Journal of Geotechnical and Geoenvironmental Engineering, ASCE, **129(11)**, 1054-1056

Chandler R.J., Crilly M.S., Montgomery-Smith, G., 1992, *A low-cost method of assessing clay desiccation for low rise buildings*, Proc. Institution of Civil Engineers and Civil Engineering, **92**, 82-89

Chandler R.J., Gutierez C.I., 1986, *The filter paper method of suction measurement*, Geotechnique, **36(2)**, 265-268

Chapuis R.P., Aubertin P.-P., 2003, *Predicting the coefficient of permeability of soils using the Kozeny-Carman equation*, EPM-RT-2003-03, Department CGM, Ecole Polytechnique de Montreal

Chapuis R.P., Legare P.-P., 1992, *A simple method for determining the surface area of fine aggregates and fillers in bituminous mixtures*, ASTM STP 1147, R.C. Meininger, Ed., ASTM, Philadelphia, 177-186

Chen J.F., Rotter J.M., Ooi J.Y., Zhong Z., 2005, *Flow pattern in a full scale silo containing iron ore*, Chemical Engineering Science, Elsevier, **60**, 3029-3041

Chen J.F., Rotter J.M., Ooi J.Y., Zhong Z., 2007, *Correlation between the flow pattern and wall pressures in a full scale experimental silo*, Engineering Structures, Elsevier, **29**, 2308-2320

Childs E.C., 1940, *The use of soil moisture characteristics in soil studies*, Journal of Soil Science, **50**, 239-252

Chin K.B., Leong E.C., Rahardjo H., 2010, *A simplified method to estimate the soil-water characteristic curve*, Canadian Geotechnical Journal, **47(12)**, 1382-1400

Clayton C.R.I., Xu M., Bloodworth A., 2006, *A laboratory study of the development of earth pressure behind integral bridge abutments*, Geotechnique, **56(8)**, 561-571

Cleary P.W., Sawley M.L., 2002, *DEM modelling of industrial granular flows: 3D case studies and the effect of particle shape on hopper discharge*, Applied Mathematics Modeling, **26**, 89-111

Cleaver J.A.S., Nedderman R.M., 1993, *The measurement of velocity distributions in conical hoppers*, Chemical Engineering Science, **48**, 3703

Coleman, J.D., 1962, *Stress/strain relations for partly saturated soils*, Geotechnique, **12(4)**, 348-350

Croney, D., Coleman, J.D., Black W.P.M., 1958, *Movement and distribution of water in soil in relation to highway design and performance*, Water and its conduction in soils, High Research Board, Special Report No. 40, 226-252

Cui, Y.J., Delage, P., 1996, *Yielding and plastic behaviour of an unsaturated compacted silt*, Geotechnique, **46(2)**, 291-311

Cunningham, M.R., 2000, *The mechanical behaviour of a reconstituted unsaturated soil*, PhD Thesis, Imperial College, University of London, London

Cutress J.O., Pulfer R.F., 1967, *X-ray investigations of flowing powders*, Powder Technology, **1**, 213-220.

Datta A., Mishra B.K., Das S.P., Sahu A., 2008, *A DEM analysis of flow characteristics of noncohesive particles in hopper*, Materials and Manufacturing Processes, **23**, 196-203

Delage P., Romero E.E., Tarantino A., 2008, *Recent developments in the techniques of controlling and measuring suction in unsaturated soils*, Toll et al. (eds), Unsaturated Soils: Advances in Geo-Engineering, Taylor and Francis Group, London, 33-52.

Drescher A., Ferjani M., 2004, *Revised model for plug/funnel flow in bins*, Powder Technology, **141**, 44-54

Drescher A., Waters A.J., Rhoades C.A., 1995, *Arching in hoppers: I. Arching theories and bulk material flow properties*, Powder Technology, **84**, 165-176

Enstad G., 1975, *On the theory of arching in mass flow hoppers*, Chemical Engineering Science, **30(10)**, 1273-1283

Escario V., Juca J.F.T, 1989, *Strength and deformation of partly saturated soils*, Proceedings of 12th International Conference on Soil Mechanics and Foundation Engineering, 43-46

Escario V., Saez J., 1986, *The shear strength of partly saturated soils*, Geotechnique, **36(3)**, 453-456

Estabragh A.R., Javadi A.A., 2008, *Effect of suction on compressibility and shear behaviour of unsaturated silty soil*, Toll et al. (eds), Unsaturated soils: Advances in Geo-Engineering, Taylor and Francis Group, London, 449-452.

Estabragh A.R., Javadi A.A., Boot J.C., 2004, *Effect of compaction pressure on consolidation behaviour of unsaturated silty soil*, Canadian Geotechnical Journal, **41(3)**, 540-550

Farouk A., Lamboj L., Kos J., 2004, *Influence of matric suction on the shear strength behaviour of unsaturated sand*, Acta Plytechnica, Czech Technical University Publishing House, **44(4)**, 11-17

Farrel D.W., Larson W.E., 1972, *Modeling the pore structure of porous media*, Water Resources Research, **3**, 699-706

Fickie K.E., Mehrabi R., Jackson R., 1989, *Density variations in a granular material flowing from a wedge-shaped hopper*, A.1.ChE. J., **35**, 853

Fitzpatrick J.J., Iqbal T., Delaney C., Twomey T., Keogh M.K., 2004, *Effect of powder properties and storage conditions on the flowability of milk powders with different fat contents*, Journal of Foog Engineering, **64**, 435-444

Fowler R.T., Glastonbury J.R., 1959, *The flow of granular solids through orifices*, Chemical Engineering Science, **10**, 150-156

Fredlund D.G., 1975, *A diffused air volume indicator for unsaturated soils*, Canadian Geotechnical Journal, **12(4)**, 533-539

Fredlund D.G., 2000, *The 1999 R.M. Hardy Lecture: The implementation of unsaturated soil mechanics into geotechnical engineering*, Canadian Geotechnical Journal, **37(5)**, 963-986

Fredlund D.G., Houston S.L., 2009, *Protocol for the assessment of unsaturated soil properties in geotechnical engineering practice*, Canadian Geotechnical Journal, **46(6)**, 694-707

Fredlund D.G., Morgenstern N.R., 1977, *Stress state variables for unsaturated soils*, Journal of Geotechnical Engineering Division, **103**, 447-466

Fredlund D.G., Morgenstern N.R., Widger R.S., 1978, *The shear strength of unsaturated soils*, Canadian Geotechnical Journal, **15(3)**, 313-321

Fredlund D.G., Rahardjo H., 1993, *Soil mechanics for unsaturated soils*, John Wiley and Sons, Inc., New York

Fredlund D.G., Vanapalli S.K., Xing A., Pufahl D.E., 1995, *Predicting the shear strength function for unsaturated soils using the soil-water characteristic curve*,

Fredlund D.G., Xing A., 1994, *Equations for the soil-water characteristic curve*, Canadian Geotechnical Journal, **31(4)**, 521-532

Fredlund D.G., Xing A., Fredlund M.D., Barbour S.L., 1996, *The relationship of the unsaturated soil shear strength to the soil-water characteristic curve*, Canadian Geotechnical Journal, **33(3)**, 440-448

Fredlund D.G., Xing A., Huang S., 1994, *Predicting the permeability function for unsaturated soils using the soil-water characteristic curve*, Canadian Geotechnical Journal, **31(3)**, 521-532

Fredlund M.D., Fredlund D.G., Wilson G.W., 1997, *Prediction of the soil-water characteristic curve from grain-size distribution and volume-mass properties*, Proceedings of the 3rd Brazilian Symposium on unsaturated soils, Rio de Janerio, Brazil, April 20-22, **1**, 13-23

Gallage C.P.K., Uchimura T., 2006, *Effects of wetting and drying on the unsaturated shear strength of a silty sand under low suction*, Proceedings of the 4th International Conference on Unsaturated Soils, **1**, Carefree, Arizona, USA, 1247-1258

Gallipoli D., Gens A., Sharma R., Vaunat J., 2003, *An elasto-plastic model for unsaturated soil incorporating the effects of degree of saturation on the mechanical behaviour*, Geotechnique, **53(1)**, 123-135

Gallipoli D., Wheeler S.J., Karstunen M., 2003, *Modelling the variation of degree of saturation in a deformable soil*, Geotechnique, **53(2)**, 681-687

Gan J.K-M., Fredlund D.G., 1996, *Shear strength characteristics of two saprolitic soils*, Canadian Geotechnical Journal, **33(4)**, 595-609

Ganesan V., Muthukumarappan K., Rosentrater K.A., 2008, *Flow properties of DDGS with varying soluble and moisture contents using Jenike shear testing*, Powder Technology, **187**, 130-137

Garcimartin A., Mankoc C., Janda A., Arevalo R., Pastor J.M., Zuriguel I., Maza D., 2006, *Flow and Jamming of granular matter through an orifice*, Depto. de F´ısica y

Mat. Apl., Universidad de Navarra, 31080 Pamplona, Spain, 471-486, http://fisica.unav.es/granular (last accessed on 25/08/2012)

Gardner R., 1937, *A method of measuring the capillary tension of soil moisture over a wide moisture range*, Soil Science Journal, **43**, 277-283

Gardner R., 1958, *Some steady state solutions of unsaturated moisture flow equations with applications to evapouration from a water table*, Soil Science Journal, **85**, 228-232

Garven E., Vanapalli S.K., 2006, *Evaluation of empirical procedures for predicting the shear strength of unsaturated soils*, ASCE Geotechnical Special Publication No. 147, **2**, 2570-2581

Goda T.J., Ebert F., 2005, *Three-dimensional discrete element simulations in hoppers and silos*, Powder Technology, **158**, 58-68

Grantham S.G., Forsberg F., 2004, *Measurement of granular flow in a silo using digital speckle radiography*, Powder Technology, **146**, 56-65

Gui M.H., Yu C.M., 2008, *Rate of strength increase of unsaturated lateritic soil*, Canadian Geotechnical Journal, **45(9)**, 1335-1343

Haghighi A., Medero G., Marinho F.A.M., Mercier B., Woodward P., 2012, *Temperature effects on suction measurement using filter paper technique*, ASTM Geotechnical Testing Journal, GTJODJ, **35(1)**, 1-8

Han K.K., Rahardjo H., Broms B.B., 1995, *Effects of hysteresis on the shear strength of a residual soil*, Alonso E.E., Delage P. (Eds), Unsaturated Soils, **2**, 499-504

Head K.H, 1986, *Manual of soil laboratory testing*, **3**, John Wiley & Sons, New York

Hilf J.W., 1956, *An investigation of pore water pressure in compacted cohesive soils*, Technical Memo 654, Denver, Bureau of Reclamation

Hillel D., 1998, *Environmental soil physics*, 1st Edition, Academic Press, London

Hirshfeld D., Radzyner Y., Rapaport D.C., 1997, *Molecular dynamics studies of granular flow through an aperture*, The European Physical Journal E, **56**, 4404-4415

Hirshfeld D., Rapaport D.C., 2001, *Granular flow from a silo: Discrete-particle simulations in three dimensions*, The European Physical Journal E, **4**, 193-199

Hodnett M.G., Tomasella J., 2002, *Marked differences between van Genuchten soil-water retention parameters for temperate and tropical soils: a new water-retention pedo-transfer functions developed for tropical soils*, Geoderma, **108**, 155-180

Hoffman C., Tarantino A., 2008, *Effect of grain size distribution on water retention behaviour of well graded coarse material*, Toll et al. (Eds), Unsaturated Soils: Advances in Geo-Engineering, Taylor and Francis Group, London, 291-297

Hoffmann C., Romero E., Alonso E.E., 2005, *Combining different controlled-suction techniques to study expansive clays*, Proceedings of International Symposium on Advanced Experimental Unsaturated Soil Mechanics, Trento, Italy, June 27-29, 2005. Tarantino A., Romero E., Cui Y.J., (eds.), A.A. Balkema, Leiden: 61-67

Houston W.N., Dye H.B., Zapata C.E., Perera Y.Y., Harraz A., 2006, *Determination of SWRC using one point measurement and standard curves*, Proceedings of the Fourth International Conference on Unsaturated Soils, Carefree, Arizona, USA, April 2-6, **2**, 1482-1493

Houston S.L., Houston W.N., Wagner A., 1994, *Laboratory filter paper suction measurements*, Geotechnical Testing Journal, GTJODJ, **17(2)**, 185-194

Houston S.L., Perez-Garcia N., Houston W.N., 2008, *Shear strength and shear volume change behaviour of unsaturated soils from triaxial test program*, Journal of Geotechnical and Geoenvironmental Engineering, ASCE, **134(11)**, 1619-1632

Hoyos L.R., Laloui L., Vassallo R., 2008, *Mechanical testing in unsaturated soils*, Journal of Geothnical and Geological Engineering, Springer, **26**, 675-689

Imre E., Rajkai K., Firgi T., Trang Q.P., Telekes G., 2006, *Closed-form functions for the soil-water retention curve od sand fractions and sand mixtures*, Proceedings of the Fourth International Conference on Unsaturated Soils, Carefree, Arizona, USA, April 2-6, **2**, 2408-2419

Iqbal T., Fitzpatrick J.J., 2006, *Effect of storage conditions on the wall friction characteristics of three food powders*, Journal of Food Engineering, **72**, 273-280

Jenike A.W., 1964, *Storage and flows of solids*, Bulletin No. 123 of the Utah Engineering Experimental Station, **53**, 26

Jennings J.E., 1961, *A revised effective stress lawfor use in the prediction of the behaviour of unsaturated soils*, Pore Pressure and Suction in soils, Butterworths, 26-30

Jennings J.E., Burland J.B., 1962, *Limitations to the use effective stresses in partly saturated soils*, Geotechnique, **12(2)**, 125-144

Johanson J.R., 1964, *Stress and velocity fields in the gravity flow of bulk solids*, Journal of Applied Mechanics, **86**, 499

Josa A., Balmaceda A., Gens A., Alonso E.E., 1992, *An elasto-plastic model for partially saturated soils exhibiting a maximum collapse*, Proceedings of 3rd International Conference on Computational Plasticity, Barcelona, **1**, 815-826

Jotisankasa A., 2005, *Collapse behaviour of a compacted silty clay*, PhD Thesis, Department of Civil and Environmental Engineering, Imperial College London, University of London, London, United Kingdom

Karube D., Kato S., Hamada, K., Honda M., 1996, *The relationship between the mechanical behaviour and the state of pore water in unsaturated soils*, JSCE Journal of Geotechnical Engineering, **34**, 83-92

Kasangaki G.J., Medero G.M., Ooi J.Y., 2012, *Factors influencing water retention characteristics of granular materials*, Proceedings of the Workshop on Advances in Multiphysical Testing of Soils and Shales, AMTSS, EPLF, Laussame, Switzerland, 3-5 September, in Laluoi L., Ferrari A. (Eds.): Multiphysical Testing of Soils and Shales, SSGG, 111-116

Kasangaki G.J., Medero G.M., Ooi J.Y., 2012, *Water retention characteristics of non-plastic granular materials*, Proceedings of the Second European Conference on Unsaturated Soils, E-UNSAT 2012, Napoli Italy, 20-22 June, in Mancuso C., Jommi C., & D'Onza F. (Eds.): Unsaturated Soils: Research and Applications 2012, **2**, 197-203

Kasangaki G.J., Towhata I., 2009, *Wet compaction and lime stabilisation to mitigate volume change potential of clayey soils*, Japanese Geotechnical Society Soils and Foundations, **49(5)**, 813-821

Kato S., Matsuoka H., Sun D.A., 1995, *A constitutive model for unsaturated soil based on SMP*, Proceedings of 1st International Conference on Unsaturated Soils, Paris, **2**, 739-744

Kawajiri S., Shibuya S., Kato S., 2010, *Effects of matric suction on elastic shear modulus for three unsaturated soils*, Proceedings of the Fifth International Conference on Unsaturated Soils, Barcelona, Spain, 6-8 September, Alonso E., Antonio G. (Eds), Unsaturated soils, **1**, CRC Press, Taylor & Francis Group, Balkema, 271-275

Ketterhagen W.R., Curtis J.S., Wassgren C.R., Hancock B.C., 2009, *Predicting the flow mode from hoppers using the discrete element method*, Powder Technology, **195**, 1-10

Karube D., 1988, *New concept of effective stress in unsaturated soil and its proving test*, Donaghe R.T., Chaney R.C., Silver M.L. (Eds), Advanced Triaxial testing of Soil

and Rocks, ASTM STP 977, American Society for Testing and Materials, Philadephia, 539-5552

Khalili N., Geiser F., Blight G.E., 2004, *Effective stress in unsaturated soil: Review with new evidence*, International Journal of Geomechanics, **4(2)** 115-126

Khalili N., Khabbaz M.H., 1998, *A unique relationship for χ for the determination of the shear strength of unsaturated soils*, Geotechnique, **48(5)** 681-687

Khoury C.N., Miller G.A., 2010, *Effects of suction hysteresis on the shear strength of unsaturated soil interfaces*, Proceedings of the Fifth International Conference on Unsaturated Soils, Barcelona, Spain, 6-8 September, Alonso E., Antonio G., (Eds), Unsaturated soils, **1**, CRC Press, Taylor & Francis Group, Balkema, 283-287

Kim T.H., Sture S., 2008, *Capillary-induced tensile strength in unsaturated sands*, Canadian Geotechnical Journal, **45(5)**, 726-737

Kim T.H., Sture S., 2004, *Effect of moisture on attraction force in beach sand*, Marine Georesources and Geotechnology, **22**, 33-47

Koliji A., Laloui L., Cusinier O., Vulliet L., 2006, *Suction induced effects on the fabric of a structured soil*, Transport in Porous Media, **64**, 261-278

Kramer S.L., Sivaneswaran N., Davis R.O., 1990, *Analysis of membrane penetration in triaxial tests*, Journal of Engineering Mechanics, **116(4)**, 773-789

Kusinska E., 2000, *Effect of tritical moisture content and slenderness ratio of a silo on pressure distribution*, International Journal of Agrophysics, **14**, 191-195

Landi G., Barletta D., Poletto M., 2011, *Modeling and experiments on the effect of air humidity on the flow properties of glass powders*, Powder Technology, **207**, 437-443

Lappalainen K., Manninen M., Alopaeus V., Aittamaa J., Dodds J., 2009, *An analytical model for capillary pressure-saturation relation for gas-liquid system in a packed-bed of spherical particles*, Transport in Porous Media, Springer Netherlands, **77**, 17-40

Leong E.C., Rahardjo H., 1997, *Review of soil-water characteristic curve equations*, Journal of Geotechnical and Geoenvironmental Engineering, ASCE, **123(12)**, 1106-1117

Leong E.C., Widiastuti S., Lee C.C., Rahardjo H., 2007, *Accuracy of suction measurement*, Geotechnique, **57(6)**, 547-556

Leverett M.C., 1941, *Capillary behaviour in porous solids*, AIME, **142(1)**, 152-169

Likos W.J., Lu N., 2002, *Filter paper technique for measurement of total soil suction*, Journal of the Transportation Research Board, No. 1786, TRB, Washington D.C., 1120-1128

Lings M.L., Dietz M.S., 2004, *An improved direct shear apparatus for sand*, Geotechnique, **54(4)**, 245-256

Lloret A., Alonso E.E., 1985, *State surfaces for partially saturated soils*, Proceedings of 11th International Conference on Soil Mechanics and Foundations, San Francisco, 557-562

Lourenco S.D.N., Toll D.G., Augarde C.E., Gallipoli D., Congreve A., Smart T., Evans F.D., 2008, *Observation of unsaturated soil by environment scanning electron microscopy in dynamic mode*, Toll et al. (Eds), Unsaturated soils: Advances in Geo-Engineering, Taylor and Francis Group, London, 145-150

Lourenco S.D.N., Toll D.G., Augarde C.E., Gallipoli D., Evans F.D., Medero G.M., 2008, *Evaluation of suction measurement by the tensiometer and the axis translation technique*, Toll et al. (Eds), Unsaturated soils: Advances in Geo-Engineering, Taylor and Francis Group, London, 213-218

Lu N., Likos W.J., 2004, *Unsaturated soil mechanics*, John Wiley and Sons, Inc., New Jersey, USA

Lu N., Likos W.J., 2006, *Suction stress characteristic curve for unsaturated soil*, Journal of Geotechnical and Geoenvironmental Engineering, **132(2)**, 131-142

Lui J.K., Peng, L.Y., 2008, *Strength and yielding of unsaturated compacted silt from Beijing-Kowloom railway embankment*, Toll et al. (Eds), Unsaturated soils: Advances in Geo-Engineering, Taylor and Francis Group, London, 471-474

Maatouk A., Leroueil S., Rochelle P.L.A., 1995, *Yielding and critical state of a collapsible unsaturated silty soil*. Géotechnique, **45(3)**, 465–477

Mankoc C., Janda A., Arevalo R., Pastor J.M., Zuriguel I., Garcimartin A., Maza D., 2007, *The flow rate of granular materials through an orifice*, Granular Matter, **9**, 407–414

Marinho F.A.M., 1994, *Shrinkage behaviour of some plastic clay*, PhD Thesis, Imperial College, University of London

Marinho F.A.M., Oliveira M., 2005, *The filter paper method revisited*, Geotechnical Testing Journal, **29(3)**, 250-258

Marinho F.A.M., Take W.A., Tarantino A., 2008, *Measurement of matric suction using tensiometric and axis translation techniques*, Journal of Geothnical and Geological Engineering, Springer, **26**, 615-631

Maswoswe J., 1985, *Stress pass for a compacted soil during collapse due to wetting*, PhD Thesis, Imperial College of Science, Technology and Medicine, University of London

Matchett A.J., 2007, *The shape of the cohesive arch in hoppers and silos – Some theoretical considerations*, Powder Technology, **171**, 133-145

Matyas E.L., Radhakrishna H.S., 1968, *Volume change characteristics of partially saturated soils*, Geotechnique, **18(4)**, 432-448

Miguel M.G., Vilar O.M., 2009, *Study of the water retention properties of a tropical soil*, Canadian Geotechnical Journal, **46(9)**, 1084-1092

Miller C. J., Yesiller N., Yaldo K., Merayyan S., 2002, *Impact of soil type and compaction conditions on soil water characteristic*, Journal of Geotechnical and Geoenvironmental Engineering, **128(9)**, 733-742

Mirzaii A., Yasrebi S.S., Gatmiri B., 2008, *Mechanical behaviour of an unsaturated clayey sand*, Toll et al. (Eds), Unsaturated soils: Advances in Geo-Engineering, Taylor and Francis Group, London, 453-458

Morozov E., Henshall J.L., Brown C.J., 2002, *Design optimisation of silo structures made from composite materials. Part 2: optimum design of the composite hopper*, Proceedings of the Institution of Mechanical Engineers, **216**, Part L, Journal of Materials: Design and Applications, 69-77

Mualem Y., 1976, *A new model for predicting the hydraulic conductivity of unsaturated porous media*, Water Resources Research, **12**, 513-522

Muira S., Toki S., 1982, *A sample preparation method and its effect on static and cyclic deformation-strength properties of sand*, Soils and Foundations, Japanese Society of Soil Mechanics and Foundation Engineering, JGS, **22(1)**, 61-77

Nedderman R.M., Tuzun U., Savage S.B., Houlsby G.T., 1982, *The flow of granular materials-1. Discharge rates from hoppers*, Chemical Engineering Science, **37**, 1597

Ng C.W.W., Chiu C.F., Rahardjo H., 2000, *Laboratory study of loosely compacted unsaturated volcanic fill*, Rahardjo, et al. (eds), Unsaturated soils for Asia, Rotterdam Balkema, ASCE, 551-556

Ng C.W.W., Menzies B., 2007, *Advanced unsaturated soil mechanics and engineering*, Taylor and Francis, Abingdon, United Kingdom

Ng C.W.W., Pang Y.W., 2000a, *Experimental investigations of the soil-water characteristics of a volcanic soil*, Canadian Geotechnical Journal, **37(6)**, 1252-1264

Ng C.W.W., Pang Y.W., 2000b, *Influence of stress state on soil-water characteristics and slope stability*, Journal of Geotechnical and Geoenvironmental Engineering, ASCE, **126(2)**, 157-166

Ng C.W.W., Xu J., Yung S.Y., 2009, *Effects of wetting-drying and stress ratio on anistropic stiffness of an unsaturated soil at very small strains*, Canadian Geotechnical Journal, **46(9)**, 1062-1076

Nishinura T., Shahrour I., Bian H.B., 2010, *Investigation of the behaviour of an unsaturated sand using a cyclic direct shear device*, Proceedings of the Fifth International Conference on Unsaturated Soils, Barcelona, Spain, 6-8 September, Alonso E., Antonio G., (Eds), Unsaturated soils, **1**, CRC Press, Taylor & Francis Group, Balkema, 329-334

Oberg A.L., Salfors G., 1997, *Determination of shear strength parameters of unsaturated silts and sands based on the water retention curves*, Geotechnical Testing Journal, **20(1)**, 40-48

Oliveira O.M., Marinho F.A.M., 2006, *Evaluation of filter paper calibration*, Proceedings of the Fourth International Conference on Unsaturated Soils, Carefree, Arizona, USA, April 2-6, **2**, 1845-1851

Ooi J.Y., Chen J.F., Rotter J.M., 1998, *Measurement of solids flow pattern in a gypsum silo*, Powder Technology, Elsevier, **99**, 272-284

Padilla J.M., Houston W.N., Lawrence C.A., Fredlund D.G., Houston S.L., Perez N.P., 2006, *An automated triaxial testing device for unsaturated soils*, Proceedings of the Fourth International Conference on Unsaturated Soils, Carefree, Arizona, USA, April 2-6, **2**, 1775-1786

Padilla J.M., Perera Y.Y., Houston W.N., Perez N., Fredlund D.G., 2006, *Quantification of air diffusion through high air entry ceramic disks*, Proceedings of the Fourth International Conference on Unsaturated Soils, Carefree, Arizona, USA, April 2-6, **2**, 1852-1863

Pariseau W.G., 1969, *Discontinuous velocity fields in granular flows of granular materials through slots*, Powder Technology, **3**, 218-226

Peterson R.W., 1988, *Interpretation of triaxial compression test results on partially saturated soils*, Donaghe et al. (Eds), Advanced Triaxial testing of Soil and Rocks, ASTM STP 977, American Society for Testing and Materials, Philadephia, 512-538

Pham H.Q., Fredlund D.G., 2008, *Equations for the entire soil-water characteristic curve of a volume change soil*, Canadian Geotechnical Journal, **45(4)**, 443-453

Pieper K., Wenzel F., 1963, *Comments on DIN1055: Design Loads for Buildings Loads in Silo Bins*. Beton und Stahlbetonbau, 6-11

Pires L.F., Reichardt K., Cooper M., Cassaro F.A.M., Dias N.M.P., Bacchi O.O.S., 2009, *Pore system changes of damaged Brazilian oxiols and nitosols induced by wet-dry cycles as seen in 2-D micromorphologic image analysis*, Anais da Academia Brasileira de Ciencias, **81(1)**, 151-161

Rajaram G., Erbach D.C., 1999, *Effect of wetting and drying on soil physical properties*, Journal of Terramechanics, **36**, 39-49

Rampino C., Mancuso C., Vinale F., 1999, *Laboratory testing of an unsaturated soil: equipment, procedures, and first experimental results*, Canadian Geotechnical Journal, **36(1)**, 1-12

Rassam D.W., Cook F.J., 2002, *Predicting the shear strength envelope of unsaturated soils*, Geotechnical Testing Journal, ASTM, **28**, 215-220

Rassam D.W., Williams D.J., 1999, *A relationship describing the shear strength of unsaturated soils*, Canadian Geotechnical Journal, **36(2)**, 363-368

Ridley A.M., 1993, *The measurement of soil moisture suction*, PhD Thesis, Imperial College, University of London.

Ridley A.M., Burland J.B., 1993, *A new instrument for the measurement of suction*, Geotechnique, **43(2)**, 321-324

Ridley A.M., Burland J.B., 1995, *A pore pressure probe for the in situ measurement of soil suction*, Proceedings of Conference on Advances in Site Investigation Practice, London

Ridley A.M., Burland J.B., 1999, *Use of the tensile strength of water for the direct measurement of high soil suction*, Canadian Geotechnical Journal, **36(1)**, 178-180

Ridley A.M., Dineen K., Burland J.B., Vaughan P.R., 2003, *Soil matrix suction: Some examples of its measurement and application in geotechnical engineering*, Geotechnique, **53(2)**, 241-253

Ridley A.M., Wray W.K., 1996, *Suction measurement: Theory and practice. A state-of-the-art review*, Proceedings of 1st International Conference on Unsaturated Soils, Paris, **3**, 1293-1322

Romero E., 1999, *Characterisation and thermo-hydromechechanical behaviour of unsaturated Boom clay: An experimental study*, PhD Thesis, Universitat Polytechnic de Catalunya, Barcelona, Spain

Romero E., Vaunat J., 2000, *Retention curves in deformable clays*, Tarantino A., Mancuso C., Eds, Experimental evidence and theoretical approaches in unsaturated soils, Rotterdam, A. A. Balkema, 91-106

Rotter J.M., 2001, *Guide for the economic design of circular metal silos*, Spon Press, London

Rose H.F., Tanaka T., 1959, *Rate of discharge of granular materials from bins and hoppers*, The Engineer, **208**, 645

Schulze D., 2008, Powders and bulk solids: Behaviour, characterisation, storage and flow, **16**, Springer Berlin Heidelberg

Sheldon H.G., Durian D.J., 2010, *Granular discharge and clogging for tilted hoppers*, Granular Matter, **12**, 579-585

Sheng D., Yao Y., Carter J.P., 2008, *A volume-stress model for sands under isotropic and critical stress states*, Canadian Geotechnical Journal, **45(11)**, 1639-1645

Sillers W.S., Fredlund D.G., 2001, *Statistical assessment of soil-water characteristic curve models for geotechnical engineering*, Canadian Geotechnical Journal, **38(6)**, 1297-1313

Sivakumar V., Wheeler S.J., 2000, *Influence of compaction procedure on the mechanical behaviour of unsaturated compacted clay. Part 1: Wetting and isotropic compression*, Geotechnique, **50(4)**, 359-368

Snider D.M., 2007, *Three fundamental granular flow experiments and CPFD predictions*, Powder Technology, **176**, 36-46

Sperl M., 2006, *Experiments on corn pressure in silo cells – translation and comment of Janssen's paper from 1895*, Granular Matter, **8**, 59-65

Take W.A., Bolton M.D., 2003, *Tensiometer saturation and reliable measurement of soil suction*, Geotechnique, **53(2)**, 159-172

Tarantino A., Mongiovi L., 2001, *Experimental procedures and cavitation mechanisms in tensiometer measurements*, Geotechnical and Geological Engineering, Kluwer Academic Publishers, **19**, 189-210

Tarantino A., Mongiovi L., 2003, *Calibration of the tensiometer for the direct measurement of matric suction*, Geotechnique, **53(1)**, 137-141

Tixier M., Pitois O., Mills P., 2004, *Experimental impact of the history of packing on the mean pressure in silos*, The European Physical Journal E, **14**, 241-247

Toll D.G., 1990, *A framework for unsaturated soil behaviour*, Geotechnique, **40(1)**, 31-44

Toll D.G., 2000, *The influence of fabric on the shear behaviour of unsaturated compacted soils*, Shackelford, et al. (Eds), Advances in unsaturated soils, ASCE, Geotechnical Special Publication, No. 99, Reston, 222-234.

Toll D.G., Ong B.H., 2003, *Critical-state parameters for an unsaturated residual sandy clay*, Geotechnique, **53(1)**, 93-103

Toll D.G., Rahman Z.A., Gallipoli D., 2008, *Critical state conditions for an unsaturated artificially bonded soil*, Toll et al. (Eds), Unsaturated Soils: Advances in Geo-Engineering, Taylor and Francis Group, London, 435-440

Tomboy O., Whenham V., De Vos M., Charlier R., Maertens J., Verbrugge J.C., 2009, *Shear strength of unsaturated soil and its influence on slope stability*, Toll et al. (Eds), Unsaturated Soils: Advances in Geo-Engineering, Taylor and Francis Group, London, 459-464

Tse E.Y.M., Ng C.W.W., 2008, *Effects of drying and wetting cycles on unsaturated shear strength*, Toll et al. (Eds), Unsaturated Soils: Advances in Geo-Engineering, Taylor and Francis Group, London, 481-486

Uchaipichat A., Khalili, N., 2009, *Experimental investigation of thermo-hydro-mechanical behaviour of an unsaturated silt*, Geotechnique, **59(4)**, 339-353

Urso M.E.D., Lawrence C.J., Adams M.J., 1999, *Pendular, funicular and capillary bridges: Results for two dimensions*, Journal of Colloid and Interface Science, **220**, 42-56

Van Genuchten M.Th., 1980, *A closed form equation for predicting the hydraulic conductivity of unsaturated soils*, Soil Science Society of the America Journal, **44**, 892-898

Vanapalli S.K., Fredlund D.G., Pufahl D.E., Clifton A.W., 1996, *Model for the prediction of shear strength with respect to soil suction*, Canadian Geotechnical Journal, **33(3)**, 379-392

Vanapalli S.K., Nicotera M.V., Sharma R.S., 2008, *Axis translation and negative water column techniques for suction control*, Journal of Geotechnical and Geological Engineering, Springer, 645-660

Vanapalli S.K., Oh W.T., Puppala A.J., 2009, *A simple method for the prediction of modulus of elasticity for unsaturated sandy soils*, Toll et al. (Eds), Unsaturated Soils: Advances in Geo-Engineering, Taylor and Francis Group, London, 503-509

Verghese T.M., Nedderman R.M., 1995, *The discharge of fine sands from conical hoppers*, Chemical Engineering Science, **50(19)**, 3143-3153

Vilar O.M., 2006, *A simplified procedure to estimate the shear strength envelope of unsaturated soils*, Canadian Geotechnical Journal, **43(10)**, 1088-1095

Walters J.K., 1973, *A theoretical analysis of stresses in axially-symmetric hoppers and bunkers*, Chemical Engineering Science, **28(3)**, 779 -789

Wang J., 2005, *The stress-strain and strength characteristics of Portaway sand*, PhD Thesis, University of Nottingham

Weir G., 2004, *A mathematical model for dilating, non-cohesive granular flows in steep-walled hopper*, Chemical Engineering Science, **59**, 149-161

Wheeler S.J., 1988, *The undrained shear strength of soils containing large gas bubbles*, Geotechnique, **38(3)**, 399 -413

Wheeler S.J., 1996, *Inclusion of specific water volume within an elasto-plastic model for unsaturated soil*, Canadian Geotechnical Journal, **33(1)**, 42-57

Wheeler S.J., Gallipoli D., Karstunen M., 2002, *Comments on the use of the Barcelona Basic Model for unsaturated soils*, International Journal for Numerical and Analytical Methods in Geomechanics, John Wiley & Sons, Ltd., **26** 1561-1571

Wheeler S.J., Karube D., 1996, *Constitutive modelling*, Alonso E.E., Delage P. (Eds), Unsaturated soils, Balkema, Rotterdam, **3**, 1323-1356

Wheeler S.J., Sharma R.S., Buisson S.R., 2003, *Coupling of hydraulic hysteresis and stress-strain behaviour in unsaturated soils*, Geotechnique, **53(1)**, 41-54

Wheeler S.J., Sivakumar V., 1995, *An elasto-plastic critical state framework for unsaturated soils*, Geotechnique, **45(1)**, 35-53

Wulfsohn D., Adams B.A., Fredlund D.G., 1998, *Triaxial Testing of unsaturated agricultural soils*, Journal of Agricultural Engineering Research, Elsevier, **69(4)**, 317-330

Yamamuro J.A., Wood F.M., 2004, *Effect of depositional method on the undrained behaviour and microstructure of sand with silt*, Soil Dynamics and Earthquake Engineering, Elsevier, **24**, 751-760

Yamamuro J.A., Wood F.M., Lade P.V., 2008, *Effect of depositional method on the microstructure of silty sand*, Canadian Geotechnical Journal, **45(11)**, 1538-1555

Yang H., Rahadjo H., Leong E.C., Fredlund D.G., 2004, *Factors affecting drying and wetting soil-water characteristic curves of sandy soils*, Canadian Geotechnical Journal, **41**, 908-920

Yang S.R., Lin H.D., Kung J.H.S., Huang W.H., 2008, *Suction-controlled laboratory testing on resilient modulus of unsaturated compacted subgrade soils*, Journal of Geotechnical and Geoenvironmental Engineering, ASCE, **134(9)**, 1375-1384

Zapata C.E., Houston W.N., Houston S.L., Walsh K.D., 2000, *Soil-water characteristic curve variability*, Proceedings of the Geo-Denver Conference, Denver, Colorado, U.S., August 5-8, Shackelford et al. (Eds), Advances in Geotechnics, 84-124

Zhang J.Y., Rudolph V., 1991, *Effect of shear friction on solid flow through an orifice*, Industrial Engineering Chemistry Research, **30**, 1977-1981

Zhang X., Li L., 2011, *Limitations in the constitutive modeling of unsaturated soils and solutions*, International Journal of Geomechanics, ASCE, **11(3)**, 174-185

Zhu H.P., Mehrabadi M.M., Massoudi M., 2007, *The frictional flow of a dense material based on the dilatant double shearing model*, Computers and Mathematics with Applications, **53**, 244 - 259

Zhu H.P., Zhou Z.Y., Yu A.B., Zulli P., 2009, *Stress fields of solid flow in a model blast furnace*, Granular Matter, Springer, **11**, 269 - 280

Zhong Z., Ooi J.Y., Rotter J.M., 2001, *The sensivity of silo flow and wall stresses to filling pattern*, Engineering Structures, Elsevier, **23**, 756-767